Distribution Agreement

In presenting this thesis or dissertation as a partial fulfillment of the requirements for an advanced degree from Emory University, I hereby grant to Emory University and its agents the non-exclusive license to archive, make accessible, and display my thesis or dissertation in whole or in part in all forms of media, now or hereafter known, including display on the world wide web. I understand that I may select some access restrictions as part of the online submission of this thesis or dissertation. I retain all ownership rights to the copyright of the thesis or dissertation. I also retain the right to use in future works (such as articles or books) all or part of this thesis or dissertation.

Signature:

_____ _____
Sharon A. Swanger   Date

Bidirectional control of dendritic mRNA translation, glutamate receptor expression, and synapse structure by the CPEB-associated polyadenylation machinery

By

Sharon A. Swanger
Doctor of Philosophy

Graduate Division of Biological and Biomedical Sciences
Neuroscience

_____
Gary J. Bassell, Ph.D.
Advisor

_____
Raymond J. Dingledine, Ph.D.
Committee Member

_____
Yue Feng, Ph.D.
Committee Member

_____
Randy A. Hall, Ph.D.
Committee Member

_____
Subhabrata Sanyal, Ph.D.
Committee Member

Accepted:

_____
Lisa A. Tedesco, Ph.D.
Dean of the James T. Laney School of Graduate Studies

_____
Date

Bidirectional control of dendritic mRNA translation, glutamate receptor expression, and synapse structure by the CPEB-associated polyadenylation machinery

By

Sharon A. Swanger
B.S., Lehigh University, 2001

Advisor: Gary J. Bassell, Ph.D.

An abstract of
a dissertation submitted to the Faculty of the
James T. Laney School of Graduate Studies of Emory University
in partial fulfillment of the requirements for the degree of
Doctor of Philosophy

Graduate Division of Biological and Biomedical Sciences
Neuroscience

2012

ABSTRACT

Bidirectional control of dendritic mRNA translation, glutamate receptor expression,

and synapse structure by the CPEB-associated polyadenylation machinery

By

Sharon A. Swanger

Neurons are highly polarized cells that extend elaborate dendritic arbors and have thousands of synaptic inputs. The post-transcriptional control of gene expression through dendritic mRNA localization and local protein synthesis is an important means for regulating postsynaptic protein expression. Moreover, translational control of dendritic mRNAs is essential for certain forms of synaptic plasticity, learning, and memory. CPEB (cytoplasmic polyadenylation element binding protein) is one RNA binding protein that regulates local translation in dendrites as well as synaptic structure and function. However, the mechanism by which it regulates these processes is unknown. Herein, we identify a poly(A) polymerase, a deadenylase, and the translation inhibitory factor neuroguidin as components of a dendritic CPEB-associated polyadenylation complex. Synaptic stimulation induces phosphorylation of CPEB, expulsion of the deadenylase from the ribonucleoprotein complex, and mRNA polyadenylation in dendrites. Furthermore, these CPEB-associated translation factors bidirectionally regulate dendritic spine morphology as well as AMPA receptor surface expression in cultured hippocampal neurons. One CPEB target mRNA is that encoding GluN2A, which is an NMDA receptor subunit and a critical regulator of synapse function and plasticity. We found that GluN2A mRNA is localized to dendrites and associates with CPEB. The dendritic transport and local translation of GluN2A mRNA is regulated by CPEB and its target sequence within GluN2A mRNA. The CPEB-associated poly(A) polymerase promotes dendritic GluN2A protein expression and surface expression of GluN2A-containing NMDA receptors; whereas, the negative translation factor neuroguidin inhibits GluN2A expression in dendrites and at the cell surface. Moreover, protein synthesis and this poly(A) polymerase are required for activity-induced translation of GluN2A and membrane insertion of GluN2A-containing NMDA receptors. These results identify a pivotal role for dendritic mRNA polyadenylation and the opposing effects of CPEB-associated translation factors in regulating receptor expression and synapse structure at glutamatergic synapses as well as activity-induced membrane insertion of NMDA receptors during synaptic plasticity.

Bidirectional control of dendritic mRNA translation, glutamate receptor expression,

and synapse structure by the CPEB-associated polyadenylation machinery

By

Sharon A. Swanger
B.S., Lehigh University, 2001

Advisor: Gary J. Bassell, Ph.D.

A dissertation submitted to the Faculty of the
James T. Laney School of Graduate Studies of Emory University
in partial fulfillment of the requirements for the degree of
Doctor of Philosophy

Graduate Division of Biological and Biomedical Sciences
Neuroscience

2012

ACKNOWLEDGEMENTS

TABLE OF CONTENTS

List of Figures and Tables

CHAPTER FIVE

APPENDIX 1

List of Abbreviations and Symbols

^{3}H   tritiated hydrogen

4E-BP   eIF4E binding protein

AMPA   α-amino-3-hydroxy-5-methyl-4-isoxazolepropionic acid

ApCPEB77   aplysia cytoplasmic polyadenylation element binding protein 77 kDa

APV   2-amino-5-phosphonopentanoate

Arc   activity-regulated cytoskeleton-associated protein

Arg3.1   activity-regulated gene 3.1

area V1   primary visual cortex

A-site   aminoacyl-site

AUG   adenine-uracil-guanine

BDNF   brain-derived neurotrophic factor

CA1   cornus ammonis 1

CA3   cornus ammonis 3

CaMKII   calcium/calmodulin-activated kinase II

CPE   cytoplasmic polyadenylation element

CPEB   cytoplasmic polyadenylation element binding protein

CPSF   cleavage and polyadenylation specificity factor

CYFIP   cytoplasmic fragile-x mental retardation interacting protein;

DIV   days in vitro

eEF   eukaryotic elongation factor

eIF   eukaryotic translation initiation factor

eRF	eukaryotic releasing factor
Fmr1	fragile X mental retardation 1
FMRP	fragile x mental retardation protein
GAP43	growth-associated protein 43
GDP	guanine diphosphate
GFP	green fluorescent protein
GluA1	AMPA-type glutamate receptor subunit 1
GluA2	AMPA-type glutamate receptor subunit 2
GluN1	NMDA-type glutamater receptor subunit 1
GluN2A	NMDA-type glutamate receptor subunit 2A
GluN2B	NMDA-type glutamate receptor subunit 2B
GTP	guanine triphosphate
hnRNP	heterogeneous nuclear ribonucleoprotein
IRES	internal ribosome entry site
IRSp53	insulin receptor tyrosine kinase substrate p53
kDa	kilodalton
KIF5	kinesin superfamily protein 5
LTD	long-term depression
LTP	long-term potentiation
MAP2	microtubule-associated protein 2
mGlu	metabotropic glutamate receptor
mRNA	messenger RNA
mTOR	mammalian target of rapamycin

Ngd	neuroguidin
NMDA	*N*-methyl-*D*-aspartate
PABP	poly(a) binding protein
PAGE	polyacrylamide gel electrophoresis
PARN	poly(a) ribonuclease
PKMζ	protein kinase m-zeta
poly(A)	poly-adenosine
PSD95	postsynaptic density protein 95
P-site	peptidyl-site
RNA	ribonucleic acid
RNP	ribonucleoprotein
S	Svedberg unit
TLS	translocated in liposarcoma
TrkB	tyrosine kinase receptor B
tRNA	transfer RNA
UTR	untranslated region
ZBP1	zipcode-binding protein 1
α	alpha
β	beta
γ	gamma
Δ	delta
μ	mu
ζ	Zeta

CHAPTER ONE

General Introduction

The brain encodes learned information by transducing experience-mediated neural activity into long-term modifications of synaptic connections. These activity-dependent alterations in synapse structure and function are generally termed synaptic plasticity. A single neuron can receive up to 10,000 synaptic inputs, but the activity-induced synaptic plasticity underlying learning occurs at particular synapses on a given neuron, not all synapses. Therefore, synaptic plasticity requires precise temporal and spatial control mechanisms. Moreover, the ability of the brain to alter synaptic connections during learning and memory relies upon new protein synthesis. Thus, the requirement for input-specific synaptic modifications during learning poses a problem: how are the newly synthesized proteins required for synaptic plasticity delivered only to specific synapses?

One model, first described by Frey and Morris, is termed the "synaptic tagging and capture" hypothesis (Frey and Morris, 1997). A molecular "tag" is formed at activated synapses during the early phase of long-lasting synaptic plasticity; this "tag" lasts only a short time and its formation is protein synthesis-independent. For the consolidation or late phase of synaptic plasticity, newly synthesized proteins from the cell body are trafficked to the dendrites and "captured" by only the "tagged" synapses (Figure 1.1A). An alternative model is that mRNA transcripts are trafficked throughout the dendritic arbor, and mRNA translation is repressed until synaptic activation leads to localized protein synthesis at the activated inputs. Thus, new proteins are synthesized at only activated synapses where they enable synaptic modification (Figure 1.1B). Locally synthesizing new proteins affords the neuron tight spatial and temporal control of signal-induced gene expression, whereas trafficking of proteins from a distant site requires not only time, but an elaborate mechanism for ensuring delivery to only the appropriate

subcellular domains. Also, several protein molecules can be locally synthesized from a single mRNA transcript, which is more economical than long-distance transport of several protein molecules synthesized within the cell body. While these two non-mutually exclusive theories underlying synapse-specific plasticity both have garnered much support, herein, the focus is on the second theory termed local protein synthesis.

The earliest support for local protein synthesis at synapses came in 1965 when David Bodian discovered polyribosomes localized near the postsynaptic membrane within in spinal motoneurons (Bodian, 1965). Polyribosomes are an array of ribosomes that are associated with an mRNA transcript and can be viewed by electron microscopy. Bodian hypothesized that "postjunctional synthetic processes involving RNA may be required for the maintenance or function of impinging boutons". Subsequently, it was shown that polyribosomes were localized at postsynaptic sites throughout the dendritic arbor of hippocampal neurons (Steward and Levy, 1982). These founding studies brought forth the hypothesis that local protein synthesis might regulate synaptic communication and generated a multitude of new scientific questions, including: 1) does protein synthesis occur in dendrites, 2) what is the relationship between synaptic activity and local protein synthesis, 3) which mRNA transcripts are localized to dendrites, 4) does dendritic protein synthesis contribute to input-specific synaptic plasticity, and 5) how is dendritic protein synthesis regulated? These fundamental questions spawned a new field of neuroscience focused on uncovering the roles for dendritic protein synthesis in regulating neuron function.

1.1 The significance of protein synthesis in synaptic plasticity, learning, and memory

In 1963, Flexner and colleagues showed that an intracerebral injection of puromycin, a protein synthesis inhibitor, interrupted long-term memory in mice (Flexner et al., 1963). Since that time, protein synthesis has been shown to be required for many types of long-term synaptic plasticity, learning, and memory. The majority of these studies have focused on plasticity at glutamatergic synapses within the cerebral cortex and hippocampus, as these brain regions are critical for consolidating short-term memory into long-term memory and memory storage (Hernandez and Abel, 2008). However, protein synthesis-dependent synaptic plasticity occurs in many other brain regions as well, including the amygdala (reviewed in Helmstetter et al., 2008), striatum (Centonze et al., 2007; Maccarrone et al., 2010; Mao et al., 2008), nucleus accumbens (Ferretti et al., 2010; Hernandez and Kelley, 2004; Kuo et al., 2007; Neasta et al., 2010; Pedroza-Llinas et al., 2009; Sun and Wolf, 2009; Wang et al., 2010b), dorsal raphe nucleus (Baker-Herman and Mitchell, 2002), ventral tegmental area (Argilli et al., 2008; Mameli et al., 2007; Schilstrom et al., 2006; Sorg and Ulibarri, 1995), thalamus (Parsons et al., 2006), and cerebellum (Karachot et al., 2001; Linden, 1996). In addition, neuromodulatory inputs to the hippocampus and cerebral cortex regulate protein synthesis-dependent plasticity and learning. These afferents include dopaminergic inputs from the ventral tegmental area (Bloomer et al., 2008; Huang and Kandel, 1995; Huang et al., 2004; Kudoh et al., 2002; Nagai et al., 2007; Navakkode et al., 2007; Schicknick et al., 2008; Smith et al., 2005; Tischmeyer et al., 2003; Wang et al., 2010a), cholinergic inputs from the medial septal nucleus and the nucleus basalis magnocellularis (Bergado et al., 2007; Frey et al., 2001; Frey et al., 2003; Massey et al., 2001; McCoy and McMahon, 2007;

Volk et al., 2007), and noradrenergic inputs from the locus ceoruleus (Bloomer et al., 2008; Gelinas et al., 2007; Gelinas and Nguyen, 2005; Straube et al., 2003; Walling and Harley, 2004). Collectively, these studies established that protein synthesis-dependent plasticity controls a variety of animal behaviors including spatial memory, motor learning, drug addiction, social and reproductive behaviors, appetitive learning, and fear conditioning. Moreover, this collection of findings underscores the critical function of protein synthesis during synaptic plasticity throughout the brain and the importance for understanding how protein synthesis controls synapse structure and function.

1.2 Activity-induced local protein synthesis in dendrites

Local protein synthesis within the postsynaptic compartment is one mechanism that contributes to new protein synthesis necessary for long-term synaptic plasticity. In support of this assertion, the protein synthetic machinery including mRNA, ribosomes, translation factors, tRNA, tRNA synthetases, and co-translational protein sorting organelles are present within dendrites and at synaptic sites (Davis et al., 1987; Gardiol et al., 1999; Steward and Levy, 1982; Steward and Reeves, 1988; Tiedge and Brosius, 1996). Synaptic ribosomal proteins and translation factors are associated with membranous cisterns positive for endoplasmic reticulum markers (Gardiol et al., 1999), and the endoplasmic reticulum-to-Golgi secretory pathway is functional in dendrites (Horton and Ehlers, 2003). Together, these findings suggest that the molecular machinery necessary for synthesizing functional cytoplasmic and membrane-bound proteins is present within dendrites.

The quest to "prove" that dendritic protein synthesis occurs required novel

techniques to separate dendritic and somatic cytoplasm. Torre and Steward developed a method for culturing neurons on a porous surface through which only neurites could extend. Following transection of the somas, the neurites were pulsed with ^{3}H-leucine and detected by autoradiography. Puromycin-sensitive labeling of proteins was observed within transected dendrites suggesting that new protein synthesis occurred in the dendritic compartment (Torre and Steward, 1992). Importantly, Torre and Steward also demonstrated that newly synthesized proteins could be glycosylated within the dendritic compartment; glycosylation is a co-translational protein modification critical for the function and localization of many proteins (Torre and Steward, 1996).

Although these studies demonstrated that proteins could be synthesized within dendrites, whether dendritic protein synthesis had any relation to synaptic plasticity was not addressed. Two well-studied forms of long-term synaptic plasticity underlying learning and memory are long-term potentiation (LTP) and long-term depression (LTD). LTP and LTD are Hebbian forms of synaptic plasticity, meaning that they are triggered by associated changes in presynaptic and postsynaptic neuronal activity and occur in a synapse-specific manner (Hebb, 1949). Synapses with correlated presynaptic and postsynaptic firing are strengthened (LTP), and uncorrelated presynaptic and postsynaptic firing leads to synapse weakening (LTD) (Bliss and Lomo, 1973; Dunwiddie and Lynch, 1978). A collection of studies in the 1980's showed that the late-phase of LTP in the hippocampus required protein synthesis (reviewed in Silva and Giese, 1994)). Fortuitously, the hippocampus has a unique laminar structure making it ideal for the study of localized protein synthesis. In the CA1 and CA3 (cornu ammonis 1 and 3) regions, the somas of pyramidal neurons are located in one layer (stratum

pyramidale) and all apical dendrites extend into another layer [stratum lucidum (CA3), radiatum, and lacunosum-moleculare]. Similarly, in the dentate gyrus, the granule cell somas are located in the stratum granulosum and extend apical dendrites into the stratum moleculare (Andersen, 2007). Neuroscientists have taken advantage of this laminar organization in their studies of dendritic protein synthesis as it provides a means to separate, either visually or mechanically, the hippocampal neuron soma from its apical dendrites.

Feig and Lipton used this distinct hippocampal structure to provide the first evidence for dendritic protein synthesis during LTP. The muscarinic receptor agonist carbachol was applied to hippocampal slices in combination with high-frequency stimulation, a paradigm known to induce LTP in the CA1 region, and this produced a three-fold increase in ^{3}H-leucine incorporation in the dendritic region (Feig and Lipton, 1993). Since the slices were only incubated in ^{3}H-leucine for 3 minutes, it was unlikely that the labeling in the dendritic compartment was due to transport of somatic proteins. More recently, local synthesis of endogenous proteins was visualized in cultured hippocampal neurons using a non-canonical amino acid that can be fluorescently labeled (Dieterich et al., 2010). The non-canonical amino acid was locally perfused onto a distal dendritic region along with brain-derived neurotrophic factor (BDNF), a neurotrophin that stimulates neural activity and can induce LTP in the hippocampus, and a protein synthesis inhibitor was applied to the bath. BDNF application induced a local increase in fluorescence suggesting that new proteins were synthesized within the perfusion area; this was the first study to allow fluorescence visualization of newly synthesized endogenous proteins.

To address whether dendritic protein synthesis is necessary for long-term synaptic plasticity, Kang and Schuman severed the CA1 pyramidal cell dendrites from the somas in hippocampal slices and induced LTP using BDNF (Kang and Schuman, 1996). LTP could be generated even in severed dendrites, and this potentiation was blocked by incubation with protein synthesis inhibitors. Huber and colleagues used a similar method to demonstrate that metabotropic glutamate receptor-dependent long-term depression (mGlu-LTD) is dependent on dendritic protein synthesis (Huber et al., 2000). These studies were the first to convincingly show that local protein synthesis is required for at least some types of long-lasting synaptic plasticity.

1.3 mRNA localization to dendrites

Autoradiography studies showed that mRNA transcripts labeled with ^{3}H-uridine were actively transported to distal dendrites (Davis et al., 1987). Subsequently, a wealth of studies have examined which mRNA transcripts are localized to dendrites and whether mRNA transport mechanisms are transcript-specific. The mRNAs encoding microtubule-associated protein 2 (MAP2) and α calcium/calmodulin-dependent kinase II (αCaMKII) were detected in hippocampal dendrites *in vivo*, whereas mRNAs encoding β-tubulin and βCaMKII were restricted to the soma (Burgin et al., 1990; Garner et al., 1988). Similarly, in cultured hippocampal neurons, MAP2 mRNA was detected in dendrites, whereas those encoding β-tubulin and growth associated protein 43 (GAP43) were not (Kleiman et al., 1990). These studies suggested that there are mRNA-specific mechanisms regulating dendritic mRNA localization.

Over the next twenty years, many mRNAs were validated as dendritic transcripts

using in situ hybridization *in vitro* or *in vivo*; these include mRNAs encoding key

plasticity-related proteins such as glutamate receptor subunits, β-actin, protein kinase M

zeta (PKMζ), BDNF, and postsynaptic scaffolding proteins including postsynaptic

density protein 95 (PSD95) and Shank1 (Bassell et al., 1998; Falley et al., 2009;

Miyashiro et al., 1994; Muddashetty et al., 2007; Muslimov et al., 2004; Tongiorgi et al.,

1997). In addition, large-scale microarray studies have attempted to identify all localized

mRNAs in cultured hippocampal neurons or the CA1 stratum radiatum (Poon et al.,

2006; Zhong et al., 2006a). The most abundant, and consistently detected, mRNA

transcripts belong to families encoding receptors, cytoskeletal proteins, synaptic signaling

molecules, translational machinery, and cell adhesion molecules. Many of these

transcripts encode proteins important for synapse formation or plasticity suggesting that

local protein synthesis could indeed provide synapses with new proteins necessary for

activity-dependent modifications.

1.3.1 Activity-induced dendritic mRNA transport

     Synaptic activity regulates dendritic mRNA localization, which further suggests

that mRNA regulation at synapses is important for neuron function. Several laboratories

have shown that seizure induction in rodents increases the dendritic localization of

specific mRNAs such as Arc/Arg3.1 (activity-regulated cytoskeleton-associated

protein/activity-regulated gene 3.1), BDNF, αCaMKII, and Homer (Link et al., 1995;

Lyford et al., 1995; Simonato et al., 2002; Tiruchinapalli et al., 2008); seizures were used

in these studies as an *in vivo* means of increasing neural activity. Notably, the mRNA

encoding Arc/Arg3.1, an immediate early gene that is transcribed after neural activity,

was targeted specifically to activated synapses in the dentate gyrus when seizure induction was followed by electrical stimulation of a specific dendritic layer (Steward et al., 1998). Similarly, Tongiorgi et al. found that epileptogenic stimuli localized BDNF mRNA to specific synaptic fields in the CA3 region of the hippocampus (Tongiorgi et al., 2004). Both forms of synapse-specific mRNA localization were dependent on *N*-methyl-*D*-aspartate (NMDA) receptor signaling (Steward and Worley, 2001; Tongiorgi et al., 2004). These data suggest that mRNA localization, not just local protein synthesis, might mediate input specificity during synaptic plasticity.

LTP induction in anaesthetized rats increased dendritic localization of αCaMKII and MAP2 mRNA in the dentate gyrus and CA1 regions of the hippocampus suggesting that a more physiological form of neural activity also induces dendritic mRNA localization *in vivo* (Roberts et al., 1998). LTP induction in the hippocampus of awake, behaving rats increased αCaMKII and Arc/Arg3.1 mRNA levels in synaptic fractions isolated from the molecular layer of the dentate gyrus (Havik et al., 2003). Interestingly, total levels of Arc/Arg3.1 mRNA were increased and synaptic localization of Arc/Arg3.1 mRNA was dependent upon NMDA receptor activity; whereas, total αCaMKII mRNA levels were not changed following LTP, and αCaMKII mRNA synaptic localization was not dependent on NMDA receptor activation (Havik et al., 2003). These findings indicated that mRNA transport might be regulated in a transcript specific-manner.

In cultured neurons, detailed studies have enabled the discovery of several signaling pathways that regulate dendritic mRNA localization. For example, depolarization-induced increases in dendritic BDNF and tyrosine kinase B (TrkB) mRNAs are dependent upon L-type calcium channels and ionotropic glutamate receptor

activation (Tongiorgi et al., 1997), whereas depolarization-induced localization of GluR1 and Fmr1 (fragile X mental retardation 1) mRNAs is dependent upon mGlu receptor activation (Antar et al., 2004; Grooms et al., 2006). Neurotrophin signaling also regulates dendritic mRNA localization (Knowles and Kosik, 1997). Specifically, neurotrophin-3 increases dendritic localization of β-actin mRNA (Eom et al., 2003), and BDNF increases dendritic localization of BDNF and TrkB mRNAs (Tongiorgi et al., 1997). These studies indicate that dendritic mRNA transport is regulated in an activity-dependent and transcript-specific manner.

1.3.2 Cis-acting elements mediate mRNA-specific dendritic transport

The asymmetric localization of specific mRNA transcripts was first visualized in embryos (Jeffery et al., 1983) and soon after in cultured fibroblasts (Lawrence and Singer, 1986). Investigations in these systems established that *cis*-acting elements within mRNA transcripts mediate asymmetric mRNA localization, and in many cases these targeting elements were found in the 3' untranslated region (UTR) of the mRNA (reviewed in Kislauskis and Singer, 1992). Based on these studies and the discovery that not all mRNAs are localized to dendrites, it was hypothesized that specific mRNAs could harbor distinct elements necessary for dendritic targeting. Indeed, several studies identified *cis*-acting elements that mediated dendritic localization of specific transcripts.

The first dendritic targeting element was identified in the 3' UTR of MAP2 mRNA; it consisted of 640 nucleotides that were necessary and sufficient for dendritic localization in both hippocampal and sympathetic neurons (Blichenberg et al., 1999). The best studied 3' UTR is that of αCaMKII mRNA, in which several dendritic targeting

elements were identified. One study found a 30 nucleotide targeting element in the proximal region of the 3' UTR that could be silenced by more distal regions, and neural activity was shown to de-repress the proximal element allowing for dendritic localization of αCaMKII mRNA (Mori et al., 2000). Another group found an αCaMKII mRNA targeting element consisting of several hundred nucleotides, which mediated dendritic targeting in unstimulated cultured neurons (Blichenberg et al., 2001). In a seminal study, Miller et al. generated mice expressing αCaMKII mRNA lacking most of the 3' UTR. In these mice, αCaMKII mRNA was restricted to the soma and proximal dendrites, and αCaMKII protein was reduced by more than 80% at the postsynaptic density; total mRNA and protein levels were reduced by approximately 50% (Miller et al., 2002). These mice exhibited deficits in LTP, spatial memory, and fear conditioning suggesting that the 3' UTR of αCaMKII mRNA was necessary for proper hippocampal function. Notably, the proximal targeting element found by Mori et al. was present in the 3' UTR of the mutant mice, indicating that this element is not sufficient for dendritic targeting of αCaMKII *in vivo* (Miller et al., 2002; Mori et al., 2000). The discovery of several dendritic targeting elements in a single 3' UTR highlights the complexity inherent in the regulatory mechanisms underlying dendritic mRNA trafficking. Further work showed that 3' UTRs mediate the targeting of several established dendritic mRNAs including β-actin (Eom et al., 2003), Arc/Arg3.1 (Kobayashi et al., 2005), BDNF (An et al., 2008), Shank1 (Bockers et al., 2004), and PKMζ (Muslimov et al., 2004). Importantly, these studies on 3' UTR-mediated mRNA localization not only advanced the understanding of dendritic mRNA transport, but also provided scientists with a tool to investigate the *cis-* and *trans*-acting factors regulating dendritic mRNA transport and translation.

1.4 Specific mRNAs are translated within dendrites

 While the synaptic localization of mRNA and polyribosomes suggest that protein synthesis occurs in dendrites, these findings do not indicate whether synthesis of a specific protein can be detected in dendrites. To address this question, several laboratories investigated protein synthesis in biochemically isolated synaptic fractions and demonstrated that proteins such as αCaMKII were synthesized (Bagni et al., 2000; Muddashetty et al., 2007; Scheetz et al., 2000; Weiler et al., 1997). However, these studies are not conclusive as these biochemical fractions are enriched for synaptic compartments, but do contain somatic material as well. In hippocampal slices, electrical stimulation of specific dendritic laminae was shown to rapidly induce a protein synthesis-dependent increase in αCaMKII immunostaining within the activated region, which was more than 100 µm from the soma (Ouyang et al., 1997; Ouyang et al., 1999; Steward and Halpain, 1999). While strongly suggestive of local synthesis of αCaMKII protein, transport of newly synthesized proteins from the soma could not be ruled out. Following the discovery that the 3' UTR of αCaMKII was sufficient to mediate dendritic localization, Erin Schuman and colleagues devised a method to visualize translation of a fluorescent reporter within dendrites (Aakalu et al., 2001). A construct containing the coding region of GFP flanked by the 5' and 3' UTR sequences of αCaMKII mRNA was generated and expressed in cultured hippocampal neurons. While GFP fluorescence in the soma was photobleached, BDNF application induced a protein synthesis-dependent increase in dendritic GFP fluorescence. A subsequent study showed that NMDA and mGlu receptor activation induced local GFP synthesis (Gong et al., 2006). Dendritic GFP synthesis was dependent upon the 3' UTR of αCaMKII suggesting that this sequence is

necessary for local synthesis of αCaMKII (Aakalu et al., 2001; Gong et al., 2006).

Notably, the sites of BDNF-induced new GFP fluorescence were closely associated with

synaptic markers (Aakalu et al., 2001), suggesting that protein synthesis occurred locally

at synapses.

To investigate dendritic synthesis of actual synaptic proteins, not just a

fluorescent reporter protein, two separate laboratories used transected dendrites of

hippocampal neurons and studied α-amino-3-hydroxy-5-methyl-4-isoxazolepropionic

acid (AMPA) receptor subunit synthesis (Ju et al., 2004; Kacharmina et al., 2000). In one

approach, isolated dendrites were transfected with a plasmid expressing myc-tagged

GluA2 and, subsequently, treated with an mGlu$_{1/5}$ agonist, which increased dendritic

synthesis and membrane insertion of this exogenously expressed GluA2 protein

(Kacharmina et al., 2000). In an alternative approach, Ju et al. transfected hippocampal

neurons with tetracysteine-tagged GluA1 or GluA2, and then treated the cells with dyes

that fluoresce upon binding to the tetracysteine motif (Ju et al., 2004). GluA1 and GluA2

were indeed synthesized in isolated dendrites and trafficked to the plasma membrane

following mGlu$_{1/5}$ receptor activation. Although the machinery necessary for successful

synthesis and transport of a membrane protein had been previously visualized in

dendrites, these were the first studies to demonstrate that a membrane protein could be

translated within the dendrite and trafficked to its functional location.

The advent of these novel techniques for visualizing local protein synthesis

generated strong support for activity-induced dendritic synthesis of plasticity-related

proteins. Moreover, these methods uncovered that different synaptic signaling

mechanisms could induce the local synthesis of various proteins within dendrites. Given

that different forms of synaptic plasticity, such as LTP and LTD, require dendritic protein

synthesis, it is important to understand how specific mRNAs are regulated in response to

particular synaptic stimuli. While some receptor-mediated signaling pathways to the

translational machinery are beginning to be uncovered, it is still largely unclear how

specific mRNAs are regulated. Moreover, new dendritic mRNA transcripts are

continuously being discovered, thus there is a constant need for investigation of the

molecular mechanisms underlying local protein synthesis.

1.5 General translational control mechanisms

The molecular mechanisms controlling protein synthesis are critical for a vast

array of cell biological processes, including the precise regulation of protein levels in

both space and time. Protein synthesis can be regulated through mechanisms affecting

general translation factors and ribosome proteins, or through mRNA-specific mechanisms

mediated by *trans*-acting factors and *cis*-acting elements. Both general and mRNA-

specific regulation are important in spatial control of translation in neurons.

1.5.1 The translation process

Translation is divided into three stages: initiation, elongation and termination,

with translation initiation being the primary point of control (Jackson et al., 2010).

Translation initiation is regulated by a complex of factors that ultimately recruit 60S

ribosomes to the start codon. First, the 43S pre-initiation complex interacts with the 5'

cap structure of the mRNA. The 43S complex consists of a 40S ribosome subunit,

eukaryotic initiation factors (eIF) 3, 1, 1A and 5, and the ternary complex, which includes

eIF2, GTP, and a methionine-loaded tRNA. The interaction between the 43S complex and the 5' cap is mediated through a scaffold protein eIF4G; this protein creates a bridge between the 43S complex and the 5' cap by interacting with eIF3 and eIF4E, the protein that directly binds the 5' cap structure (Lamphear et al., 1995). The scaffolding protein eIF4G also interacts with poly(A) binding protein (PABP), which binds the poly(A) tail at the 3' end of the mRNA. It is this eIF4G-PABP interaction that circularizes the mRNA and permits translational regulation through factors that bind the 3' UTR (Wells et al., 1998). Once the 43S pre-initiation complex binds the mRNA, it scans the mRNA from 5' to 3' until it reaches the AUG initiation codon. The tRNA base pairs with the AUG codon and a stable complex is formed. Following GDP hydrolysis by eIF2, most initiation factors are released and the 60S ribosome subunit binds the mRNA forming the translation-competent 80S ribosome complex. Of note, some mRNA transcripts contain internal ribosome entry sites (IRES) where components of the 43S complex can bind and initiate translation independent of the 5' cap structure. These mRNA transcripts might be insensitive to some general mechanisms of translational control as not all eIFs are needed for IRES-mediated translation initiation (Jackson et al., 2010).

Translation elongation is orchestrated by repetitive actions of the 80S ribosome, eukaryotic elongations factors (eEFs), and aminoacyl-charged tRNAs. Together, these molecules decode the mRNA sequence to form a nascent polypeptide. The ternary complex containing eEF1A, aminoacyl-tRNA, and GTP enters the ribosome A- (aminoacyl-) site and binds the mRNA in a codon-dependent manner following GTP hydrolysis by eEF1A. Translocation of the ternary complex to the ribosome P- (peptidyl-) site is regulated by eEF2-mediated GTP hydrolysis. Both eEF1A and eEF2 are regulated

by post-translational modifications, which control translation elongation (Mathews et al.,
2007; Merrick and Nyborg, 2000). Translation termination is mediated through two
releasing factors (eRFs); eRF1 recognizes the stop codon and GTP hydrolysis by eRF3
releases the polypeptide chain from the 80S ribosome (Salas-Marco and Bedwell, 2004).
The mechanisms by which translation termination occurs are still being elucidated, and,
compared to translation initiation and elongation, little is known regarding regulation of
the termination process.

1.5.2 General mechanisms controlling translation initiation

The two most common general translational control mechanisms are regulation of
eIF2 phosphorylation and the association between eIF4E and eIF4G. eIF2 is part of the
tRNA ternary complex, which is only functional when eIF2 is bound to GTP. If eIF2 is
phosphorylated, then, after GTP hydrolysis and release of eIF2-GDP from the initiation
complex, eIF2 will tightly bind and sequester the guanine exchange factor eIF2B
preventing the exchange of GDP for GTP (Rowlands et al., 1988). Thus, eIF2
phosphorylation decreases translation by reducing the levels of functional ternary
complexes. The interaction between eIF4E, the cap-binding protein, and eIF4G is critical
for cap-dependent translation initiation as it forms part of the bridge connecting the 43S
pre-initiation complex to the mRNA. A family of proteins termed eIF4E inhibitory
proteins regulate this interaction by binding eIF4E and preventing its binding to eIF4G
(Gingras et al., 1998; Pause et al., 1994; Richter and Sonenberg, 2005). The mammalian
target of rapamycin (mTOR) signaling pathway regulates a subset of eIF4E inhibitory
proteins, called eIF4E binding proteins (4E-BPs). mTOR-mediated phosphorylation of

4E-BPs disrupts their interaction with eIF4E, which allows eIF4E to bind eIF4G and facilitates translation initiation (Hay and Sonenberg, 2004).

While these general mechanisms can affect all mRNA transcripts, their activation can be spatially restricted through localized signaling, and, as such, these mechanisms can regulate local protein synthesis. In this regard, eIF2, eIF4E, eIF4G, 4E-BPs, and components of the mTOR signaling pathway are localized to synapses and regulated by synaptic activity (Asaki et al., 2003; Carroll et al., 2006; Kanhema et al., 2006; Menon et al., 2004; Moon et al., 2009; Smart et al., 2003; Takei et al., 2009; Tang et al., 2002). Long-term synaptic plasticity, learning, and memory are regulated by eIF2 phosphorylation as well as mTOR signaling (Antion et al., 2008a; Antion et al., 2008b; Banko et al., 2005; Costa-Mattioli et al., 2007; Hoeffer et al., 2008; Slipczuk et al., 2009; Tang et al., 2002). Moreover, mTOR signaling can be locally activated in dendrites and regulates dendritic synthesis of an αCaMKII 3' UTR reporter protein (Gong et al., 2006; Takei et al., 2004). Together, these findings suggest that synaptic signaling to the general translational machinery regulates local protein synthesis and is critical for synapse function.

1.6 mRNA-specific mechanisms of translational control

Specific subsets of mRNA can be controlled through regulation of *trans*-acting factors that associate with specific mRNA sequences or structures. These regulatory mechanisms are activated through specific extracellular signals, at distinct developmental stages, or within particular subcellular compartments and, thus, are important in the precise temporal and spatial regulation of translation (Jackson et al., 2010). Here, the

focus will be on regulatory mechanisms mediated by specific *trans*-acting factors that

interact with 3' UTR *cis*-acting elements including RNA binding proteins, mRNA-

specific eIF4E inhibitory proteins, and regulators of cytoplasmic polyadenylation. It is

important to note that specific elements within the 5' UTR are also key regulators of

translation; these include IRESs, complex secondary structure, and upstream open

reading frames (Hellen and Sarnow, 2001; Morris and Geballe, 2000; Pickering and

Willis, 2005).

1.6.1 RNA binding proteins and ribosome recruitment

RNA binding proteins can regulate translation through interacting with specific

elements that are most often located in the 3' UTR of mRNA transcripts (Abaza and

Gebauer, 2008). Many RNA binding proteins have conserved functions across species

and cell types indicating their importance. In addition, several RNA binding proteins

have critical roles in the spatial and temporal regulation of mRNA-specific translation

(Burd and Dreyfuss, 1994). Two mechanisms by which RNA binding proteins regulate

translation are through blocking translation initiation complex formation or preventing

60S ribosomal subunit recruitment to the initiation complex (Jackson et al., 2010).

Though not discussed in detail here, RNA binding proteins can also regulate translation

through micro-RNAs and the RNA-induced silencing complex as well as interactions

with eEF2 and eEF1A (Chen and Huang, 2011; Hussey et al., 2011; Jin et al., 2004;

Muddashetty et al., 2011).

One mRNA-specific mechanism for inhibiting 43S initiation complex formation

is through mRNA-specific eIF4E inhibitory proteins. These proteins can either provide a

direct link between the 3' UTR and the 5' cap structure or create a bridge by interacting with an RNA binding protein (Abaza and Gebauer, 2008). The first mRNA-specific eIF4E inhibitory protein identified was maskin, which is a critical regulator of maternal mRNA translation in *Xenopus* oocytes (Cao and Richter, 2002; Groisman et al., 2000). Maskin interacts with eIF4E and the RNA binding protein cytoplasmic polyadenylation element binding protein (CPEB) to repress translation initiation (Stebbins-Boaz et al., 1999). CPEB provides mRNA specificity in this translational control mechanism as it binds *cis*-acting cytoplasmic polyadenylation element (CPE) sequences present in the 3' UTR of a subset of mRNAs (Paris et al., 1991). In neurons, the RNA binding protein FMRP (fragile X mental retardation protein) has been shown to interact with the eIF4E binding protein called Cytoplasmic FMRP Interacting Protein (CYFIP, also known as Sra-1), and this interaction mediates translational repression of FMRP target mRNAs (Napoli et al., 2008). Finally, Pumilio2 is an mRNA binding protein that binds a specific 3' UTR sequence present in some mRNAs, and it inhibits translation initiation by interacting directly with the 5' cap and preventing eIF4E binding (Cao et al., 2010; Wharton et al., 1998). Interestingly, CPEB, FMRP, CYFIP, and Pumilio2 are all expressed in neurons and have critical functions in regulating dendrite morphology and long-term synaptic plasticity (Bassell and Warren, 2008; Fiore et al., 2009; Menon et al., 2004; Richter, 2007; Schenck et al., 2003; Schenck et al., 2004; Vessey et al., 2010; Vessey et al., 2006; Ye et al., 2004).

RNA binding proteins can also regulate the formation of the 80S ribosome complex. Heterogeneous nuclear ribonucleoproteins (hnRNPs) K and E1 are two RNA binding proteins that interact with CU-rich regions in the 3' UTR of specific mRNAs and

inhibit joining of the 60S ribosomal subunit with the initiation complex in reticulocytes (Ostareck et al., 2001). Zipcode binding protein (ZBP1) binds a specific 54 nucleotide sequence in the 3' UTR of β-actin mRNA and was shown to repress β-actin translation through blocking 80S ribosome formation in reticulocyte lysates (Huttelmaier et al., 2005). Interestingly, Src kinase phosphorylates hnRNPs K and E1 as well as ZBP1 and, in each case, leads to translation activation by disrupting the interaction between the RNA binding protein and its target mRNA (Huttelmaier et al., 2005; Ostareck-Lederer et al., 2002). Phosphorylation of RNA binding proteins is a common mechanism regulating stimulus-induced protein synthesis and is a mechanism integral to the work presented here. The reversible regulation provided by phosphorylation of synaptic RNA binding proteins is a mechanism apt for mediating input-specific activation of translation.

1.6.2 Cytoplasmic polyadenylation

Most mRNA transcripts acquire a long stretch of adenine residues at the 3' end prior to nuclear export. In the cytoplasm, the poly(A) tail regulates mRNA stability as well as translation through the recruitment of PABP (Millevoi and Vagner, 2010). As stated above, PABP interacts with eIF4G to circularize the mRNA and facilitate translation by tethering the initiation factors to the mRNA. Therefore, a longer poly(A) tail, which recruits more PABP molecules, facilitates translation initiation, whereas a short poly(A) tail represses translation (Wells et al., 1998). The poly(A) tail of a subset of mRNAs is regulated in the cytoplasm, and this process is mediated by 3' UTR CPE sequences and the associated RNA binding protein CPEB.

Cytoplasmic polyadenylation occurs in many cell types, but the regulatory

mechanisms have only been delineated in *Xenopus* oocytes (Figure 1.2). In these cells,

CPEB associates not only with CPE-containing mRNAs and the eIF4E inhibitory protein

maskin, as mentioned above, but also several other translational regulators including: (1)

cleavage and polyadenylation specificity factor (CPSF), which binds the polyadenylation

hexanucleotide AAUAAA, (2) Gld2, a poly(A) polymerase, (3) PARN, a deadenylating

enzyme, and (4) symplekin, a scaffold protein upon which the ribonucleoprotein (RNP)

complex is assembled (Richter, 2007). CPE-containing mRNAs undergo poly(A) tail

shortening in the cytoplasm, a process mediated by the offsetting activities of Gld2 and

PARN (Barnard et al., 2004; Kim and Richter, 2006). That is, these two CPEB-anchored

enzymes are constitutively active, but because PARN is the more active, the tails remain

short even though Gld2 is continuously catalyzing poly(A) addition. Upon progesterone

stimulation, the kinase Aurora A phosphorylates CPEB leading to expulsion of PARN

from the RNP complex and default polyadenylation. The newly elongated poly(A) tail

recruits PABP, which binds eIF4G and helps it displace maskin from eIF4E, thereby

recruiting the 40S ribosomal subunit to the 5' end of the mRNA (Cao et al., 2006; Kim

and Richter, 2006; Stebbins-Boaz et al., 1999). Precise temporal regulation of maternal

mRNA translation is vital for development, and CPEB-mediated translation repression

and subsequent stimulus-induced translation activation is a key molecular mechanism

underlying this developmental process.

1.7 Bidirectional control of dendritic mRNA translation by mRNA binding proteins

Dendritic protein synthesis has two distinct phases: translational repression during

transport and translational activation at synapses. The dendritic targeting elements

identified for several mRNA transcripts showed no obvious sequence similarities.

Subsequently, investigations regarding dendritic mRNA transport and translation focused

on *trans*-acting RNA binding proteins and their cognate *cis*-acting sequences. As

discussed above, RNA binding proteins can: 1) bind mRNAs at specific *cis*-acting

elements, 2) regulate spatial and temporal mRNA translation, and 3) reversibly repress

and activate translation through stimulus-induced post-translational modifications.

Therefore, the reversible translational control mediated by RNA binding proteins is well-

suited for regulating dendritic protein synthesis (Figure 1.3).

1.7.1 RNA binding proteins mediate dendritic mRNA transport

mRNAs are transcribed, processed, and assembled into ribonucleoprotein

particles (RNPs) in the nucleus and then exported to the cytoplasm (Farina and Singer,

2002). RNPs are large, heterogeneous granules (~1000S) that can contain multiple

mRNA transcripts and several *trans*-acting factors, including RNA binding proteins

(Kanai et al., 2004). At least some RNA binding proteins assembled into RNPs in the

nucleus remain associated with RNPs during trafficking to distal locations and are

required for RNP transport (Kress et al., 2004; Oleynikov and Singer, 2003); however, it

is likely that transport RNPs also recruit additional factors after export to the cytoplasm

(Sossin and DesGroseillers, 2006).

In neurons, RNPs are actively transported on microtubules; this has been

demonstrated in living neurons by labeling endogenous mRNAs as well as expressing

exogenous 3' UTR targeting elements that associate with fluorescent proteins (Knowles et

al., 1996; Rook et al., 2000). Several lines of evidence support a role for RNA binding

proteins in microtubule-based mRNA transport. Neuronal RNPs were isolated from brain

tissue by immunoprecipitation of the kinesin protein KIF5, a microtubule motor (Kanai et

al., 2004). The isolated RNPs contained mRNA transcripts as well as RNA binding

proteins, such as Staufen1 and 2, FMRP, and ZBP1. Staufen proteins have a key role in

RNP transport in many cell types, including neurons; however, the mechanism by which

Staufen regulates mRNA transport remains unclear (Miki et al., 2005). A recent report

illustrates that different mRNA transcripts are trafficked in distinct RNPs, and that

Staufen 2 regulates the inclusion of MAP2 mRNA in dendritic transport RNPs, but not β-

actin or αCaMKII mRNAs (Mikl et al., 2011). Thus, it is likely that mRNA-specific

binding proteins control targeting of mRNAs into particular RNPs. In this regard, FMRP,

which binds a subset of dendritic mRNAs, has been shown to interact with KIF5, and

mutating the KIF5-binding domain within FMRP restricts its dendritic localization as

well as that of at least one FMRP target mRNA (Dictenberg et al., 2008). Similar to the

effect on dendritic mRNAs, neurotrophin application, depolarization, and glutamate

receptor activation induce transport of RNA binding proteins to dendrites (Doyle and

Kiebler, 2011). Furthermore, altering the expression of dendritic RNA binding proteins or

mutating their cognate *cis*-acting elements can restrict the basal and activity-induced

dendritic transport of their target mRNAs (Kiebler and Bassell, 2006).

1.7.2 Translational repression and synaptic activation of local protein synthesis

The precise activation of translation beneath distinct synaptic sites is critical for

the proposed model of local protein synthesis. Importantly, RNP transport granules are

considered to be translationally silenced because they contain components of RNA

processing bodies, which are sites of translational repression, and do not incorporate radio-labeled amino acids (Eulalio et al., 2007; Krichevsky and Kosik, 2001). In neurons, both depolarization and BDNF application induce several mRNAs to shift from the cellular fractions containing markers of transport RNPs to the fractions containing polyribosomes (Krichevsky and Kosik, 2001; Shiina et al., 2005). While these studies indicate that synaptic activity can redistribute mRNAs from a repressed state to a translation-ready state, no detailed molecular mechanisms describing dendritic transport and bidirectional control of translation have been described for a specific mRNA.

The mechanism regulating β-actin mRNA transport and local translation is likely the best studied for any localized mRNA. If one synthesizes findings from several cellular systems, a detailed mechanism for ZBP1-mediated transport, translational repression, and local translation of β-actin mRNA can be constructed. β-actin mRNA localization to neurites is dependent upon ZBP1 and the 54 nucleotide zipcode sequence in the 3' UTR of β-actin mRNA to which ZBP1 binds (Bassell et al., 1998; Eom et al., 2003; Ross et al., 1997; Zhang et al., 2001). In neuroblastoma cells, ZBP1 co-localizes with β-actin mRNA within the nucleus and at distal cytoplasmic sites (Huttelmaier et al., 2005). In reticulocyte lysates, ZBP1 was shown to repress the translation of reporter mRNAs in a zipcode-dependent manner, and a non-phosphorylatable mutant form of ZBP1 could not be de-repressed to activate translation of β-actin mRNA (Huttelmaier et al., 2005). In axonal growth cones, BDNF application induces local β-actin synthesis that is dependent upon Src-mediated phosphorylation of ZBP1 (Sasaki et al., 2010). While much of this mechanism has been delineated using *in vitro* assays, neuronal cell lines, and over-expressed constructs, the nexus of observations provides a clear example of

how mRNA transport, translational silencing, and local translational activation can be linked. What remains to be fully tested is whether an RNA binding protein-mediated mechanism can control mRNA transport, translation repression, and local translation in dendrites.

1.8 Cytoplasmic polyadenylation element binding protein

CPEB-mediated translational repression and, subsequent, stimulus-induced translational activation allows for the timely synthesis of proteins necessary for oocyte maturation. Similarly, precise translational control is required for stimulus-induced translation at synapses. Therefore, it is intriguing to consider that a similar bidirectional mechanism could provide temporal and spatial control of activity-induced synaptic protein synthesis. Indeed, CPEB is localized to synapses and has been shown to regulate dendritic mRNA transport, local protein synthesis, and long-term synaptic plasticity (Richter, 2007). However, the mechanism through which CPEB regulates dendritic mRNA translation and synaptic plasticity is unknown, and this will be the focus of the thesis work presented herein.

1.8.1 The CPEB family of RNA binding proteins

CPEB belongs to a family of RNA binding proteins that is characterized by two RNA recognition motifs and a C-terminal zinc finger domain, all of which contribute to their RNA binding activities (Hake et al., 1998; Huang et al., 2006; Kurihara et al., 2003; Theis et al., 2003). The CPEB family of proteins is separated into two subgroups: CPEB1 and CPEB2 proteins. The CPEB1 proteins interact with CPE sequences, which have

consensus sequence UUUUUAU (Paris et al., 1991); whereas, the CPEB2 proteins have been shown to bind to a U-rich loop structure within select mRNAs (Huang et al., 2006; Wang and Cooper, 2010). Vertebrates have one CPEB1 protein isoform, which is called CPEB, and three CPEB2 proteins called CPEB2, CPEB3, and CPEB4 (Kurihara et al., 2003; Theis et al., 2003). All four CPEB proteins are expressed in the mammalian brain (Theis et al., 2003; Wu et al., 1998). Invertebrates have two CPEB isoforms. In *Aplysia*, the two isoforms are called ApCPEB77 and ApCPEB49, but ApCPEB77 is the predominant neuronal isoform and is referred to as ApCPEB in the literature and herein (Liu and Schwartz, 2003; Si et al., 2003a; Si et al., 2003b). Both *Aplysia* isoforms are part of the CPEB1 sub-family of proteins. *In Drosophila,* the CPEB proteins are called Orb and Orb2; Orb is a CPEB1 protein and is only expressed in germ cells, whereas Orb2 is a CPEB2 protein and is expressed in many tissues, including the nervous system (Keleman et al., 2007; Lantz et al., 1992). CPEB2 proteins have been implicated in learning and memory in *Drosophila,* mice, and humans (Keleman et al., 2007; Pavlopoulos et al., 2011; Vogler et al., 2009); however, they will not be discussed in further detail here as they do not mediate CPE-dependent polyadenylation, which is the focus of this work.

1.8.2 The role of CPEB in synaptic plasticity, learning, and memory

CPEB has been shown to regulate synaptic plasticity, learning, and memory in several studies. The CPEB knockout mice show altered memory extinction as well as reduced theta burst- and growth hormone-induced LTP in the hippocampus (Alarcon et al., 2004; Berger-Sweeney et al., 2006; Zearfoss et al., 2008). In Purkinje neurons of the cerebellum, expression of a non-phosphorylatable mutant form of CPEB reduced LTD,

increased the number and length of dendritic spines, and slowed motor learning (McEvoy et al., 2007). In the *Xenopus* retinotectal system, CPEB regulates dendritic growth, synapse strength, and synaptic responses to visual stimuli (Bestman and Cline, 2008). In *Aplysia*, ApCPEB regulates serotonin-induced long-term synaptic facilitation and synapse expansion (Liu et al., 2006; Miniaci et al., 2008; Si et al., 2003a). In sum, these findings strongly support an evolutionarily conserved function for CPEB in regulating neuronal morphology and synapse function.

1.8.3 Synaptic activity regulates CPEB phosphorylation

A necessary component of mechanisms underlying synaptic protein synthesis is reversible regulation by synaptic activation. In hippocampal slices, CPEB phosphorylation is increased following LTP induction and decreased during LTD (Atkins et al., 2005). One study suggested that Aurora A kinase phosphorylates CPEB (Huang et al., 2002); whereas, another study found that CaMKII mediates CPEB phosphorylation, and that Aurora A kinase does not phosphorylate CPEB in an *in vitro* assay (Atkins et al., 2004). While the kinase involved in neuronal CPEB phosphorylation remains unclear, both studies showed that activity-induced CPEB phosphorylation is dependent on NMDA receptor activation in hippocampal neurons (Atkins et al., 2004; Huang et al., 2002). Furthermore, Atkins et al. showed that protein phosphatase 1 activity keeps CPEB phosphorylation low in hippocampal neurons (Atkins et al., 2004). Together, these data illustrate that opposing kinase and phosphatase activities function to reversibly regulate CPEB phosphorylation in neurons. However, in all of these studies, CPEB phosphorylation was assayed in biochemical fractions or whole cell lysates; thus, it

remains unclear whether CPEB phosphorylation is regulated within the dendritic

compartment of intact neurons.

1.8.4 CPEB-mediated regulation of mRNA transport and translation

     The CPE sequence is sufficient for targeting mRNA to dendrites, and the 3' UTR

of several established dendritic mRNAs, including MAP2, αCaMKII, and BDNF, contain

CPE sequences that regulate their dendritic localization (Huang et al., 2003; Oe and

Yoneda, 2010; Wells et al., 2001; Wu et al., 1998). CPEB interacts with kinesin and

dynein, and exhibits bidirectional, microtubule-dependent movement in dendrites of

cultured hippocampal neurons (Huang et al., 2003). Furthermore, mutating the kinesin-

binding domain of CPEB restricts the dendritic localization of endogenous MAP2 mRNA

(Huang et al., 2003). In *Aplysia*, CPEB is required for localization of syntaxin mRNA

during long-term facilitation (Liu et al., 2006). Collectively, these studies indicate that

CPEB and the CPE sequence can regulate dendritic mRNA transport. In addition, CPEB

shuttles between the cytoplasm and nucleus, and it interacts with known target mRNAs

within the nucleus (Ernoult-Lange et al., 2009; Rouget et al., 2006). In oocytes, the CPE

sequence represses translation and does so with greater efficacy for RNA injected into the

nucleus as compared to RNA injected into the cytoplasm (Lin et al., 2010). Altogether,

these findings support a model whereby CPEB binds CPE-containing mRNAs in the

nucleus, represses translation, and controls mRNA localization.

     The CPE sequence is implicated in neuronal mRNA polyadenylation and

translation as well. Endogenous αCaMKII mRNA undergoes NMDA receptor-mediated

polyadenylation and translation *in vivo* and in synaptic fractions isolated from

hippocampal tissue (Huang et al., 2002; Wu et al., 1998). The CPE sequences within the

αCaMKII 3' UTR are required for stimulus-induced polyadenylation when the mRNA is

injected into oocytes (Wu et al., 1998). In cultured hippocampal neurons, these αCaMKII

CPE sequences are necessary for glutamate-induced synthesis of a GFP reporter protein

(Wells et al., 2001). In *Aplysia,* the CPE-containing N-actin mRNA is polyadenylated

following serotonin stimulation, and the CPE sequences are necessary for

polyadenylation of this mRNA when injected into oocytes (Liu and Schwartz, 2003; Si et

al., 2003a). In Purkinje neurons, expression of a non-phosphorylatable mutant form of

CPEB reduced activity-induced expression of IRSp53 (insulin receptor tyrosine kinase

substrate p53), a synaptic protein encoded by a CPE-containing mRNA (McEvoy et al.,

2007). This study suggests that CPEB phosphorylation regulates synthesis of IRSp53, but

the roles of mRNA polyadenylation and protein synthesis in activity-induced IRSp53

protein expression were not addressed.

       Collectively, this evidence is suggestive of a role for CPEB in neuronal mRNA

polyadenylation, but there is no evidence directly linking CPEB to activity-induced

polyadenylation in neurons. Furthermore, synaptic mRNA polyadenylation has only been

studied in biochemical fractions that, while enriched for synaptic compartments, often

contain somatic material. Therefore, it is yet unclear whether mRNA polyadenylation

occurs in intact dendrites. In addition, work in the oocyte system has shown that CPEB

can only regulate mRNA polyadenylation and translation in conjunction with other

translation factors, and CPEB-associated translational regulators in the brain have not

been studied. The identification of such factors and investigating their roles in local

mRNA translation as well as synapse structure and function are objectives of this thesis.

1.8.5 Putative CPEB-associated translational regulators in the brain

The factors involved in CPEB-mediated translational regulation in oocytes are the poly(A) polymerase Gld2, deadenylase PARN, scaffolding protein symplekin, and eIF4E inhibitory protein maskin. The poly(A) polymerase Gld2 is expressed in the mammalian brain and was recently shown to regulate long-term memory in *Drosophila* (Kwak et al., 2008; Rouhana et al., 2005), suggesting that this translation regulator could play a role in neuronal mRNA polyadenylation and synaptic plasticity. There is no mammalian homolog of maskin, but another eIF4E inhibitory protein called neuroguidin (Ngd) was recently identified in the brain (Jung et al., 2006). In oocytes, exogenously expressed Ngd interacts with CPEB and inhibits translation of CPE-containing mRNAs. However, it is unclear whether Ngd interacts with CPEB or regulates mRNA translation in the brain. To date, there have been no studies investigating the expression or function of either PARN or symplekin in neurons. The goal of this thesis is to determine whether these molecules interact with CPEB in neurons and regulate dendritic mRNA polyadenylation, local protein synthesis, and synapse structure and function.

1.9 Thesis hypothesis and objectives

Regulating dendritic protein synthesis requires a mechanism that links mRNA transport, translational repression, and local activation of protein synthesis. The established roles for CPEB in synaptic plasticity and translational regulation in oocytes suggest that this RNA binding protein could mediate a bidirectional control mechanism underlying synaptic protein synthesis. Thus, we hypothesize that CPEB regulates synapse structure and function by interacting with an activity-regulated polyadenylation complex

that controls dendritic protein synthesis. In this thesis, we address this hypothesis through four specific aims. First, we examine whether CPEB is part of a complex of translation factors that is regulated by synaptic activity in dendrites. Second, we examine whether CPEB and associated factors regulate dendritic mRNA polyadenylation. Third, we determine whether these translation factors regulate dendritic spine morphology and synapse strength. Finally, we determine whether CPEB and associated factors control dendritic translation of a CPE-containing mRNA.

The thesis work presented here establishes that a CPEB-associated translation complex controls dendritic mRNA polyadenylation and dendritic spine morphology as well as the dendritic transport of GluN2A mRNA and activity-induced GluN2A synthesis and membrane insertion. This collection of findings reveals that CPEB associates with several factors to mediate bidirectional control of dendritic mRNA polyadenylation and activity-induced local protein synthesis in neurons. Moreover, this work identifies a new mechanism regulating activity-induced NMDA receptor expression, and thus, advances our understanding of the molecular mechanisms underlying plasticity at glutamatergic synapses.

Figure 1.1 Theoretical models for the input-specific delivery of synaptic proteins.

(A) "Synaptic tagging and capture" model: (1) synaptic activation forms a "tag" at particular synapses and induces a synapse-to-soma signal that (2) leads to new protein synthesis and dendritic transport of synaptic proteins. (3) The newly synthesized proteins are "captured" at only the activated synapses. (B) Local protein synthesis model: (1) mRNA transcripts are trafficked to dendrites, and (2) synaptic activation activates translation beneath particular synapses, and thus, (3) newly synthesized proteins are delivered specifically to activated synapses.

Figure 1.1

A. "Synaptic tagging and capture" model
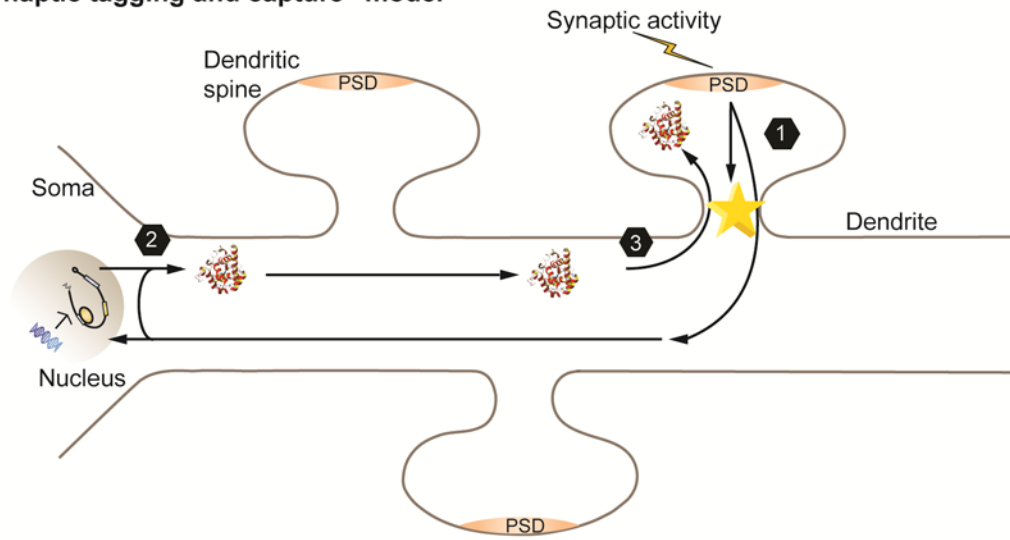
B. Local protein synthesis model
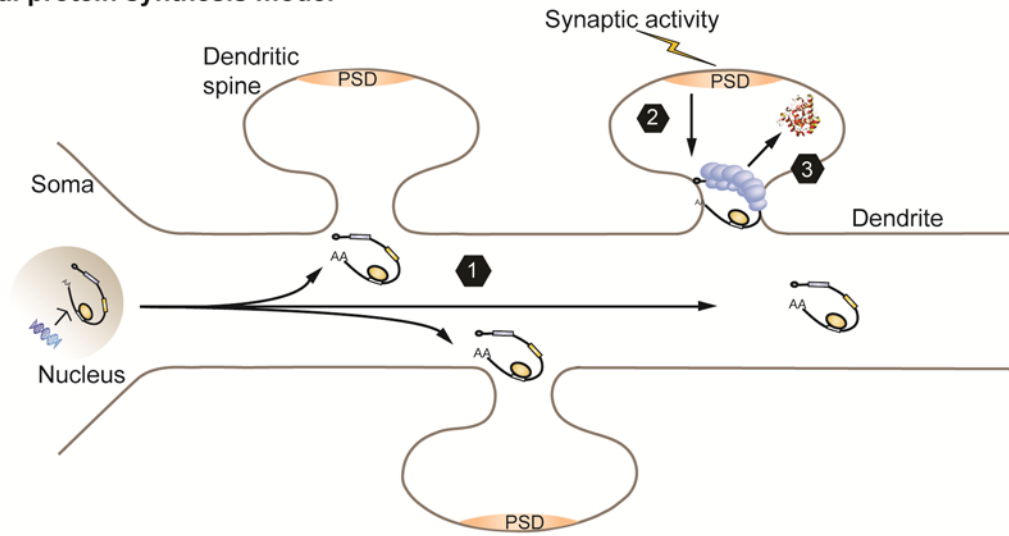
Figure 1.2
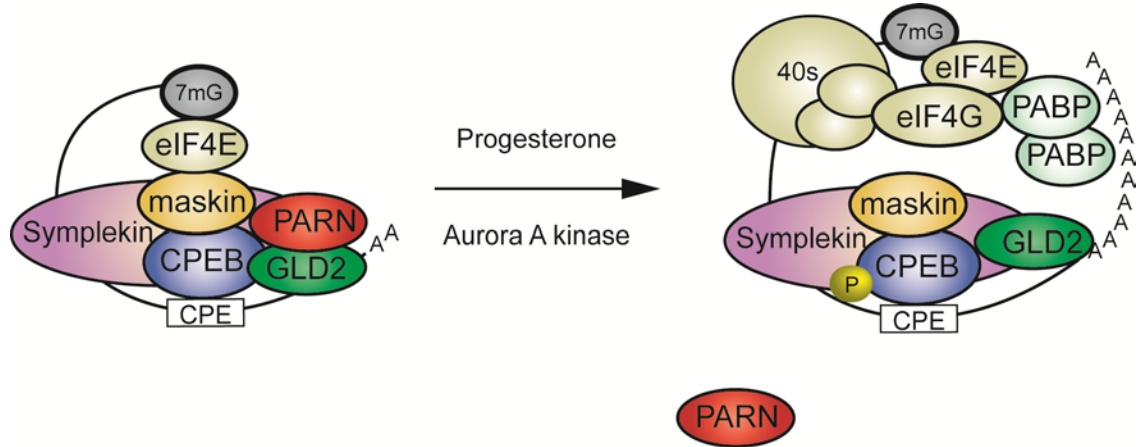
Figure 1.2 Model of cytoplasmic polyadenylation in *Xenopus* oocytes. CPE-containing

mRNAs are bound by CPEB, which in turn binds a complex of translation factors

including the poly(A) polymerase Gld2, deadenylase PARN, eIF4E inhibitory protein

maskin, and scaffolding protein symplekin. Progesterone activates Aurora A kinase-

mediated phosphorylation of CPEB. CPEB phosphorylation facilitates translation

initiation by recruiting the 40S ribosome subunit to bind eIF4E, and it does so through

two mechanisms: 1) disrupting the interaction between PARN and CPEB, which leads to

Gld2-mediated poly(A) tail elongation and subsequent PABP recruitment, and 2)

disrupting the interaction between maskin and eIF4E, which allows eIF4G to bind eIF4E

(Kim and Richter, 2006; Stebbins-Boaz et al., 1999).

Figure 1.3 Model of RNA binding protein-mediated dendritic mRNA transport, translational repression, and local activation of protein synthesis. (1) The RNA binding protein and target mRNA are assembled into a RNP within the nucleus and exported to the cytoplasm. (2) The RNA binding protein represses mRNA translation and interacts with an anterograde microtubule motor that mediates dendritic localization of the RNP. (3) Once localized to a synapse, synaptic signaling activates local translation, possibly through a reversible post-translational modification of the RNA binding protein. (4) Local activation of translation leads to the synthesis of new proteins at specific synapses. (5) The RNA binding protein interacts with a retrograde microtubule motor to return to the soma, where it is shuttled into the nucleus to, perhaps, retrieve another mRNA molecule (adapted from Bassell and Warren, 2008).

Figure 1.3
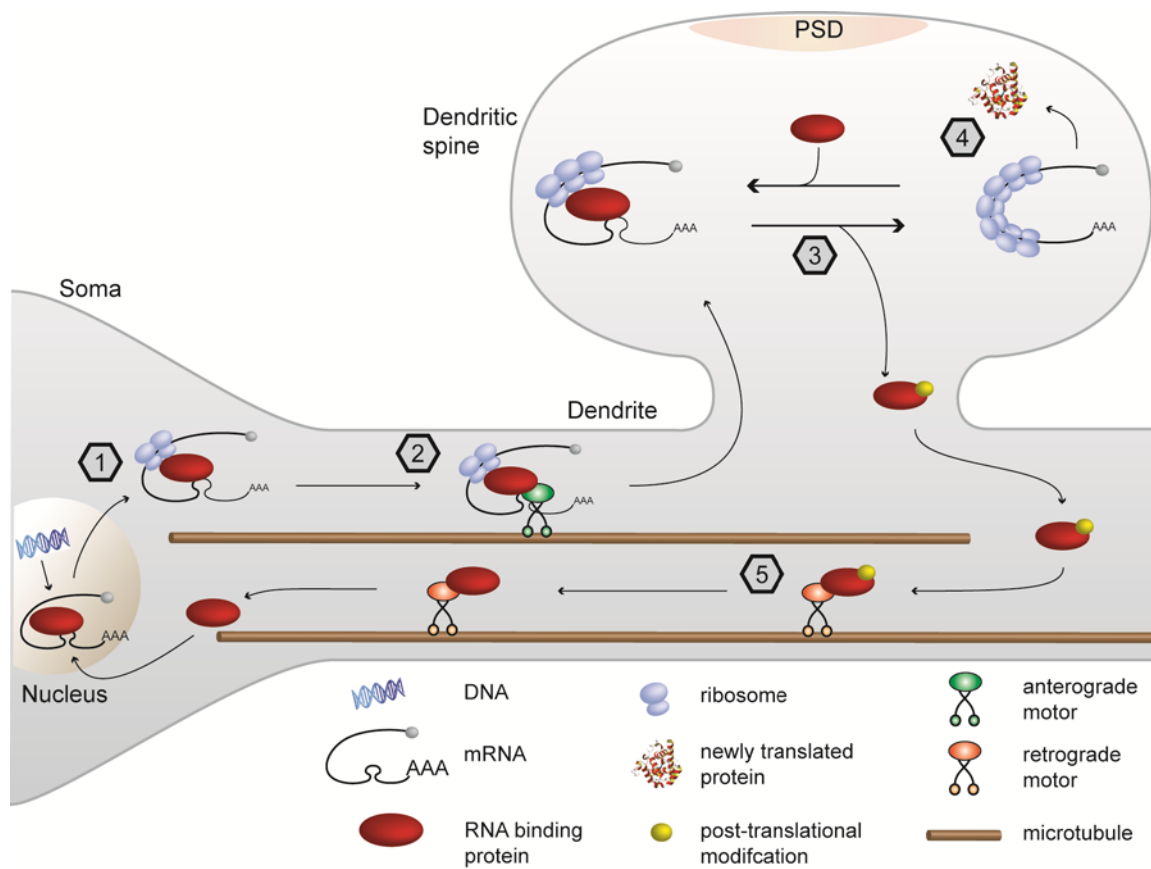
CHAPTER TWO:

The CPEB-associated polyadenylation complex is regulated by activity and controls

dendritic mRNA polyadenylation

Parts of this chapter are adapted from:

Swanger, S.A., Bassell, G.J. Gross, C., High-resolution fluorescence in situ hybridization to detect mRNAs in neuronal compartments *in vitro* and *in vivo*. *Method Mol Biol.* 2011;714:103-123.

Udagawa, T.*, Swanger, S.A.*, Takeuchi, K., Kim, J.H., Nalavadi, V., Shin, J., Lorenz, L.J., Zukin, R. S., Bassell, G.J., and Richter, J.D. Bidirectional control of mRNA translation and synaptic plasticity by the cytoplasmic polyadenylation complex. *Mol Cell.* In press. (* equal contribution)

2.1 Introduction

In the mammalian nervous system, experience-induced modifications of synaptic connections (synaptic plasticity) are thought to underlie learning and memory (Kandel, 2001). These modifications require activity-dependent protein synthesis, which likely involves specific mRNA translation at or near synapses (Sutton and Schuman, 2006). In the hippocampus, two forms of synaptic plasticity, late-phase LTP and mGlu-LTD, require dendritic protein synthesis (Huber et al., 2000; Kang and Schuman, 1996). LTP enhances synaptic efficacy while LTD reduces it; thus, it seems axiomatic that each form of plasticity would depend upon the translation of some unique sets of mRNAs that respond to different synaptic signaling events (Costa-Mattioli et al., 2009; Richter and Klann, 2009; Wang et al., 2009; Zukin et al., 2009). Indeed, dendrites harbor many different mRNAs (Eberwine et al., 2002; Poon et al., 2006), ribosomes (Steward and Levy, 1982), mRNA binding proteins (Bassell and Kelic, 2004), micro-RNAs (Schratt, 2009), and RISC (Banerjee et al., 2009), supporting the idea of stimulus- and mRNA-specific control of synaptic protein synthesis.

One protein involved in neuronal mRNA translation is the RNA binding protein CPEB (Wu et al., 1998), which binds CPE sequences in 3' UTRs and modulates poly(A) tail length. In *Xenopus* oocytes, a number of CPEB-associated factors have been identified including: (1) cleavage and polyadenylation specificity factor (CPSF), which binds the hexanucleotide AAUAAA, (2) Gld2, a poly(A) polymerase, (3) PARN, a deadenylase, (4) maskin, which interacts with the cap-binding factor eIF4E, and (5) symplekin, a scaffold protein upon which the ribonucleoprotein (RNP) complex is assembled (Richter, 2007). When tethered to mRNAs by CPEB, PARN activity is

dominant to that of Gld2, leading to poly(A) tail shortening of CPE-containing mRNAs (Barnard et al., 2004; Kim and Richter, 2006). Upon stimulation of oocytes to re-enter meiosis, the kinase Aurora A phosphorylates CPEB, leading to expulsion of PARN from the RNP complex and default polyadenylation by Gld2. The poly(A) tail then serves as a platform for PABP, which binds eIF4G and helps it displace maskin from eIF4E, thereby recruiting the 40S ribosomal subunit to the mRNA (Kim and Richter, 2006; Richter, 2007; Stebbins-Boaz et al., 1999).

In the brain, CPEB regulates synaptic plasticity and certain hippocampal-dependent memories (Alarcon et al., 2004; Berger-Sweeney et al., 2006; McEvoy et al., 2007; Zearfoss et al., 2008). NMDA receptor activation promotes Aurora A- and/or calcium/calmodulin-dependent protein kinase II (CaMKII)-dependent CPEB phosphorylation (Atkins et al., 2004; Huang et al., 2002), triggering mRNA-specific polyadenylation and translation (Du and Richter 2005; Huang et al. 2002; McEvoy et al. 2007; Wu et al. 1998). Although CPEB stimulates polyadenylation in neurons, the mechanism by which it does so is unknown. Moreover, whether polyadenylation occurs in dendrites to control the local mRNA translation necessary for synaptic plasticity is also unknown. Indeed, CPEB can repress translation without influencing polyadenylation (Groisman et al., 2006), and it also modulates alternative splicing (Lin et al., 2010), indicating that cytoplasmic 3' end processing does not necessarily affect plasticity. Finally, maskin is not detected in mammals, thus implicating other factors involved in CPEB-mediated translation. In this regard, mammalian neurons contain neuroguidin (Ngd), a CPEB and eIF4E-binding protein that may function in a manner analogous to maskin (Jung et al., 2006).

The observations showing that CPEB is localized to synapses, that it modulates plasticity, and that local protein synthesis is necessary for LTP and LTD suggest that cytoplasmic polyadenylation could mediate local protein synthesis and synaptic efficacy. To investigate this possibility, we focused on the factors that control polyadenylation and translation and found that CPEB, symplekin, Gld2, PARN, and Ngd formed a complex in dendrites of hippocampal neurons. NMDA stimulation promoted phosphorylation of CPEB and expulsion of PARN from the complex, and coincidentally induced a rapid increase in dendritic poly(A) levels. Furthermore, Gld2 and PARN bidirectionally regulated poly(A) RNA levels in dendrites and NMDA-induced polyadenylation was blocked by inhibiting CPEB phosphorylation. These findings indicate that the CPEB-associated complex regulates cytoplasmic polyadenylation in dendrites, which could be a bidirectional mechanism for regulating mRNA-specific translation at hippocampal synapses.

2.2 Results

2.2.1 The cytoplasmic polyadenylation machinery is localized to dendrites and synapses

CPEB has been detected in dendrites and at synapses in cultured hippocampal neurons (Huang et al., 2002; Wu et al., 1998); however, the factors that mediate CPEB-dependent translational control in mammalian neurons have not been determined. Gld2, PARN, Ngd, and symplekin were examined as possible CPEB partners. To determine the expression and subcellular distribution of these proteins *in vivo*, mouse brain sections were immunostained, and high-resolution confocal images of the hippocampus were analyzed. First, at low magnification, CPEB, Gld2, PARN, Ngd, and symplekin were

detected in the CA1, CA3, and dentate gyrus regions (Figure 2.1A). High magnification

confocal images allowed visualization of CPEB, Gld2, PARN and Ngd immunoreactivity

within cell bodies and MAP2-positive dendrites throughout the hippocampus (dentate

gyrus is shown; Figure 2.1B). The signal within MAP2-positive regions appeared

punctate, which is consistent with staining of RNA transport granules within neuronal

processes (Kiebler and Bassell, 2006). To examine the dendritic localization in more

detail, deconvolution and digital image analysis were used to trace individual dentate

granule cell dendrites across serial z-planes (Figure 2.1B). With this approach, CPEB,

Gld2, PARN and Ngd granules were detected in distal dendrites more than 50 μm from

the cell body. In contrast, immunoreactivity for a splicing factor, hnRNP A1, was

restricted to nuclei and cell bodies. 3D reconstructions of confocal z-series showed that

the punctate immunostaining of CPEB, Gld2, PARN, and Ngd did not overlap or

surround DAPI-stained nuclei, indicating that the punctate signal is not within cell bodies

(Figure 2.2A). In addition, the expression of CPEB, Gld2, PARN, Ngd, and symplekin

was analyzed in synaptoneurosomes isolated from mouse hippocampus. Each protein was

prominently expressed in synaptoneurosomes, which were enriched for the synaptic

protein PSD-95 and contained little glial fibrillary acidic protein (GFAP; Figure 2.2B).

Additional immunostaining revealed that these proteins are expressed in the cerebellum

and visual cortex (Figure 2.3A,B), two brain areas wherein CPE-containing mRNAs

undergo activity-induced mRNA polyadenylation (Shin et al., 2004; Wu et al., 1998).

To further investigate the subcellular distribution of these proteins, cultured

hippocampal neurons were immunostained for CPEB, Gld2, PARN, Ngd, and symplekin

after being grown for 17 days *in vitro* (*DIV*). The specificity of antibodies against Gld2,

PARN, and Ngd was confirmed using shRNA-mediated knockdown followed by immunocytochemistry in cultured neurons, and mRNA and protein knockdown were assessed by PCR and western blotting (Figure 2.4). The immunoreactivity showed extensive dendritic localization of these proteins, and the signal was granular and extended beyond multiple dendritic branch points (Figure 2.5). The immunoreactivity for hnRNP A1 was restricted to the nucleus and cell body. These data suggest that the cytoplasmic polyadenylation apparatus resides in discrete granules trafficked to dendrites.

2.2.2 Interaction and co-localization of CPEB complex proteins

To investigate whether these translational regulators formed a multi-protein complex, their interactions were analyzed by co-immunoprecipitation from neuroblastoma cell lysates. Endogenous symplekin co-immunoprecipitated GFP-tagged CPEB and GFP-tagged Gld2 (Figure 2.6A). In addition, FLAG-tagged PARN co-immunoprecipitated with symplekin and GFP-tagged CPEB (Figure 2.6B), and FLAG-tagged CPEB co-immunoprecipitated with symplekin, GFP-tagged PARN (Figure 2.6C), and GFP-tagged Gld2 (Figure 2.6D). Neither FLAG tagged protein co-immunoprecipitated tubulin or GFP alone (Figure 2.6E). Taken together, these data suggest that CPEB, PARN, Gld2, and symplekin form a multi-protein complex in neuronal cells. Simultaneously, my collaborators performed co-immunoprecipitations from mouse brain lysates. They found that symplekin co-immunoprecipitated with PARN, Ngd, and CPEB and that Ngd co-immunoprecipitated with symplekin from mouse brain lysates (Udagawa et al., in press); thus, confirming that this complex of translation factors associate in the brain.

To assess whether the CPEB-associated complex components were co-localized in dendrites, cultured neurons were co-immunostained for symplekin and each other component, and deconvolved images were analyzed for 3D co-localization (Figure 2.7A). CPEB, PARN, Gld2 and Ngd were non-randomly co-localized with symplekin (probability > 0.95), while GluR1 was not (Figure 2.7B). The Mander's coefficient, the fraction of total signal that is co-localized, for each co-localized pair was between 0.24 and 0.38 demonstrating that significant levels of CPEB, PARN, Gld2, and Ngd were co-localized with symplekin in dendritic granules (Figure 2.7C). These proteins were also detected within dendritic spines; 3D reconstructions of phalloidin fluorescence (Figure 2.7D) showed that 23.1% ± 1.24% of spines contained symplekin immunoreactivity and 80.1% ± 2.54% of symplekin-positive spines also contained CPEB, Gld2, PARN, or Ngd immunoreactivity (n = 40 cells, 1196 spines). These data indicate that the cytoplasmic polyadenylation machinery forms complexes in dendrites and at synapses.

CPEB has been previously shown to interact with the microtubule motor kinesin, and thus, it was hypothesized that CPEB might be necessary for the dendritic transport of its associated translational regulators. To address this hypothesis, lentiviral shRNA was used to knock down CPEB expression, and total protein levels as well as the ratio of dendritic to somatic expression of Gld2, PARN, and Ngd were analyzed. CPEB knockdown was confirmed by western blotting (Figure 2.8A). There were no significant alterations in the total protein levels of Gld2, PARN, or Ngd following knockdown of CPEB (Figure 2.8B). However, CPEB depletion caused approximately a 40% decrease in the dendritic immunofluorescence for PARN and Gld2 and a 30% decrease in dendritic Ngd immunofluorescence (Figure 2.8C-E). These data suggest that CPEB regulates the

localization of these translational factors to dendrites and, perhaps, that Gld2, PARN, and Ngd are co-transported with CPEB into dendrites.

2.2.3 PARN is expelled from the polyadenylation complex following NMDA-induced CPEB phosphorylation

In oocytes, polyadenylation is activated by CPEB S174 or T171 phosphorylation (species-dependent) (Hodgman et al., 2001; Mendez et al., 2000), which induces PARN expulsion from the CPEB-containing complex (Kim and Richter, 2006). NMDA receptor activation elicits CPEB T171 phosphorylation in mammalian neurons (Atkins et al., 2004; Huang et al., 2002), but whether this occurs in dendrites is unknown. To assess this possibility, hippocampal neurons were treated with NMDA (100 nM for 30 seconds) and immunostained for phosphorylated CPEB (pCPEB) or total CPEB (Figure 2.9A). Quantification of the mean immunofluorescence intensities in dendrites (≥ 75 μm from the soma) showed that NMDA stimulation increased dendritic pCPEB by 90%, while total dendritic CPEB levels were not significantly affected (Figure 2.9B). In synaptoneurosomes from cortical neuron cultures, NMDA treatment increased synaptic pCPEB ~2.5 fold compared to control (Figure 2.9C). These data suggest that NMDA receptor activation leads to rapid CPEB phosphorylation at synapses.

To determine whether NMDA receptor activation alters the composition of the dendritic CPEB-associated protein complex, hippocampal neurons were treated with NMDA, co-immunostained for the complex components, and analyzed for 3D co-localization (Figure 2.10A). Although NMDA did not alter CPEB or Gld2 co-localization with symplekin, it significantly reduced the co-localization of PARN with symplekin as

well as CPEB with PARN (Figure 2.10B-E). Total protein levels of Gld2 and PARN

were not affected (Figure 2.10F,G). Inhibitors of Aurora A and CaMKII, two enzymes

that phosphorylate CPEB T171 in neurons (Atkins et al., 2004; Huang et al., 2002),

occluded NMDA-induced CPEB phosphorylation in dendrites (Figure 2.11A) and at

synapses (Figure 2.11B). These same inhibitors of Aurora A and CaMKII blocked the

NMDA-induced reduction of PARN co-localization with symplekin, suggesting that

CPEB phosphorylation triggers the release of PARN from dendritic CPEB-containing

complexes (Figure 2.12). PARN expulsion was also indicated by biochemical data;

membrane depolarization of neuroblastoma cells increased CPEB phosphorylation

(Figure 2.13A) and decreased co-immunoprecipitation of FLAG-tagged PARN with wild

type (WT) CPEB, but not a non-phosphorylatable mutant form of CPEB (CPEB-AA)

(Figure 2.13B-D). Thus, activity-induced CPEB phosphorylation disrupts the interaction

between PARN and CPEB-containing complexes in neuronal cells.

*2.2.4 Dendritic polyadenylation is induced by NMDA receptor activation and
bidirectionally regulated by PARN and Gld2*

To investigate whether polyadenylation occurs in dendrites upon synaptic activity,

neurons were processed for fluorescence in situ hybridization (FISH) with oligo(dT)

probes, which detected punctate poly(A) RNA in the soma, dendritic and axonal arbors,

and at synapses (Figure 2.14). Oligo(dT) probes accurately detected the decreasing

proximal-to-distal gradient of poly(A) RNA in dendrites (Bassell et al. 1994), and

oligo(dA) FISH yielded negligible signal (Figure 2.15). To assess dendritic poly(A)

levels, the mean oligo(dT) fluorescence intensity was measured in dendritic regions ≥ 75

μm from the soma. NMDA treatment for 30 seconds resulted in a 55% increase in FISH intensity compared to vehicle-treated neurons (Figure 2.16A,B); this effect was abrogated by the NMDA receptor antagonist amino-5-phosphonovaleric acid (APV; Figure 2.16C). NMDA did not affect dendritic αCaMKII mRNA levels (Figure 2.17A-C), indicating negligible transcript transport to distal dendrites during the brief stimulation period.

Since Gld2 and PARN were putative regulators of dendritic polyadenylation, the co-localization of these enzymes with poly(A) mRNA was examined before and after NMDA receptor activation. Cultured hippocampal neurons were processed for oligo(dT) FISH and immunostained for either Gld2 or PARN, followed by 3D co-localization analysis. Under basal conditions, both Gld2 and PARN showed significant co-localization with poly(A) mRNA in distal dendrites (Figure 2.18A). Interestingly, NMDA treatment increased the amount of co-localization between Gld2 and poly(A) mRNA (Figure 2.18B), whereas the co-localization between PARN and poly(A) mRNA was decreased following NMDA treatment (Figure 2.18C). These data suggest that PARN is expelled from dendritic mRNA-containing complexes after NMDA stimulation, while Gld2 remains in the RNPs. The increase in co-localization between poly(A) and Gld2 following NMDA is likely due to the increase in poly(A) RNA signal in particular granules, perhaps specifically those granules that contain Gld2.

To determine if dendritic polyadenylation was sensitive to Gld2 or PARN levels, neurons were transduced with lentiviruses expressing Gld2- or PARN-specific shRNA or a control (see Figure 2.4 for knockdown efficiency). Depletion of Gld2 significantly reduced both basal and NMDA-stimulated dendritic oligo(dT) FISH signals relative to controls (Figure 2.19A), indicating that this enzyme regulates steady-state and activity-

induced levels of dendritic poly(A) RNA. Depletion of PARN significantly increased

basal levels of dendritic oligo(dT) FISH signal and decreased poly(A) RNA levels

following NMDA stimulation (Figure 2.19B). These data suggest that PARN regulates

steady-state and activity-induced poly(A) tail length of at least some mRNAs and,

perhaps, that increased NMDA receptor signaling leads to degradation of dendritic

mRNAs in PARN-deficient cells.

2.2.5 NMDA-induced polyadenylation is dependent upon CPEB phosphorylation

　　　　To directly assess whether CPEB phosphorylation and PARN expulsion regulate

dendritic polyadenylation, oligo(dT) FISH intensity was quantified in the dendrites of

neurons expressing CPEB-WT or CPEB-AA (Figure 2.20A). The expression and

localization of CPEB-WT and CPEB-AA in dendrites were similar (data not shown).

Steady-state dendritic oligo(dT) FISH intensity was reduced by both CPEB-WT (20%)

and CPEB-AA (28%) expression compared to control cells. NMDA treatment increased

dendritic oligo(dT) FISH intensity in control (56.9%) and CPEB-WT expressing (89.0%)

neurons, whereas CPEB-AA expression blocked this effect (Figure 2.20B). In addition,

pre-treatment with Aurora A or CaMKII inhibitors occluded the NMDA-induced increase

in dendritic oligo(dT) FISH intensity (Figure 2.20C,D). From these data, it is inferred that

the dendritic mRNA polyadenylation machinery is regulated by NMDA receptor activity,

and that CPEB phosphorylation leads to PARN extrusion from this complex resulting in

mRNA polyadenylation in dendrites.

Figure 2.1 CPEB, PARN, Gld2, Neuroguidin and symplekin are expressed in the hippocampus and localize to dendrites. (A) Confocal images of mouse hippocampus immunostained for CPEB, PARN, Gld2, Ngd and symplekin (scale bar is 200 µm). (B) Mouse hippocampal sections were co-immunostained for MAP2 (red) and CPEB, Gld2, PARN, Ngd and hnRNP A1 (green), and z-series were acquired with a confocal microscope. Images show dentate granule cell bodies (GC) and the molecular layer (ML). The open arrowheads point to a proximal dendrite and closed arrowheads follow a single dendrite through serial z-stacks across 1.6 µm (scale bars are 10 µm).
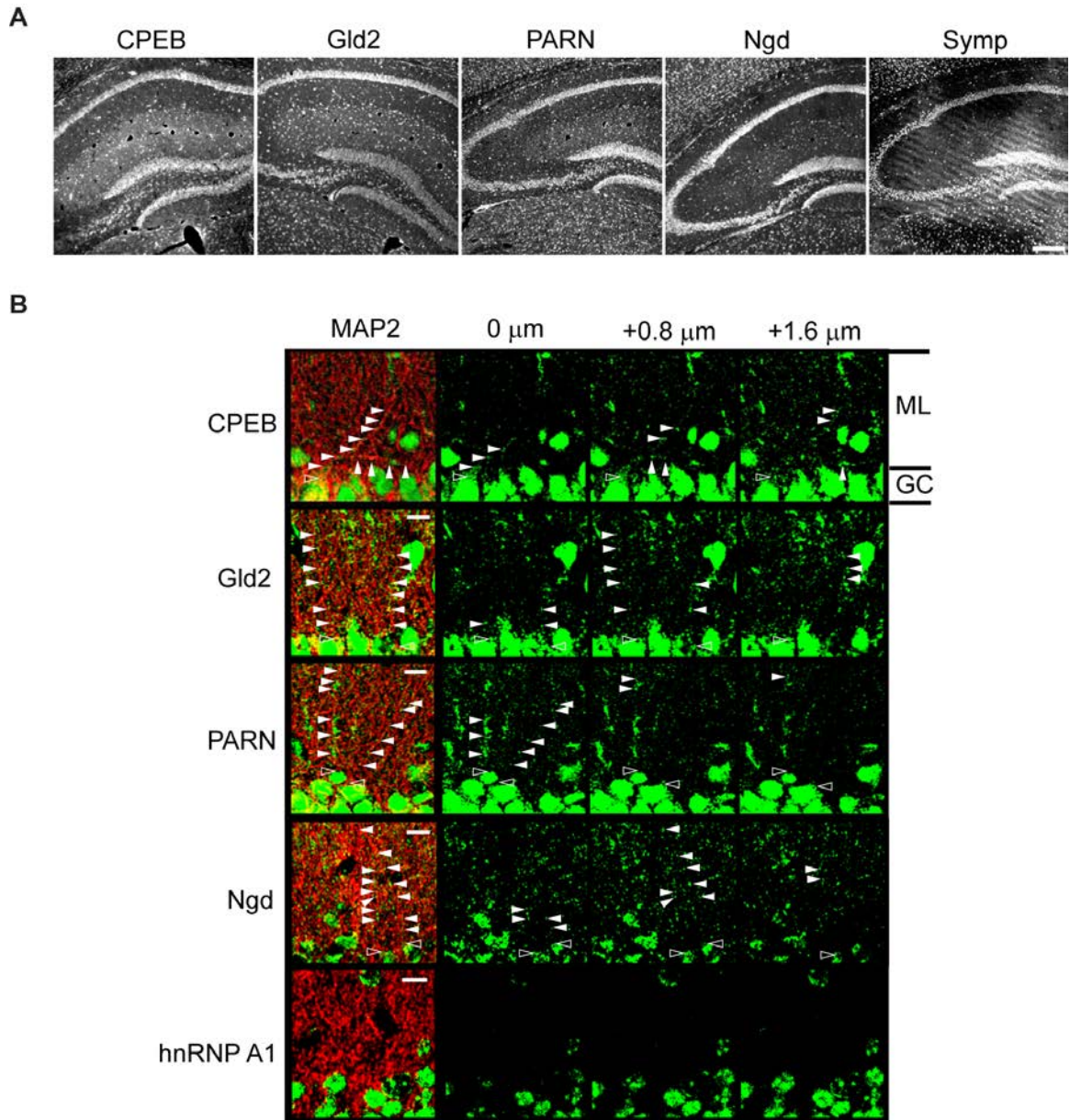
Figure 2.1

Figure 2.2
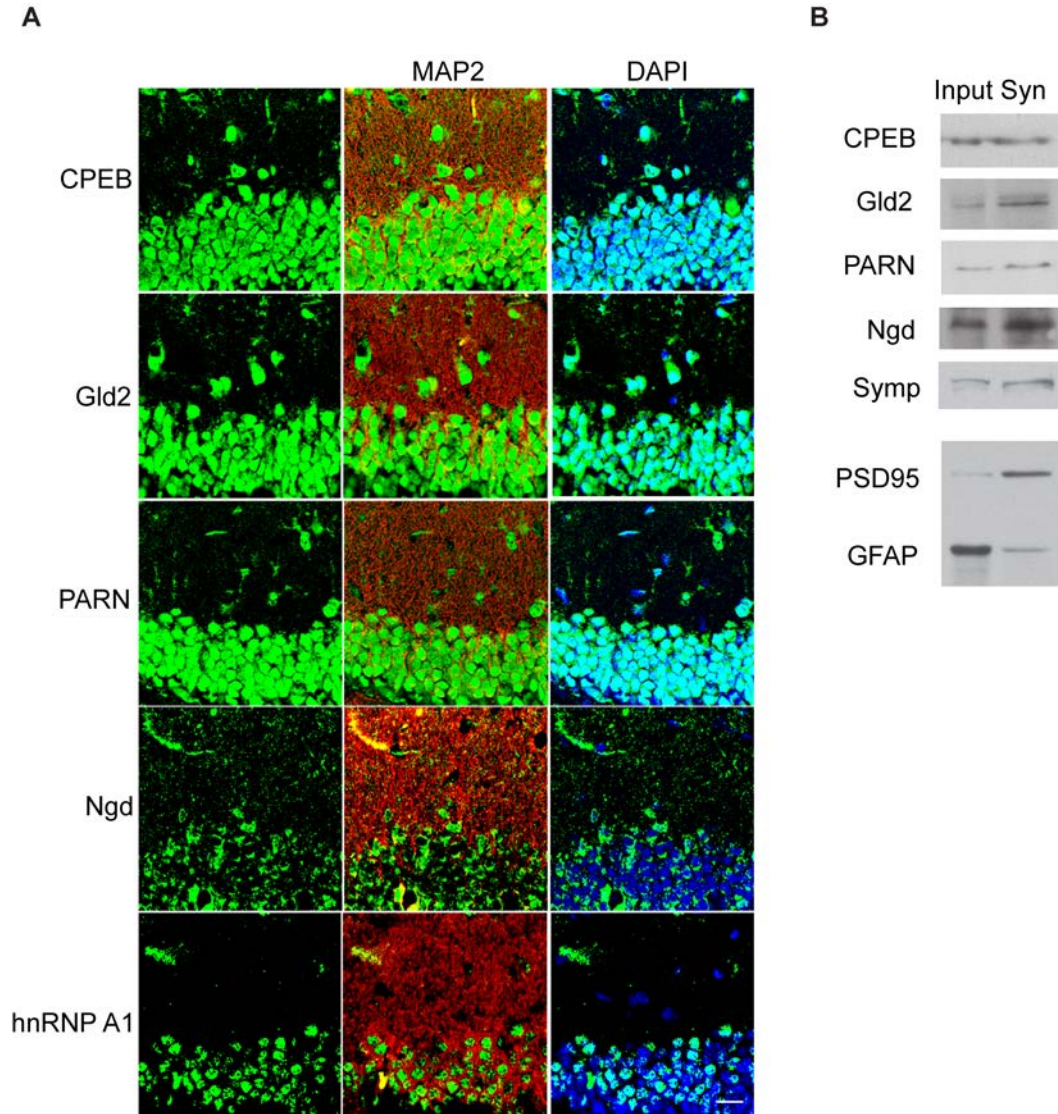
Figure 2.2 CPEB, PARN, Gld2 and Ngd are expressed at synapses. (A) Coronal

sections of the mouse dentate gyrus were co-immunostained for CPEB, Gld2, PARN,

Ngd, or hnRNP A1 (green) and MAP2 (red), then stained with DAPI to identify nuclei

(blue). Scale bar is 20 µm. (B) Equal amounts of protein from mouse forebrain

homogenate (Input) and synaptoneurosomes (Syn) were immunoblotted for CPEB,

PARN, Gld2, Ngd and symplekin. PSD95 and GFAP western blots demonstrate

enrichment of the synaptic fractions.

Figure 2.3
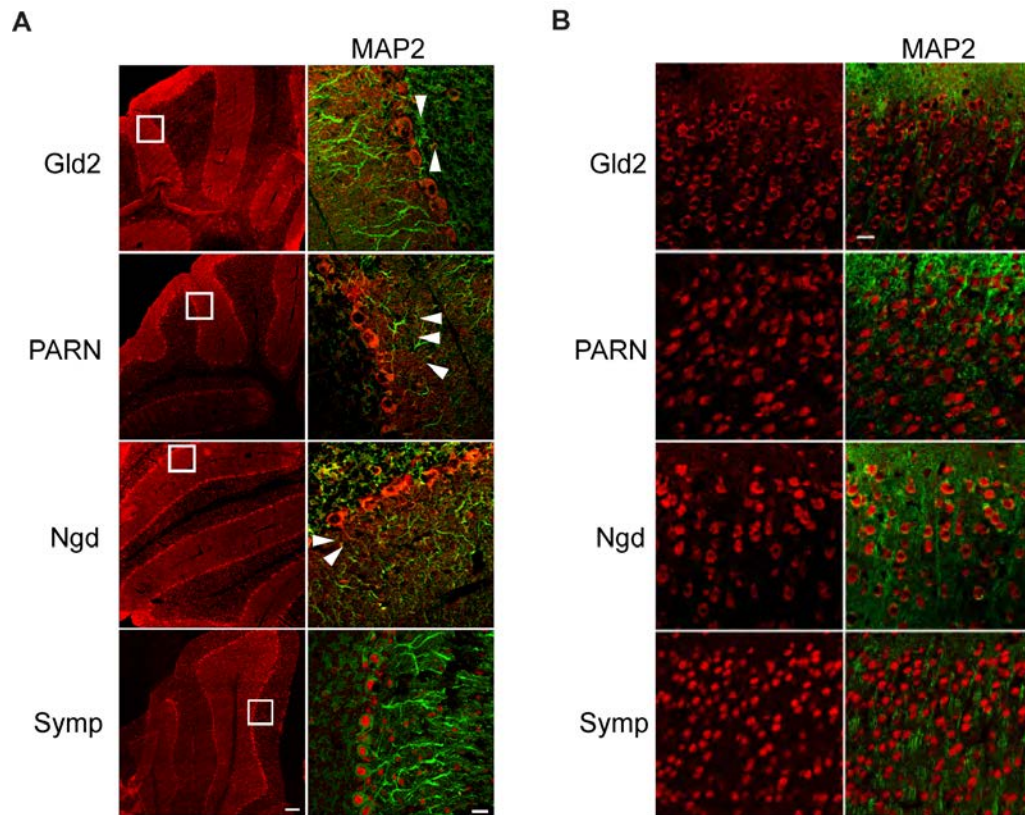
Figure 2.3 Putative CPEB interacting partners are expressed in brain regions where CPEB regulates mRNA translation. (A) Sagittal sections of mouse cerebellum were co-immunostained for Gld2, PARN, Ngd or symplekin (red) and MAP2 (green). Arrowheads point to Purkinje neuron dendrites. Scale bars are 200µm (left panels) and 20µm (right panels). (B) Coronal sections of mouse cortex (area V1 is shown) were co-immunostained for Gld2, PARN, Ngd or symplekin (red) and MAP2 (green). Scale bar is 20µm.

Figure 2.4 Specificity of antibodies and shRNA against Gld2, PARN, and Ngd.

Hippocampal neurons were transduced with lentiviruses expressing scramble shRNA, GFP alone, Gld2 shRNA, PARN shRNA, and Ngd shRNA for 3-4 days. (A) RNA levels were assessed by PCR, and protein levels were assessed by (B) western blot, and (C) immunocytochemistry.

Figure 2.4
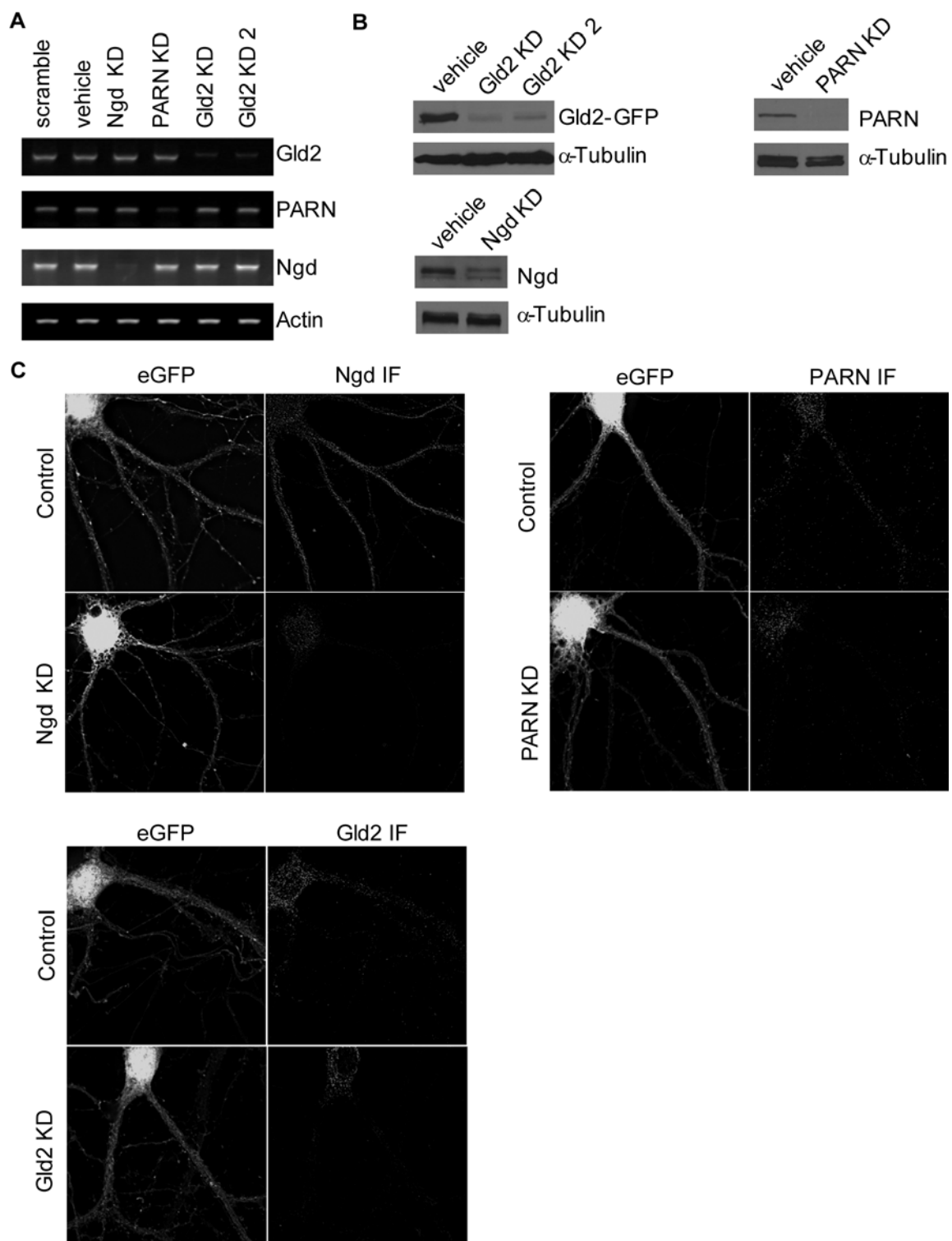
Figure 2.5
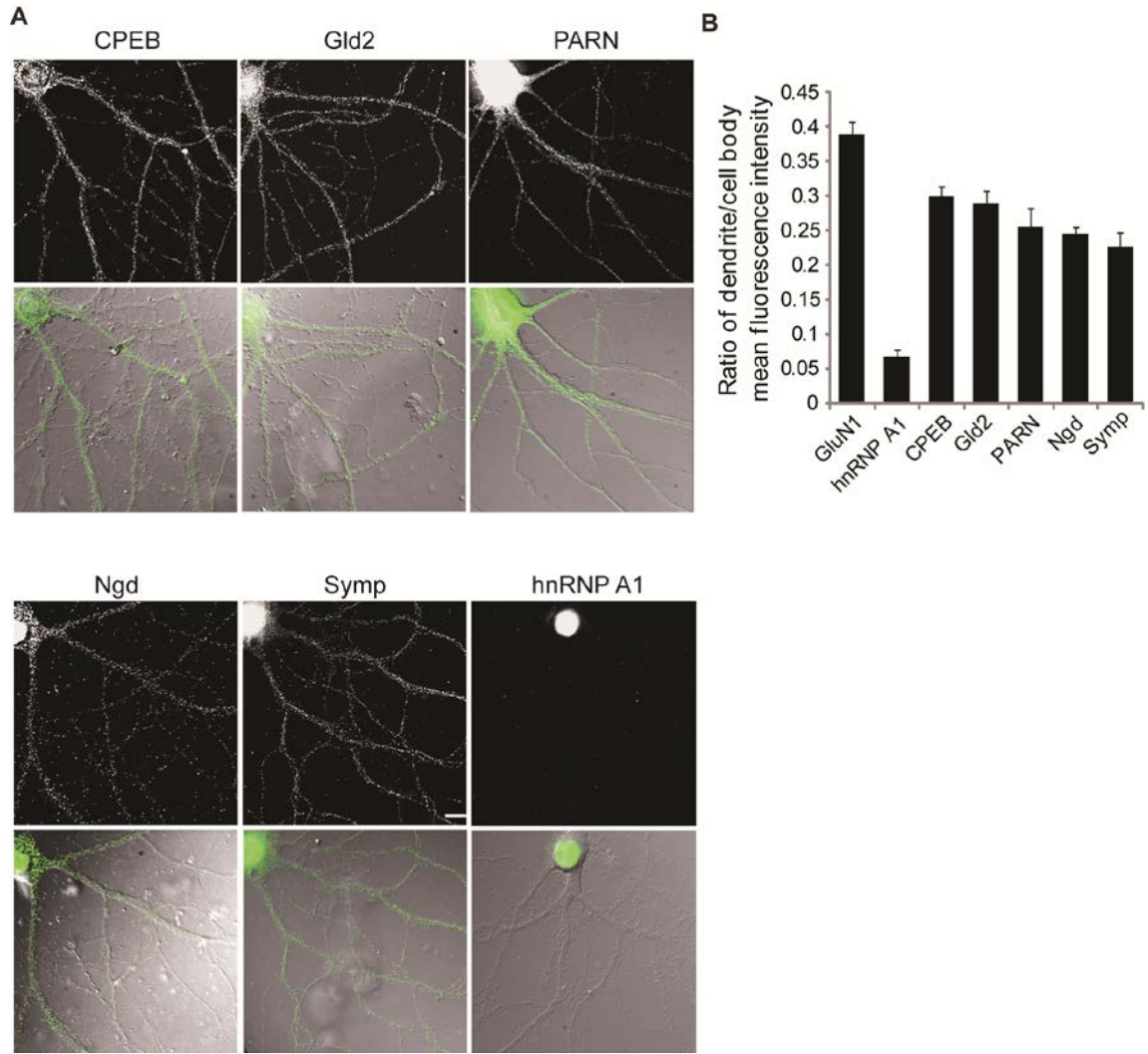
Figure 2.5 CPEB, Gld2, PARN, Ngd and Symplekin localize to dendrites in cultured hippocampal neurons. (A) 17 *DIV* hippocampal neurons were immunostained for CPEB, Gld2, PARN, Ngd, symplekin, or hnRNP A1 (red). DIC images are shown with immunofluorescence overlay. Scale bar is 5 µm. (B) The mean fluorescence intensity within distal dendritic regions (> 75 μm from the soma) and somas were determined and are presented as a ratio (n = 30 cells). hnRNP A1 and GluN1 (images not shown) are negative and positive controls, respectively.

Figure 2.6
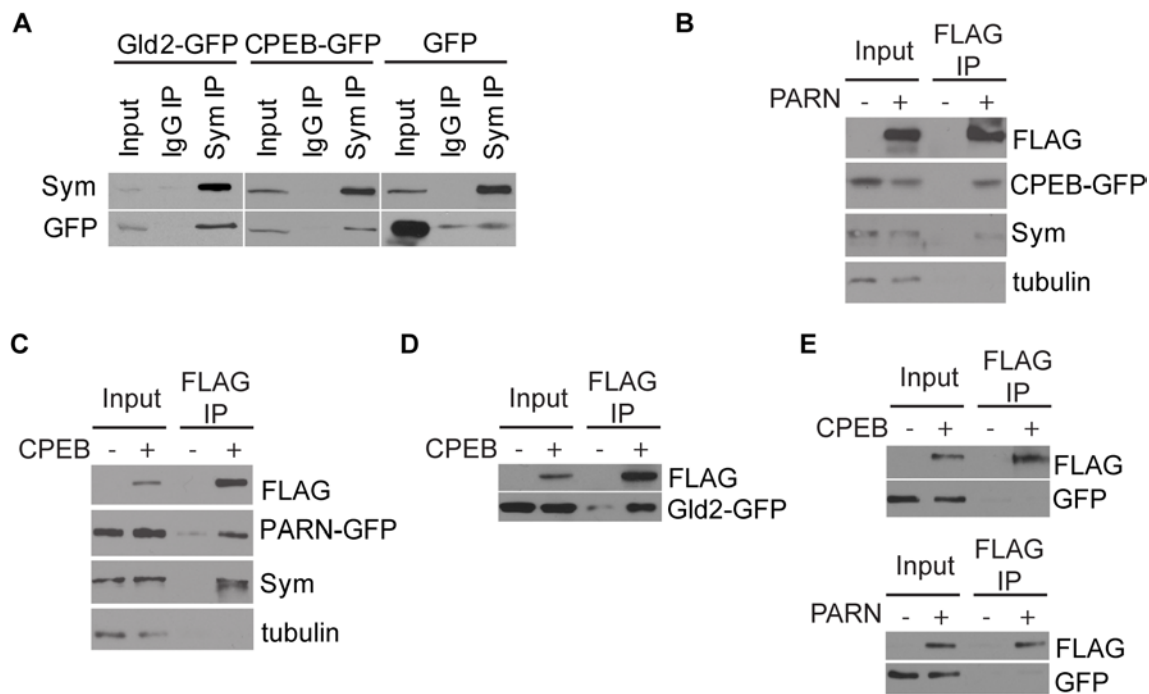
Figure 2.6 Interaction of CPEB-containing cytoplasmic complex proteins. (A)

Lysates from mouse neuroblastoma cells (Neuro2A cells) expressing GFP or GFP-Gld2

were used for co-immunoprecipitation with symplekin antibodies or an IgG control,

followed by western blotting for symplekin and GFP. Lysates from Neuro2A cells

expressing (B) FLAG-PARN and CPEB-GFP, (C) FLAG-CPEB and PARN-GFP, (D)

FLAG-CPEB and Gld2-GFP, or (E) GFP and FLAG-CPEB or FLAG-PARN were co-

immunoprecipitated with FLAG antibodies, then western blotted for FLAG, GFP,

symplekin, or tubulin (negative control) as shown.

Figure 2.7 The CPEB-associated polyadenylation complex is present in dendrites and at synapses. (A) Hippocampal neurons (17 *DIV*) were co-immunostained for symplekin (red) and CPEB, Gld2, PARN, Ngd, or GluA1 (green); the images were deconvolved and analyzed for 3D co-localization within dendritic regions. Images shown are 3D reconstructions of straightened dendritic regions. Pixels with overlapping signals are shown in white; the scale bar is 10 µm. (B) The probability of non-random co-localization in 3D reconstructions was determined for symplekin and CPEB, Gld2, PARN, Ngd or GluA1. (C) Mander's overlap coefficients were computed for each co-localized pair. (D) High-magnification images and 3D reconstructions depict co-localization in dendritic spines (green: phalloidin; red: symplekin; blue: CPEB, Gld2, PARN or Ngd; scale bar is 0.5 µm).

Figure 2.7

A

B

C

D
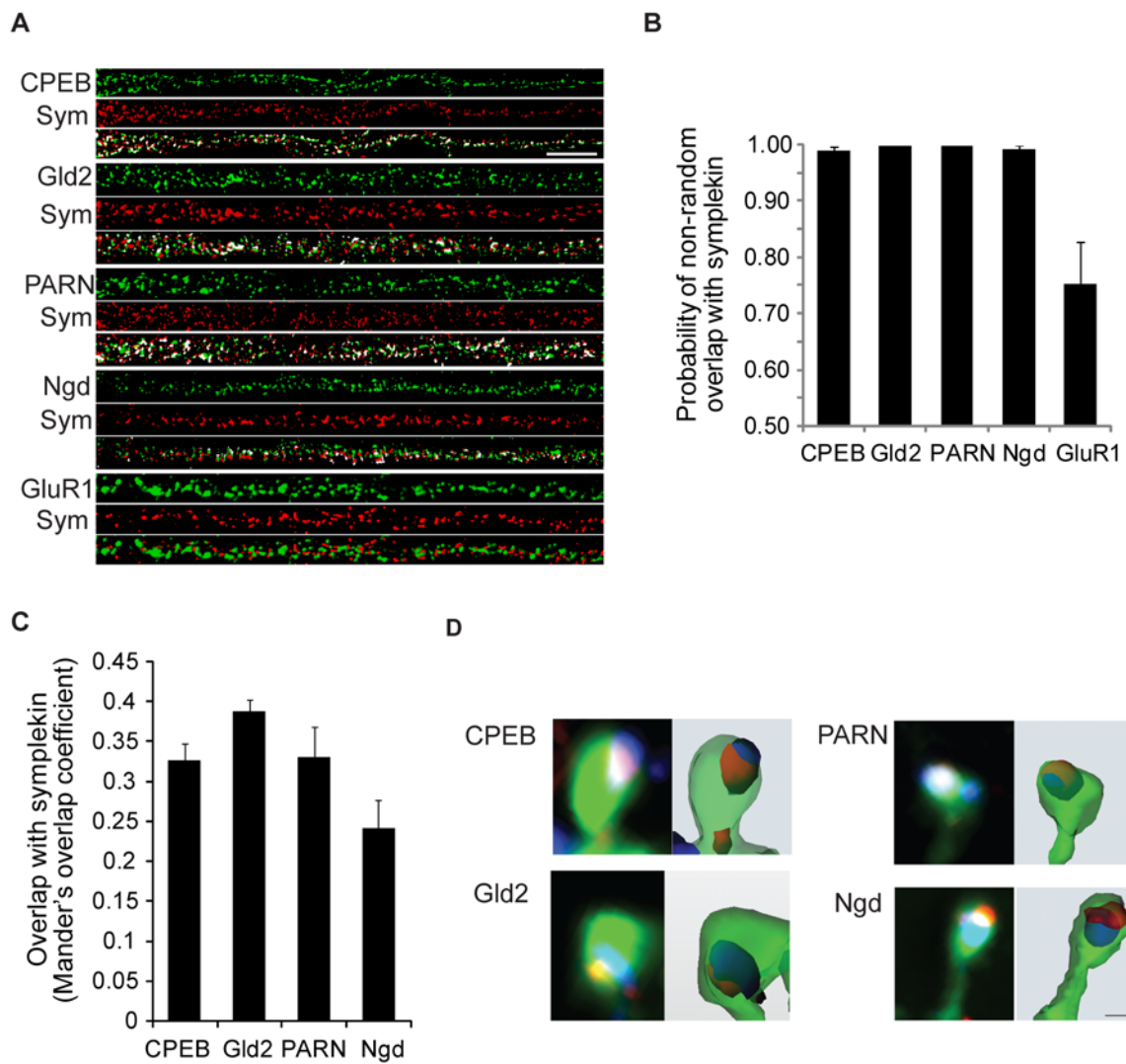
Figure 2.8 CPEB regulates the dendritic localization of Gld2, PARN, and Ngd. (A)

14 *DIV* hippocampal neurons were treated with either control or CPEB shRNA lentivirus

for 4 days, then lysed and immunoblotted for CPEB, Gld2, PARN, Ngd, and α-tubulin

(loading control). (B) Total protein levels were quantified by densitometry and analyzed

by Student's t-test, and the graphed values were normalized to the mean of the control

group (CPEB: $p = 0.001$, Gld2: $p = 0.981$, PARN: $p = 0.599$, Ngd: $p = 0.437$). (C-E) 14

DIV hippocampal neurons were treated with lentivirus as above, and then fixed and

immunostained for either Gld2, PARN, or Ngd. The lentivirus also expressed GFP and is

shown here to illustrate neuron morphology. Proximal and distal (> 75 µm from the

soma) dendrite immunofluorescence signals were quantified and are graphed as a ratio

(distal/proximal). Control versus CPEB knockdown groups were analyzed by Student's t-

test (Gld2: $p = 0.001$, PARN: $p = 0.001$, Ngd: $p = 0.024$).

Figure 2.8
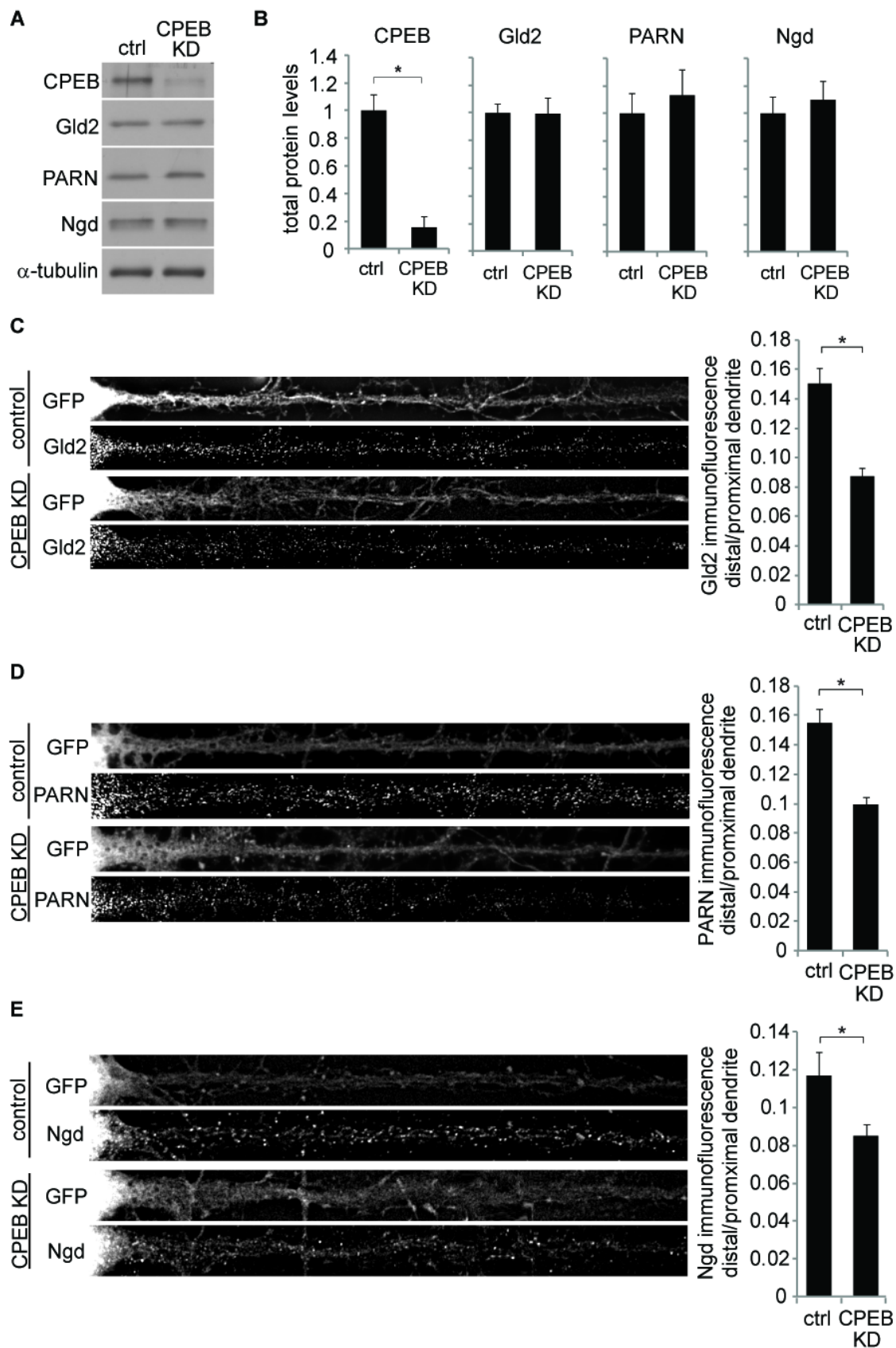
Figure 2.9
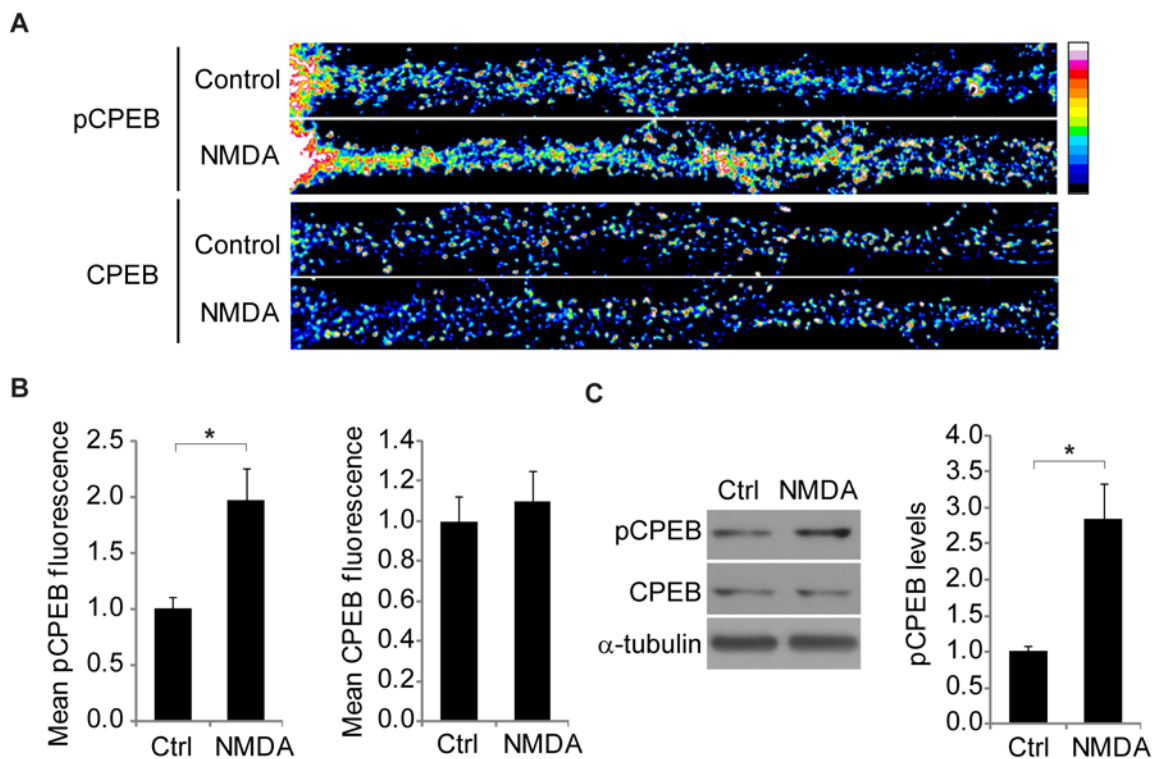
Figure 2.9 NMDA receptor activation increases CPEB phosphorylation at synapses.

(A) Hippocampal neurons treated with vehicle (Ctrl) or 100 nM NMDA (30 sec) were

immunostained for pCPEB or total CPEB. Immunoreactivity is illustrated with

straightened dendrites and a 16-color intensity map shown at right. The scale bar is 10

μm. (B) The mean fluorescence intensity for pCPEB and total CPEB were quantified in

distal dendritic regions $\geq$ 75 μm from the cell body, and the graphed values are

normalized to the mean of the control group ($n = 45$ dendrites, $*p = 0.002$, Student's t-

test). (C) Synaptoneurosomes from cortical neuron cultures were immunoblotted for

pCPEB, CPEB and tubulin (loading control), and then quantified by densitometry.

pCPEB levels were normalized to total CPEB, and the graphed values were normalized to

the control group mean ($n = 6$, $*p = 0.003$, Student's t-test).

Figure 2.10 NMDA receptor activation reduces co-localization between PARN and the CPEB complex. (A) Representative images of 17 *DIV* hippocampal neurons treated with NMDA or vehicle and co-immunostained for: CPEB and symplekin, Gld2 and symplekin, PARN and symplekin, or CPEB and PARN. The white voxels contain both signals. The scale bar is 5µm. (B-E) Hippocampal neurons treated with vehicle or 100 nM NMDA (30 sec) were co-immunostained and 3D co-localization analyses were performed. The histograms display the Mander's overlap coefficients ($n = 45$ dendrites, D: *$p = 0.01$, E: *$p = 0.003$, Student's *t*-test). (F,G) Mean fluorescence intensities for Gld2 and PARN were measured in dendrites using ImageJ, and the graphed values were normalized to control group mean (n = 45 dendrites).

Figure 2.10
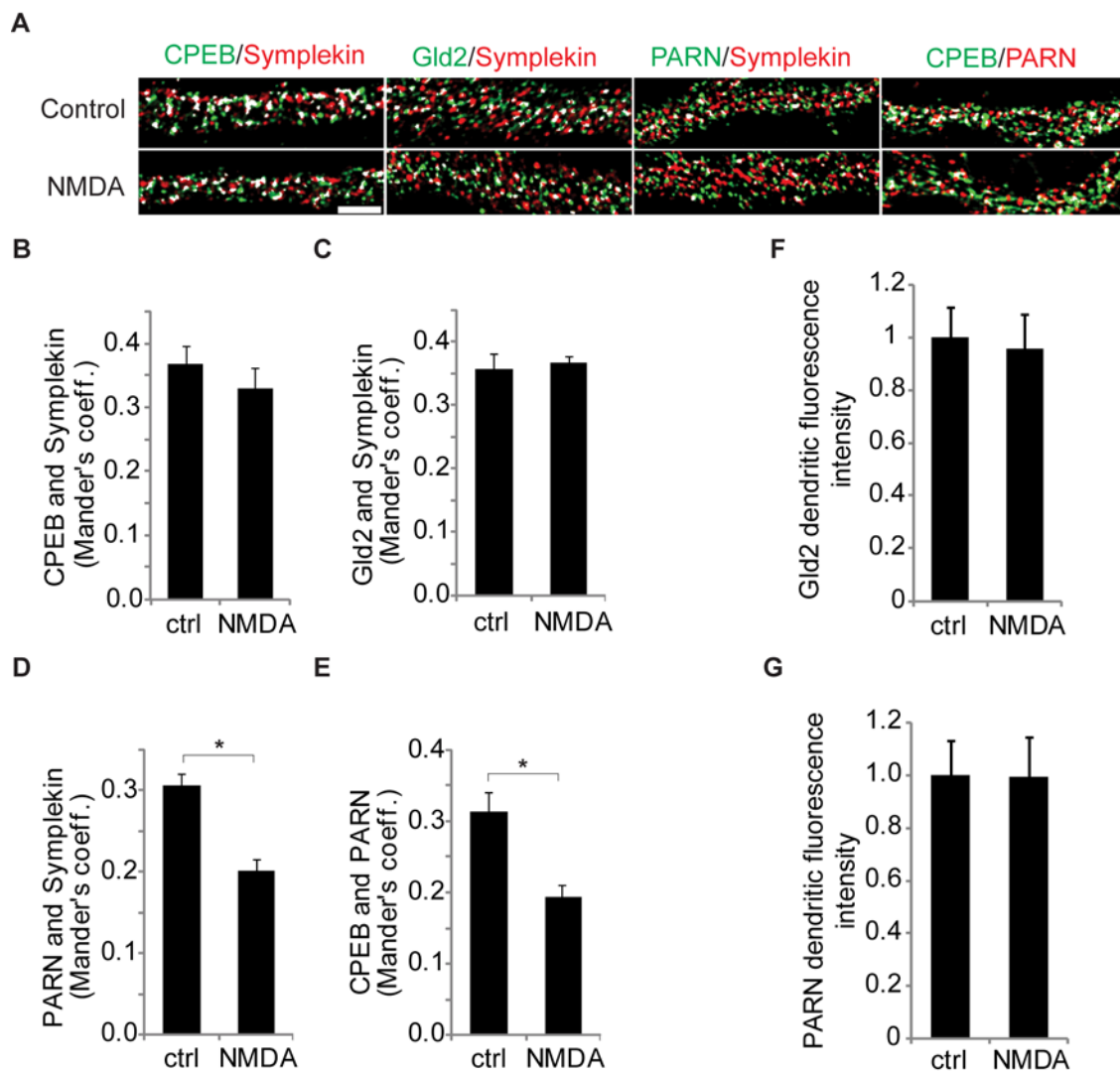
Figure 2.11 Pharmacological inhibition of CaMKII and Aurora A kinase blocks CPEB phosphorylation. (A) Synaptoneurosomes isolated from cortical neuron cultures were pretreated with vehicle, KN93 (CaMKII inhibitor), or ZM447473 (Aurora A inhibitor) and treated with vehicle or NMDA. Immunoblots for pCPEB, CPEB, and α-tubulin were quantified by densitometry, and the graphed values were normalized to the untreated group mean (n = 6, ANOVA post-hoc Dunnett's test, $*p = 0.001$). *(B)* Mean dendritic pCPEB immunoreactivity was quantified in neurons pre-treated with vehicle, KN93 or ZM447473, and treated with vehicle or NMDA for 30 seconds. All graphed values were normalized to the untreated group mean (n = 45; Kruskal-Wallis test, $*p = 0.007$).

Figure 2.11

A
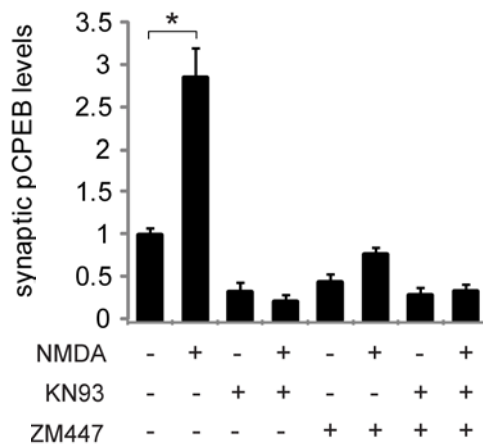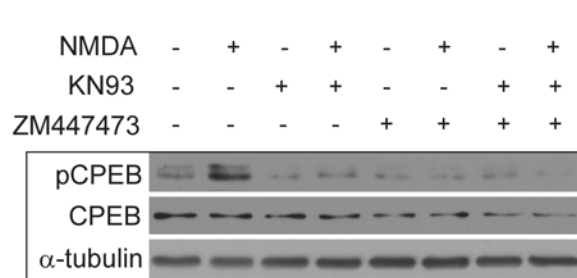
B
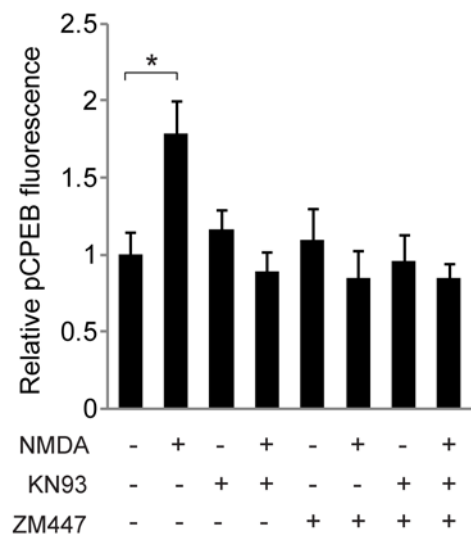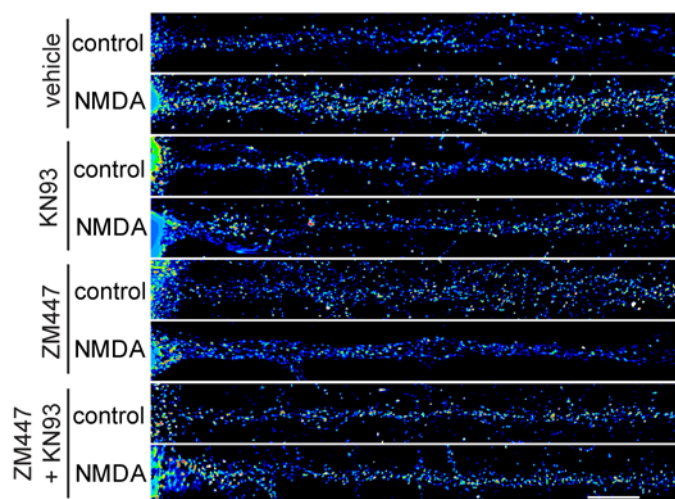
Figure 2.12
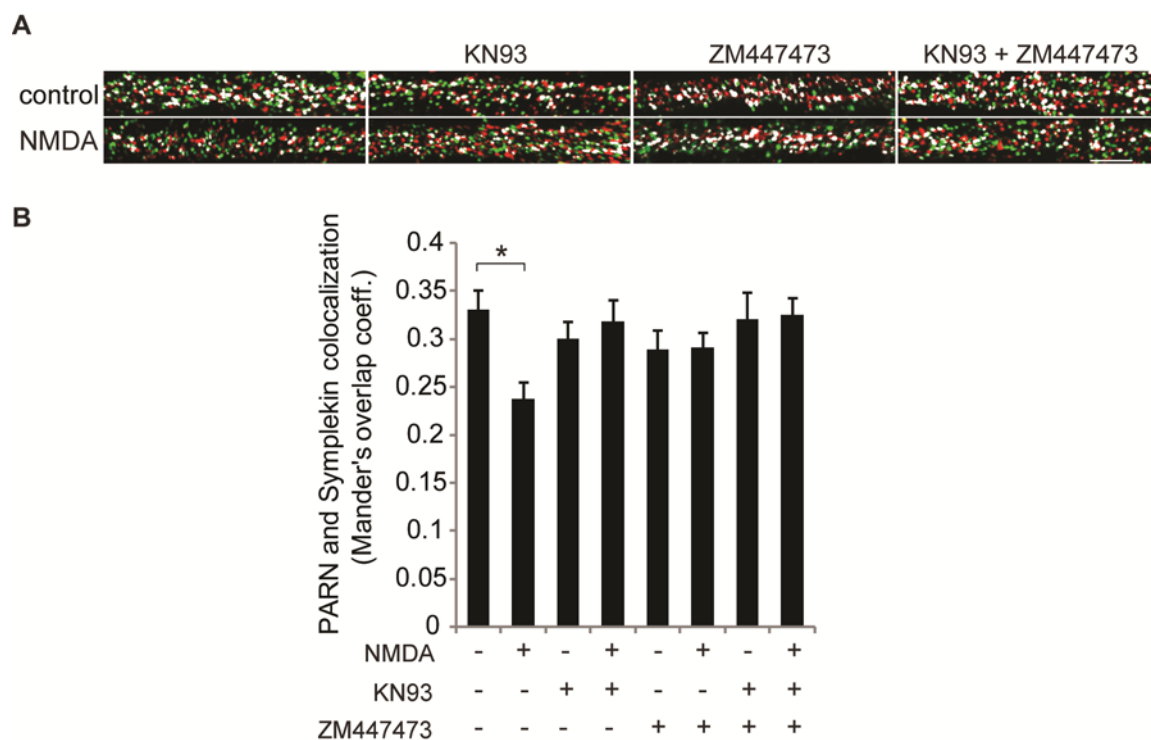
Figure 2.12 Aurora A and CaMKII inhibitors block the NMDA-induced decrease in co-localization between PARN and symplekin. (A) Co-localization between PARN and symplekin was quantified in neurons treated with vehicle, KN93 or ZM447473 and vehicle or NMDA, followed by co-immunostaining for PARN and symplekin. (B) Groups were compared using a one-way ANOVA and Bonferroni t-tests (n = 40; *p = 0.003; KN93 vs. KN93+NMDA p = 0.983; ZM447473 vs. ZM447473+NMDA p = 0.999, KN93+ZM447473 vs. KN93+ZM447473+NMDA p = 0.901).

Figure 2.13
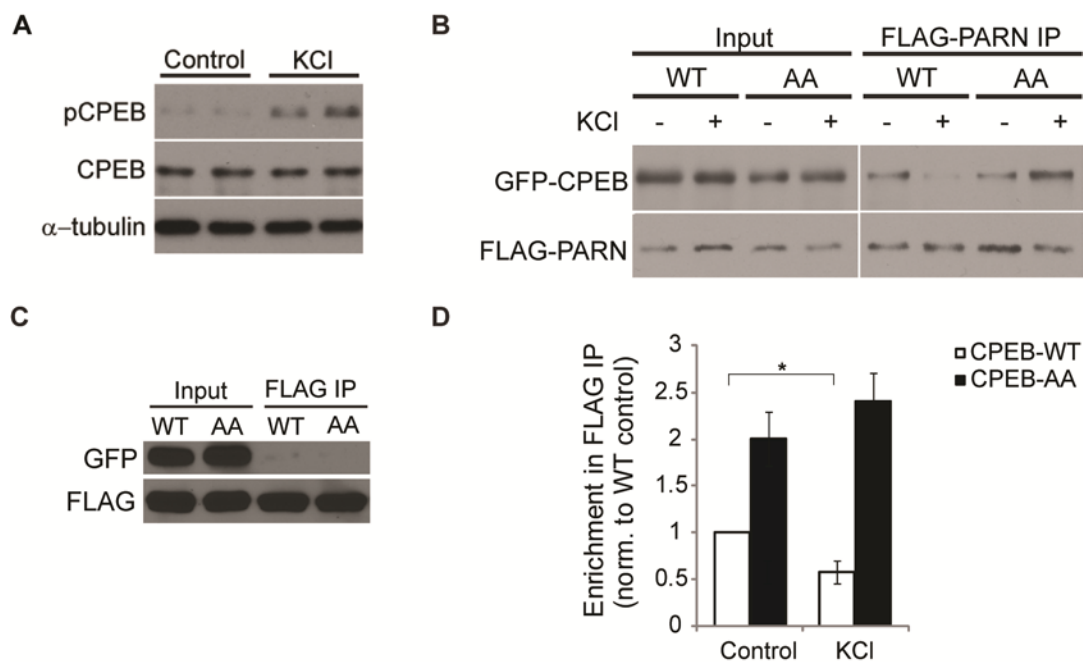
Figure 2.13 Activity-induced CPEB phosphorylation disrupts the association between PARN and CPEB. (A) Neuroblastoma cells were treated with vehicle (Control) or 90 mM KCl for 5 min in duplicate, and lysates were immunoblotted for pCPEB, CPEB, and α-tubulin (a loading control). (B) Neuroblastoma cells expressing FLAG-PARN and GFP-tagged CPEB-WT or CPEB-AA were treated with vehicle or 90 mM KCl (5 min). Cell lysates were immunoprecipitated with FLAG antibodies and immunoblotted for GFP and FLAG. (C) Neuroblastoma cells were transfected to express FLAG and GFP-tagged CPEB-WT and CPEB-AA. After 24 hours, cell lysates were immunoprecipitated with FLAG antibodies and immunoblotted for GFP and FLAG. (D) Immunoblots were quantified by densitometry; the IP values were normalized to input values and all graphed values were normalized to WT control levels (n = 6; *$p = 0.024$, one-way ANOVA post-hoc Tukey's test).

Figure 2.14 FISH detection of poly(A) mRNA in dendrites and axons of cultured hippocampal neurons. (A) A specific poly(A) mRNA signal is detected in the cell body and dendrites of a 16 *DIV* neuron (DIC overlay, top left). The poly(A) mRNA signal maintains high signal-to-noise ratio in distal dendrites (>100μm from the cell body, top center). RFP fluorescence (top right) can be visualized in tandem with poly(A) mRNA FISH (bottom left). Synapsin immunostaining shows poly(A) mRNA granules at synapses (bottom center). (B) Poly(A) mRNA granules are detected in dendritic spines (top left) filled with RFP signal (top right) and overlap with synapsin staining (bottom right). (C) Poly(A) mRNA is detected in the cell body and neurites of a 3 *DIV* neuron (DIC overlay, top left). The poly(A) mRNA signal extends the length of the axon (top right) and into the growth cone (arrowheads, bottom panels).

Figure 2.14
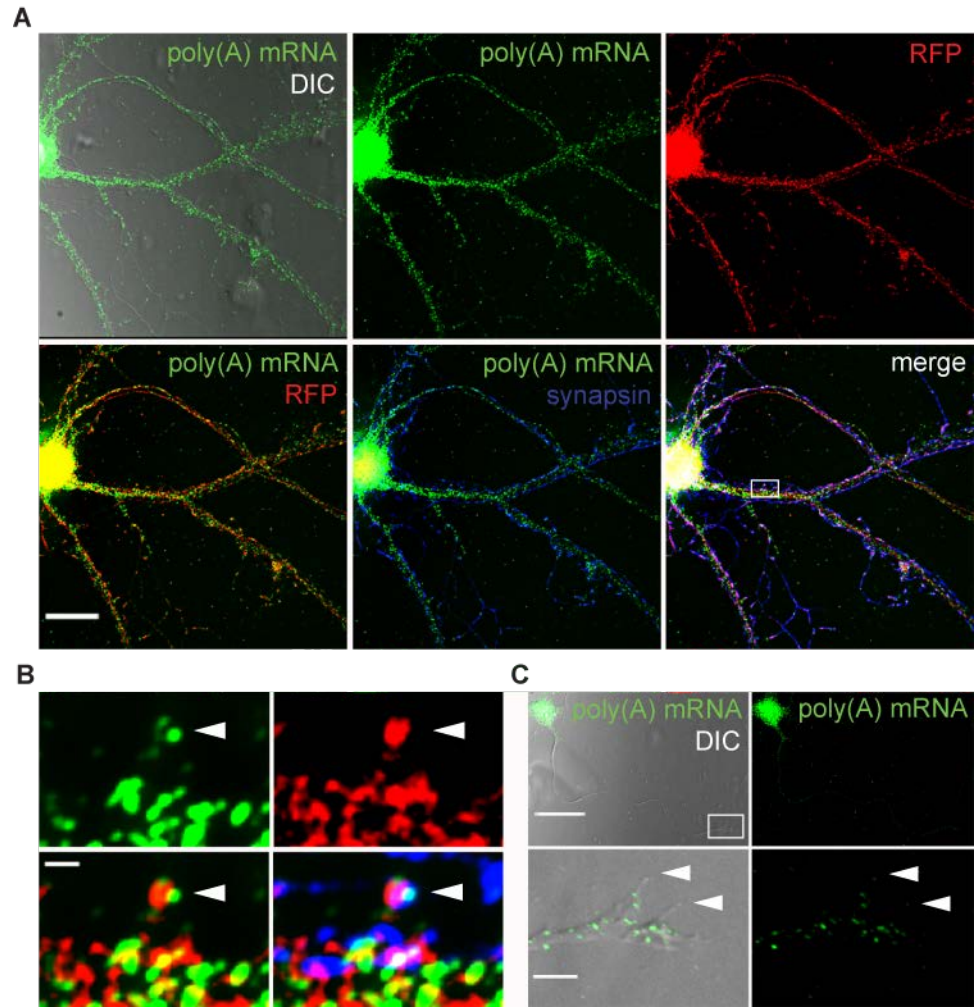
Figure 2.15
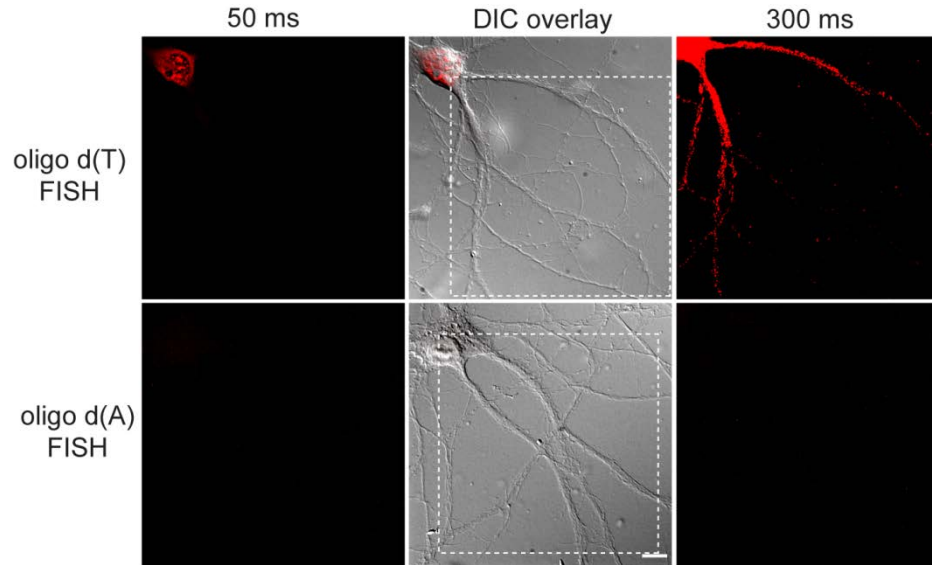
Figure 2.15 Oligo(dT) probes specifically detect poly(A) mRNA in neurons. Images

depict 17 *DIV* hippocampal neurons processed for FISH with digoxigenin-labeled

oligo(dT) (top panels) or oligo(dA) (bottom panels) probes. Left panel images were

captured with 50 ms exposure times. Center panels show FISH overlay with DIC images.

The area traced with the white dotted line is shown in the right panels; 300 ms exposure

times were used to capture these images.

Figure 2.16 NMDA-induced dendritic polyadenylation. (A) Poly(A) RNA FISH was

performed on 17 *DIV* hippocampal neurons treated with vehicle or NMDA (100 nM, 30

sec). The scale bar is 10 µm. The images at right show high magnification of the punctate

poly(A) FISH signal in distal dendrites within the white box in left images. Images were

pseudo-colored using a 16 color intensity map (right). Mean poly(A) pixel intensity

versus distance from the cell body was plotted for the shown images. (B) Mean poly(A)

FISH signals were quantified in dendritic regions ≥ 75 µm from the cell body, and the

graphed values were normalized to the mean of the control group ($n = 38\text{-}40$, *$p = 0.008$,

Student's *t*-test). (C) Poly(A) FISH was performed on dendrites following NMDA, APV,

or NMDA + APV treatment of neurons. Mean dendritic poly(A) FISH signals were

quantified and all graphed values were normalized the control group mean ($n = 30$, *$p =$

0.01, APV vs. APV+NMDA $p = 0.717$, one-way ANOVA post-hoc Tukey's test).

Figure 2.16
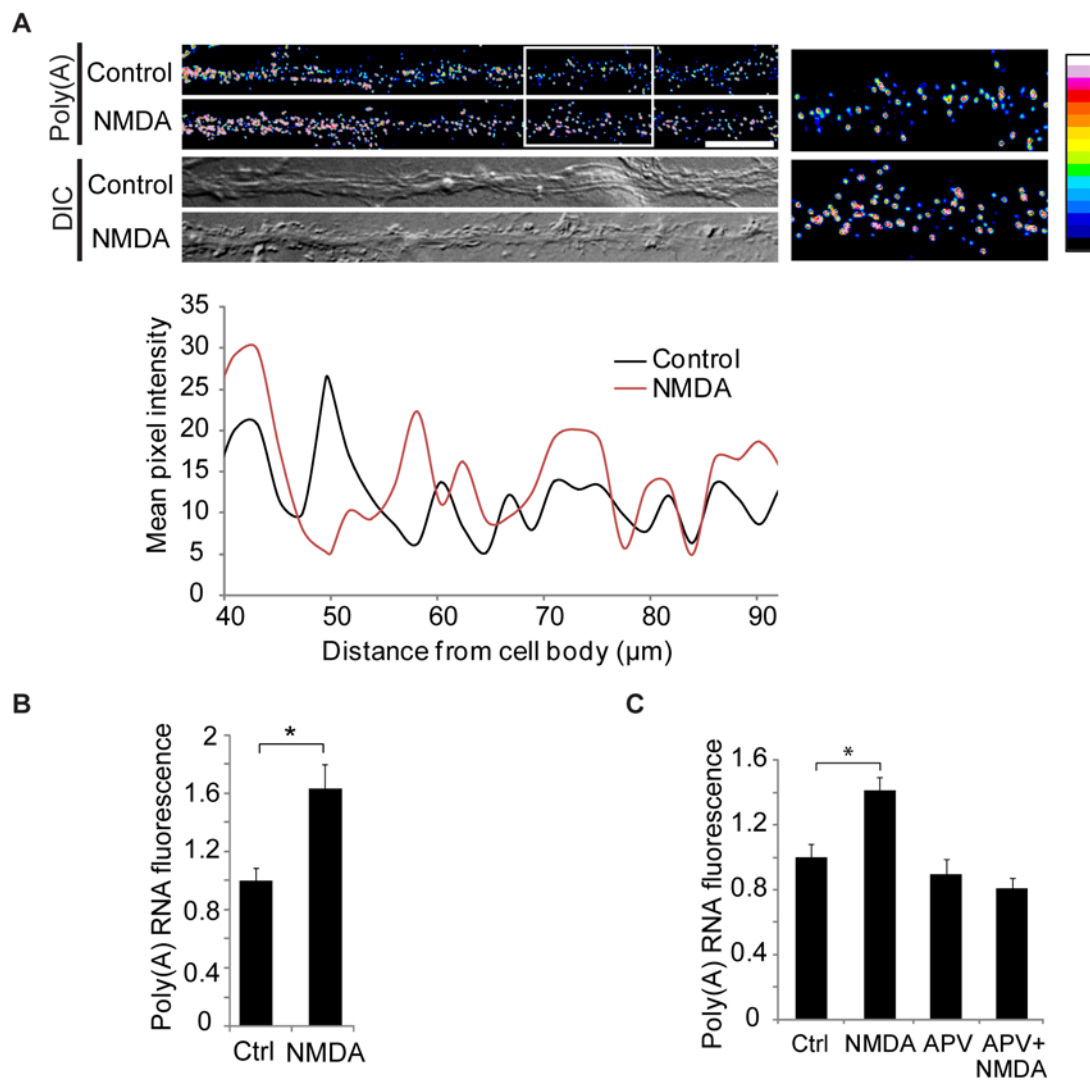
Figure 2.17
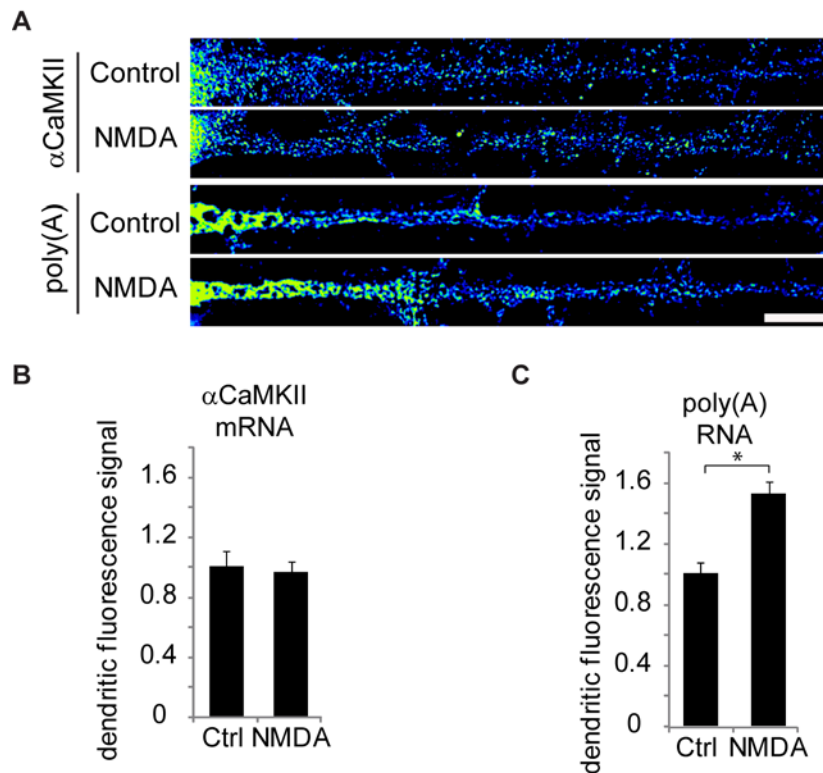
Figure 2.17 Brief NMDA stimulation does not increase dendritic αCaMKII mRNA levels. (A) Control and NMDA-treated hippocampal neurons were processed for αCaMKII and poly(A) FISH. (B,C) Dendritic FISH signals were quantified using ImageJ and the graphed values were normalized to control group mean (αCaMKII: n = 36, Control vs. NMDA, $p = 0.580$; poly(A): n = 40, *$p = 0.001$, Student's t-test).

Figure 2.18
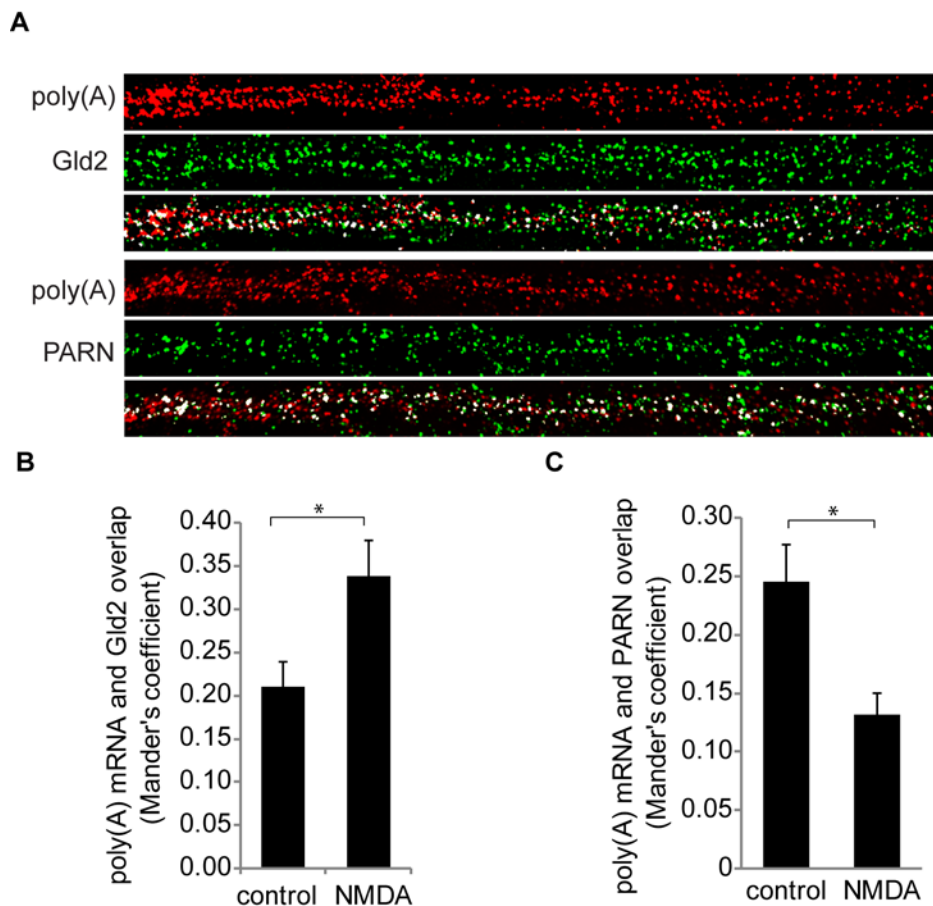
Figure 2.18 NMDA reduces the co-localization of PARN with poly(A) mRNA. (A)
Co-localization analyses were performed on neurons processed for poly(A) FISH and
immunostained for Gld2 or PARN. The images are of control neurons; the scale bar is
10µm and the white signal represents overlapping pixels. (B) Mander's overlap
coefficients for poly(A) RNA co-localized with Gld2 in control and NMDA-treated
neurons were plotted in the histogram (n = 45, Mann-Whitney test, $*p = 0.004$). (C)
Mander's overlap coefficients for poly(A) RNA co-localized with PARN in control and
NMDA-treated neurons were plotted in the histogram (n = 40, Mann-Whitney test, $*p =$
0.001).

Figure 2.19
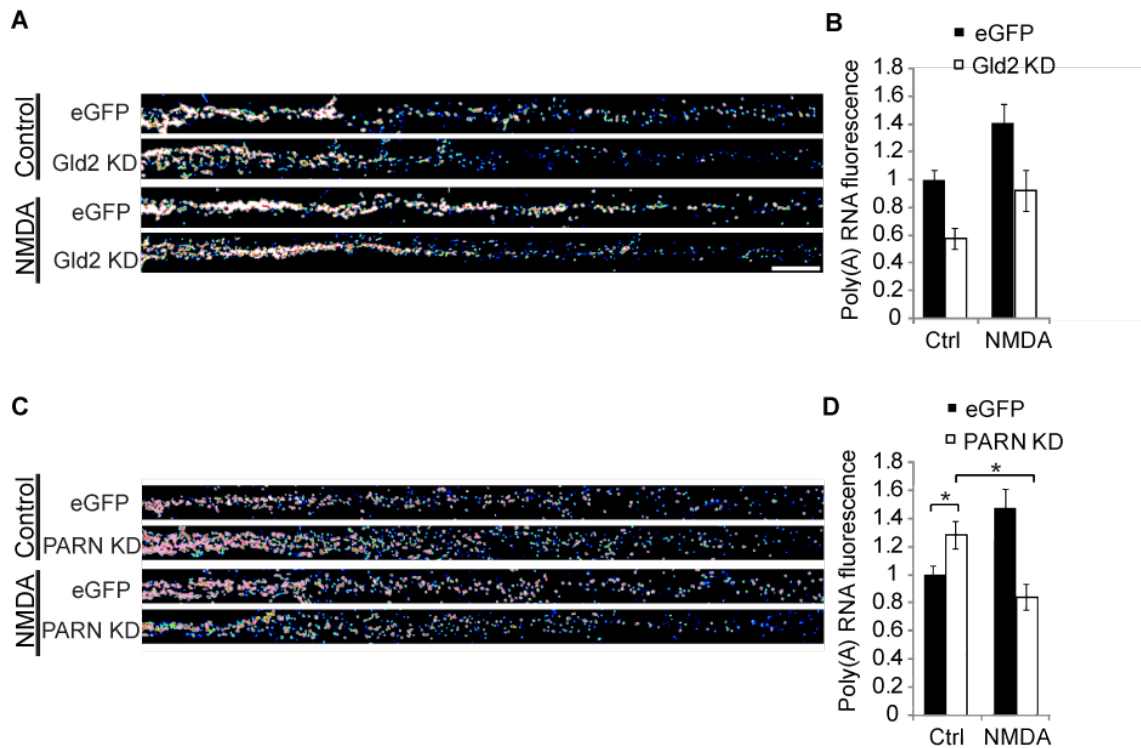
Figure 2.19 Gld2 and PARN bidirectionally regulate dendritic mRNA polyadenylation. (A) Poly(A) FISH was performed on neurons transduced with control or Gld2 shRNA-expressing lentivirus and treated with vehicle or NMDA. (B) Mean poly(A) FISH signals were quantified in distal dendrites, and the graphed values were normalized to the mean of the control group ($n = 50$, two-way ANOVA, main effects: treatment, $p = 0.0061$, and genotype, $p = 0.009$, interaction effect: $p = 0.2733$). (C) Poly(A) FISH was performed on neurons transduced with control or PARN shRNA-expressing lentivirus and treated with vehicle or NMDA. (D) Mean poly(A) FISH signals were quantified in distal dendrites, and the graphed values were normalized to the mean of the control group ($n = 50$, two-way ANOVA, Tukey's test $*p < 0.05$).

Figure 2.20 NMDA-induced dendritic polyadenylation is dependent upon CPEB phosphorylation. (A) 14 *DIV* hippocampal neurons expressing mCherry, mCherry-CPEB-WT, or mCherry-CPEB-AA were treated with vehicle or 100 nM NMDA (30 sec), fixed, and processed for oligo(dT) FISH. (B) Mean oligo(dT) fluorescence intensity was quantified in distal dendritic regions, and all graphed values were normalized to the mean of the CPEB-WT control group (n = 35-40 cells; $*p = 0.045$, $^{+}p = 0.033$, $^{\ddagger}p = 0.003$, $^{\#}p = 0.005$; one-way ANOVA post-hoc Tukey's test). (C) Hippocampal neurons pre-treated with vehicle, KN93 or ZM447473, and then treated with vehicle or NMDA were processed for oligo(dT) FISH. (D) Distal dendritic oligo(dT) FISH intensities were quantified as above, and all graphed values were normalized to the untreated group mean ($n = 35$-40, one-way ANOVA, post-hoc Dunnett's test, $*p = 0.043$).

Figure 2.20
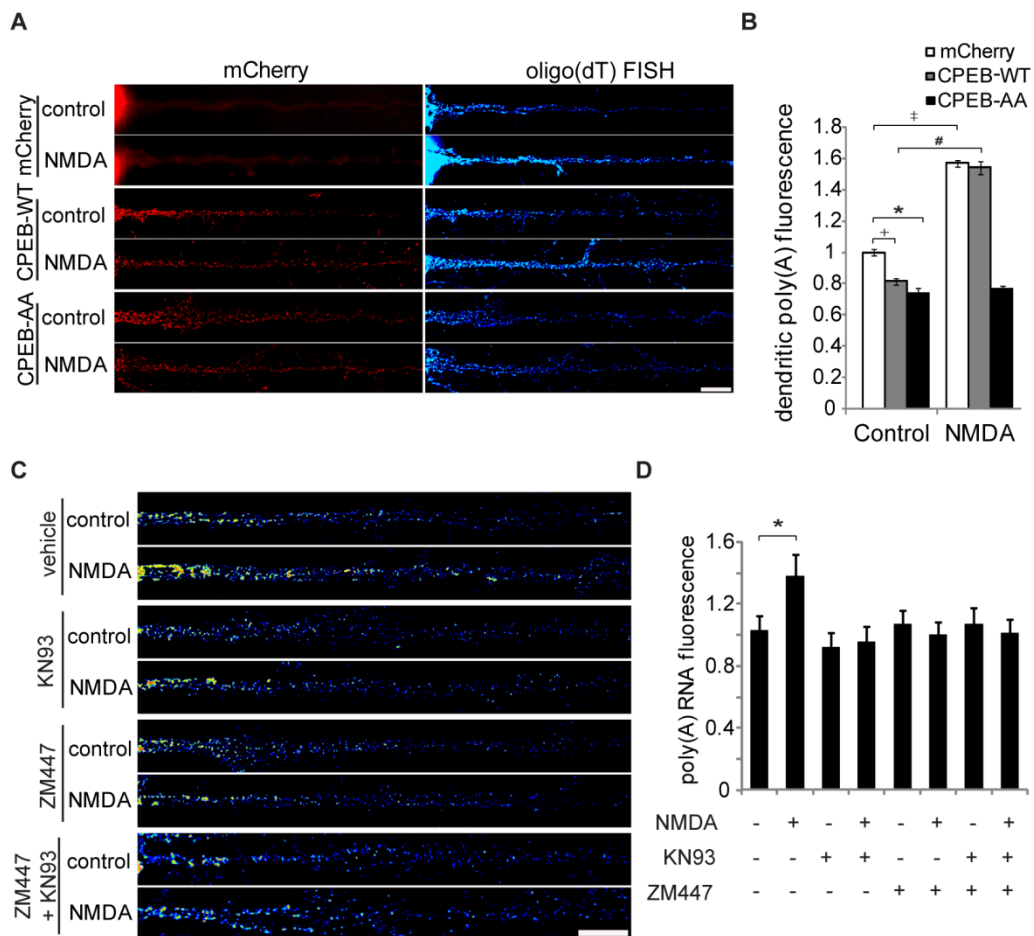
2.3 Discussion

Although CPEB has been previously established as an important regulator of local protein synthesis in neurons, the underlying mechanisms have, until now, been unknown. Herein, the data show that a CPEB-associated polyadenylation complex is localized to dendrites where it is activated by NMDA receptor signaling and controls mRNA polyadenylation. CPEB associates with a complex of translational regulators including the poly(A) polymerase Gld2, deadenylase PARN, and eIF4E binding protein Ngd and regulates their dendritic localization. Gld2 and PARN exert bidirectional control of dendritic poly(A) RNA levels, and NMDA receptor activation leads to mRNA polyadenylation through CPEB phosphorylation and subsequent expulsion of PARN from the mRNP complex. Based on these data, we propose that the CPEB-associated complex represses translation of CPE-containing mRNAs until NMDA receptor activation at synapses, which leads to local CPEB phosphorylation, mRNA polyadenylation and, perhaps, translation initiation.

Polyadenylation of synaptic mRNA transcripts is likely a key mechanism controlling neuron function. In rats, αCaMKII mRNA is polyadenylated in the visual cortex following light-induced neuronal activation (Wu et al., 1998). In Purkinje neurons of the mouse cerebellum, tissue plasminogen activator mRNA is polyadenylated following glutamate stimulation (Shin et al., 2004). In *Aplysia*, actin mRNA is polyadenylated during serotonin-induced long-term facilitation (Liu and Schwartz, 2003; Si et al., 2003a). In each case, neuronal activity leads to an increase in synaptic levels of the respective proteins, suggesting that mRNA polyadenylation leads to an increase in protein synthesis (Liu and Schwartz, 2003; Shin et al., 2004; Si et al., 2003a; Wu et al.,

1998). Furthermore, each of these mRNAs contains CPE sequences in the 3' UTR that regulate mRNA polyadenylation (Huang et al., 2002; Liu and Schwartz, 2003; Shin et al., 2004; Si et al., 2003a; Wells et al., 2001; Wu et al., 1998). In this thesis, it is shown that CPEB, Gld2, and PARN regulate dendritic mRNA polyadenylation in hippocampal neurons. Similar to CPEB, Gld2 and PARN are also expressed in both the visual cortex and the cerebellum, suggesting that these CPEB-associated factors could regulate mRNA polyadenylation in these brain regions as well. A host of other CPE-containing mRNA transcripts also undergo activity-dependent polyadenylation in hippocampal neurons, including AMPA receptor binding protein and MAP2 (Du and Richter, 2005). Thus, it is likely that the CPEB-associated complex regulates the polyadenylation and translation of a specific subset of dendritic mRNAs to mediate effects upon synaptic function.

As shown in this chapter, activity-induced CPEB phosphorylation is required for extrusion of PARN from the mRNP complex and dendritic mRNA polyadenylation. These data provide strong support for the hypothesis that a phosphorylation-dependent mechanism underlies CPEB-mediated translational control. However, concurrent work has suggested that the *Aplysia* CPEB isoform (ApCPEB) functions as a prion-like protein to regulate mRNA translation and long-term facilitation at synapses (Si et al., 2003a; Si et al., 2003b). As of now, it is unclear whether this function is conserved in any other organism. It is unlikely that mammalian CPEB confers prion-like properties as it lacks the extended N-terminal glutamine-rich domain necessary for multimerization. However, it is possible that other mammalian CPEB family members, such as CPEB3 and CPEB4, could be functionally homologous to ApCPEB as these molecules contain an extended glutamine-rich N-terminal region (Theis et al., 2003). Although further work is necessary

to clarify the differing roles of neuronal CPEB across species, it is clear from my work and that of others that CPEB is regulated by a phosphorylation-dependent mechanism in mammalian neurons (Atkins et al., 2005; Atkins et al., 2004; Huang et al., 2002; McEvoy et al., 2007), and that CPEB phosphorylation regulates mRNA polyadenylation.

The signaling cascade leading to CPEB phosphorylation and subsequent polyadenylation has also been a point of contention in the field. In *Xenopus* oocytes, Aurora A kinase catalyzes CPEB phosphorylation; however, in hippocampal neurons, one study suggested that Aurora A is responsible for CPEB phosphorylation (Huang et al., 2002), while another study suggested that CaMKII mediates CPEB phosphorylation and that, at least *in vitro*, Aurora A does not phosphorylate mammalian CPEB (Atkins et al., 2004). In Purkinje neurons, Aurora A kinase-mediated phosphorylation of CPEB regulates LTD expression (McEvoy et al., 2007). Herein, it is demonstrated that inhibitors of both Aurora A kinase and CaMKII block NMDA receptor-mediated CPEB phosphorylation. Since simultaneous application of both inhibitors does not have an additive effect on CPEB phosphorylation, it is possible that Aurora A and CaMKII function in the same signaling pathway. In this regard, it has been shown that neuronal depolarization leads to CaMKII-mediated phosphorylation of glycogen synthase kinase-3-β (GSK-3-β), which inhibits GSK-3 activity (Song et al., 2010). GSK-3 activity inhibits Aurora A kinase-mediated phosphorylation of CPEB in oocytes and astrocytes (Jones et al., 2008; Sarkissian et al., 2004). Thus, it is possible that NMDA receptor signaling activates Aurora A kinase through CaMKII-mediated inhibition of GSK-3, which leads to elevated levels of phosphorylated CPEB.

My data show that the CPEB-associated polyadenylation complex regulates

dendritic mRNA polyadenylation, but it remains unclear how this mechanism might contribute to long-lasting synaptic plasticity. Synaptic modifications are made rapidly but must also be maintained in order to support long-term alterations in synaptic efficacy. αCaMKII mRNA is one established CPEB target that undergoes polyadenylation and is critical for long-term synaptic plasticity. One proposed model for long-term synaptic modification by CPEB is through a positive-feedback mechanism whereby activation of CPEB-mediated polyadenylation leads to increased translation of αCaMKII molecules, which are then incorporated into active CaMKII holoenzymes; thus, leading to further CPEB phosphorylation and translation of αCaMKII (Aslam et al., 2009). One could imagine a similar positive feedback mechanism for any plasticity-related protein that would increase NMDA receptor signaling to the CPEB-associated polyadenylation machinery. Thus, further understanding the regulation and function of CPEB-mediated local protein synthesis will provide insight regarding, not only the importance of mRNA polyadenylation at synapses, but also the newly synthesized proteins necessary for the long-term synaptic modifications underlying synaptic plasticity, learning, and memory.

2.4 Experimental Procedures

Neuron culture and drug treatment

Rat hippocampal neuron cultures were prepared from E18 embryos as described previously (Goslin and Banker, 1998) with the following modifications. Hippocampal neurons were cultured in Neurobasal media (Invitrogen) supplemented with Glutamax (Invitrogen) and NS21 (Chen et al., 2008). For NMDA treatment, hippocampal neurons were treated with 100 nM NMDA (Tocris Bioscience) for 30 seconds. Inhibitors were applied for 30 min prior to NMDA application as follows: 100 nM ZM447473 (Tocris Bioscience), 10 µM KN-93 (Millipore), and 50 µM APV (Tocris Bioscience).

Antibodies

Rabbit polyclonal CPEB, pCPEB (Tay et al., 2003), PARN (Kim and Richter, 2006), Ngd (Jung et al., 2006), and Gld2 antibodies as well as mouse monoclonal symplekin (BD Biosciences) (Kim and Richter, 2006) antibodies were described previously. For immunocytochemistry, the following antibody dilutions were used: rabbit polyclonal anti-CPEB (1:100), goat polyclonal anti-CPEB (1:200, Santa Cruz Biotechnology), anti-pCPEB (1:500), anti-symplekin (1:100), anti-PARN (1:2000), anti-Gld2 (1:100), anti-MAP2 (1:2,000, Sigma Aldrich), anti-synapsin (1: 2,000), anti-Ngd (1:1,000), anti-GluN1 (1:500, BD Biosciences), anti-GluA1 (1:100, Millipore), anti-hnRNP A1 (1:500, gift from Dr. Yue Feng). Secondary antibodies were used at 1:1000; Cy2- and Cy3-conjugated anti-mouse IgG, Cy5-conjugated anti-goat, and Cy5-conjugated anti-rabbit IgG (Jackson Immunoresearch). For immunohistochemistry, antibodies were incubated as follows: rabbit polyclonal anti-CPEB (1:200), anti-Gld2 (1:100), anti-PARN (1:200),

anti-Ngd (1:100), anti-hnRNP A1 (1:200), and mouse monoclonal anti-MAP2 (1:200)

and anti-symplekin (1:100, BD Biosciences). Cy2-conjugated anti-mouse and Cy3-

conjugated anti-rabbit IgG were used at 1:200 (Jackson Immunoresearch). For western

blotting, the following antibody dilutions were used: anti-CPEB (1:2,000), anti-pCPEB

(1:1000), anti-symplekin (1:2000), anti-PARN (1: 2,000), anti-Ngd (1:1000), anti-Gld2

(1:500), anti-PSD-95 (1:2000, Millipore), anti-glial fibrillary acid protein (GFAP, 1:3000,

Millipore), anti-GFP (1:3,000, Clontech), anti-FLAG (1:2000, Sigma Aldrich), and anti-

α-tubulin (1:20,000, Sigma Aldrich).

DNA construction and cell transfection

For expression vectors, CPEB, CPEB-AA (S174A/S180A), and PARN cDNA

were cloned into the pFUGW-GFP lentiviral vector using BsrG1/EcoR1 sites, and Gld2

cDNA was cloned into the pFUGW-GFP using Nde1/EcoR1 to make C-terminal GFP

fusion proteins. Triple FLAG cDNA was constructed and appended to the 5' end of

mCherry cDNA using PCR; the product was flanked with 5' Age1 and 3' BsrG1 sites.

eGFP was removed from pFUGW using the Age1/BsrG1 sites and FLAG-mCherry was

inserted at the same sites. CPEB, CPEB-AA, and PARN were cloned into pFUW-FLAG-

mCherry using the BsrG1/EcoR1 sites. Neuro2A cells and hippocampal neurons were

transfected using Lipofectamine 2000 (Invitrogen) according to the manufacturer's

instructions, except that hippocampal neurons were transfected with 1/5 of the suggested

amounts of DNA and transfection reagent.

Synaptoneurosome preparation

Synaptoneurosomes were prepared from mice at postnatal day 18 - 21 (P18 - P21) as described previously (Hollingsworth et al., 1985; Scheetz et al., 2000). Briefly, the dissected hippocampus was homogenized on ice in 10 volumes of homogenization buffer containing (in mM): 118 NaCl, 4.7 KCl, 1.2 $MgSO_4$, 2.5 $CaCl_2$, 1.53 KH_2PO_4, 212.7 glucose, and 1 DTT, pH 7.4, and supplemented with Complete protease inhibitors (Roche Applied Science). A sample of the total homogenate was removed and kept on ice. The homogenate was passed through three 100 µm nylon mesh filters, followed by one 11 µm filter (MLCWP 047 Millipore) and centrifuged at 1000 x *g* for 10 min. The synaptoneurosome pellets were resuspended in the same buffer. To prepare synaptoneurosomes from cultures, 8-10 million cortical neurons were washed briefly with ice-cold 1x PBS, then scraped in ice-cold homogenization buffer, and processed as described above. Protein concentrations were estimated using the Bradford Protein Assay (BioRad). Samples were boiled in sodium dodecyl sulfate (SDS) sample buffer and processed by SDS-polyacrylamide gel electrophoresis (PAGE).

Co-immunoprecipitation

Neuro2A cells were lysed and immunoprecipitations were performed as described previously (Kim and Richter, 2006). Samples were boiled in SDS sample buffer and processed by SDS-PAGE. Two percent of each lysate was used as the input standard.

Western blotting

Protein samples were transferred from polyacrylamide gels to PVDF membranes, and

then western blotted with antibodies as mentioned above. Densitometry was performed using ImageJ software.

Immunofluorescence and fluorescence in situ hybridization

Mouse brains from male C57BL/6 mice aged postnatal day 21 (P21) and cultured hippocampal neurons were processed for immunofluorescence as described previously (Muddashetty et al., 2007). Fluorescence *in* situ hybridization (FISH) was performed on cultured hippocampal neurons as described (Swanger et al., 2011a).

Lentivirus production and shRNA knockdown

All the knockdown lentiviral constructs were prepared on pLentiLox3.7-Syn (kind gift from M. Sheng). The details of the construction method are available at http://www.sciencegateway.org/protocols/lentivirus/index.htm. Targeting sequences were chosen in the coding region based on the criteria described previously (Naito et al., 2004). Several shRNA sequences against each gene were cloned into the vectors and those showing most effective knockdown were used further. Targeting sequences of each gene used were: Gld2: 5' atgcacaattcaactttca 3', PARN: 5' atgaagaagaacgcaaaa 3', Ngd: 5' gtggagattcgcacggttt 3'. Lentiviruses were produced using the lentiviral vector mentioned above with packaging vectors pSPAX2 and pMD2.G in HEK293T cells. Transfection was performed in 10 or 15 cm dishes in OptiMEM (GIBCO) using Lipofectamine 2000 (Invitrogen) according to the manufacturer's instructions. Three hours after transfection the medium was replaced with DMEM with FBS and the virus-containing medium was collected and filtered two days later.

For knockdown experiments in the cultured neurons, lentiviruses were added to the cultures at 12-14 *DIV* and experiments were conducted 3-4 days later. To measure the level of knockdown, RT-PCR, western blotting, and immunostaining were performed. In the case of Gld2, western blotting was performed using cells transduced with ectopic GFP-tagged Gld2, as the antibody detected nonspecific bands at around the size of endogenous Gld2 by western blotting. Note that this nonspecific signal appears only in western blotting using neuron lysates as Gld2 immunostaining showed significantly lower signal in knockdown neurons compared to control.

Microscopy and image analysis

Coronal brains sections were imaged with a Zeiss (Oberkochen) LSM510 confocal microscope. Images were prepared using Imaris (Bitplane, Inc.). Cultured neurons were imaged with a Nikon TE200 or a Nikon Ti inverted microscope using a 60x 1.4NA Plan Apo objective and a cooled CCD camera (Photometrics). Within each experiment, all treatment groups were imaged with the same acquisition settings and within the same imaging session. Z-series were obtained at 0.15 μm steps. Image stacks were deconvolved using a 3D blind constrained iterative algorithm (AutoQuant, CyberMetrics). Quantification of immunofluorescence and FISH signals were performed using ImageJ. Mean fluorescence intensities were quantified within a cellular region, and mean background fluorescence intensities were quantified from an adjacent, non-cellular region. Dendrites were straightened using the Straighten plugin for ImageJ. Plots of pixel intensity versus distance from the soma were created using ImageJ; mean pixel intensity was quantified in 10 pixel wide line starting at the edge of the soma and extending 100

µm along the dendrite. Quantitative co-localization analysis was performed on volume rendered, 3D-reconstructed distal dendritic regions using Imaris COLOC software (Bitplane, Inc.) as described (Zhang et al., 2006). Co-localized regions were analyzed using automatic thresholds and Mander's overlap coefficients were used to report the degree of overlap (Costes et al., 2004; Manders et al., 1993). To assess protein localization within dendritic spines, Imaris Filament Tracer software was used to build a 3D reconstruction from images of 488-phalloidin (Invitrogen) stained neurons. The background signal was subtracted from the immunostaining in the Cy3 and Cy5 channels. The percentage of spines positive for immunoreactivity was computed using Filament Tracer software. All images shown within a single figure panel are presented with identical threshold settings. The experimenter was blind to treatment and/or group during image acquisition and image analysis.

Statistical analyses

The statistical analyses were performed using PASW 18.0 (IBM). All datasets were evaluated for homogeneity of variances using Levene's test. If Levene's test was significant, the data were transformed using a square root transformation. Normality was assessed for each dataset using the Kolmogorov-Smirnov test. Normally distributed datasets were evaluated with Student's *t*-test for two group comparisons, and an ANOVA and post-hoc pairwise comparisons for 3 or more groups. Non-normal datasets were analyzed using Mann-Whitney test for two groups and Kruskal-Wallis test for 3 or more groups. Alpha was set at 0.05, and all graphs are shown as mean ± standard error of the mean (S.E.M.), unless specified otherwise in the figure legends.

CHAPTER THREE

Gld2 and Neuroguidin bidirectionally regulate dendritic spine morphology and

AMPA receptor surface expression in hippocampal neurons

Parts of this chapter are adapted from:

Udagawa, T.*, Swanger, S.A.*, Takeuchi, K., Kim, J.H., Nalavadi, V., Shin, J., Lorenz, L.J., Zukin, R. S., Bassell, G.J., and Richter, J.D. Bidirectional control of mRNA translation and synaptic plasticity by the cytoplasmic polyadenylation complex. *Mol Cell.* In press. (* equal contribution)

3.1 Introduction

Long-term synaptic plasticity at glutamatergic synapses is mediated by structural and functional alterations. Dendritic spines form the postsynaptic structure at most glutamatergic synapses, and these dynamic dendritic protrusions change in size and shape during synaptic plasticity, learning, and memory (Alvarez and Sabatini, 2007). The morphology of dendritic spines is tightly correlated with synaptic efficacy, postsynaptic density size, and synaptic AMPA receptor number (Harris et al., 1992; Harris and Stevens, 1989). During LTP, there are concurrent increases in dendritic spine size, synapse strength, and GluA1 surface expression; on the other hand, LTD induces a decrease in each of these measures (Kopec et al., 2007; Matsuzaki et al., 2004; Park et al., 2006) (Okamoto et al., 2004; Wang et al., 2007; Yang et al., 2008).

Local protein synthesis has been shown to regulate the functional alterations during synaptic plasticity. Dendritic protein synthesis is necessary for the respective increase and decrease in synaptic strength during BDNF-induced LTP and mGlu-LTD (Huber et al., 2000; Kang and Schuman, 1996). AMPA receptor surface expression has been shown to be directly regulated by local synthesis of GluA1 and GluA2 (Ju et al., 2004; Kacharmina et al., 2000; Sutton et al., 2006). In addition, many locally synthesized proteins such as αCaMKII, PSD95, and Arc/Arg3.1 play critical roles in the modulation or trafficking of AMPA receptors (Chowdhury et al., 2006; Gross et al., 2010; Muddashetty et al., 2007; Nakamoto et al., 2007; Shepherd et al., 2006; Waung et al., 2008). Therefore, the pathways that control local translation are critically linked to synaptic plasticity and AMPA receptor surface expression. While there is no direct evidence connecting dendritic protein synthesis to spine morphology, LTP-induced spine

expansion has been shown to require protein synthesis (Fifkova et al., 1982; Tanaka et al., 2008; Yang et al., 2008). Furthermore, plasticity-inducing stimuli lead to translocation of polyribosomes, mRNA transcripts, mRNA binding proteins, and translation factors into spines (Havik et al., 2003; Ostroff et al., 2002; Smart et al., 2003; Yoshimura et al., 2006; Zhang et al., 2012). Thus, it is plausible that local protein synthesis would regulate dendritic spine morphology in conjunction with synapse strength.

CPEB is one regulator of local protein synthesis that has been shown to regulate synaptic plasticity, neural circuit development, dendritic spine morphology, and learning and memory across the taxonomic system. In mice, CPEB is required for specific types of synaptic plasticity and learning in both the hippocampus and the cerebellum (Alarcon et al., 2004; Berger-Sweeney et al., 2006; McEvoy et al., 2007). Expression of a non-phosphorylatable mutant form of CPEB in Purkinje neurons leads to increased dendritic spine number and length (McEvoy et al., 2007). Altering CPEB expression or activity in the retinotectal system of the *Xenopus laevis* tadpole brain leads to attenuated dendritic growth, reduced synapse strength, and diminished response to visual stimuli (Bestman and Cline, 2008). In *Aplysia californica*, CPEB-dependent protein synthesis regulates serotonin-induced long-term facilitation as well as synapse formation (Si et al., 2003a). Together, these studies suggest that CPEB-mediated mRNA polyadenylation and translation has a critical and conserved function in neurons.

As shown in the previous chapter, an activity-regulated complex of translation factors associates with CPEB at synapses; these factors include the poly(A) polymerase Gld2, the deadenylase PARN, and the eIF4E binding protein neuroguidin (Ngd). Gld2

and PARN bidirectionally regulate dendritic poly(A) RNA levels under unstimulated

conditions. Following NMDA receptor activity, CPEB is phosphorylated resulting in

expulsion of PARN from the mRNP complex and subsequent mRNA polyadenylation in

dendrites. Neuroguidin is an eIF4E binding protein that was previously shown to repress

translation in a CPE-dependent manner (Jung et al., 2006). Interestingly, in *Drosophila*

melanogaster, a homolog of Gld2 is required for long-term memory formation (Kwak et

al., 2008). Based on these findings and the role of CPEB in synaptic plasticity, we

hypothesized that Gld2, PARN, and Ngd also regulate synapse structure and function.

Here, we report that depletion of Gld2 reduced the proportion of mature dendritic spines

and decreased the surface expression of GluA1 in cultured hippocampal neurons, while

depletion of Ngd increased the proportion of mature spines and GluA1 surface

expression. The results of this study suggest a bidirectional mechanism for regulating

dendritic spine structure and synapse strength through post-transcriptional mRNA

regulation.

3.2 Results

3.2.1 CPEB-associated translation factors regulate dendritic spine morphology

To examine whether Gld2, PARN, and Ngd regulate dendritic spine number,

dendritic spine density was assayed following shRNA-mediated depletion of the

individual translation factors. Cultured hippocampal neurons were treated with lentiviral

shRNA against Gld2, PARN, or Ngd, and then transfected with fluorescently-tagged

Lifeact, a small actin-binding peptide, which was used to trace neuron morphology

(Figure 4.1). Dendritic spines were counted and measured with an automated method

using Imaris Filament Tracer (Swanger et al., 2011b). Knockdown of Gld2, PARN, and Ngd each significantly increased dendritic spine density (Figure 4.2A,B), indicating that the cytoplasmic polyadenylation complex regulates dendritic spine formation and, perhaps, synapse formation.

Spine density can increase in response to elevated synaptic stimulation or as a homeostatic response to decreased synaptic activity (Kirov and Harris, 1999). Therefore, how the shRNA manipulations affected hippocampal neuron structure was further investigated by analyzing spine head width and length. Spine head width is positively correlated with AMPA receptor number and postsynaptic density size, and long spines with thin heads are generally associated with weaker synapses compared to short spines with wide heads (Alvarez and Sabatini, 2007; Bourne and Harris, 2007; Bourne and Harris, 2008). Depletion of Gld2 did not affect spine length, but significantly reduced spine head width, suggesting a decrease in synapse size and, possibly, strength (Figure 4.2C,D). PARN depletion increased spine length, but had no effect on spine head width. A concurrent increase in length and decrease in spine head width would suggest the formation of weaker synapses, but a change in spine length alone is difficult to interpret. Ngd knockdown significantly decreased spine length and increased spine width (Figure 4.2C,D), suggesting an increase in synapse size and strength.

As a final measure of how Gld2, PARN, and Ngd depletion affected spine morphology, spines were classified as mushroom, stubby, or thin according to spine length, spine head width, and spine neck width. Mushroom spines are most often associated with mature synapses having large postsynaptic densities, whereas stubby and thin spines are associated with weaker, smaller synapses (Harris et al., 1992; Harris and

Stevens, 1989). Spine classification analysis showed that Gld2 knockdown increased the proportion of immature (stubby-shaped) spines and decreased the incidence of mature (mushroom-shaped) spines, which is indicative of reduced synaptic efficacy. Conversely, Ngd depletion reduced the proportion of immature (thin-shaped) spines and increased the proportion of mature spines suggesting that Ngd knockdown increased synaptic efficacy (Figure 4.2E). PARN knockdown did not significantly alter the incidence within any spine class. Together, these data demonstrate that the CPEB-associated factors regulate synapse number and spine shape. Furthermore, Gld2 and Ngd bidirectionally regulate dendritic spine maturation, which is strongly correlated to synapse strength.

3.2.2 Gld2 and Ngd bidirectionally regulate GluA1 surface expression

Synapse strength is largely regulated by synaptic AMPA receptor content; strong glutamatergic synapses have greater numbers of AMPA receptors as compared to weaker synapses (Malinow and Malenka, 2002). To determine whether Gld2 and Ngd also regulate AMPA receptor surface expression, surface protein biotinylation assays were used to assess the surface levels of the GluA1 subunit of AMPA receptors following shRNA-mediated depletion of Gld2 or Ngd. Gld2 knockdown significantly reduced GluA1 surface expression, whereas Ngd knockdown significantly increased GluA1 expression (Figure 4.3A,B). Total levels of GluA1 were not altered under either knockdown condition. These data indicate that the CPEB-associated translation complex regulates synaptic AMPA receptor content and, perhaps, synapse strength.

Figure 3.1
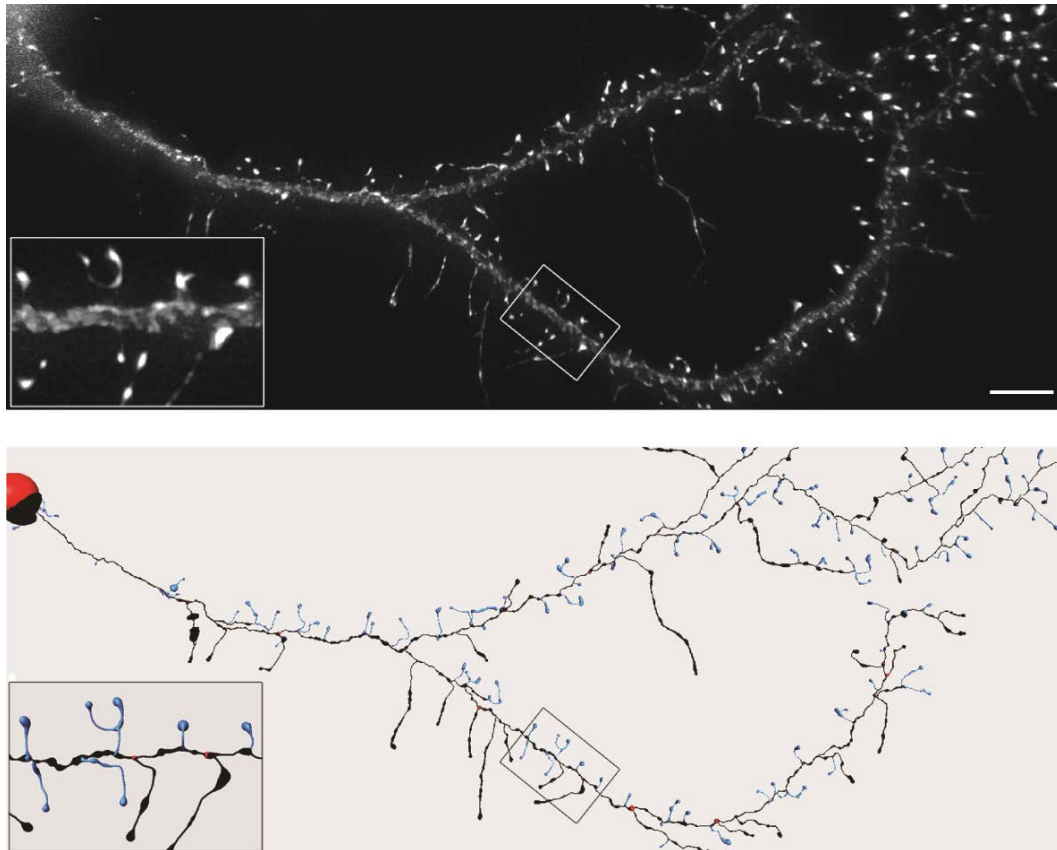
Figure 3.1 Dendritic spines were analyzed in Lifeact transfected neurons. *13 DIV* hippocampal neurons were transduced with lentivirus expressing GFP and shRNA against Gld2, PARN, or Ngd. At *16 DIV*, hippocampal neurons were transfected with Lifeact-RFP (top panel) and fixed 24 hrs later. Imaris Filament Tracer software was used to prepare a trace (bottom panel) of the dendrites (black) and spines (blue) from images of the RFP fluorescence signal.

Figure 3.2 Gld2 and Ngd bidirectionally regulate dendritic spine morphology. (A)

Cultured hippocampal neurons were treated with control, Gld2, PARN, or Ngd shRNA

and transfected with Lifeact-RFP. Images of Lifeact fluorescence are shown and spines

from each class are depicted (stubby: closed arrowheads, mushroom: open arrowheads,

thin: arrows). Scale bar is 5 μm. (B) Spine density was calculated as the number of spines

per 10 μm of dendrite, and groups were compared using the Kruskal-Wallis test (n = 65 -

75 cells; $*p = 0.005$, $\# p = 0.011$, $^{\ddagger} p = 0.003$). (C) Spine length was measured for each

spine, and the cumulative frequency for each group is plotted. Each KD group was

compared to control using the Kolmogorov-Smirnov test ($n = 65$ - 75 cells, 4552 - 5348

spines; Gld2 KD: $p = 0.82$, PARN KD: $p = 0.001$, Ngd KD, $p = 0.004$). (D) The

maximum spine width was measured for each spine, binned as shown on the x-axis, and

graphed as cumulative frequency (Kolmogorov-Smirnov test; $n = 65$ - 75 cells, 4552 -

5348 spines; Gld2 KD, $p = 0.02$, PARN KD, $p = 0.56$, Ngd KD, $p = 0.001$). (E) Spines

were classified as stubby, mushroom, or thin based on their length, head width, and neck

width. Each KD group was compared to the control group using the chi-square test ($* p =$

0.001, $\# p = 0.022$, $^{\ddagger} p = 0.034$).

Figure 3.2
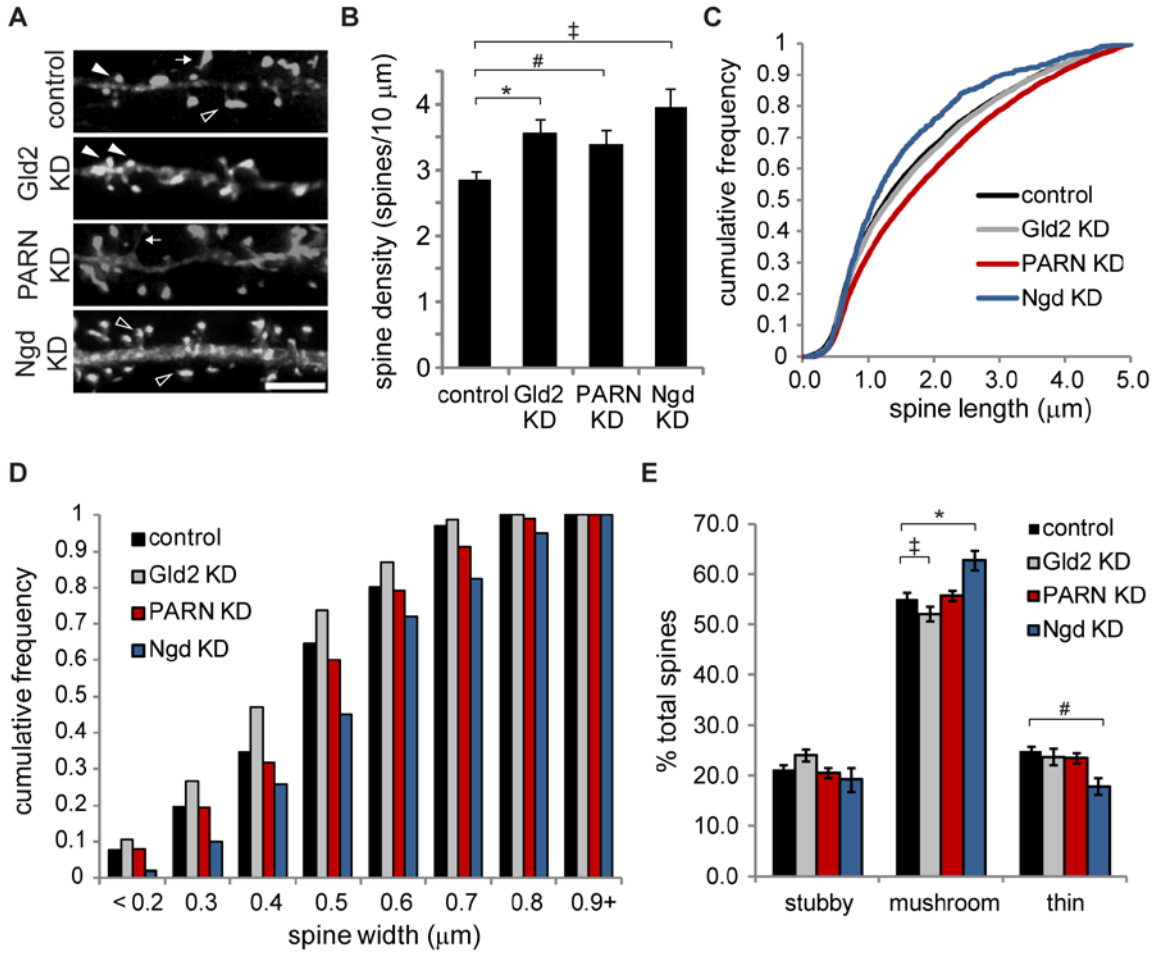
Figure 3.3 Gld2 and Ngd bidirectionally regulate GluA1 surface expression. (A) *14 DIV* hippocampal neurons were transduced with either control (ctrl), Gld2 shRNA, or Ngd shRNA lentivirus particles. After 3-4 days, surface proteins were biotinylated under ice-cold conditions and precipitated using Neutravidin-conjugated beads. Surface protein precipitates and total lysates were processed for western blotting with anti-GluA1 and anti-α-tubulin antibodies. (B) Surface GluA1 levels were determined by densitometry of western blots. Surface GluA1 levels were normalized to total GluA1 levels, and α-tubulin was used as a loading control for total lysates. Control and KD levels were compared using Student's t-test, and the graphed values were normalized to the control group mean (n = 6, * $p = 0.022$, # $p = 0.029$). (C) Total GluA1 levels were determined by densitometry and normalized to the α-tubulin levels. Control and KD levels were compared using Student's t-test, and the graphed values were normalized to the control group mean (n = 6, ctrl vs. Gld2 KD $p = 0.583$, ctrl vs. Ngd KD $p = 0.467$).

Figure 3.3
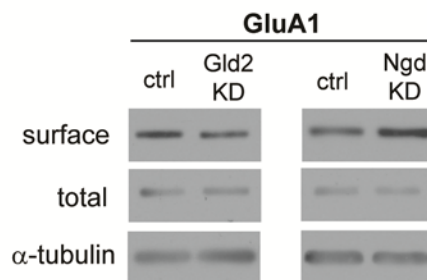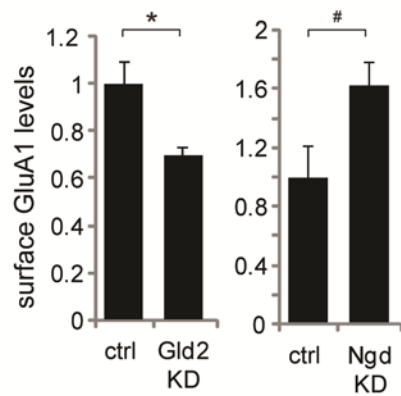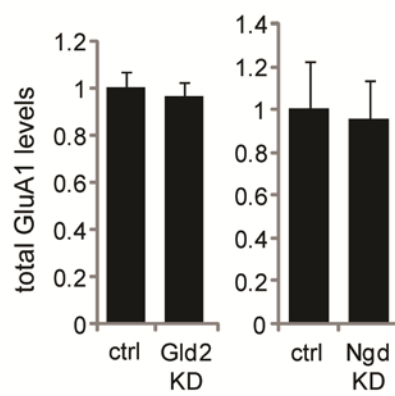
3.3 Discussion

In this study, we have shown that the CPEB-associated factors Gld2 and Ngd bidirectionally regulate synapse structure and AMPA receptor surface expression. Gld2 depletion from hippocampal neurons decreased dendritic spine size and AMPA receptor surface expression, while Ngd depletion enhanced dendritic spine size and AMPA receptor surface expression. In parallel, my collaborators tested whether depletion of these CPEB-associated factors regulated theta burst stimulation-induced LTP (TBS-LTP) in the dentate gyrus. Indeed, Gld2 depletion attenuated protein synthesis-dependent TBS-LTP, whereas Ngd depletion enhanced TBS-LTP (Udagawa et al., in press). Together, these complementary studies reveal that these CPEB-associated translational regulators control synaptic structure, receptor expression, and plasticity in a bidirectional manner.

Depletion of Gld2 had an overall inhibitory effect on synapse efficacy as shown by the immature dendritic spine morphology, reduced AMPA receptor surface expression, and attenuated TBS-LTP (Udagawa et al., in press). These findings suggest that Gld2 activity is important for maintaining synapse strength and for synapse potentiation. Consistent with this assertion, the expression of a dominant-negative form of Gld2 inhibits long-term memory formation in *Drosophila* (Kwak et al., 2008). Similarly, CPEB has previously been shown to regulate dendritic spine morphology, synapse strength, and synaptic plasticity (Alarcon et al., 2004; Bestman and Cline, 2008; McEvoy et al., 2007; Zearfoss et al., 2008). In this thesis, it was shown that CPEB co-localizes with Gld2 at synapses, but the role of CPEB in the Gld2-mediated regulation of synapse structure and function is not clear. Gld2 has no RNA binding activity, so in order to regulate mRNA polyadenylation it must interact with an RNA binding protein such as

CPEB. While our studies indicate that Gld2 and CPEB likely regulate synapse structure and function as part of a polyadenylation complex, Gld2 could mediate its synaptic effects through other RNA binding proteins as well. In this regard, Gld2 does interact with Gld3 and RNP8 in *C. elegans*, and, by binding to different mRNAs, these proteins employ Gld2 to antagonize one another and propel cells down different lineages (Kim et al. 2009). In the mammalian brain, Gld2 is only known to interact with CPEB, but one could envision how Gld2 might interact with different RNA binding proteins, and thus, activate different mRNAs in a synaptic stimulation-dependent manner.

Depletion of Ngd from hippocampal neurons resulted in dendritic spine maturation, increased AMPA receptor surface expression, and enhanced TBS-LTP (Udagawa et al., in press), suggesting that Ngd functions to repress synapse strength and potentiation. Ngd has previously been shown to be important for neural tube closure and neural crest cell migration in developing *Xenopus* embryos (Jung et al., 2006). Our work is the first to elucidate a role for Ngd in the mammalian nervous system. The only known interacting partners for Ngd are CPEB and eIF4E, thus we propose that one mechanism by which Ngd regulates synapse structure and function is by repressing the translation of CPE-containing mRNAs. However, it remains unclear whether CPEB is necessary for the interaction of Ngd with eIF4E, so it is possible that Ngd blocks translation initiation of other mRNAs as well.

As shown in the previous chapter, NMDA treatment of hippocampal neurons causes PARN expulsion from the CPEB-containing RNP complex and PARN regulates dendritic mRNA polyadenylation. These observations suggest that PARN might play a critical role in dendritic translation and possibly synapse structure and function.

However, PARN knockdown has only a modest affect on synaptic spine morphology in cultured neurons and no significant effect on TBS-evoked LTP in the dentate gyrus (Udagawa et al., in press). It is possible that the loss of PARN may not have been sufficient to overcome other negative regulators of translation in the same RNP complexes, such as Ngd. Alternatively, PARN might control the deadenylation of mRNAs when LTP is induced by different stimulation protocols, or in response to stimuli that evoke LTD. Nevertheless, PARN depletion did significantly increase spine number and length, which are two important morphological properties that regulate neuron function. This study is the first to investigate the function of PARN in the brain, and thus much further work is necessary to clarify the synaptic role of this deadenylase.

Based on our findings, we propose a model whereby CPEB and its associated regulatory factors assemble in an RNP with CPE-containing mRNAs and are transported to dendrites. In this RNP, Ngd functions to repress translation and synapse potentiation. Upon synapse activation, the RNP becomes de-repressed allowing for Gld2-mediated polyadenylation and translation initiation, which facilitates potentiation of synapse strength. The synaptic localization of these factors suggests that the bidirectional control mechanism described here likely mediates activity-induced local protein synthesis. However, it cannot be ruled out that somatic translational regulation by these factors contributes to the observed effects on synapse structure and function. In the future, it will be interesting to determine whether Gld2 and Ngd also regulate activity-induced changes in dendritic spine morphology and AMPA receptor surface expression.

Another remaining question is which mRNA targets of the CPEB-associated complex are regulated at synapses and contribute to activity-induced synaptic

modifications. It is conceivable that local protein synthesis of structural components could play an important role in regulating activity-induced structural plasticity. MAP2 mRNA is a CPE-containing dendritic mRNA that undergoes activity-induced polyadenylation and translation in synaptic fractions (Du and Richter, 2005; Huang et al., 2003). MAP2 stabilizes microtubules and is regulated by activity in dendritic spines (Quinlan and Halpain, 1996). Moreover, microtubules modulate dendritic spine formation and maturation (Dent et al., 2011). Thus, MAP2 is one interesting candidate that could contribute to the regulation of synapse structure and function by the CPEB-associated translational complex. Local synthesis of plasticity-related signaling molecules, neurotransmitter receptors, and scaffolding proteins could also contribute to structural and functional synaptic plasticity. Some candidate CPE-containing mRNAs are αCaMKII, calmodulin, AMPA receptor binding protein, tissue plasminogen activator, and BDNF (Du and Richter, 2005; Oe and Yoneda, 2010; Shin et al., 2004). Identifying the locally synthesized proteins regulated by the CPEB-associated complex will be integral to understanding how local protein synthesis controls synapse structure and function.

3.4 Experimental Procedures

Hippocampal neuron culture

Rat hippocampal neuron cultures were prepared from E18 embryos as described

previously (Goslin and Banker, 1998) with the following modifications. Neurons were

cultured in Neurobasal media supplemented with Glutamax and NS21 (Chen et al.,

2008). Neurons used for imaging were plated at low density on poly-L-lysine coated

coverslips, and neurons used for biotinylation experiments were plated at high density on

poly-L-lysine-coated tissue culture plastic dishes.

Lentiviral shRNA knockdown

All the shRNA lentiviral constructs were prepared on pLentiLox3.7-Syn. The targeting

sequences for each gene are as follows: Gld2: 5' atgcacaattcaactttca 3', PARN: 5'

atgaagaagaacgcaaaa 3', Ngd: 5' gtggagattcgcacggttt 3'. Lentiviruses were produced using

the lentiviral vector mentioned above with packaging vectors pSPAX2 and pMD2.G in

HEK293T cells. Transfection was performed in 10 or 15 cm dishes in OptiMEM

(GIBCO) using Lipofectamine 2000 (Invitrogen) according to the manufacturer's

instructions. Three hours after transfection the medium was replaced with DMEM with

FBS and the virus-containing medium was collected and filtered two days later (provided

by J.D. Richter). For knockdown experiments in cultured neurons, lentiviruses were

added to the cultures at 13 *DIV* and experiments were conducted 3-4 days later. To

measure the level of knockdown, RT-PCR, western blotting, and immunostaining were

performed.

DNA transfection

Hippocampal neurons were transfected with Lifeact, a 17 amino acid peptide

(MGVADLIKKFESISKEE), fused to C-terminal RFP (Riedl et al., 2008; Riedl et al.,

2010) at 16 *DIV* using the calcium phosphate transfection method (the Lifeact construct

was kindly provided by Dr. Roland Wedlich-Soeldner). After 24 hours, the neurons were

fixed and the coverslips were mounted on slides using propyl gallate-containing media.

Fluorescence imaging and dendritic spine analysis

Cultured neurons were imaged with a Nikon Ti inverted microscope using a 60x 1.4NA

Plan Apo objective and a cooled CCD camera (Photometrics). Within each experiment,

all treatment groups were imaged with the same acquisition settings and within the same

imaging session. Z-series were obtained at 0.15 μm steps. Image stacks were

deconvolved using a 3D blind constrained iterative algorithm (AutoQuant,

CyberMetrics). Spine morphology and density were analyzed using Imaris Filament

Tracer (Bitplane, Inc.) as described in Appendix A.1 (Swanger et al., 2011b). Spine

classifications were as follows: stubby spines = length $\leq$ 1μm; mushroom spines = length

$\leq$ 3μm, end point diameter/minimum diameter $\geq$ 1.5μm; long, thin spines = length $\leq$ 5μm,

endpoint diameter/minimum diameter $\leq$ 1.5μm. The experimenter was blind to conditions

during imaging and image analysis.

Receptor biotinylation and western blotting

Surface protein biotinylation was performed as previous described (Ehlers, 2000).

Briefly, high density 17 *DIV* hippocampal neuron cultures were placed on ice and rinsed

twice with ice-cold PBS containing 1 mM $MgCl_2$ and 0.01 mM $CaCl_2$, then incubated on

ice with the PBS solution containing 1 mg/ml Sulfo-NHS-Biotin (Thermo Scientific) for

20 minutes. Cultures were then rinsed 3 times with PBS solution containing 50 mM

glycine to quench the biotin reactivity. Neurons were scraped in ice-cold lysis buffer (150

mM NaCl, 50 mM Tris, 50 mM NaF, 1 mM EDTA, 1 mM EGTA, 1% Triton, 0.2% SDS,

and protease inhibitors), then sonicated and centrifuged for 15 minutes. Supernatants

were added to Neutravidin beads and rotated at 4ºC for 2 hours, then washed 4 times with

lysis buffer; 2% of the supernatant volume was kept for SDS-PAGE analysis. Laemmli

buffer was added to the samples, and they were boiled for 5 minutes, followed by SDS-

PAGE and western blotting. The following antibodies were used: anti-GluR1 (1:2000,

Millipore) and anti-α-tubulin (1:20,000, Sigma Aldrich).

Statistical analysis

Statistical analyses were completed using PASW 18.0 statistical software (IBM). All

datasets were analyzed for equal variances using Levene's test and normality using the

Kolmogorov-Smirnov test. Non-normal datasets were analyzed using the Kruskal Wallis

test for multiple group comparisons, and normal datasets were analyzed using either a

one-way ANOVA or Student's t-test. Cumulative distributions were compared using the

Kolmogorov-Smirnov test. Alpha was set at 0.05, and Bonferroni corrections were

applied when multiple comparisons were made within a single dataset.

CHAPTER FOUR

CPEB and associated translation factors regulate activity-induced dendritic

GluN2A mRNA translation and NMDA receptor membrane insertion

4.1 Introduction

Long-term synaptic plasticity is the best understood molecular mechanism underlying learning and memory in the brain. Some forms of long-lasting synaptic plasticity, such as BDNF-induced LTP and mGlu-dependent LTD, require the rapid synthesis of new proteins within dendrites (Huber et al., 2000; Kang and Schuman, 1996). Locally synthesized synaptic proteins likely contribute to the synaptic modifications that mediate these forms of synaptic plasticity (Steward and Schuman, 2001; Sutton and Schuman, 2006). For example, the local translation of αCaMKII was shown to be critical for hippocampal LTP and memory consolidation in mice (Miller et al., 2002). Also, the endocytosis of AMPA receptors is critical for mGlu-LTD and is dependent on the rapid synthesis of Arc/Arg3.1, a locally synthesized protein that interacts with the endocytic machinery (Chowdhury et al., 2006; Rial Verde et al., 2006; Waung et al., 2008). However, in these cases, the detailed mechanism and translation factors governing the activity-induced translation were not investigated. Identifying the functions of newly synthesized proteins and the mechanisms underlying their local synthesis is critical for understanding how experience induces changes at individual synapses.

As shown in this thesis, the CPEB-associated poly(A) polymerase Gld2 regulates dendritic poly(A) RNA levels (Figure 2.19), dendritic spine morphology (Figure 3.2), and surface expression of AMPA receptors (Figure 3.3). In addition, my collaborators have shown that Gld2 regulates theta-burst LTP in the hippocampus (Udagawa et al., in press). To better understand how Gld2 activity regulates these processes, my collaborators performed a screen for mRNA transcripts whose poly(A) tail is regulated by Gld2.

Following Gld2 knockdown in hippocampal neurons, mRNA was fractionated using thermal elution from poly(U)-Sepharose columns and analyzed by microarray (Figure 4.1A) (Du and Richter, 2005; Simon et al., 1996; Udagawa et al., in press). Approximately 100 mRNAs showed reduced poly(A) tail length as a result of Gld2 knockdown in the microarray analysis (Figure 4.1B), and five were selected and validated by qRT-PCR (Figure 4.1C). One mRNA that was validated as having a shortened poly(A) tail following Gld2 knockdown was GluN2A, an NMDA receptor subunit. Although Gld2 likely influences neuron function by regulating many mRNAs, the post-transcriptional regulation of GluN2A mRNA was focused upon because of the critical role of NMDA receptors in synaptic plasticity.

NMDA receptors are tetrameric glutamate-gated ion channels and are usually composed of two GluN1 subunits and two GluN2 subunits (Traynelis et al., 2010). GluN2A and GluN2B are the predominate GluN2 subunits expressed in hippocampal pyramidal neurons, and they differentially regulate NMDA receptor channel properties, protein interactions, and trafficking (Lau and Zukin, 2007). The expression of NMDA receptor subunits are differentially regulated in both development and synaptic plasticity. GluN2B expression is high early in development, and GluN2A is expressed in an activity-dependent manner later during development (Yashiro and Philpot, 2008). During plasticity, the insertion and expression of GluN2A and GluN2B are tightly regulated (Bellone and Nicoll, 2007; Sobczyk and Svoboda, 2007). Specifically, LTP induction in the hippocampus increases GluN2A expression (Williams et al., 2003; Williams et al., 1998; Zhong et al., 2006b), and LTP has been shown to increase the surface expression of GluN2A-containing NMDA receptors in adult CA1 pyramidal neurons (Grosshans et al.,

2002). Furthermore, sensory activation in the visual cortex increases the expression of GluN2A, which is dependent on protein synthesis (Philpot et al., 2007; Quinlan et al., 1999). Interestingly, NMDA receptor activity blocks the translation of GluN2B protein (Chen and Bear, 2007). NMDA receptors are critical regulators of LTP induction, but they also contribute to LTP expression. NMDA receptor insertion underlies LTP expression at mossy fiber-CA3 synapses in the hippocampus (Kwon and Castillo, 2008; Rebola et al., 2008), and the NMDA receptor component of excitatory postsynaptic potentials is increased during LTP at Schaffer collateral-CA1 synapses (Peng et al., 2010). Interestingly, this increase was shown to be mediated by NR2A-containing receptors, suggesting that activity-induced expression of GluN2A might regulate the inciting plasticity event as well as future synaptic activation.

Given these reports and our finding that Gld2 regulates GluN2A mRNA polyadenylation, we hypothesized that the CPEB-associated polyadenylation complex locally regulates GluN2A mRNA and NMDA receptor expression at synapses. While several studies have shown that GluN1 mRNA is localized to dendrites (Benson, 1997; Gazzaley et al., 1997; Miyashiro et al., 1994), it remains unclear whether any other NMDA receptor subunit mRNA is also asymmetrically localized in neurons. Here, it is demonstrated that GluN2A mRNA is localized to hippocampal neuron dendrites *in vivo* and *in vitro*. Moreover, CPEB interacted with GluN2A mRNA and regulated its dendritic transport. In addition, chemical LTP increased the surface expression of GluN2A-containing NMDA receptors in a protein synthesis-dependent manner, and the synthesis and insertion of GluN2A was bidirectionally regulated by the CPEB-associated translation factors Gld2 and Ngd. Finally, the 3' UTR of GluN2A mRNA mediated

dendritic protein synthesis in a CPE-dependent manner. These findings indicate that

CPEB-mediated post-transcriptional regulation of GluN2A mRNA is a novel mechanism

for regulating NMDA receptor expression during synaptic plasticity.

Figure 4.1 Identification of mRNAs whose polyadenylation is controlled by Gld2.

(A) Cultured hippocampal neurons were transduced with control or Gld2 shRNA-expressing lentivirus for 4 days, and then RNA was extracted. A portion of the sample was used for microarray analysis (total) while the remainder was applied to poly(U) Sepharose, followed by washing, elution at 65°C, and microarray analysis (poly(A)). RNAs eluting at $50°C$ have poly(A) tails ~50 nucleotides, while $65°C$ eluates contain only RNAs with longer poly(A) tails. All analyses were performed with two biologic replicates. (B) Venn diagram showing that, upon Gld2 knockdown, 25 and 124 mRNAs were significantly reduced in total and poly(A) RNA ($65°C$ eluates) fractions, respectively. Among them, 22 mRNAs were detected in both samples. (C) Selected mRNAs were examined by qRT-PCR using gene specific primers; the mRNA levels in the Gld2 knockdown samples (total and poly(A) fraction) were normalized to the control levels (adapted from Udagawa, et al., in press).

Figure 4.1
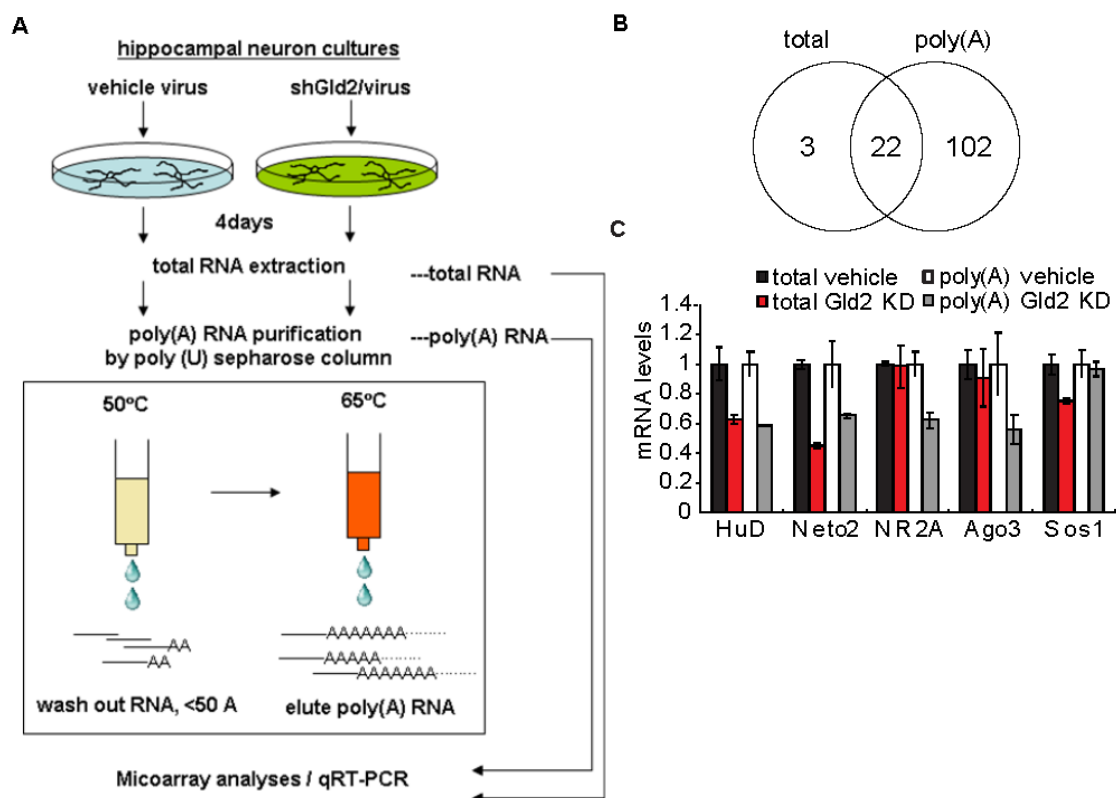
4.2 Results

4.2.1 CPEB interacts with GluN2A mRNA

My collaborators discovered that Gld2 depletion reduced the poly(A) tail length of GluN2A mRNA (Figure 4.1), but Gld2 must be tethered to mRNA through an RNA binding protein in order to exert its poly(A) polymerase activity. As shown in this thesis, Gld2 interacts with the RNA binding protein CPEB (Figure 2.6), and both Gld2 and CPEB localize to synapses (Figures 2.2 and 2.7). Therefore, we examined whether CPEB interacts with GluN2A mRNA. Importantly, GluN2A mRNA contains a CPE sequence in the 3' UTR, and this sequence is conserved across species (Figure 4.2A). To determine if CPEB associates with GluN2A mRNA, FLAG-tagged CPEB was immunoprecipitated from hippocampal neuron lysates and mRNA levels in the precipitates were quantified using real-time PCR. GluN2A mRNA was significantly enriched in FLAG-CPEB immunoprecipitates as compared to FLAG-mCherry control immunoprecipitates, whereas the non-CPE containing mRNAs γ-actin and GluN1 were not (Figure 4.2B). The established CPEB target mRNA αCaMKII served as a positive control (Wu et al., 1998) and was also significantly enriched in the FLAG-CPEB precipitates compared to control.

To determine whether the CPE sequence within the GluN2A 3' UTR mediates this interaction, constructs were generated to encode GFP appended to either the native 933 nucleotide sequence at the 3' end of the rat GluN2A 3' UTR or the same sequence with the CPE mutated (Figure 4.2C). These constructs were transfected into neuroblastoma cells along with either FLAG-tagged CPEB or FLAG and immunoprecipitated using FLAG antibodies. Quantitative real-time PCR using GFP-specific primers demonstrated that the GluN2A 3' UTR mRNA was significantly enriched in FLAG-CPEB

immunoprecipitates compared to control precipitates. However, the mRNA containing a

mutated CPE sequence was not significantly enriched, and neither was the non-CPE

containing 3' UTR of β-actin mRNA. Taken together, these data demonstrate that CPEB

associates with GluN2A mRNA and that the CPE sequence within the 3' UTR is required

for this interaction.

4.2.2 GluN2A mRNA is localized to dendrites

CPEB has been shown to localize to dendrites, and it has been shown in this thesis

that the CPEB-associated translational regulators Gld2 and Ngd are localized to dendrites

(Figures 2.2 and 2.5). To begin to examine whether GluN2A mRNA could be regulated

by this complex within dendrites, the subcellular localization of GluN2A mRNA was

analyzed using FISH on mouse brain sections and cultured hippocampal neurons.

GluN2A mRNA was localized to distal dendritic compartments of cortical neurons and

hippocampal CA1 neurons *in vivo*, whereas β-tubulin mRNA, a non-dendritic transcript,

was restricted to the cell body and proximal dendrites (Figure 4.3A,B). GluN2A sense

sequence probes showed negligible FISH signal on mouse brain sections. FISH on

cultured hippocampal neurons confirmed the dendritic localization of GluN2A mRNA

(Figure 4.4). The ratio of dendrite to soma FISH fluorescence for GluN2A mRNA was

similar to αCaMKII and PSD95 mRNAs, two known dendritic mRNAs (Muddashetty et

al., 2007), and significantly greater than that of β-tubulin mRNA. GluN2A sense and

scramble sequence probes showed negligible signal. Taken together, these data indicate

that GluN2A mRNA is localized to dendrites, which suggests that it could be translated

locally at synapses.

4.2.3 CPEB and the CPE sequence regulate dendritic localization of GluN2A mRNA

CPEB has been shown to interact with microtubule motors, and the CPE sequence is sufficient to localize mRNA to dendrites (Huang et al., 2003). To determine whether CPEB regulates the dendritic localization of GluN2A mRNA, hippocampal neurons were transduced with lentiviral shRNA against CPEB (knockdown shown in Figure 2.8) and processed for GluN2A mRNA FISH. Depletion of CPEB resulted in a 50% decrease in the number of dendritic GluN2A mRNA granules compared to control (Figure 4.5), suggesting that CPEB indeed regulates the dendritic transport of GluN2A mRNA.

Next, we examined whether the 3' UTR of GluN2A mRNA was sufficient to localize mRNA to dendrites, and if so, whether the CPE sequence was required for dendritic mRNA localization. To do so, hippocampal neurons were transfected with GFP alone or GFP constructs harboring either the native GluN2A 3' UTR, ΔCPE-GluN2A 3' UTR, or β-actin 3' UTR sequences used above (see Figure 4.3C), then fixed and processed for GFP mRNA FISH (Figure 4.6A). The β-actin 3' UTR and the GFP only constructs were used as positive and negative controls for dendritic localization, respectively. Quantification of a ratio between dendritic and somatic fluorescence signals revealed that the GluN2A 3' UTR targeted GFP mRNA to dendrites at a level similar to the β-actin 3' UTR and resulted in significantly more dendritic GFP FISH signal than GFP alone (Figure 4.6B). The ΔCPE-GluN2A 3' UTR did not target GFP mRNA to distal dendrites, suggesting that the CPE sequence is required for the 3' UTR-mediated dendritic localization of GluN2A mRNA.

4.2.4 Gld2 and Ngd bidirectionally regulate dendritic GluN2A protein expression

As shown in the previous chapter, the CPEB-associated translation factors Gld2 and Ngd bidirectionally regulate dendritic spine morphology (Figure 3.2) and AMPA receptor surface expression (Figure 3.3). Given that GluN2A mRNA is bound by CPEB, we sought to determine if Gld2 and Ngd regulated the expression of GluN2A protein in hippocampal neurons. Upon Gld2 knockdown in hippocampal neurons, total GluN2A protein levels decreased by 31% as evaluated by western blotting (Figure 4.7A). In addition, the dendritic GluN2A protein levels were decreased by approximately 20% following Gld2 knockdown, whereas the NMDA receptor subunit GluN1 protein levels were unaffected (Figure 4.7B,C). Conversely, the depletion of Ngd resulted in a 40% increase in total GluN2A protein levels (Figure 4.8A). Tubulin protein levels were not affected, but expression of GluN1 increased by approximately 20%. Dendritic GluN2A protein levels were increased by 30% following Ngd knockdown, while dendritic GluN1 levels were not changed (Figure 4.8B,C). Together, these data indicate that Gld2 and Ngd bidirectionally regulate GluN2A protein levels in dendrites of hippocampal neurons.

4.2.5 Gld2 and Ngd bidirectionally regulate the surface expression of GluN2A-containing NMDA receptors

The functional location for NMDA receptors is at the cell surface. To determine whether reducing Gld2 or Ngd levels affected NMDA receptor surface expression, surface biotinylation assays were performed on cultured hippocampal neurons following Gld2 or Ngd knockdown. GluN1, GluN2A, and GluN2B protein levels were analyzed as these are the major NMDA receptors subunits expressed in hippocampal pyramidal

neurons (Figure 4.9A). Gld2 depletion reduced GluN2A surface levels by 64% and GluN1 surface levels by 36%, but GluN2B surface levels were not significantly altered by Gld2 knockdown (Figure 4.9B). Thus, Gld2 depletion significantly reduced the ratio of surface GluN2A/GluN2B protein levels. Gld2 depletion significantly reduced total GluN2A protein levels; whereas, total GluN2B levels were significantly increased following Gld2 KD, and total GluN1 levels were not significantly altered (Figure 4.9C). The depletion of Ngd from hippocampal neurons increased GluN2A surface expression by 83% and increased GluN1 surface expression by 34%, whereas Ngd knockdown did not alter GluN2B surface levels (Figure 4.10A,B). In addition, the ratio of GluN2A/GluN2B surface protein levels was increased following Ngd depletion. The total levels for GluN2A and GluN1 were also increased, but total GluN2B levels were not significantly changed (Figure 4.10C). Together, these data demonstrate that Gld2 and Ngd regulate the total and surface expression of GluN2A and suggest that Gld2 and Ngd bidirectionally control surface NMDA receptor expression as well as the ratio of surface GluN2A- and GluN2B-containing NMDA receptors.

4.2.6 Chemical LTP induces a protein synthesis-dependent increase in GluN2A-containing NMDA receptor surface expression

NMDA receptors are dynamically regulated at synapses following activity, and several studies have shown that GluN2A protein expression is increased during LTP in the hippocampus (Grosshans et al., 2002; Philpot et al., 2007; Williams et al., 2003; Williams et al., 1998; Zhong et al., 2006b). We sought to elicit a similar LTP-induced increase in GluN2A expression in cultured hippocampal neurons. To do so, we used an

established NMDA receptor-dependent chemical LTP paradigm that is induced by treating hippocampal neurons with glycine (200 µM) for 3 minutes (Lu et al., 2001). Chemical LTP increased dendritic GluN2A expression by 39%, and this increase was blocked by incubation with the protein synthesis inhibitor anisomycin (Figure 4.11).

It has been established that this chemical LTP paradigm induces a significant increase in miniature and evoked excitatory postsynaptic potentials as well as surface AMPA receptor expression (Lu et al., 2001; Petrini et al., 2009; Shang et al., 2009), but it was necessary to confirm that LTP was being induced in our system. To do so, molecular determinants of long-term synaptic potentiation were measured, including phosphorylation of GluA1 at Ser845 and Ser831 as well as surface levels of GluA1 (Barria et al., 1997; Esteban et al., 2003). The chemical LTP paradigm led to a sustained increase in GluA1 phosphorylation (Figure 4.12A,B) as well as GluA1 surface expression (Figure 4.12C). These findings confirm that this established LTP paradigm works in our system and that GluN2A expression can be increased during long-term synaptic potentiation in cultured hippocampal neurons.

It is possible that protein synthesis of individual receptor subunits could contribute to activity-dependent changes in NMDA receptor membrane insertion. To address this hypothesis, we examined whether chemical LTP stimulation induced a protein synthesis-dependent change in the surface or total expression of the GluN1, GluN2A, and GluN2B subunits of NMDA receptors (Figure 4.13A). Chemical LTP increased the surface expression of GluN1 by 25% and GluN2A by 27% and these increases were blocked by anisomycin treatment (Figure 4.13B). In addition, chemical LTP increased the total levels of GluN1 by 30% and GluN2A by 35%, and these

increases were also blocked by anisomycin treatment (Figure 4.13C). Neither the total nor the surface expression of GluN2B was significantly altered by chemical LTP treatment. Together, these data suggest that chemical LTP induces a protein synthesis-dependent increase in the surface expression of GluN2A-containing NMDA receptors.

4.2.7 Chemical LTP induces CPEB phosphorylation and dendritic mRNA polyadenylation

The data presented thus far indicate that chemical LTP induces the synthesis of GluN2A and increases the surface expression of GluN2A-containing NMDA receptors. Given that basal expression of GluN2A is regulated by Gld2 and Ngd, it was hypothesized that the chemical LTP-induced synthesis and membrane insertion of GluN2A would also be regulated by Gld2 and Ngd. To address this hypothesis, it was first necessary to evaluate the effects of this LTP inducing stimulation paradigm on the CPEB-associated complex. Glycine application induced a sustained increase in CPEB phosphorylation for at least 20 min (Figure 4.14A). Furthermore, glycine treatment led to a significant increase in dendritic poly(A) RNA signal within 30 seconds (Figure 4.14B), similar to the previous findings with NMDA stimulation (Figure 2.16). These data suggest that this glycine-mediated chemical LTP paradigm indeed activates the CPEB complex and induces dendritic mRNA polyadenylation.

4.2.8 Gld2 depletion occludes and Ngd depletion potentiates the chemical LTP-induced synthesis and surface expression of GluN2A

To determine whether activity-induced GluN2A synthesis and surface expression

were regulated by Gld2 and Ngd, the surface and total levels of GluN2A protein were assayed following Gld2 or Ngd depletion and chemical LTP treatment. Gld2 knockdown occluded the chemical LTP-induced increase in both surface and total expression of GluN2A (Figure 4.15A). Ngd knockdown potentiated the chemical LTP-induced increase in GluN2A surface expression and increased total GluN2A expression similarly with and without chemical LTP stimulation (Figure 4.15B). Together, these data indicate that Gld2 is required for the chemical LTP-induced synthesis and membrane insertion of GluN2A, whereas Ngd inhibits chemical LTP-induced membrane insertion of GluN2A.

4.2.9 Gld2 is required for increased dendritic GluN2A expression during chemical LTP

Given that GluN2A mRNA as well as Gld2 and Ngd are localized to dendrites, we next investigated whether Gld2 and Ngd regulated the dendritic expression of GluN2A protein during chemical-induced LTP. Gld2 depletion decreased basal GluN2A expression as shown above, and blocked the chemical LTP-induced increase in dendritic GluN2A expression (Figure 4.16A). Ngd depletion increased basal and chemical LTP-induced GluN2A expression similarly (Figure 4.16B). These data on dendritic protein expression are consistent with the observed effects of Gld2 and Ngd on total expression levels shown in Figure 4.15. In addition, these data suggest that the CPEB-associated translation factors Gld2 and Ngd could regulate chemical LTP-induced synthesis of GluN2A in dendrites.

4.2.10 GluN2A mRNA is translated in dendrites in a CPE-dependent manner

Two methods were employed to investigate whether GluN2A is locally

synthesized in neurons. First, to evaluate endogenous GluN2A protein, synaptoneurosome fractions were prepared from mouse hippocampus and activated with glutamate (10 µM) and glycine (100 µM). GluN2A protein levels were significantly increased in the activated synaptoneurosome samples compared to vehicle-treated samples, and this effect was blocked by anisomycin treatment (Figure 4.17). These data suggest that GluN2A can be synthesized at synapses; however, these enriched synaptic fractions contain small amounts of somatic material, so these data do not unequivocally indicate synaptic translation.

Therefore, to further analyze whether GluN2A mRNA is translated locally, a fluorescence translation assay was used to determine whether the 3' UTR of GluN2A is sufficient to mediate dendritic mRNA translation. Based on previous studies, we generated a construct containing the coding region of Dendra2, a photoconvertible fluorescent protein, flanked by a portion of the GluN2A 5' UTR and the GluN2A 3' UTR sequence used above in Figure 4.4 (see Figure 4.18A for construct schematic) (Wang et al., 2009; Welshhans and Bassell, 2011). A dual palmitoylation sequence from GAP-43 was added to the 5' end of the Dendra2 coding sequence to limit protein diffusion by anchoring to local membrane compartments (Sasaki et al., 2010). Dendra2 initially shows green fluorescence, but can be converted to its red fluorescent form using ultraviolet light. Synthesis of Dendra2 protein can be monitored by measuring the recovery of green fluorescence within the photoconverted region. The limited diffusion ensures that new green fluorescence in the photoconverted region is not due to movement of green fluorescent Dendra2 molecules into the photoconverted region from adjacent regions (see schematic in Figure 4.18B).

Following transfection of Dendra2-GluN2A 3' UTR into cultured hippocampal neurons, live-cell imaging was used to measure photoconversion of Dendra2 and the recovery of green fluorescence in a distal dendritic region. When chemical LTP was induced following photoconversion, there was a significant increase in the green fluorescence recovery over time and this increase was blocked by anisomycin treatment (Figure 4.19). The requirement of protein synthesis indicates that the recovery of green fluorescence is indeed a result of newly synthesized Dendra2 protein. There was no fluorescence recovery when only vehicle solution was applied suggesting that this new protein synthesis requires synaptic activation. Furthermore, when a Dendra2 construct lacking the 3' UTR of GluN2A was transfected into hippocampal neurons, chemical LTP induced no change in fluorescence recovery; this suggests that the 3' UTR of GluN2A is sufficient to mediate dendritic mRNA translation. Taken together, these data indicate that this fluorescence assay indeed measures local protein synthesis in dendrites and that the GluN2A 3' UTR mediates the dendritic synthesis of a fluorescent reporter protein.

Whether the CPEB complex regulates dendritic translation of the GluN2A 3' UTR reporter was examined using a Dendra2-GluN2A 3' UTR construct having the mutated CPE sequence shown in Figure 4.2C. While chemical LTP induced significant fluorescence recovery in neurons expressing Dendra2-GluN2A 3' UTR, there was no significant fluorescence recovery in neurons expressing Dendra2-GluN2A-ΔCPE 3' UTR (Figure 4.20). These data suggest that the CPE sequence is required for dendritic translation of the GluN2A 3' UTR reporter protein.

Figure 4.2 CPEB interacts with GluN2A mRNA. (A) GluN2A mRNA contains a conserved CPE sequence in the 3' UTR. (B) FLAG-mCherry-CPEB or FLAG-mCherry plasmids were transfected into hippocampal neurons and immunoprecipitated from lysates with FLAG antibodies. GluN2A, γ-actin, GluN1, and αCaMKII mRNA levels in input and FLAG immunoprecipitates were quantified by real-time PCR in triplicate. Precipitated mRNA levels were normalized to input levels for each sample, and the graphed values were normalized to the FLAG-mCherry γ-actin group mean. The data were analyzed by one-way ANOVA and post-hoc Bonferroni t-tests (n = 6 independent experiments, * $p = 0.009$, # $p = 0.002$, γ-actin: $p = 0.205$, GluN1: $p = 0.468$). (C) Neuroblastoma cells were transfected with either FLAG-mCherry-CPEB or FLAG-mCherry and GFP appended to the GluN2A, ΔCPE-GluN2A, or β-actin 3' UTR. GFP mRNA levels in FLAG immunoprecipitates and input samples were quantified by real-time PCR. The data were normalized and analyzed as described above, and the graphed values were normalized to the FLAG-mCherry GluN2A group mean (n = 6, * $p = 0.015$, ΔCPE-GluN2A: $p = 0.282$, β-actin: $p = 0.200$).

Figure 4.2

A

```
GluN2A                              ~140nt        ~17nt
human  5'UGUC--UUUUAAUUU-------AAUAAA-----poly(A) 3'
cattle 5'UGUC--UUUUAUUUU-------AAUAAA-----poly(A) 3'
rat    5'UGUCUUUUUUAAUUU-------AAUAAA-----poly(A) 3'
mouse  5'UGUC-UUUUUAAUUU-------AAUAAA-----poly(A) 3'
                  CPE              Poly(A)
                                   signal
```

B

C 3' UTR

```
GluN2A      5' --UUUUUAAUUU--3'
ΔCPE-GluN2A 5' --GGATCCAUUU--3'
```

Figure 4.3

A

β-tubulin   GluN2A   A'   GluN2A sense

B

β-tubulin   GluN2A   GluN2A sense
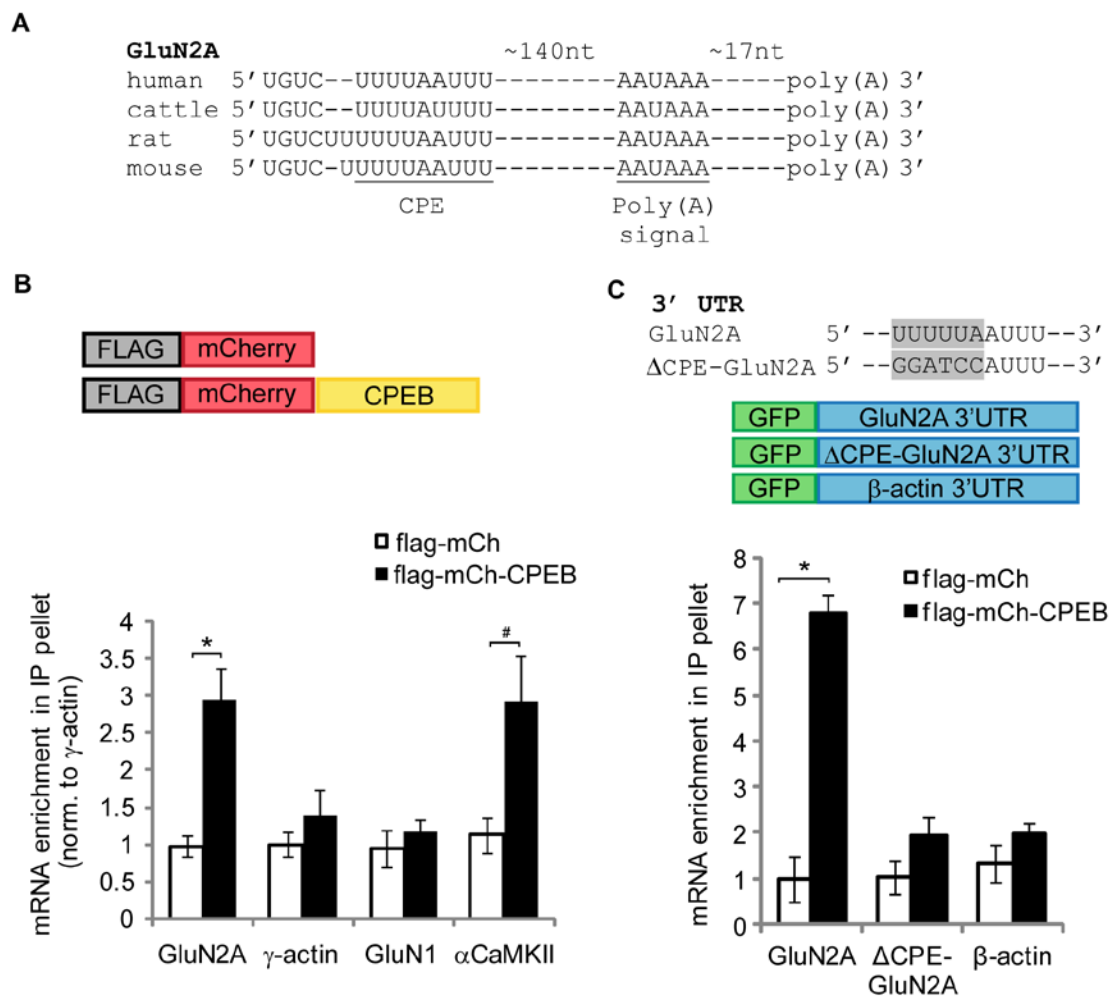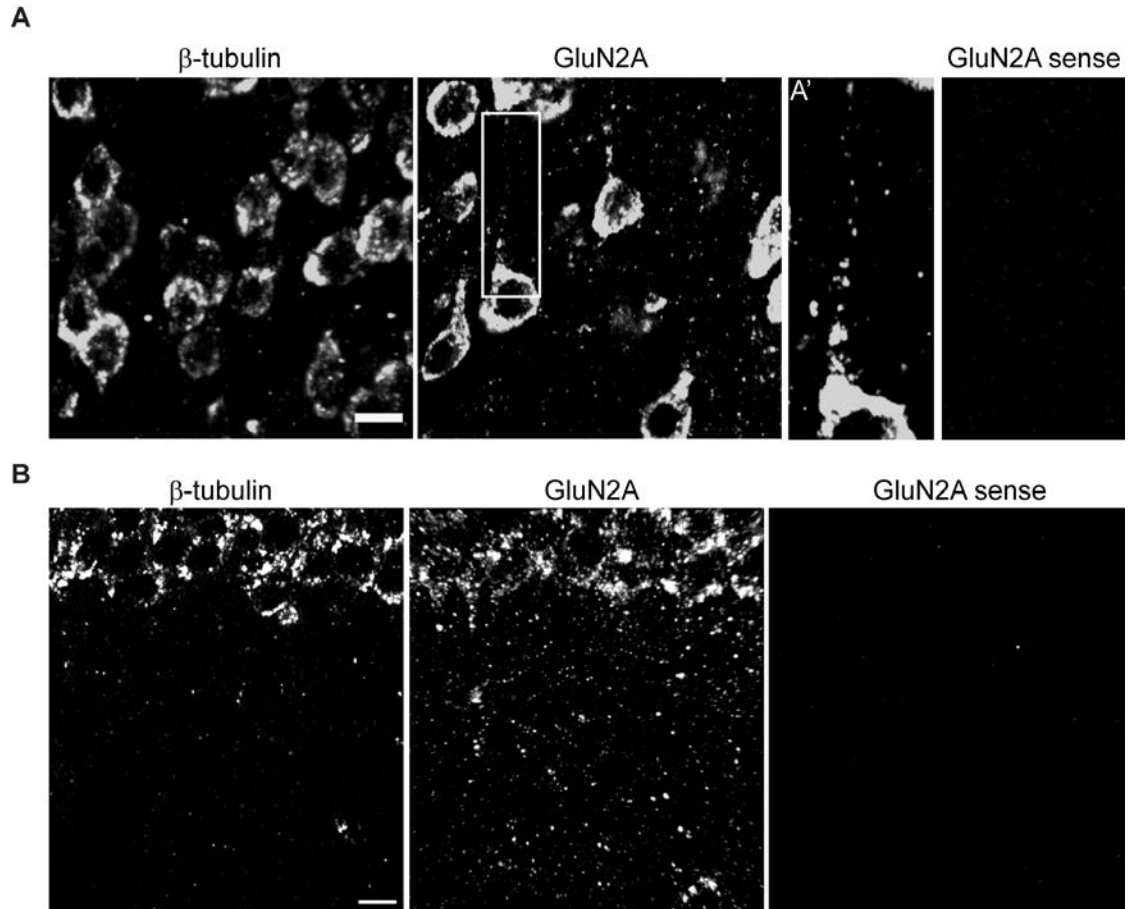
Figure 4.3 GluN2A mRNA is localized to dendrites *in vivo*. FISH was performed on mouse brain sections using riboprobes against β-tubulin and GluN2A. GluN2A sense sequence probes were used as a control. Confocal z-stacks were acquired of (A) a cortical region (A' is a magnified image of the white box) and (B) the hippocampal CA1 region, and merged z-planes are shown as maximum intensity projections. Scale bars are 10 µm.
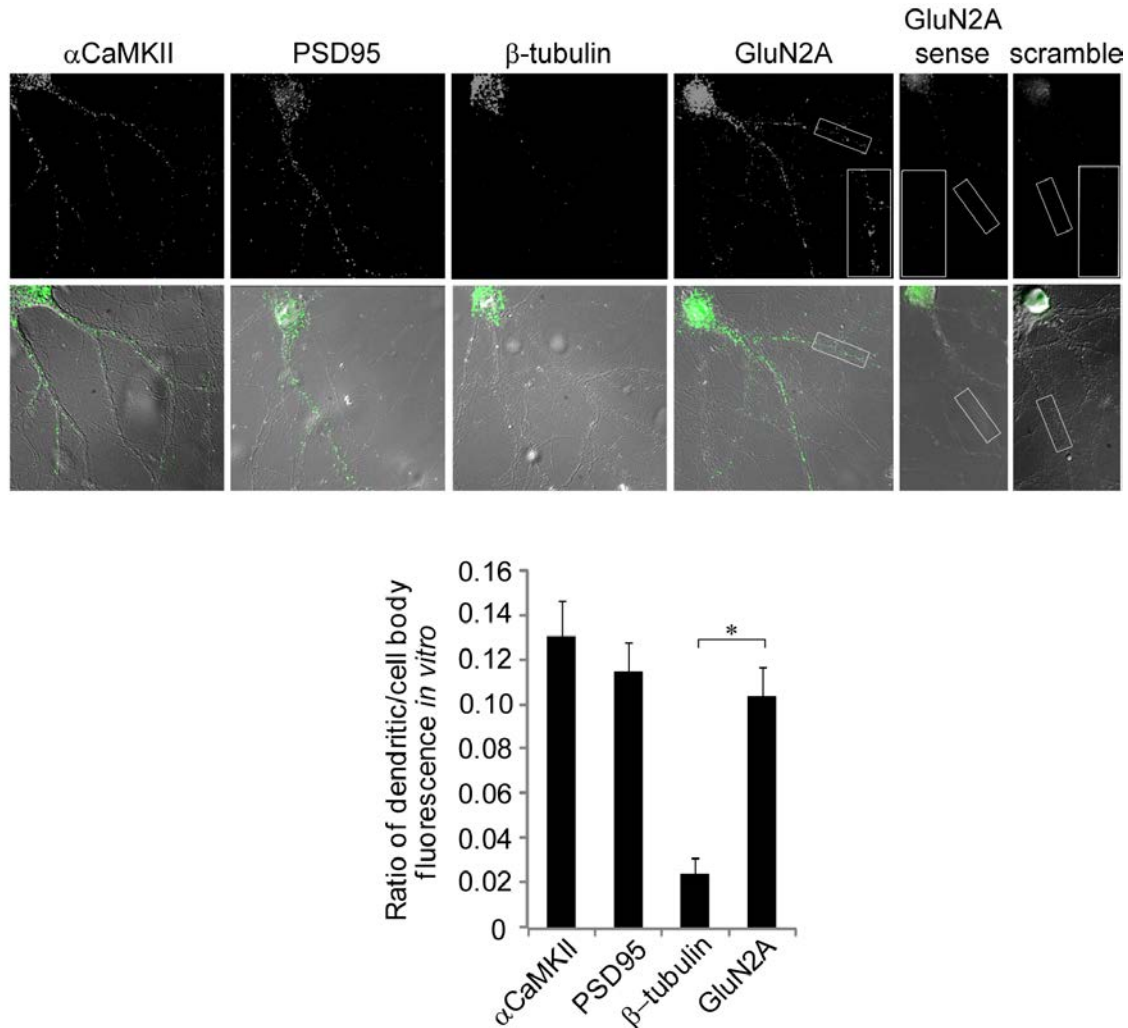
Figure 4.4

Figure 4.4 GluN2A mRNA is localized to dendrites in cultured hippocampal

neurons. FISH was performed on cultured hippocampal neurons with oligonucleotide

probes specific for αCaMKII, PSD95, β-tubulin and GluN2A as well as probes with a

scrambled sequence and GluN2A sense sequence. Dendritic and cell body fluorescence

intensities were quantified and plotted as a ratio (n = 25 - 30 cells, *p = 0.001, αCaMKII

vs. GluN2A: p = 0.563; PSD95 vs. GluN2A: p = 0.903, one-way ANOVA, post-hoc

Dunnett's test).

Figure 4.5
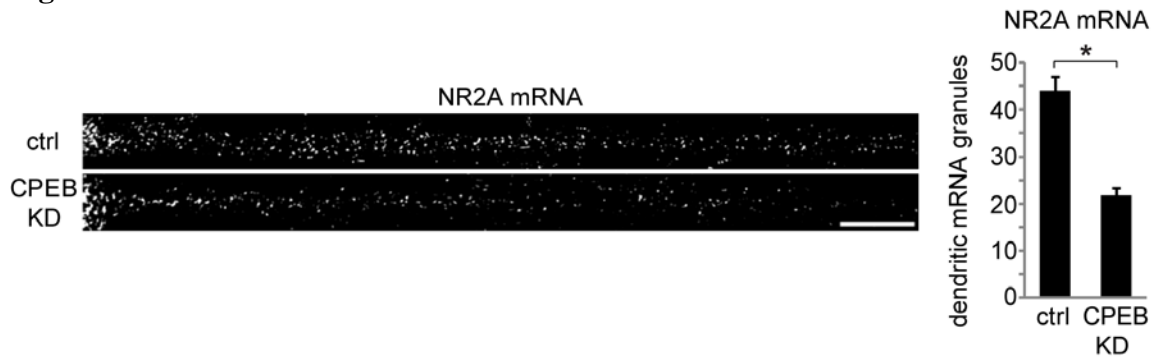
Figure 4.5 CPEB regulates the dendritic localization of GluN2A mRNA. Cultured

hippocampal neurons were treated with either control or CPEB shRNA lentiviruses for 4

days, then fixed and processed for GluN2A FISH. The scale bar is 10 µm. The number of

dendritic mRNA granules were counted using Image J and normalized to the area of the

dendritic region. The groups were compared using Student's t-test (n = 25 - 30 cells, $*p <$

0.001).

Figure 4.6

A

B
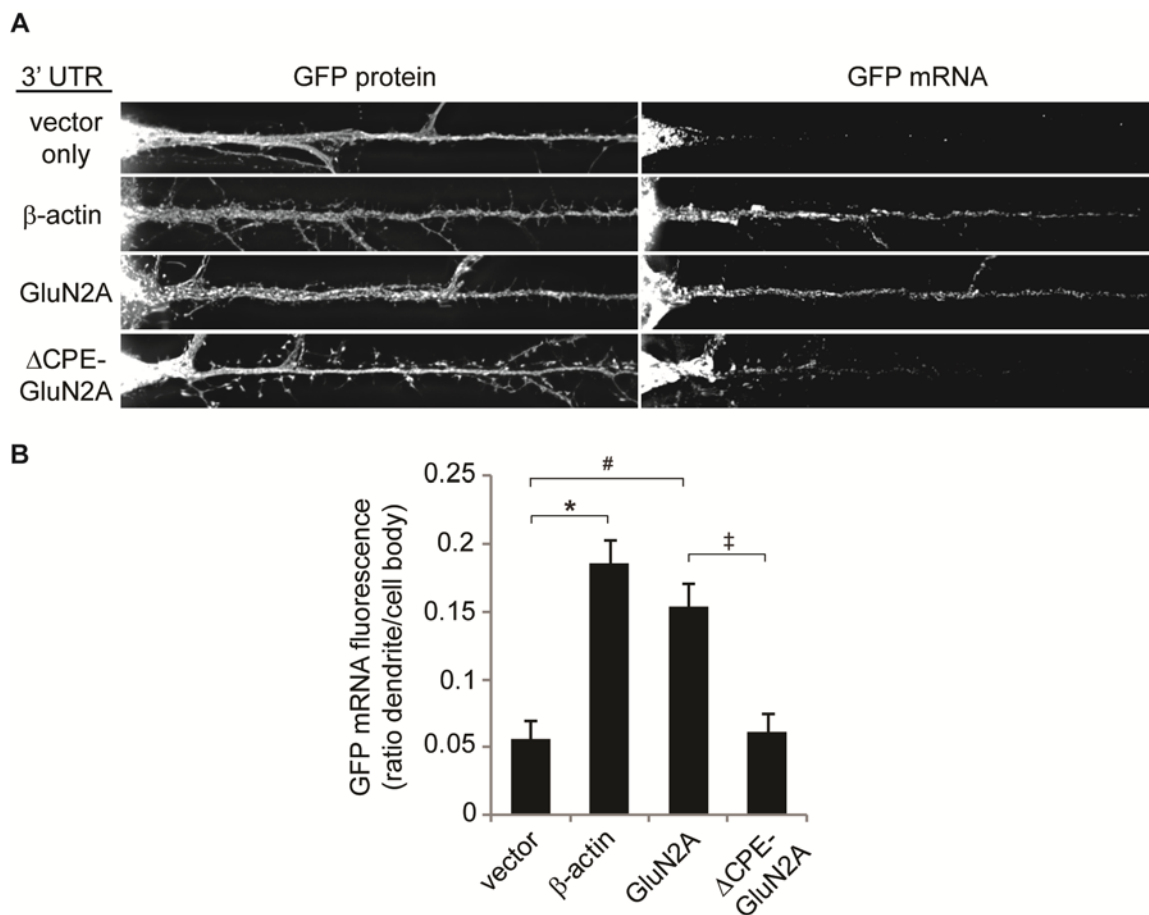
Figure 4.6 The CPE sequence is required for dendritic localization of the GluN2A mRNA 3' UTR. (A) Cultured hippocampal neurons were transfected with plasmids containing the coding region of GFP and the vector 3' UTR, β-actin 3' UTR, GluN2A 3' UTR or ΔCPE-GluN2A 3' UTR. After 12 hours, the neurons were fixed and processed for GFP mRNA FISH. Representative images of GFP protein fluorescence and GFP mRNA FISH fluorescence signals are shown. (B) GFP FISH fluorescence was quantified in both the cell body and a dendritic region, and graphed as the ratio of dendritic fluorescence to cell body fluorescence. Groups were compared using a one-way ANOVA and post-hoc Bonferroni t-tests (n = 18 - 25 cells, * $p = 0.001$, # $p = 0.001$, ‡ $p = 0.001$, β-actin vs. GluN2A: $p = 0.242$, vector vs. ΔCPE-GluN2A: $p = 0.798$).

Figure 4.7 Gld2 depletion decreases dendritic GluN2A protein expression. (A) High-density cultured hippocampal neurons (11 *DIV*) were transduced with control or Gld2 shRNA lentivirus for 4 days, followed by western blotting for GluN2A and α-tubulin (a loading control). The graphed values were normalized to the control group mean (n = 4, *p = 0.025, Student's t-test). (B) 11 *DIV* hippocampal neurons were treated with control or Gld2 shRNA lentivirus and immunostained for GluN2A or GluN1 4 days later. (C) Somatic and dendritic fluorescence intensities were quantified and treatment conditions were compared by Student's t-test (n = 30 - 35 neurons, *p = 0.020, GluN2A cell body: p = 0.668, GluN1 cell body: p = 0.903 , GluN1 dendrite: p = 0.849). The graphed values were normalized to the control group means.

Figure 4.7
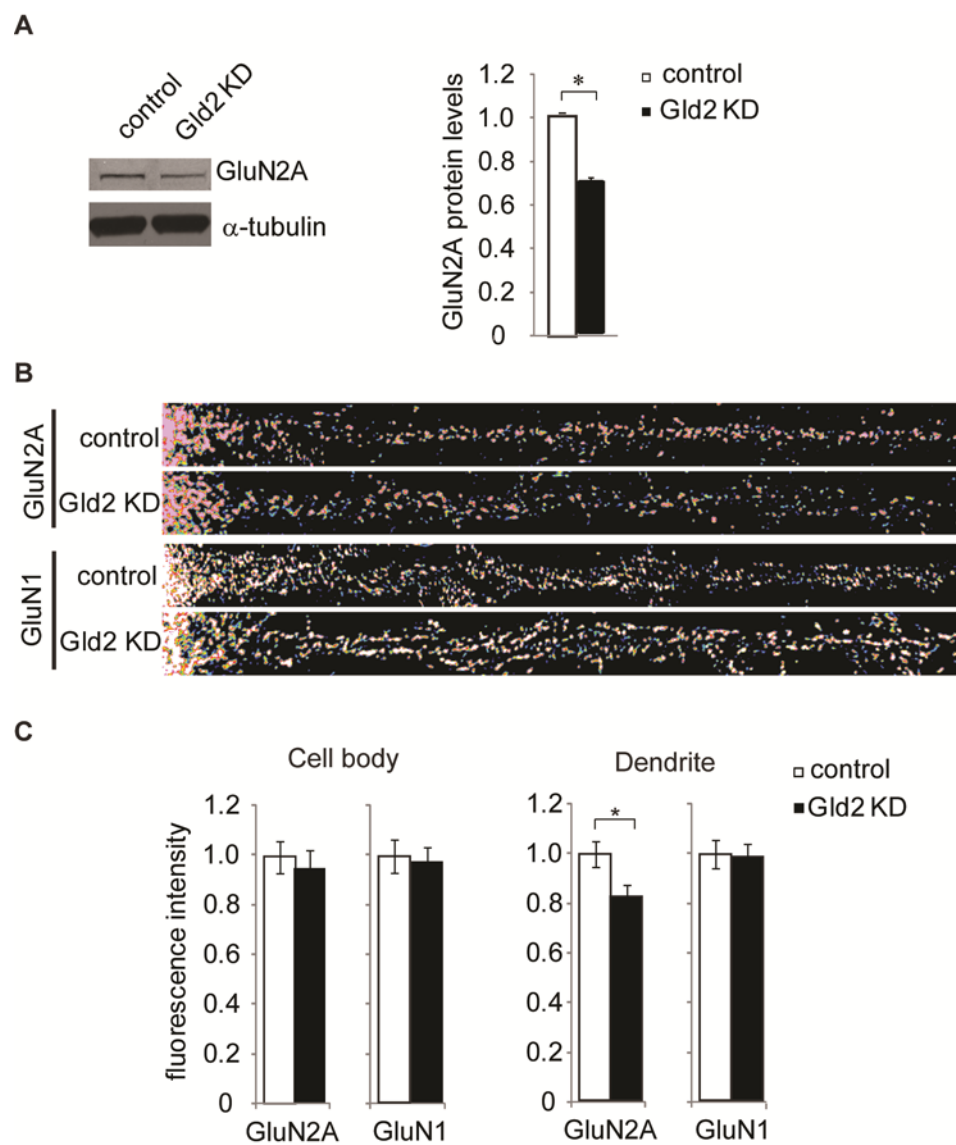
Figure 4.8 Ngd depletion increases dendritic GluN2A protein expression. (A) High-density cultured hippocampal neurons (11 *DIV*) were transduced with control or Ngd shRNA lentivirus for 4 days, followed by western blotting for GluN2A, GluN1, and α-tubulin (a loading control). Control and KD groups were compared using paired t-tests (n = 4, *p = 0.015, #p = 0.023). (B) 11 *DIV* hippocampal neurons were treated with control or Ngd shRNA lentivirus and immunostained for GluN2A or GluN1 4 days later. *(C)* Somatic and dendritic fluorescence intensities were quantified and treatment conditions were compared by Student's t-test (n = 30 - 35 neurons, *p = 0.025, GluN2A cell body: p = 0.805). The graphed values were normalized to the control group means.

Figure 4.8
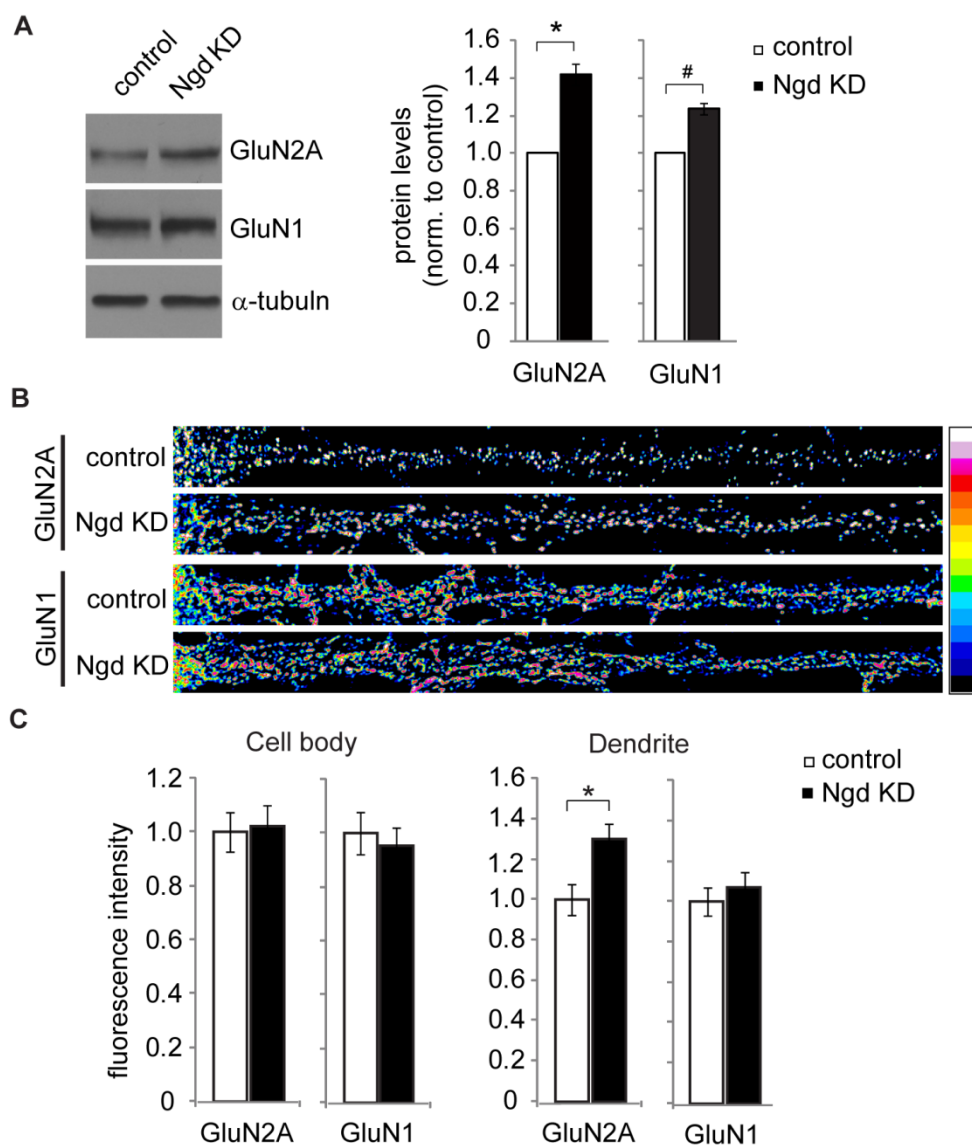
Figure 4.9 Gld2 depletion reduces surface expression of GluN2A-containing NMDA receptors. 14 *DIV* hippocampal neurons were treated with control or Gld2 shRNA lentivirus for 4 days, and then surface proteins were biotinylated and precipitated. (A) Total and precipitated proteins were immunoblotted for GluN2A, GluN2B, GluN1, and α-tubulin (loading control). (B) Surface protein levels were compared between control and Gld2 KD using paired t-tests (n = 6, * $p = 0.019$, # $p = 0.022$, ‡ $p = 0.021$, GluN2B: $p = 0.380$). (C) Total protein levels were compared as above (n = 6, * $p = 0.047$, # $p = 0.036$, GluN1: $p = 0.117$).

Figure 4.9
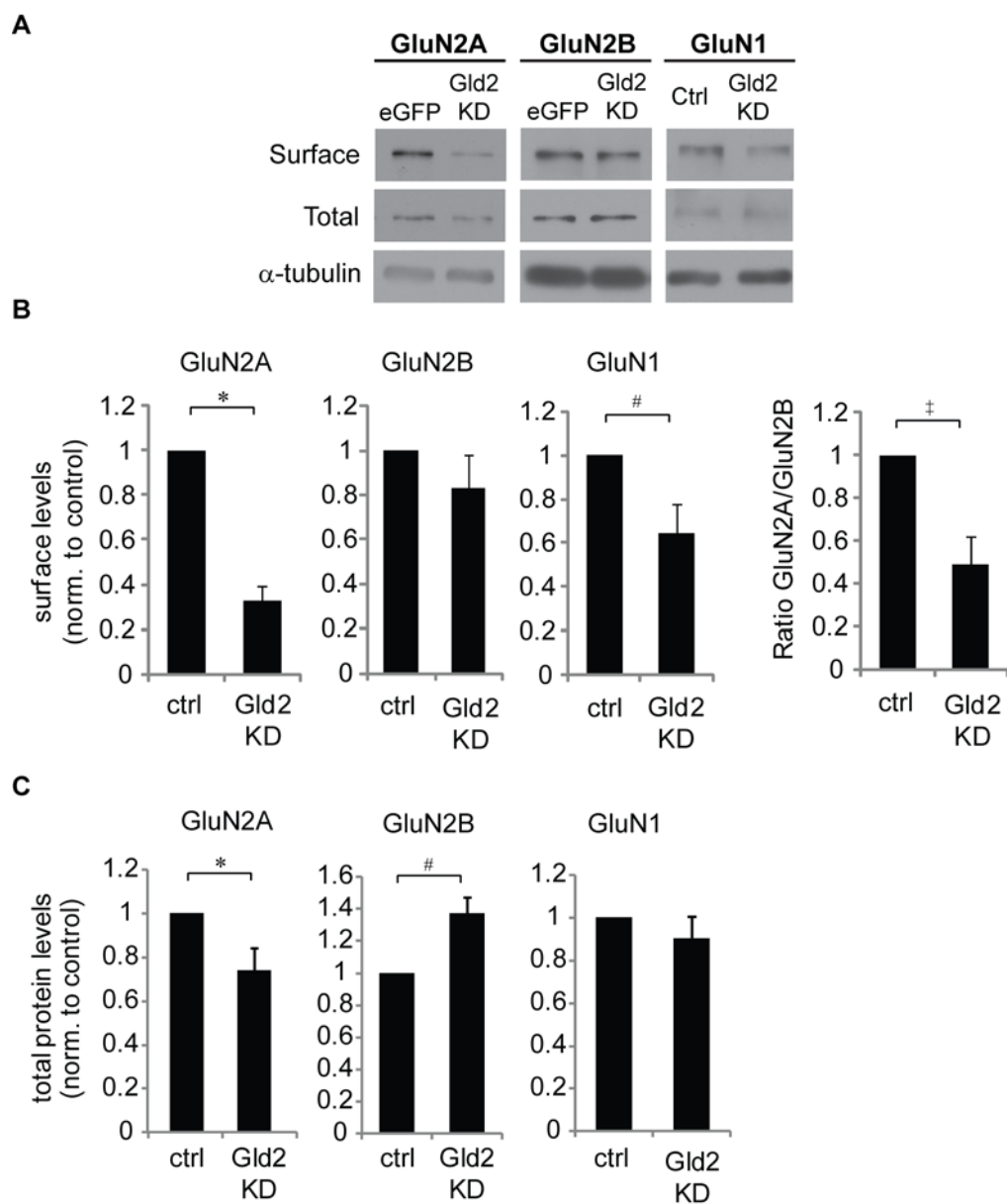
Figure 4.10 Ngd depletion increases surface expression of GluN2A-containing NMDA receptors. 14 *DIV* hippocampal neurons were treated with control or Ngd shRNA lentivirus for 3 days, and then surface proteins were biotinylated and precipitated. (A) Total and precipitated proteins were immunoblotted for GluN2A, GluN2B, GluN1, and tubulin (loading control). (B) Surface protein levels were compared between control and Gld2 KD using paired t-tests (n = 6, * $p = 0.020$, # $p = 0.018$, ‡ $p = 0.032$, GluN2B: $p = 0.580$). (C) Total protein levels were compared as above (n = 6, * $p = 0.026$, # $p = 0.004$, GluN2B: $p = 0.486$).

Figure 4.10
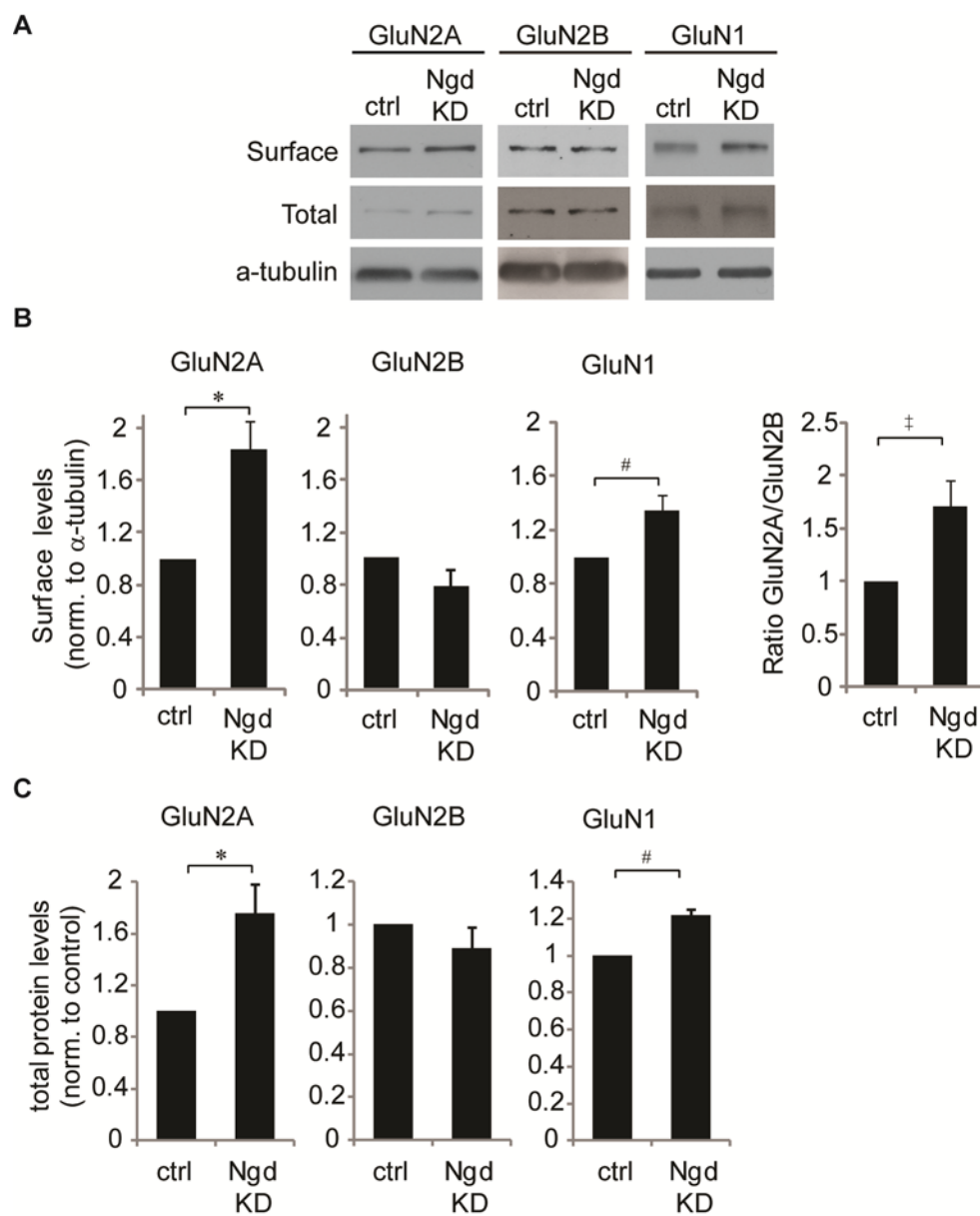
Figure 4.11
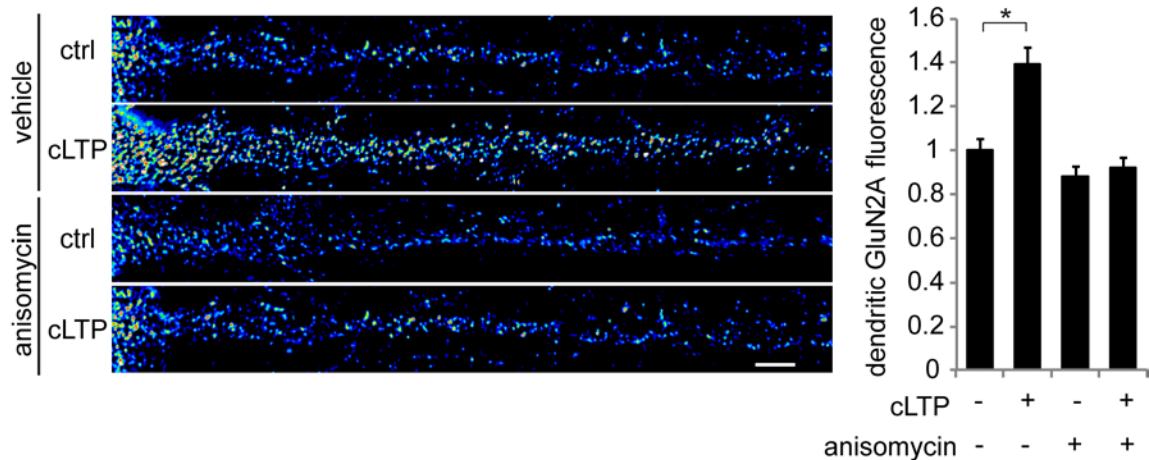
Figure 4.11 Chemical LTP induces a protein synthesis-dependent increase in dendritic GluN2A protein expression. Hippocampal neurons were treated with glycine or a control solution for 3 min, and then incubated in bathing solution without glycine for 30 min. In addition, the neurons were treated with either anisomycin or vehicle throughout the experiment. After fixation, the neurons were processed for GluN2A immunofluorescence and the distal dendritic signal was measured. The graphed values were normalized to the mean of the untreated group, and the groups were compared with a one-way ANOVA and post-hoc Bonferroni t-tests (n = 28 - 32 cells, * p = 0.001, anisomycin vs. anisomycin/cLTP: p = 0.589).

Figure 4.12 Glycine-induced chemical LTP leads to GluA1 phosphorylation and membrane insertion in cultured hippocampal neurons. Hippocampal neurons were treated with 200 µM glycine for 30 sec, 3 min, or 3 min followed by 10 min or 20 min in bathing solution without glycine. (A,B) Cell lysates were immunoblotted for phosphorylated GluA1 (pGluA1-S845 or -S831), total GluA1, and α-tubulin (loading control). Glycine-treated groups were compared to untreated (0 min) using a one-way ANOVA and post-hoc Dunnett's tests (n = 5 experiments; (A) 30 sec: $p = 0.002$, 3 min: $p = 0.002$, 10 min: $p = 0.001$, 20 min: $p = 0.001$; (B) 30 sec: $p = 0.001$, 3 min: $p = 0.002$, 10 min: $p = 0.005$, 20 min: $p = 0.005$). (C) Hippocampal neurons were treated with control or 200 µM glycine for 3 min, and then incubated in bathing solution for 30 min. Surface proteins were biotinylated and precipitated, and then total and precipitated protein samples were immunoblotted for GluA1 and α-tubulin (loading control). Surface levels were compared using a paired t-test (n = 6, * $p = 0.013$).

Figure 4.12
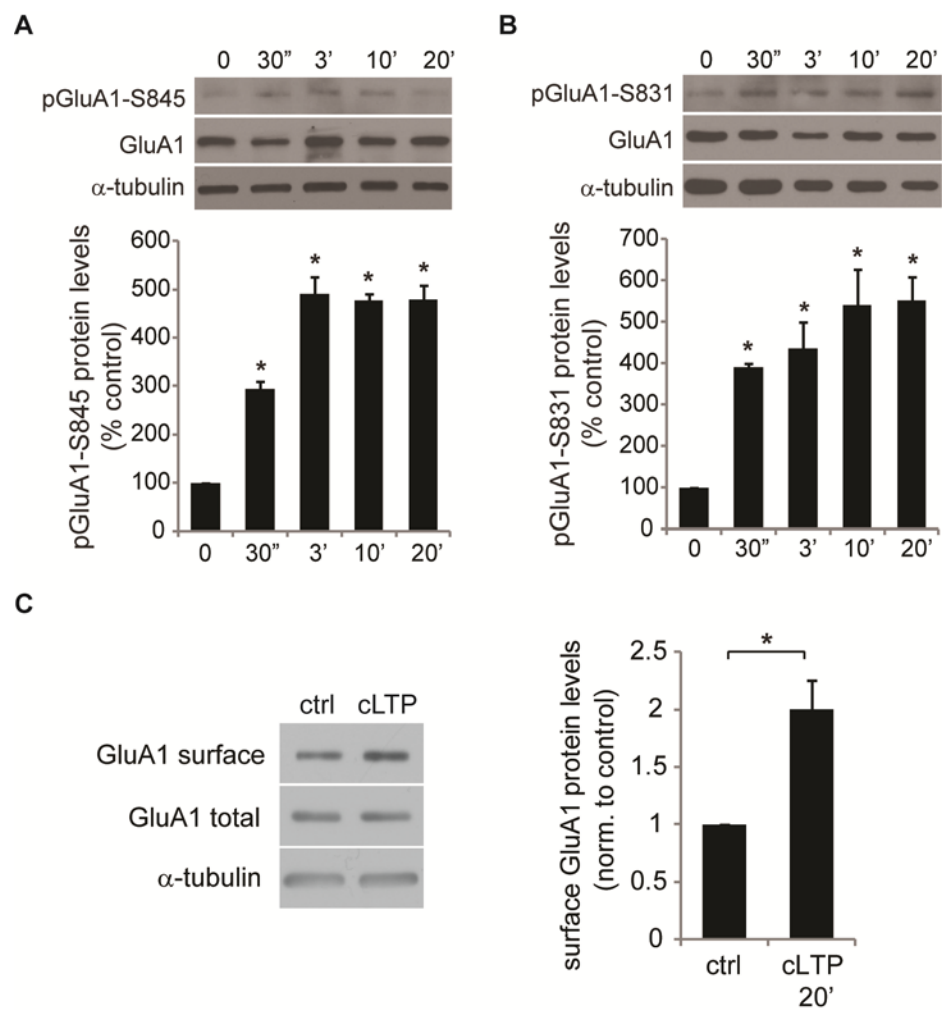
Figure 4.13 Chemical LTP induces a protein synthesis-dependent increase in the surface expression of GluN2A-containing NMDA receptors. Hippocampal neurons were treated with anisomycin or DMSO for 30 minutes in cLTP bathing solution, and then treated with either vehicle or glycine for 3 min followed by a 30 min incubation without glycine. (A) Surface proteins were biotinylated, and total and surface proteins were immunoblotted for GluN1, GluN2A, GluN2B, and α-tubulin (loading control). (B) Surface and (C) total protein levels were compared using repeated measures one-way ANOVA and post hoc Bonferroni t-tests (n = 6; surface GluN1: * $p = 0.001$, aniso vs. aniso/cLTP: $p = 0.999$, surface GluN2A: # $p = 0.022$, aniso vs. aniso/cLTP: 0.999, surface GluN2B: one-way ANOVA $p = 0.643$; total GluN1: * $p = 0.020$, aniso vs. aniso/cLTP: $p = 0.982$, total GluN2A: # $p = 0.015$, aniso vs. aniso/cLTP: $p = 0.884$, total GluN2B: one-way ANOVA, $p = 0.814$).

Figure 4.13
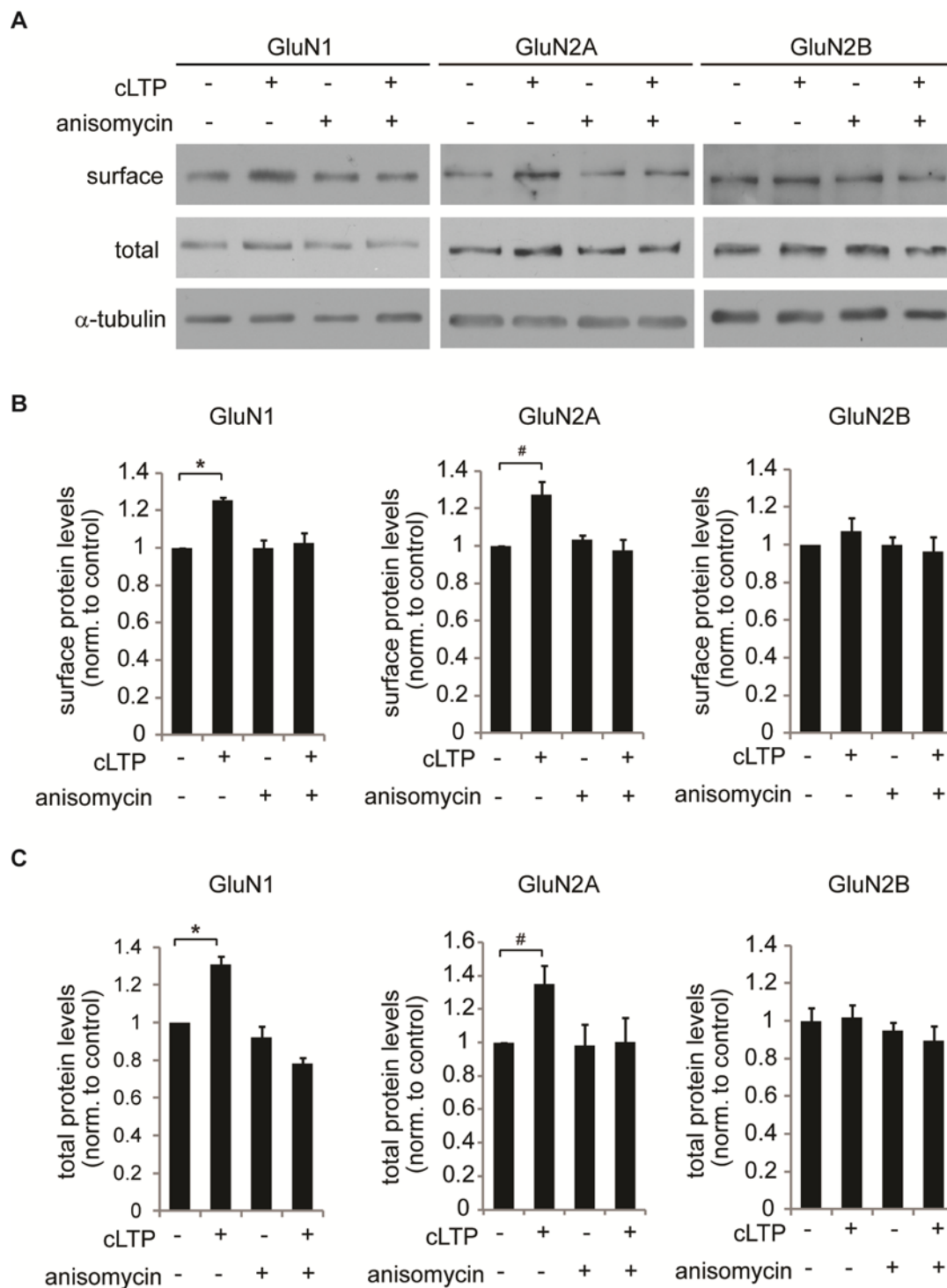
Figure 4.14
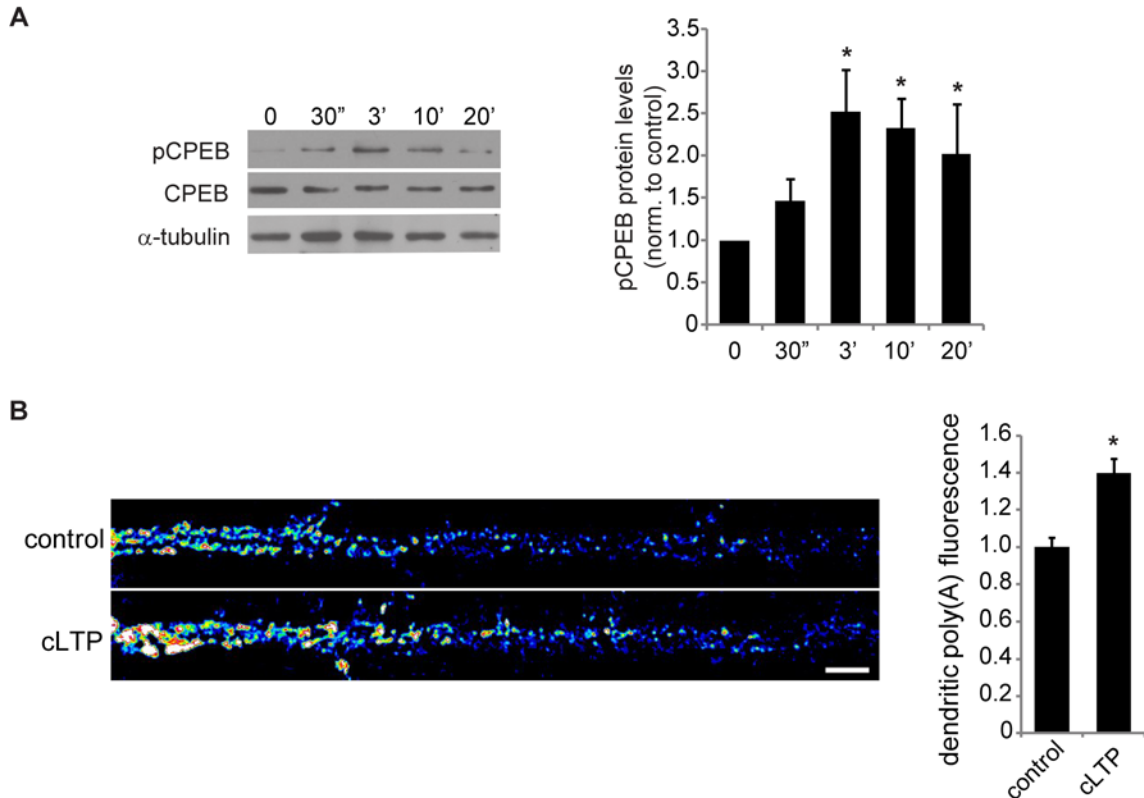
Figure 4.14 Chemical LTP induces CPEB phosphorylation and dendritic mRNA polyadenylation. (A) Hippocampal neurons were treated with 200 μM glycine for 30 sec, 3 min, or 3 min followed by 10 min or 20 min in bathing solution without glycine. Cell lysates were immunoblotted for phosphorylated CPEB, total CPEB, and α-tubulin (loading control). Glycine-treated groups were compared to untreated (0 min) using a repeated measures one-way ANOVA and post-hoc Dunnett's tests (n = 5 experiments; 30 sec: $p = 0.014$, 3 min: $p = 0.008$, 10 min: $p = 0.007$, 20 min: $p = 0.011$). (B) Hippocampal neurons were treated with 200 μM glycine or vehicle for 30 seconds, then fixed and processed for oligo (dT) FISH. Representative images are shown, and the dendritic poly(A) fluorescence signals were quantified. The graphed values were normalized to the control group mean (n = 40 - 45 cells, Student's t-test, * $p = 0.012$).

Figure 4.15 Gld2 and Ngd bidirectionally regulate chemical LTP-induced GluN2A surface expression. Hippocampal neurons were treated with control, Gld2 shRNA, or Ngd shRNA lentiviruses for 3 days and vehicle or glycine for 3 min followed by a 30 min incubation without glycine. Surface proteins were biotinylated, and total and surface proteins were immunoblotted for GluN2A and α-tubulin (loading control). Groups were analyzed by repeated measures two-way ANOVA and post hoc Bonferroni t-tests (n = 6). (A) Surface: cLTP main: $p = 0.089$, Gld2 KD main: $p = 0.001$, interaction: $p = 0.001$, * $p = 0.001$, # $p = 0.007$, Gld2 KD/vehicle vs. Gld2 KD/cLTP: $p = 0.043$. Total: cLTP main: $p = 0.072$, Gld2 KD main: $p = 0.001$, interaction: $p = 0.001$, * $p = 0.015$, # $p = 0.005$, Gld2 KD/vehicle vs. Gld2 KD/cLTP: $p = 0.397$ (B) Surface: cLTP main: $p = 0.001$, Ngd KD main: $p = 0.001$, interaction: $p = 0.006$, * $p = 0.012$, # $p = 0.001$, ‡ $p = 0.002$. Total: cLTP main: $p = 0.005$, Ngd KD main: $p = 0.001$, interaction: 0.940.

Figure 4.15
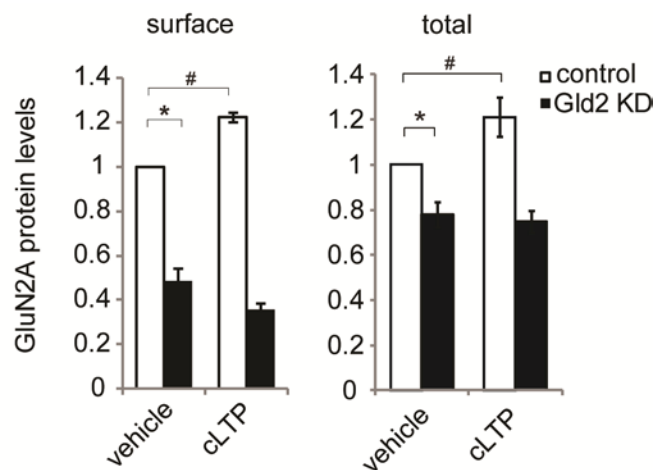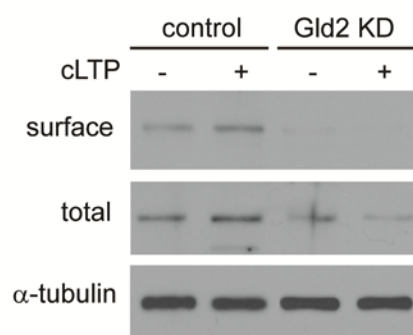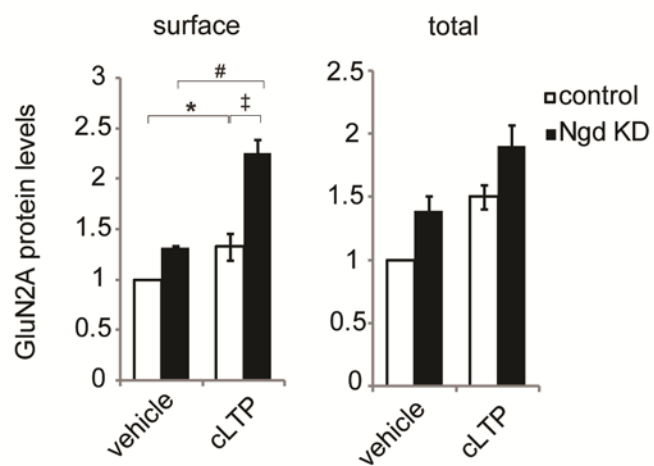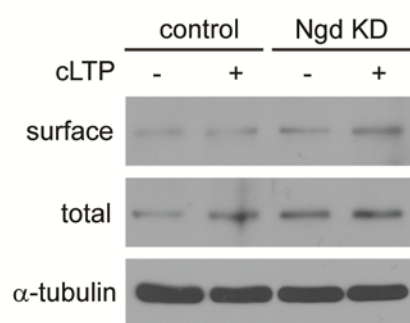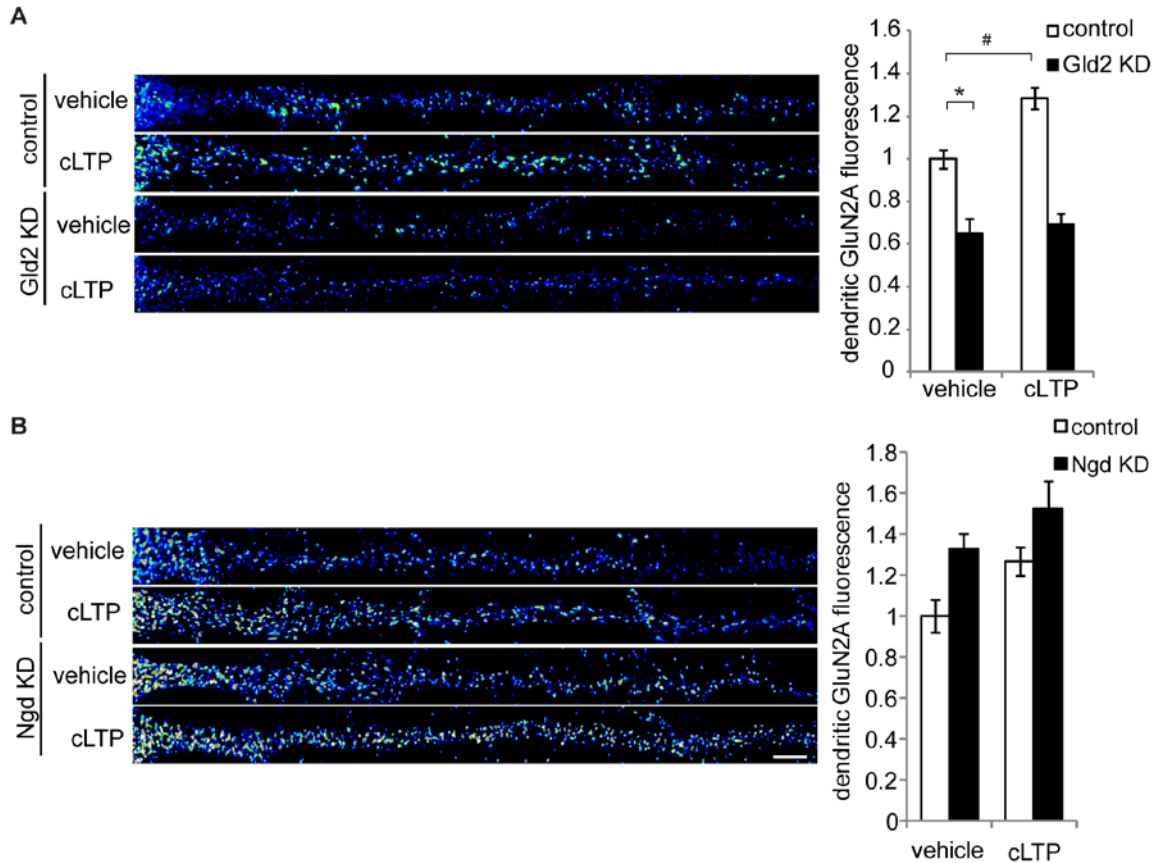
Figure 4.16

Figure 4.16 Gld2 depletion occludes the chemical LTP induced synthesis of GluN2A.

Hippocampal neurons were treated with control, Gld2 shRNA, or Ngd shRNA

lentiviruses for 3 days, then treated with glycine or vehicle for 3 min followed by a 30

min incubation in bathing solution without glycine. After fixation, neurons were

processed for GluN2A immunofluorescence and distal dendritic fluorescence signals

were quantified. (A) Groups were compared by two-way ANOVA and post-hoc

Bonferroni t-tests (n = 25 - 28 cells, cLTP main: $p = 0.001$, Gld2 KD main: $p = 0.001$,

interaction: $p = 0.007$, * $p = 0.009$, # $p = 0.001$, Gld2 KD vehicle vs. cLTP: $p = 0.987$).

(B) Groups were compared by two-way ANOVA (n = 29 - 31 cells, cLTP main: $p =$

0.173, Ngd KD main: $p = 0.347$, interaction: $p = 0.397$). The graphed values were

normalized to the mean of the untreated, control groups.

Figure 4.17
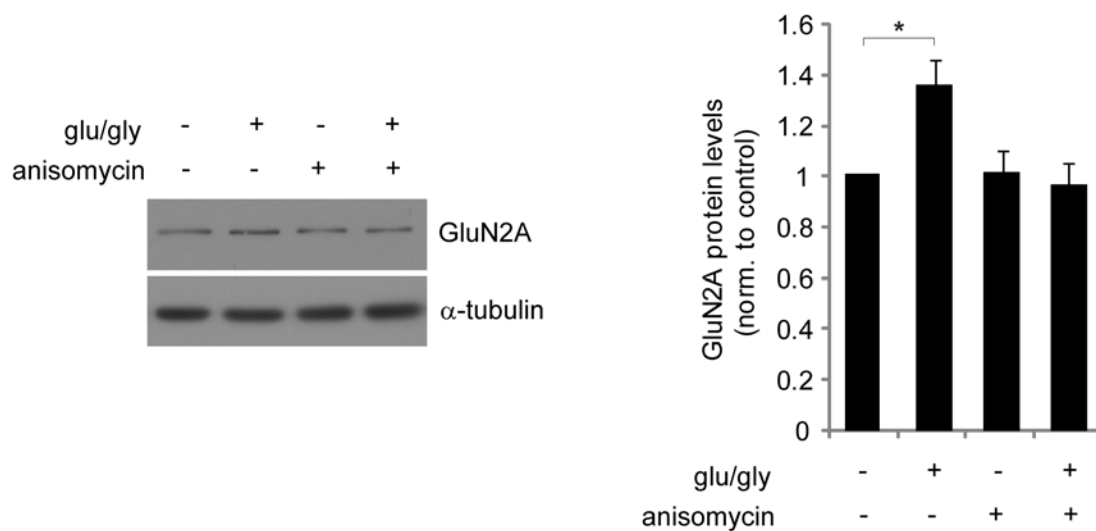
Figure 4.17 GluN2A protein is synthesized in synaptoneurosome fractions.

Synaptoneurosome fractions were prepared from mouse hippocampus and treated with vehicle or anisomycin for 15 minutes followed by vehicle or glutamate/glycine treatment for 10 min. Protein samples were immunoblotted for GluN2A and α-tubulin (loading control), and protein levels were quantified by densitometry. The groups were compared by a repeated measures one-way ANOVA and post-hoc Bonferroni t-tests (n = 6, * p = 0.013, anisomycin vs. anisomycin + glu/gly: p = 0.622).

Figure 4.18 Schematic of Dendra2 fluorescent reporter and translation assay. (A) A

plasmid was constructed containing a portion of the GluN2A 5' UTR, a dual

palmitoylation sequence (Pal2), the Dendra2 coding sequence, and a portion of the

GluN2A 3' UTR (Dendra2-GluN2A 3' UTR). (B) Dendra2-GluN2A 3' UTR is transfected

into cultured neurons, and Dendra2 fluorescence is monitored using live-cell imaging

with 488 nm and 563 nm lasers. The initial image shows green Dendra2 fluorescence and

no red fluorescence (left). A 405 nm laser is used to photoconvert Dendra2 in a distal

dendritic region (> 75 µm from the cell body), and an image acquired immediately

following photoconversion shows the loss of green fluorescence and the appearance of

red fluorescence (time point: 0 min). Time-lapse imaging is used to monitor fluorescence

for 1 hr (30 and 60 min time points are shown). After photoconversion, green

fluorescence is used to measure new protein synthesis, and stable red fluorescence shows

that Dendra2 does not diffuse and allows for constant visualization of the dendritic

region.

Figure 4.18

A

| GluN2A 5' UTR | Pal2 | Dendra2 | GluN2A 3' UTR |

B
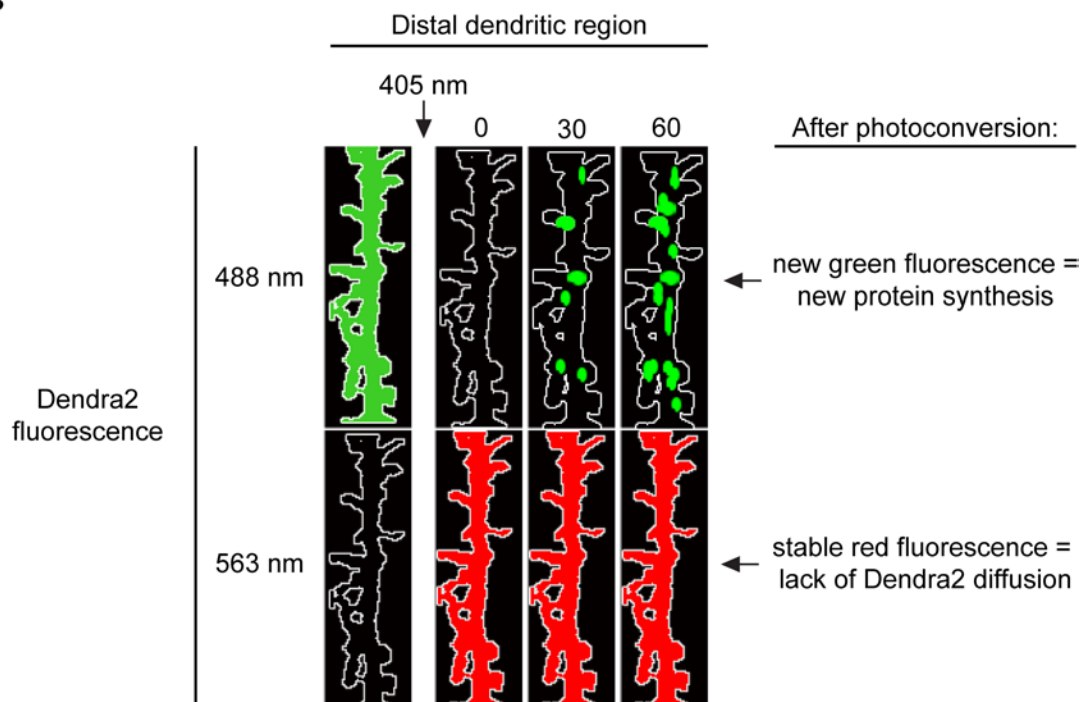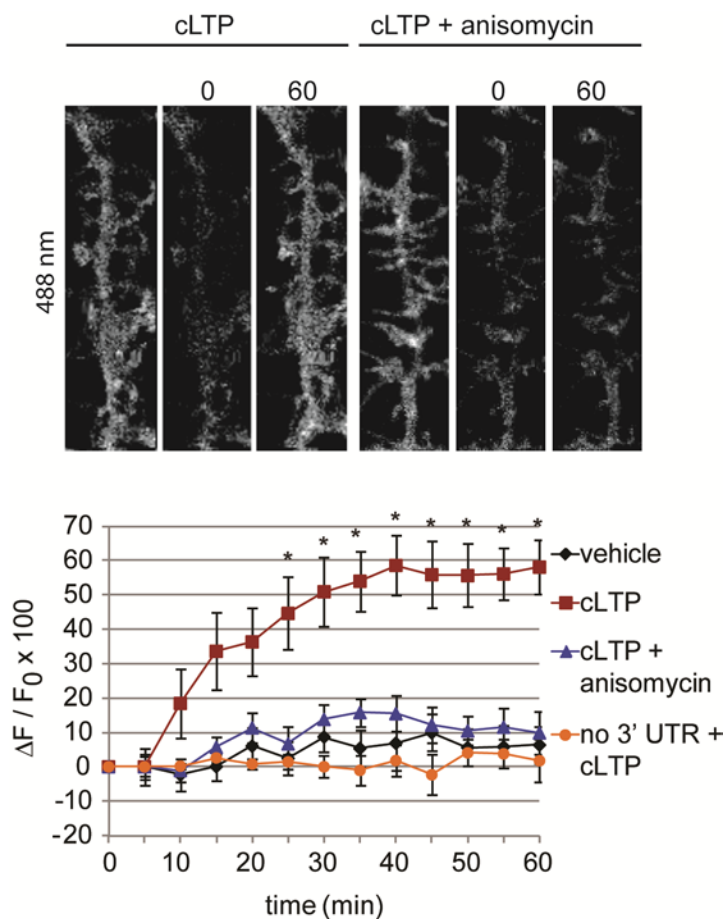
Figure 4.19

Figure 4.19 GluN2A 3' UTR mediates dendritic synthesis of a reporter protein. 14

DIV hippocampal neurons were transfected with either Dendra2-GluN2A 3' UTR or

Dendra2 alone. After 48 hours, live imaging was used to measure Dendra2 fluorescence.

Neurons were treated with vehicle or anisomycin for 30 min prior to imaging. An initial

image was acquired, and then, Dendra2 was photoconverted and imaged (time point 0

min). Cells were then either treated with vehicle or glycine for 3 min and returned to

bathing solution without glycine for time-lapse imaging (time point 5 min).

Representative images from the cLTP or cLTP + anisomycin groups show the initial

image and the time-lapse images at 0 and 60 min using the 488 nm laser.

Figure 4.20
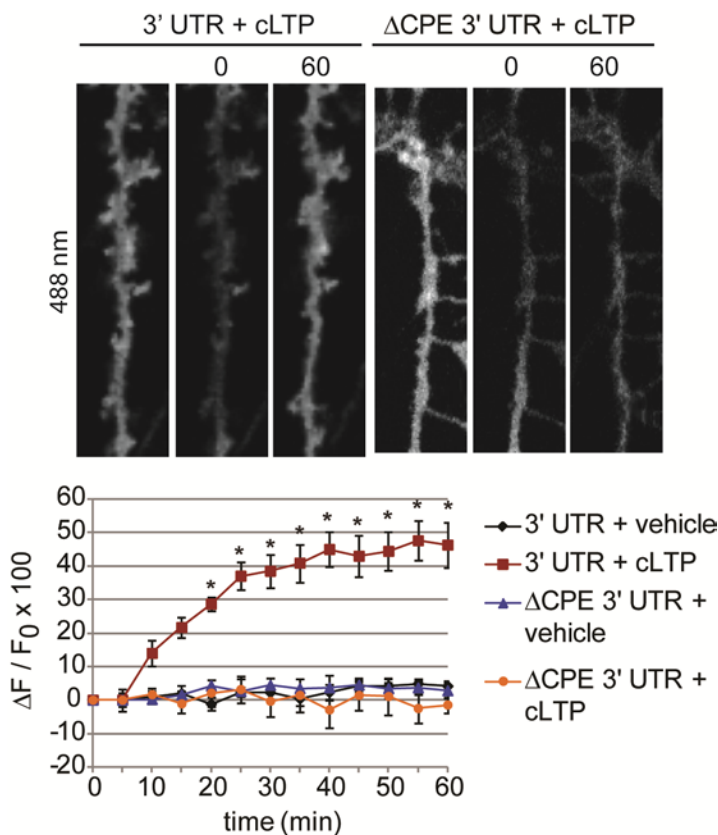
Figure 4.20 The CPE sequence is required for chemical LTP-induced synthesis of a GluN2A 3' UTR reporter in dendrites. 14 *DIV* hippocampal neurons were transfected with either Dendra2-GluN2A 3' UTR or Dendra2-ΔCPE-GluN2A 3' UTR. After 48 hours, live imaging was used to measure Dendra2 fluorescence. An initial image was acquired, and then, Dendra2 was photoconverted and imaged (time point 0 min). Cells were then either treated with vehicle or glycine for 3 min and then returned to bathing solution without glycine for time-lapse imaging (time point 5 min). Representative images from the cLTP-treated 3' UTR and ΔCPE-3' UTR groups show the initial image and the time-lapse images at 0 and 60 min using the 488 nm laser.

4.3 Discussion

Here, we have identified a molecular mechanism by which CPEB regulates activity-induced local mRNA translation in hippocampal neurons. Moreover, this work reveals a novel mechanism underlying activity-dependent insertion of GluN2A-containing NMDA receptors during synaptic plasticity. GluN2A mRNA is bound by CPEB and transported into dendrites in a CPE-dependent manner. The CPEB-associated complex inhibits GluN2A mRNA translation through the eIF4E binding protein Ngd, and LTP activates the Gld2-dependent translation of GluN2A mRNA. Furthermore, the membrane insertion of GluN2A-containing NMDA receptors is inhibited by Ngd and promoted by Gld2, and Gld2-mediated translation of GluN2A is required for LTP-induced insertion of NMDA receptors. Finally, the 3' UTR of GluN2A promotes LTP-induced dendritic translation of a reporter protein in a CPE-dependent manner. These findings indicate that post-transcriptional regulation of GluN2A mRNA by CPEB and its associated translational regulators is a critical determinant of activity-induced NMDA receptor expression.

In the synaptic protein synthesis field, many studies have focused on AMPA receptors as they are turned over rapidly at synapses, and changes in synaptic AMPA receptors are thought to be largely responsible for the long-term alterations in excitatory postsynaptic potentials during plasticity (Kessels and Malinow, 2009). However, many studies suggest that NMDA receptor expression and trafficking are altered during synaptic plasticity as well (Lau and Zukin, 2007; Yashiro and Philpot, 2008). In particular, one study has shown that during mGlu-LTD there is protein synthesis-dependent internalization of NMDA receptors and a reduction in NMDA receptor

currents (Snyder et al., 2001). In this study, GluN2A was focused on because it is a target of Gld2 activity and is implicated in synaptogenesis, synaptic remodeling, and plasticity (Camilla and Nicoll 2007; Lau and Zukin 2007). Furthermore, the differential expression of GluN2A and GluN2B subunits critically regulates NMDA receptor function in the hippocampus (MacDonald et al., 2006; Smith et al., 2009; Yashiro and Philpot, 2008). LTP induction leads to GluN2A production (Williams et al. 1998; Wang et al. 2002), suggesting that GluN2A might play a role in LTP expression as well as induction. In addition, LTP induction in the adult rat hippocampus leads to the membrane insertion of GluN2A-containing receptors (Grosshans et al. 2002). It is also possible that GluN2A synthesis might be required to enhance future synaptic responses (Smith et al., 2009). Herein, it is shown that protein synthesis is necessary for LTP-induced NMDA receptor insertion in cultured hippocampal neurons. While direct evidence that local protein synthesis is necessary for this process is lacking, the data herein support the assertion that local synthesis of NMDA receptor subunits could contribute to this activity-dependent NMDAR insertion. Indeed, GluN2A mRNA is localized to dendrites, GluN2A protein is synthesized in synaptoneurosome fractions, and the GluN2A 3' UTR regulates dendritic translation of a reporter protein in a CPE-dependent manner. An additional study that would further support these findings would be to use the fluorescence translation assay applied herein to measure the dendritic synthesis of a Dendra2-GluN2A fusion protein. Importantly, this study shows that Gld2 and Ngd regulate the dendritic levels of endogenous GluN2A protein following chemical LTP stimulation. We propose that the CPEB-associated translation regulators Gld2 and Ngd help maintain GluN2A homeostasis at synapses and tune synapses by providing the proper level and/or

stoichiometry of NMDA receptor subunits.

Gld2 is an important regulator of neuronal function as it promotes dendritic spine maturation, theta-burst LTP, dendritic mRNA polyadenylation as well as AMPA and NMDA receptor surface expression. In support of this assertion, a dominant negative Gld2 mutant inhibits long-term memory in *Drosophila* (Kwak et al. 2008). Here, 102 mRNAs were identified as having reduced poly(A) tail size following depletion of Gld2. Twenty-seven of these mRNAs have been implicated in synaptic plasticity and/or nervous system disorders. For example, HuD is involved in dendritic morphogenesis and associative and spatial memory (Bolognani et al. 2007), Sos1 links glutamate receptors to the Erk signaling pathway (Tian et al. 2004), and Neto2 affects kainate receptor function (Zhang et al. 2009). GluN2A was focused on in this study, but it is likely that Gld2 could affect plasticity through many targets. Other neuronal mRNAs polyadenylated in the cytoplasm such as those encoding αCaMKII (Du and Richter 2005; Wu et al. 1998), AMPA receptor binding protein (Du and Richter 2005), and tissue plasminogen activator (Shin et al. 2004), were not detected as having diminished poly(A) tail length following Gld2 knockdown. These results might indicate that a second poly(A) polymerase also functions in the cytoplasm of neurons; possible candidates include canonical poly(A) polymerase (Huang et al. 2002) or Gld4 (Burns et al. 2011).

While it is clear that altering the expression of Ngd affects basal levels of GluN2A protein, the observation that GluN2A expression is increased by chemical LTP even following Ngd depletion suggests that either Ngd does not function to inhibit activity-induced GluN2A translation or that it does not do so alone. Perhaps, other translation regulators play an important role in the activation of GluN2A translation

following stimulation, one such factor might be the deadenylase PARN. The role of

PARN in regulating GluN2A was not investigated here, but it is likely that PARN is

present in RNPs containing GluN2A as it is known to interact with CPEB and Gld2. It is

possible that Ngd represses the basal translation of GluN2A, while PARN plays an

integral role in activity-induced translation. Future studies are needed to tease apart the

role of these two translational repressors in regulating GluN2A translation. The enhanced

LTP-mediated membrane insertion of GluN2A following Ngd depletion suggests that

there is either increased availability of GluN2A protein or increased potential for

translation of GluN2A protein. Ngd enhances GluN2A expression under basal conditions,

so it possible that upon synaptic activation a larger pool of available NMDA receptors is

responsible for increased insertion. Alternatively, the depletion of Ngd likely increases

the potential for synaptic activation as shown by increased GluA1 surface expression, and

could thus increase the activation of local translation. To understand the role of protein

synthesis in this process, further experiments need to be completed wherein a protein

synthesis inhibitor is used in conjunction with Ngd depletion.

The data in this chapter describe a new molecular mechanism and identify critical

factors controlling dendritic GluN2A levels and NMDA receptor insertion in

hippocampal neurons. Translational control of any particular mRNA is often a complex

process involving factors that influence different steps in translation. Indeed, GluN2A

translation is also regulated in part by an FMRP-microRNA pathway (Edbauer et al.

2010). Although local translation of GluN2A was not addressed in the Edbauer et al.

study, FMRP does regulate the translation of particular dendritic mRNAs in response to

mGluR-mediated signaling (Bassell and Warren 2008). If one presumes that unique as

well as shared mRNAs are translated in response to NMDA receptor- and mGluR-mediated signaling, then it becomes evident how combinations of newly synthesized proteins could impart characteristics to synapses that are exclusive to a particular signaling cascade. Here, we demonstrate that an LTP inducing stimulation leads to increased NR2A-containing NMDA receptors in a protein synthesis-dependent manner. FMRP is a critical regulator of protein synthesis during mGlu-dependent LTD. If FMRP indeed regulates dendritic GluN2A mRNA translation during LTD, it will be interesting to discover how local regulation of GluN2A mRNA functions during synaptic depression. The continued investigation of GluN2A mRNA regulation, as well as that of other dendritic mRNAs, in response to specific signaling events will be critical for understanding the role of local protein synthesis in bidirectional synaptic plasticity.

4.4 Experimental Procedures

Hippocampal neuron culture and drug treatments

Rat hippocampal neuron cultures were prepared from E18 embryos as described

previously (Goslin and Banker, 1998). Neurons were cultured for 14-21 *DIV* on poly-L-

lysine coated tissue culture plastic for biochemical experiments, glass coverslips for fixed

imaging experiments, and glass-bottom dishes for live-cell imaging experiments. For

chemical LTP experiments, hippocampal neurons were incubated in bathing solution (in

mM: 150 NaCl, 2 $CaCl_2$, 5 KCl, 10 HEPES, 30 glucose, 0.0005 TTX, 0.001 strychnine,

0.02 bicuculline methiodide, pH 7.4.) for 30 minutes, then 200 µM glycine was added to

the bathing solution for 3 min. The glycine containing solution was then removed and

neurons were incubated in the bathing solution (without glycine) for 30 minutes unless

otherwise indicated in the figure legends. For anisomycin experiments, either 40 µM

anisomycin or equal volume of DMSO was applied to the neurons 30 minutes prior to

and maintained throughout the duration of each experiment.

DNA constructions and neuron transfection

A 933 nucleotide sequence of the GluN2A 3' UTR was cloned from rat brain cDNA.

Within the cloned portion of the GluN2A 3' UTR, the CPE sequence was mutated using

QuikChange XL (Agilent). CPE mutants were confirmed using the inserted BamHI

restriction site and sequenced. The XhoI and BspE1 restriction sites were used to clone

the 3' UTRs into peGFP-C1 (Clontech) and pDendra2-C1 (Welshhans and Bassell, 2011).

A portion of the 5' UTR (-1352 to -338) was a gift of G. Bai at University of Maryland.

PCR was used to add NheI and AgeI restriction sites flanking the 5' UTR, and these sites

157

were used to clone it upstream of Dendra2 coding region in pDendra2-C1. All primers used for cloning and mutagenesis are provided in Table 4.1. FLAG-mCherry and FLAG-mCherry-CPEB constructs were generated as described in *2.4 Experimental Procedures.*

Antibodies

For immunocytochemistry, the following antibody dilutions were used: anti-GluN2A (1:100, Millipore), anti-GluN2B (1:100, Millipore), and anti-GluN1 (1:100, BD Biosciences). For western blotting, the following antibody dilutions were used: anti-GluN2A (1:500), anti-GluN2B (1:500), anti-GluN1 (1:2000), anti-pGluR1-S831 and pGluR1-S845 (1:500, Cell Signaling Technologies), anti-GluR1 (1:2000, Millipore), anti-pCPEB (1:2000), anti-CPEB (1:500), and anti-α-tubulin (1:20,000, Sigma Aldrich).

Immunofluorescence and fluorescence in situ hybridization

Cultured hippocampal neurons were processed for immunofluorescence as described previously (Muddashetty et al., 2007). Fluorescence *in* situ hybridization (FISH) was performed on cultured hippocampal neurons and mouse brain sections as previously described (Swanger et al., 2011a). Antisense oligonucleotide probes (Biosearch Technologies) were conjugated to Cy-3b (GE Healthcare) and used to detect GluN2A, β-tubulin, PSD95, αCaMKII, and GFP mRNAs. Sense GluN2A sequence probes and scrambled probes (Sasaki et al., 2010) were used as controls. The oligonucleotide probe sequences are provided in Table 4.2. For FISH on brain sections, riboprobes were reverse transcribed from the following cDNAs: β-tubulin, GenBank Accession No. NM_023279, nt 231 - 1203 and GluN2A, GenBank Accession No. NM_008170.2.

FLAG immunoprecipitations and RNA extraction

Hippocampal neurons or neuroblastoma cells were lysed with buffer containing: 150 mM
NaCl, 50 mM Tris, 1 mM $MgCl_2$, protease inhibitors (Roche), RNAse inhibitors
(Promega), and 1% Nonidet P40, pH 7.4. Agarose beads conjugated to M2 anti-FLAG
antibodies (Sigma Aldrich) were washed 3 times with PBS, and then incubated with
neuron lysates for 2 hrs rotating at 4ºC. The beads were then washed 4 times with lysis
buffer. Five percent of the input was kept for analysis of total mRNA. RNA was
extracted from the input and IP samples using Trizol LS (Invitrogen) according to the
manufacturer's instructions.

Quantitative real-time PCR

mRNAs were reverse transcribed with random hexamer primers by Superscript III
(Invitrogen) according to manufacturer's instructions. PCR was performed in triplicate
with specific primers and SYBR II dye in a light cycler (Roche). mRNA quantification
was done by the relative quantification method. A standard curve was created by serial
dilution of the total RNA. The crossing point (cp) values for each dilution were plotted
against the assigned copy numbers (a relative number assuming the highest concentration
as 1000 copies). For the experimental samples, the relative copy number of the mRNA
was calculated using its cp value and standard curve. The list of primers is provided in
Table 4.1.

Surface biotinylation

Surface protein biotinylation was performed as previously described (Ehlers, 2000).

Briefly, high density hippocampal neuron cultures were placed on ice and rinsed twice with ice-cold PBS containing 1mM $MgCl_2$ and 0.01 mM $CaCl_2$, then incubated on ice with the PBS solution containing 1 mg/ml Sulfo-NHS-Biotin (Thermo Scientific) for 20 minutes. Cultures were then rinsed 3 times with PBS solution containing 50 mM glycine to quench the biotin reactivity. Neurons were scraped in ice-cold lysis buffer (150 mM NaCl, 50 mM Tris, 1% Triton, 0.2% SDS, and protease inhibitors), then sonicated and centrifuged for 15 minutes. Supernatants were added to Neutravidin beads and rotated at 4ºC for 2 hours, then washed 4 times with lysis buffer; 2% of the supernatant volume was kept for SDS-PAGE analysis. Laemmli buffer was added to the samples, and they were boiled for 5 minutes, followed by SDS-PAGE and western blotting.

Fixed image acquisition and analysis

Coronal brains sections were imaged with a Zeiss (Oberkochen) LSM510 confocal microscope. Images were prepared using Imaris (Bitplane, Inc.). Cultured neurons were imaged with a Nikon Ti inverted microscope using a 60x 1.4NA Plan Apo objective and an HQ2 cooled CCD camera (Photometrics). Within each experiment, all treatment groups were imaged with the same acquisition settings and within the same imaging session. Z-series were obtained at 0.15 μm steps. Image stacks were deconvolved using a 3D blind constrained iterative algorithm (AutoQuant, CyberMetrics). Quantification of immunofluorescence and FISH signals were performed using ImageJ. Mean fluorescence intensities were quantified within in a cellular region, and mean background fluorescence intensities were quantified from an adjacent, non-cellular region. Dendrites were straightened using the Straighten plugin for ImageJ. For dendritic granule counts, a

dendritic region was chosen in ImageJ and a threshold level was determined that included

all granules above background. The threshold was applied and the Particle Analysis

function was used to compute the number of RNA granules within the area. The same

threshold was used across all images and groups. The representative images shown

within a single figure panel are presented with identical threshold settings.

Local translation assay and live-cell imaging

Neurons were transfected with the Dendra2 reporter constructs using Lipofectamine 2000

and were used for imaging 48 hours after transfection. A Nikon A1R microscope, NIS-

Elements software, and a 60× objective (Nikon Apo TIRF, NA 1.49) were used for live-

cell imaging. The neurons were maintained at 37°C and 5% CO_2 throughout the

experiment. Thirty minutes prior to imaging, the growth media was removed from

MatTek dishes and was exchanged with cLTP bathing solution (without glycine). For

some experiments, neurons were pretreated with anisomycin (40 μm) or vehicle control

(DMSO) during this 30 min period. Distal dendritic regions were chosen on 3-4 neurons

within a dish and were imaged with both the 488 and 561 nm lasers. These regions were

photoconverted using the 405 nm laser and imaged immediately after using the 488 and

561 nm lasers. Neurons were then exposed either to glycine (200 μM) or vehicle control

and imaged using the 488 and 561 nm laser every 5 min for 60 min. In order for a

dendritic region to be included in the analysis, the 488 nm signal had to decrease by 75%

and the 561 nm signal had to increase by 50%. Mean fluorescent intensity was measured

in the dendritic region at each time point and background subtracted. These intensity

measurements were then normalized to the first image acquired following addition of

glycine or vehicle and graphed as $\Delta F/F_0 \times 100$. In each experiment, green fluorescence was measured outside of the photoconverted region to control for photobleaching, and red fluorescence was measured within the photoconverted region to monitor Dendra2 diffusion.

Statistical analysis

Each experiment was repeated a minimum of three independent times and all analysis was completed using SPSS (IBM). All datasets were analyzed for normality using the Shapiro-Wilk's test. If the data were normally distributed then a Student's t-test or ANOVA (one-way, two-way, or repeated-measures) was performed. Significant ANOVA analyses were followed by post-hoc tests as mentioned in each figure legend. If the data were not normally distributed, then the non-parametric Kruskal-Wallis or Mann-Whitney tests were performed. The specific statistical test used in each experiment is given in its figure legend. Significance was set as $p \leq 0.05$ and adjusted for the number of pairwise comparisons when necessary. All data are graphed as mean ± SEM.

	forward primer	reverse primer
GluN2A 3' UTR cloning	5'-cgcgcg<u>ctcgag</u>atgtggctcagatgctttcc-3'	5'-cgcgcg<u>tccgga</u>tttctcattttcatatcaattggcag-3'
CPE mutant	5'-gaagtatatactatggttgtcttcttgtagtatgtct**<u>ggtacc</u>**attttgttcaatgtgatatcaactgttttaaggaatg-3'	5'-cattccttaaaacagttgatatcacattgaacaaaat**<u>ggtacc</u>**agacatactacaagaagacaaccatagtatatac ttc-3'
GluN2A 5' UTR	gcgcgc<u>gctagc</u>gcagcaagtgtgtatgtgtgt	gcgcgc<u>accggt</u>gagccctggctcagctttct
qPCR GluN2A	gggctgctcttctccatcagc	cccttgtctgaaaccatgtccac
qPCR GluN1	tctggccaggaggagagacagag	tgtcattaggccccgtacagatcacc
qPCR γ-actin	ctggtggatctctgtgagcac	aaacgttcccaactcaaggc
qPCR αCaMKII	gctgccaagattatcaacacc	cacgctccagcttctggt
qPCR GFP	aaggacgacggcaactacaag	atgccgttcttctgcttgtcg
qPCR Dendra2	ccggttcttttgtcaagacc	ctgcctcgtcttgcagttc

Table 4.1 Primers used for cloning, mutagenesis, and quantitative real-time PCR (qPCR). Underlined sequences are restriction cut sites introduced for cloning. The mutated nucleotides within the CPE sequence primer are bold and underlined.

NR2A antisense	5' ggagcaa**t**atgatgctg**t**tgacctcaagga**t**gaccgaaga**t**agctgtca**tt** 3'
	5' cctc**t**actgtg**t**taggg**t**tggac**t**cattgagag**t**gagaggatgc**t**gtccttg 3'
	5' ggtgca**t**atacgggtag**t**tg**t**tacgaa**t**attcctctc**t**gtacttccat**t**ggg 3'
	5' gcata**t**cccagcccacaaagc**t**gttgtccac**t**gttgtc**t**tgataaagc**t**ga 3'
NR2A sense	5' aa**t**gacagcta**t**c**t**tcggtca**t** cc**t**tgagg**t**caacagcatcata**t**tgctcc 3'
	5' caagga**c**agca**t**cctctcac**t**ctcaatgag**t**ccaaccc**t**aacacag**t**agagg 3'
	5' cccaa**t**ggaag**t**acagagagga**a**ta**t**tcgtaacaac**t**acccgtata**t**gcacc 3'
	5' tcagc**t**ttatcaagacaacag**t**ggacaacagc**t**ttgtgggc**t**gggata**t**gc 3'
GFP antisense	5' gtgg**t**gcagatgaac**t**tcagggtcagc**t**tgccgtagg**t**gg 3'
	5' ggcgga**t**cttgaag**t**tcaccttgatgccg**t**tcttctgc**t**t 3'
	5' cacgaac**t**ccagcaggacca**t**gtgatcgcgct**t**ctcgttg 3'

Table 4.2 Oligonucleotide sequences for FISH probes. The bold thymidine residues are those that have been amino-modified and conjugated to either digoxigenin or a fluorophore.

CHAPTER FIVE

General Discussion

Parts of this chapter are adapted from:

Swanger, S.A., Bassell, G.J. Making and breaking synapses through local mRNA regulation. *Curr Opin Genet Dev.* 2011 Aug;21(4):414-21.

Udagawa, T.*, Swanger, S.A.*, Takeuchi, K., Kim, J.H., Nalavadi, V., Shin, J., Lorenz, L.J., Zukin, R. S., Bassell, G.J., and Richter, J.D. Bidirectional control of mRNA translation and synaptic plasticity by the cytoplasmic polyadenylation complex. *Mol Cell.* In press. (* equal contribution)

Neuronal communication occurs on a millisecond time scale, but must induce changes that last a lifetime. These life-long changes underlying synaptic plasticity require modification of the synaptic molecular composite, and this is mediated, in part, by locally synthesized proteins. Neurons have an intricate morphology with thousands of synaptic compartments and signaling micro-domains, and local protein synthesis is a mechanism that functions with the temporal and spatial precision required to regulate individual synapses during experience-mediated plasticity.

The data in this thesis describe one molecular mechanism that mediates local mRNA regulation in dendrites and modulates the synaptic protein composite as well as synapse structure and function. We have identified a multi-protein complex that associates with the synaptic mRNA binding protein CPEB and consists of the poly(A) polymerase Gld2, the deadenylase PARN, the eIF4E binding protein Ngd, and the scaffolding protein symplekin. CPEB modulates the transport of these translation factors as well as CPE-containing mRNAs into dendrites. These mRNP complexes are locally activated through NMDA receptor-mediated phosphorylation of CPEB, which leads to the expulsion of PARN from CPEB-associated mRNPs and Gld2-dependent polyadenylation of associated CPE-containing mRNAs. GluN2A mRNA is localized to dendrites, and the CPE sequence within the 3' UTR of GluN2A regulates dendritic mRNA localization and local translation. The CPEB associated translation regulators Gld2 and Ngd bidirectionally regulate the dendritic expression of NR2A protein as well as the surface expression of NR2A-containing NMDA receptors. Moreover, the data herein show that increased NMDA receptor surface expression during chemically induced LTP is dependent upon protein synthesis. Furthermore, Gld2 is required for this

activity-induced insertion of GluN2A-containing NMDA receptors. Gld2 promotes and Ngd inhibits dendritic spine maturation and AMPA receptor surface expression. In total, this thesis has determined that CPEB regulates dendritic mRNA translation through a multi-protein complex of polyadenylation and translation factors. Moreover, the data herein demonstrate that the post-transcriptional regulation of GluN2A mRNA by CPEB and associated factors is a novel mechanism for regulating activity-induced NMDA receptor surface expression during synaptic plasticity. Based on these results, we propose that local regulation of GluN2A mRNA in dendrites is one means by which CPEB, Gld2, and Ngd modulate synapse structure and function.

5.1 RNA binding proteins mediate mRNA transport and bidirectional translational control in dendrites

CPEB has an established role in mRNA regulation in neuronal dendrites as well as in modulating synaptic plasticity and neuronal structure (Alarcon et al., 2004; Berger-Sweeney et al., 2006; Bestman and Cline, 2008; McEvoy et al., 2007; Wells et al., 2001; Zearfoss et al., 2008). However, the data presented herein are the first to elucidate a molecular mechanism by which CPEB regulates dendritic mRNA localization and translation at synapses. Based on these data, we propose a model for the bidirectional control of activity-induced local translation through CPEB-mediated dendritic mRNA polyadenylation (Figure 5.1). Dendritic mRNA transcripts that contain CPE sequences are bound by CPEB, which in turn is associated with PARN, Gld2, symplekin, and Ngd. These mRNAs would have relatively short poly(A) tails, and Ngd is bound to eIF4E, the cap binding factor, and thus, the translation of the bound mRNAs is blocked at the

initiation step. NMDA receptor activation promotes phosphorylation of CPEB and expulsion of PARN from the RNP complex. Gld2 then catalyzes poly(A) addition to the CPE-containing mRNAs, which we surmise leads to the displacement of Ngd from eIF4E, the binding of eIF4G to eIF4E, and translational enhancement of the mRNA. In sum, this mechanisms permits translational repression until the phosphorylation of CPEB at synapses, and thus, allows for local activation of translation. The bidirectional control mediated by this complex of translation factors is well-suited for permitting translational repression during mRNA transport into dendrites. Indeed, the data herein show that CPEB and the CPE sequence are required for the efficient dendritic transport of at least one mRNA transcript, GluN2A. We also show that CPEB is necessary for the efficient transport of Gld2, PARN, and Ngd, suggesting that this complex is transported as a unit into dendrites; thus, further indicating that bound mRNAs are likely repressed during transport by the presence of the negative translational regulators PARN and Ngd. Importantly, this mechanism provides the elements necessary for local delivery of synaptic proteins during synaptic activation as proposed by the local protein synthesis model (Figures 1.1 and 1.2).

As mentioned previously, there are also other mRNA binding proteins that are localized to dendrites and regulate synaptic protein synthesis. Besides CPEB, the best-studied dendritic RNA binding proteins are ZBP1 and FMRP (Bassell and Warren, 2008; Doyle and Kiebler, 2011; Swanger and Bassell, 2011). For both proteins, there have been bidirectional translational control mechanisms proposed for specific localized mRNAs. ZBP1 regulates β-actin mRNA translation through repressing translation until the local phosphorylation-dependent release of mRNA in growth cones (Sasaki et al., 2010;

Welshhans and Bassell, 2011), and it is proposed to function similarly in dendrites, although this has not been shown directly (Eom et al., 2003; Perycz et al., 2011; Tiruchinapalli et al., 2003; Zhang et al., 2001). An elegant mechanism for FMRP-mediated translation repression and local activation in dendrites has also been delineated. FMRP interacts with miR-125a and the RISC complex at synapses to repress the translation of PSD95 mRNA, and mGlu receptor activation leads to dephosphorylation of synaptic FMRP resulting in the release of PSD95 mRNA and loss of the miRNA-mediated translational repression (Muddashetty et al., 2011). FMRP has also been shown to regulate the localization of some dendritic mRNAs (Antar et al., 2005; Dictenberg et al., 2008; Kao et al., 2010; Muddashetty et al., 2007), though it is unknown whether FMRP regulates the localization of PSD95 mRNA. Importantly, as shown in this thesis, CPEB and associated factors are integrally involved in mRNA localization, translational repression, dendritic mRNA polyadenylation, and dendritic protein synthesis.

Together, these studies support a critical role for mRNA binding proteins in the post-transcriptional regulation of localized mRNAs. Some established mechanisms for mRNA binding protein-mediated regulation of localized mRNAs in neuronal dendrites and growth cones are illustrated in Figure 5.2. While these mechanisms provide an understanding of how the precise spatial and temporal control of localized mRNAs occurs in neurons, in the majority of cases only one mRNA target has been studied in detail. In the future, it will be critical to search for additional mRNA targets regulated by similar molecular mechanisms in order to understand the full impact of these mRNA binding proteins at synapses. For instance, it is likely that CPEB-mediated regulation of GluN2A mRNA is of great importance for normal synaptic function, but one report

proposed that as many as 7% of brain mRNAs might undergo activity-dependent polyadenylation (Du and Richter, 2005); several mRNAs identified in this study contain CPE sequences and a few have been shown to localize to dendrites (Burgin et al., 1990; Kindler et al., 1996; Kleiman et al., 1990; Tongiorgi et al., 2004). In order to fully understand how CPEB, Gld2, PARN, and Ngd regulate synapse function through local protein synthesis, it is critical to investigate the post-transcriptional regulation of these localized mRNA transcripts as well.

5.2 Stimulus-specific local protein synthesis

Given the collection of differentially regulated mRNA transcripts and binding proteins present in dendrites, one can envision that different synaptic signaling pathways might regulate particular mRNA binding proteins and, thus, mediate the localized synthesis of a particular set of proteins. For example, CPEB and FMRP have at least two validated overlapping target mRNAs, GluN2A and αCaMKII (Bagni et al., 2000; Edbauer et al., 2010; Wu et al., 1998). These are two critical synaptic proteins so it is not surprising that there are multiple means of regulating their protein levels at synapses. However, it remains unclear how CPEB and FMRP might differentially regulate the synthesis of these target mRNAs. It is clear that mGlu activation leads to FMRP-mediated translation at synapses (Ronesi and Huber, 2008), and, based on this thesis and other work, it is clear that NMDA receptor activation induces CPEB-mediated local mRNA polyadenylation and translation (Huang et al., 2002; Wells et al., 2001; Wu et al., 1998). However, how these two mechanism act in concert is unclear. CPEB and associated factors appear to regulate hippocampal LTP (Alarcon et al., 2004; Zearfoss et

al., 2008), whereas FMRP appears to regulate LTD, although it has been implicated in

some forms of hippocampal LTP as well (Auerbach and Bear, 2010; Connor et al., 2011;

Huber et al., 2002). Interestingly, in the cerebellum, disrupting CPEB activation by

mutating the phosphorylation sites reduces mGlu-dependent LTD at the parallel fiber-

Purkinje neuron synapse and reduces dendritic spine size; whereas, depletion of FMRP

leads to enhanced LTD at these synapses and enlarged dendritic spines (Koekkoek et al.,

2005; McEvoy et al., 2007). The purpose of these overlapping synaptic mechanisms for

regulating local translation remain unclear, and how these mechanisms might

differentially regulate hippocampal synapses as compared to cerebellar synapses also

remains unstudied. Understanding how these mechanisms function together, and whether

they do so cooperatively or antagonistically, is paramount to understanding how locally

synthesized proteins are integrated into the existing synaptic composite and contribute to

synapse function and plasticity.

5.3 Synaptic regulation by mRNA binding proteins in health and disease

As shown in this thesis, Gld2 and Ngd, two CPEB-associated translation factors,

have important roles in bidirectionally regulating the surface expression of glutamate

receptors and dendritic spine morphology. Furthermore, it has been previously shown

that CPEB has a critical function in hippocampal synaptic plasticity and memory

extinction (Alarcon et al., 2004; Berger-Sweeney et al., 2006; Zearfoss et al., 2008), and

my collaborators discovered that Gld2 and Ngd also critically regulate LTP in the dentate

gyrus (Udagawa et al., in press). Interestingly, disrupting Gld2 activity in the mushroom

body of *Drosophila* blocks courtship memory formation, which supports a role for Gld2

in learning and memory (Kwak et al., 2008). In addition, CPEB has an important function in regulating cerebellar LTD, Purkinje neuron morphology, and motor learning (McEvoy et al., 2007). As shown in this thesis, Gld2, PARN, and Ngd are also expressed and localized to dendrites in Purkinje neurons of the cerebellum (Figure 2.3), suggesting that these factors could also mediate CPEB-dependent mRNA polyadenylation and translation in this brain region. Importantly, the findings presented herein suggest that CPEB and associated factors have critical roles in mediating proper synapse function in the hippocampus. This work motivates future investigations of their roles in other brain regions such as the cortex and cerebellum where activity-dependent polyadenylation of CPE-containing mRNAs has been shown to occur (Shin et al., 2004; Wu et al., 1998).

Thus far, CPEB and the associated neuronal translation factors identified herein have not been implicated in any neurological disease. Yet, in a recent report, the dendritic expression and NMDA receptor-mediated synthesis of Down syndrome cell adhesion molecule (DSCAM) was shown to be dysregulated in a mouse model of Down syndrome (Alves-Sampaio et al., 2010). DSCAM mRNA contains several CPE sequences and is localized to dendrites. In this Down syndrome mouse model, excess NMDA receptor-mediated translation results in elevated DSCAM protein levels and disrupted dendrite development in hippocampal neurons. In addition, BDNF protein levels and BDNF-induced local translation are elevated in this mouse model; interestingly, BDNF is also a CPE-containing mRNA that is locally translated (An et al., 2008; Oe and Yoneda, 2010; Troca-Marin et al., 2011). Although these reports did not determine whether CPEB-mediated mRNA regulation of either DSCAM or BDNF mRNA was disrupted in this disease model, moving forward it will be important to investigate whether these mRNAs

are indeed locally regulated by CPEB, Gld2, PARN, and Ngd, and whether dysregulation of this mechanism might contribute to the altered protein expression seen in the disease model. If so, then perhaps this translation complex could be targeted as a means to correct DSCAM and BDNF protein expression levels. Alternatively, even if this translational mechanism is not the cause of the dysregulated synthesis of DSCAM and BDNF in this disease model, perhaps altering the function or expression of the CPEB-associated translation factors could correct the protein levels through a mechanism functioning in parallel to that which is disrupted.

Indeed, the hypothesis that dysregulated translation might be corrected through targeting mechanisms parallel to those that are disrupted in disease states is one that has been considered extensively of late. For instance, a recent study showed that the excess protein synthesis and behavioral impairments in a mouse model of fragile X syndrome could be corrected by cross breeding these mice with those modeling tuberous sclerosis, which a disease model that exhibits decreased synaptic protein synthesis (Auerbach et al., 2011). In this study, the authors focused on rescuing general protein synthesis levels at synapses as the mouse model of tuberous sclerosis alters protein synthesis through a global regulatory mechanism. However, one could imagine that if an mRNA-specific translational regulatory mechanism is dysregulated in a disease state, then altering the function of another mRNA-specific regulatory mechanism, which controls an overlapping set of target transcripts, might correct aberrant translation of at least some synaptic mRNAs. In this regard, several dendritic translational regulators are associated with neurological disorders such as intellectual disability, autism and dementia (Bramham, 2007; Kumar-Singh, 2011; Sokol et al., 2011). For instance, loss of the RNA

binding protein FMRP causes fragile X syndrome, which is characterized by intellectual disability, autistic features, seizures, anxiety, and hyperactivity (Gross et al., 2011a). Mice lacking FMRP show exaggerated synaptic protein synthesis, enhanced mGlu-LTD, decreased dendritic spine size, and excess internalization of GluA1-containing receptors (Huber et al., 2002; Irwin et al., 2002; Nakamoto et al., 2007). In most cases, FMRP represses translation of target mRNAs including, PSD-95, αCaMKII, and GluA1 (Dolen et al., 2007; Gross et al., 2010; Kao et al., 2010; Muddashetty et al., 2007; Zalfa et al., 2003), but there is also evidence that FMRP enhances translation of some mRNAs (Bechara et al., 2009; Fahling et al., 2009; Gross et al., 2011b). Interestingly, FMRP and CPEB share at least two mRNA targets namely GluN2A and αCaMKII mRNA (Edbauer et al., 2010; Wu et al., 1998). While it is unknown whether dendritic GluN2A mRNA translation is dysregulated in FMRP-deficient neurons, it has been shown that αCaMKII is excessively translated at synapses in the mouse model of fragile X syndrome (Bagni et al., 2000; Kao et al., 2010; Muddashetty et al., 2007). Given that the work presented herein has delineated the molecular mechanism by which CPEB regulates at least one mRNA transcript, it will be interesting to determine whether manipulating this mechanism could counterbalance the disrupted translation resulting from the loss of FMRP.

The RNA binding protein translin is also associated with regulation of local protein synthesis as well as learning and memory (Finkenstadt et al., 2000; Kobayashi et al., 1998; Li et al., 2008; Muramatsu et al., 1998). Translin knockout mice have altered spatial memory, fear learning, and anxiety behaviors as well as increased incidence of seizures compared to wild type mice (Stein et al., 2006). Translin has been shown to

regulate the dendritic targeting of BDNF mRNA through an interaction with a constitutive dendritic targeting element with the coding region of BDNF (Chiaruttini et al., 2009). Interestingly, not all isoforms of BDNF are trafficked to dendrites; it appears that some 3' UTRs silence the coding region dendritic targeting element (An et al., 2008; Chiaruttini et al., 2009; Wu et al., 2011). Moreover, there is a known human mutation in BDNF (G694A) that causes altered brain structure, psychiatric disorders, and memory deficits (Bath et al., 2011; Bath et al., 2012; Bath and Lee, 2006; Krishnan et al., 2007; Pezawas et al., 2004; Soliman et al., 2010). When this mutation is introduced in a mouse model it disrupts the interactions between BDNF mRNA and translin as well as dendritic targeting of BDNF mRNA in hippocampal neurons (Chiaruttini et al., 2009). Together, these data suggest that translin may function to regulate dendritic synthesis of BDNF and neurological function. BDNF mRNA contains CPE sequences in the 3' UTR and the dendritic localization of BDNF mRNA has been shown to be regulated by these sequences (Oe and Yoneda, 2010). Furthermore, an isoform of BDNF mRNA harboring a long 3' UTR is localized to dendrites, and disrupting the dendritic localization of this isoform in mice leads to altered dendritic spine pruning and synaptic plasticity (An et al., 2008). Interestingly, activity specifically induces translation of the dendritically localized BDNF isoform (Lau et al., 2010). It is unclear whether CPEB or its associated factors regulate BDNF translation, but it is plausible that manipulating the function of the CPEB-associated complex could ameliorate the disrupted translin-mediated post-transcriptional regulation caused by the human mutation. Future work needs to be completed to test this hypothesis, but the possibility of using the findings described herein in translational research aimed at developing disease therapies enhances the significance of

understanding the basic mechanisms underlying local protein synthesis at synapses.

5.4 Input-specific local protein synthesis

  The models for input-specific delivery of synaptic proteins presented herein (Figure 1.1) suggest that proteins could be specifically captured at activated synapses (synaptic tagging model) or that new proteins might be synthesized specifically at activated synapses (local protein synthesis model). The data presented herein indicate that localized synthesis of the GluN2A subunit might contribute to the activity-dependent regulation of NMDA receptor expression. One could imagine that synaptic activation could lead to localized activation of CPEB-associated mRNP complexes, which results in newly synthesized NMDA receptor subunits and subsequent membrane insertion of new receptors (Figure 5.3). Indeed, bidirectional alterations in synaptic activity have been shown to alter the NMDA receptor currents and composition at specific synapses (Lee et al., 2010; Sobczyk and Svoboda, 2007). However, to date, only one study has convincingly shown that localized protein synthesis can be synapse-specific, and this study was performed in cultured *Aplysia* neurons (Wang et al., 2009). The serotonin-induced local synthesis of sensorin occurred only at activated sensory-to-motor neuron synapses. Interestingly, sensorin protein synthesis occurs in pre-synaptic terminals, but requires post-synaptic activation and cross-talk between the pre- and post-synaptic compartments. In order to study post-synaptic local protein synthesis in mammalian neurons, a combination of advanced technologies will likely have to be used. For instance, glutamate uncaging at individual dendritic spines could be used to induced localized synaptic activation in neurons expressing a fluorescent local translation reporter

such as that used herein (Figure 4.18).

Further evidence supporting input-specific protein synthesis can be garnered from studies demonstrating the synapse-specific delivery of mRNA transcripts. The studies by Steward et al. and Tonigiorgi et al. show that BDNF and Arc/Arg3.1 mRNA transcripts can also be specifically captured at activated synapses (Steward et al., 1998; Tongiorgi et al., 2004). Synaptic capture of mRNA requires transport of macromolecules following activity, and it is currently unclear whether mRNA transport followed by local translation could underlie rapid synaptic modifications during synaptic plasticity. It is likely, however, that synapse-specific localization of mRNA transcripts, and subsequent local translation, could underlie maintenance of altered synapse structure and function. Thus, these findings regarding mRNA localization provide further support for the importance of local protein synthesis in regulating modulations of synapse structure and function during the late-phase of synaptic plasticity as well as long-term maintenance of altered synaptic functions underlying long-lasting memory.

Another interesting aspect of synaptic regulation that has been poorly studied thus far is how RNPs are targeted to specific synaptic sites within dendrites. In one study, myosin Va was shown to mediate transport of RNPs containing the RNA binding protein TLS (translocated in liposarcoma) (Yoshimura et al., 2006), but how RNPs are targeted to those specific dendritic spines was not addressed. It is possible that a local signal directs RNPs being transported on microtubules to divert onto actin filaments of a particular dendritic spine, or, perhaps, RNPs are anchored within the dendritic shaft beneath synaptic sites and a subsequent signal leads to RNP translocation into the spine (Doyle and Kiebler, 2011). In fact, both mechanisms have been identified for the

targeting of RNPs to specific sites in *Drosophila* (Delanoue and Davis, 2005; Zimyanin et al., 2008), but neither has been directly studied in neuronal dendrites. In this thesis, we have shown that CPEB regulates the transport of Gld2, PARN and Ngd as well as GluN2A mRNA into dendrites, and we have also demonstrated that CPEB and associated factors are present within dendritic spines. However, it remains unclear whether CPEB regulates the targeting of mRNPs to spines and whether this process is activity-dependent. Future studies using live-imaging of fluorescently-tagged proteins and mRNA molecules could be used to address the roles of CPEB, kinesin, and myosin proteins in trafficking of mRNPs to specific synapses.

5.5 Concluding remarks

The thesis work presented here addresses, in part, three of the fundamental questions in the field of synaptic protein synthesis, as proposed earlier in this thesis: 1) how is dendritic protein synthesis regulated, 2) what is the relationship between synaptic plasticity and local protein synthesis, and 3) which mRNA transcripts are localized and translated in dendrites? Herein, we have shown that the CPEB-associated enzymes Gld2 and PARN regulate dendritic mRNAs by controlling the poly(A) tail length of CPE-containing associated mRNAs. Furthermore, we have demonstrated that a chemically-induced form of LTP activates the synaptic CPEB-associated complex and leads to dendritic mRNA polyadenylation as well as CPE-mediated dendritic mRNA translation. Finally, we have identified that GluN2A mRNA is localized to dendrites and that chemical LTP induces the protein synthesis-dependent insertion of GluN2A-containing NMDA receptors in hippocampal neurons. The collection of findings presented here

describes a novel mechanism for regulating dendritic protein synthesis as well as the activity-dependent regulation of synaptic NMDA receptors. Given the critical function of NMDA receptors and synaptic protein synthesis in health and disease, this body of work has great implications for future studies aimed at understanding and manipulating the molecular mechanisms underlying synaptic plasticity.

Figure 5.1
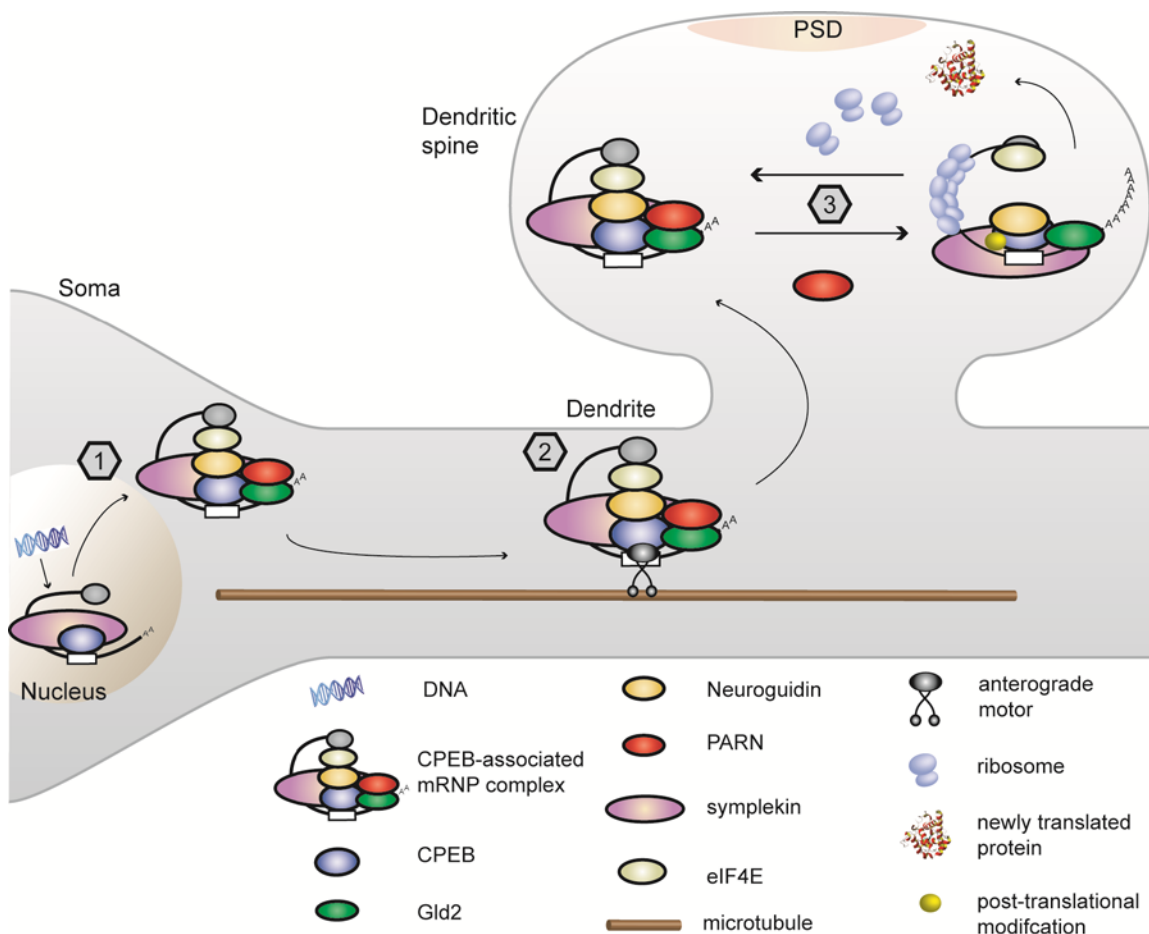
Figure 5.1 CPEB-mediated dendritic mRNA transport and bidirectional control of translation. (1) CPEB binds CPE-containing mRNAs in the nucleus where it also associates with some components of the CPEB-associated complex and with other translation factors in the cytoplasm (Lin et al., 2010). (2) CPEB binds kinesin and regulates the transport of the associated translational regulators and mRNAs into dendrites. (3) Once localized to synapses, the CPEB-associated mRNP is activated by NMDA receptor signaling, which results in CPEB phosphorylation, extrusion of PARN, and Gld2-dependent mRNA polyadenylation.

Figure 5.2 Local mRNA regulation in growth cone guidance and spine morphogenesis. This model illustrates the mechanisms controlling local mRNA transport and translation in developing axons and dendrites. mRNA transport (at right): Microtubule motor proteins, adaptors, and RNA binding proteins mediate mRNA transport, while suppressing mRNA translation. (1) At the growth cone, cues signal through surface receptors to directly activate the translation machinery. (2) A secreted molecule from the post-synaptic cell can activate pre-synaptic translation by regulating mRNA binding proteins. (3) Localized mRNAs are regulated by multiple mechanisms, such as two different RNA binding proteins. Receptor-mediated signaling can lead to post-translational modification of RNA binding proteins and de-repression. (4) miRNAs and RISC suppress translation within dendrites, and post-synaptic receptor signaling can alleviate miRNA-mediated silencing and promote local mRNA translation. Locally synthesized proteins include several classes of molecules with local and distal functions (adapted from Swanger and Bassell, 2011)).

Figure 5.2
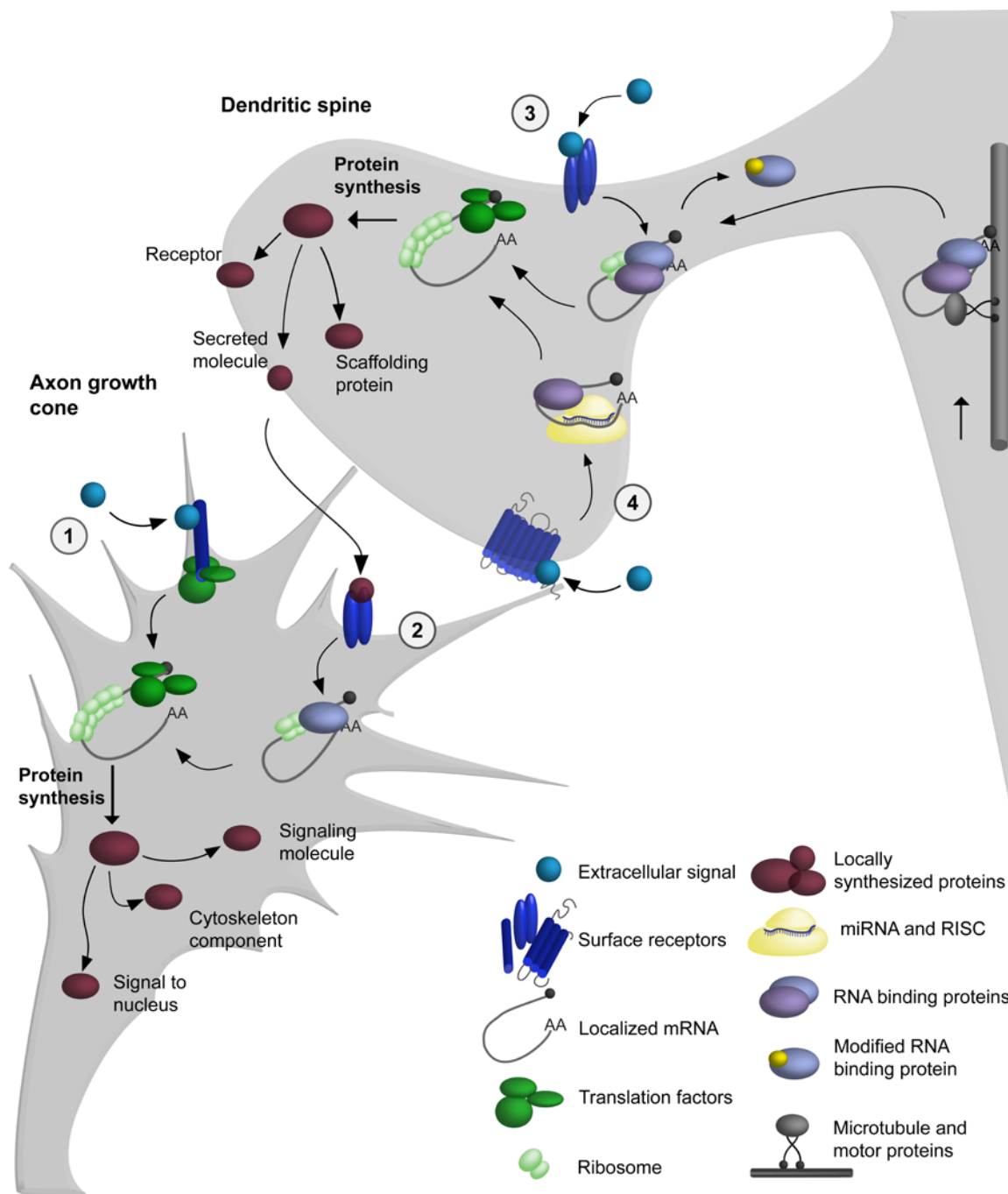
Figure 5.3 Model for CPEB-mediated local translation of GluN2A mRNA at synapses. GluN2A mRNA is localized to synapses through a CPE-dependent mechanism. (1) NMDA receptor activation leads to CPEB phosphorylation through a mechanism involving (2) Aurora A kinase and CaMKII. (3) CPEB phosphorylation causes PARN to be expelled from mRNP complexes containing GluN2A mRNA and results in Gld2-dependent mRNA polyadenylation. (4) Poly(A) tail elongation leads to the recruitment of PABP and the disruption of the Ngd-eIF4E interaction, which subsequently allows ribosome recruitment and GluN2A mRNA translation. (5) Post-transcriptional control of GluN2A mRNA by the CPEB-associated complex regulates the levels of GluN2A-containing NMDA receptors at synapses.

Figure 5.3
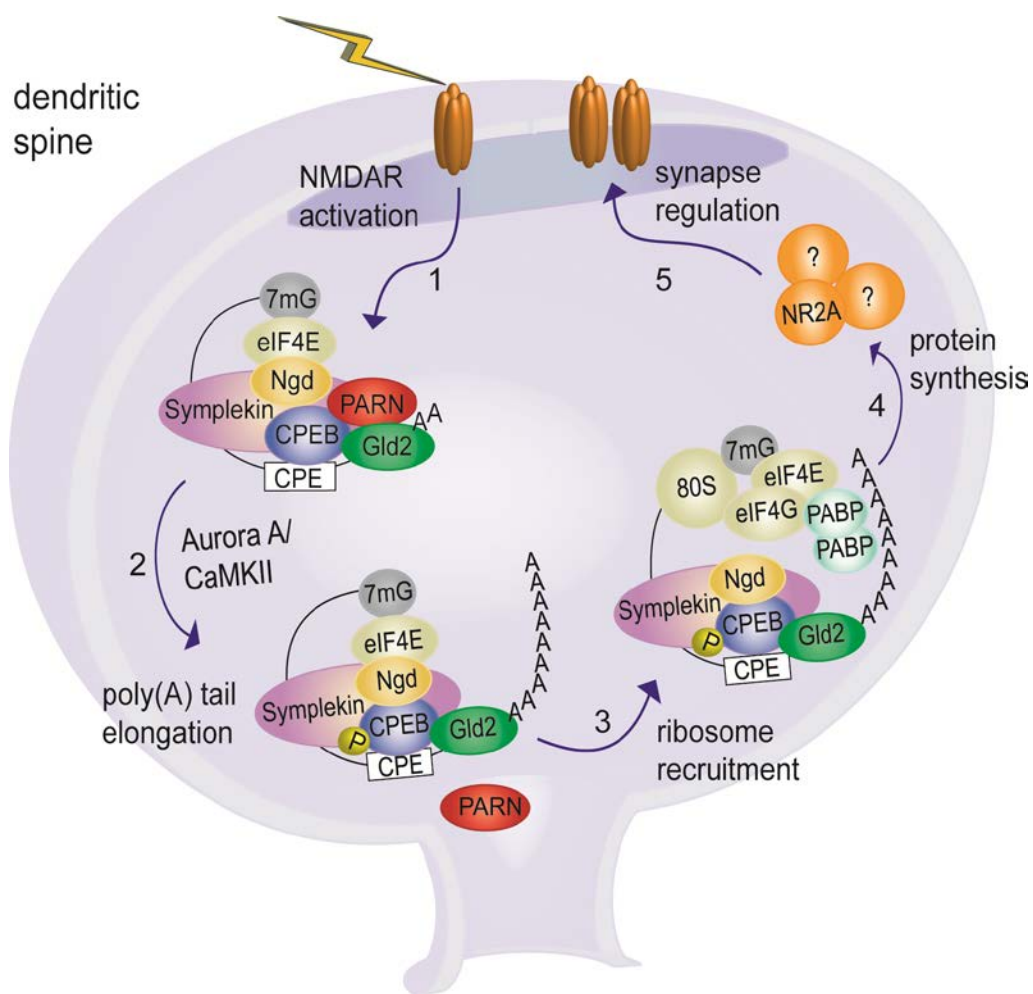
REFERENCES

Aakalu, G., Smith, W.B., Nguyen, N., Jiang, C., and Schuman, E.M. (2001). Dynamic visualization of local protein synthesis in hippocampal neurons. Neuron *30*, 489-502.

Abaza, I., and Gebauer, F. (2008). Trading translation with RNA-binding proteins. RNA *14*, 404-409.

Alarcon, J.M., Hodgman, R., Theis, M., Huang, Y.S., Kandel, E.R., and Richter, J.D. (2004). Selective modulation of some forms of schaffer collateral-CA1 synaptic plasticity in mice with a disruption of the CPEB-1 gene. Learn Mem *11*, 318-327.

Alvarez, V.A., and Sabatini, B.L. (2007). Anatomical and physiological plasticity of dendritic spines. Annu Rev Neurosci *30*, 79-97.

Alves-Sampaio, A., Troca-Marin, J.A., and Montesinos, M.L. (2010). NMDA-mediated regulation of DSCAM dendritic local translation is lost in a mouse model of Down's syndrome. J Neurosci *30*, 13537-13548.

An, J.J., Gharami, K., Liao, G.Y., Woo, N.H., Lau, A.G., Vanevski, F., Torre, E.R., Jones, K.R., Feng, Y., Lu, B., and Xu, B. (2008). Distinct role of long 3' UTR BDNF mRNA in spine morphology and synaptic plasticity in hippocampal neurons. Cell *134*, 175-187.

Andersen, P. (2007). The hippocampus book (Oxford ; New York, Oxford University Press).

Antar, L.N., Afroz, R., Dictenberg, J.B., Carroll, R.C., and Bassell, G.J. (2004). Metabotropic glutamate receptor activation regulates fragile x mental retardation protein and FMR1 mRNA localization differentially in dendrites and at synapses. J Neurosci *24*, 2648-2655.

Antar, L.N., Dictenberg, J.B., Plociniak, M., Afroz, R., and Bassell, G.J. (2005). Localization of FMRP-associated mRNA granules and requirement of microtubules for activity-dependent trafficking in hippocampal neurons. Genes Brain Behav *4*, 350-359.

Antion, M.D., Hou, L., Wong, H., Hoeffer, C.A., and Klann, E. (2008a). mGluR-dependent long-term depression is associated with increased phosphorylation of

S6 and synthesis of elongation factor 1A but remains expressed in S6K-deficient mice. Mol Cell Biol *28*, 2996-3007.

Antion, M.D., Merhav, M., Hoeffer, C.A., Reis, G., Kozma, S.C., Thomas, G., Schuman, E.M., Rosenblum, K., and Klann, E. (2008b). Removal of S6K1 and S6K2 leads to divergent alterations in learning, memory, and synaptic plasticity. Learn Mem *15*, 29-38.

Argilli, E., Sibley, D.R., Malenka, R.C., England, P.M., and Bonci, A. (2008). Mechanism and time course of cocaine-induced long-term potentiation in the ventral tegmental area. J Neurosci *28*, 9092-9100.

Asaki, C., Usuda, N., Nakazawa, A., Kametani, K., and Suzuki, T. (2003). Localization of translational components at the ultramicroscopic level at postsynaptic sites of the rat brain. Brain Res *972*, 168-176.

Aslam, N., Kubota, Y., Wells, D., and Shouval, H.Z. (2009). Translational switch for long-term maintenance of synaptic plasticity. Mol Syst Biol *5*, 284.

Atkins, C.M., Davare, M.A., Oh, M.C., Derkach, V., and Soderling, T.R. (2005). Bidirectional regulation of cytoplasmic polyadenylation element-binding protein phosphorylation by Ca2+/calmodulin-dependent protein kinase II and protein phosphatase 1 during hippocampal long-term potentiation. J Neurosci *25*, 5604-5610.

Atkins, C.M., Nozaki, N., Shigeri, Y., and Soderling, T.R. (2004). Cytoplasmic polyadenylation element binding protein-dependent protein synthesis is regulated by calcium/calmodulin-dependent protein kinase II. J Neurosci *24*, 5193-5201.

Auerbach, B.D., and Bear, M.F. (2010). Loss of the fragile X mental retardation protein decouples metabotropic glutamate receptor dependent priming of long-term potentiation from protein synthesis. J Neurophysiol *104*, 1047-1051.

Auerbach, B.D., Osterweil, E.K., and Bear, M.F. (2011). Mutations causing syndromic autism define an axis of synaptic pathophysiology. Nature *480*, 63-68.

Bagni, C., Mannucci, L., Dotti, C.G., and Amaldi, F. (2000). Chemical stimulation of synaptosomes modulates alpha -Ca2+/calmodulin-dependent protein kinase II mRNA association to polysomes. J Neurosci *20*, RC76.

Baker-Herman, T.L., and Mitchell, G.S. (2002). Phrenic long-term facilitation requires spinal serotonin receptor activation and protein synthesis. J Neurosci *22*, 6239-6246.

Banerjee, S., Neveu, P., and Kosik, K.S. (2009). A coordinated local translational control point at the synapse involving relief from silencing and MOV10 degradation. Neuron *64*, 871-884.

Banko, J.L., Poulin, F., Hou, L., DeMaria, C.T., Sonenberg, N., and Klann, E. (2005). The translation repressor 4E-BP2 is critical for eIF4F complex formation, synaptic plasticity, and memory in the hippocampus. J Neurosci *25*, 9581-9590.

Barnard, D.C., Ryan, K., Manley, J.L., and Richter, J.D. (2004). Symplekin and xGLD-2 are required for CPEB-mediated cytoplasmic polyadenylation. Cell *119*, 641-651.

Barria, A., Muller, D., Derkach, V., Griffith, L.C., and Soderling, T.R. (1997). Regulatory phosphorylation of AMPA-type glutamate receptors by CaM-KII during long-term potentiation. Science *276*, 2042-2045.

Bassell, G.J., and Kelic, S. (2004). Binding proteins for mRNA localization and local translation, and their dysfunction in genetic neurological disease. Curr Opin Neurobiol *14*, 574-581.

Bassell, G.J., and Warren, S.T. (2008). Fragile X syndrome: loss of local mRNA regulation alters synaptic development and function. Neuron *60*, 201-214.

Bassell, G.J., Zhang, H., Byrd, A.L., Femino, A.M., Singer, R.H., Taneja, K.L., Lifshitz, L.M., Herman, I.M., and Kosik, K.S. (1998). Sorting of beta-actin mRNA and protein to neurites and growth cones in culture. J Neurosci *18*, 251-265.

Bath, K.G., Akins, M.R., and Lee, F.S. (2011). BDNF control of adult SVZ neurogenesis. Dev Psychobiol.

Bath, K.G., Jing, D.Q., Dincheva, I., Neeb, C.C., Pattwell, S.S., Chao, M.V., Lee, F.S., and Ninan, I. (2012). BDNF Val66Met Impairs Fluoxetine-Induced Enhancement of Adult Hippocampus Plasticity. Neuropsychopharmacology *37*, 1297-1304.

Bath, K.G., and Lee, F.S. (2006). Variant BDNF (Val66Met) impact on brain structure and function. Cogn Affect Behav Neurosci *6*, 79-85.

Bechara, E.G., Didiot, M.C., Melko, M., Davidovic, L., Bensaid, M., Martin, P., Castets, M., Pognonec, P., Khandjian, E.W., Moine, H., and Bardoni, B. (2009). A novel

function for fragile X mental retardation protein in translational activation. PLoS Biol *7*, e16.

Bellone, C., and Nicoll, R.A. (2007). Rapid bidirectional switching of synaptic NMDA receptors. Neuron *55*, 779-785.

Benson, D.L. (1997). Dendritic compartmentation of NMDA receptor mRNA in cultured hippocampal neurons. Neuroreport *8*, 823-828.

Bergado, J.A., Frey, S., Lopez, J., Almaguer-Melian, W., and Frey, J.U. (2007). Cholinergic afferents to the locus coeruleus and noradrenergic afferents to the medial septum mediate LTP-reinforcement in the dentate gyrus by stimulation of the amygdala. Neurobiol Learn Mem *88*, 331-341.

Berger-Sweeney, J., Zearfoss, N.R., and Richter, J.D. (2006). Reduced extinction of hippocampal-dependent memories in CPEB knockout mice. Learn Mem *13*, 4-7.

Bestman, J.E., and Cline, H.T. (2008). The RNA binding protein CPEB regulates dendrite morphogenesis and neuronal circuit assembly in vivo. Proc Natl Acad Sci U S A *105*, 20494-20499.

Blichenberg, A., Rehbein, M., Muller, R., Garner, C.C., Richter, D., and Kindler, S. (2001). Identification of a cis-acting dendritic targeting element in the mRNA encoding the alpha subunit of Ca2+/calmodulin-dependent protein kinase II. Eur J Neurosci *13*, 1881-1888.

Blichenberg, A., Schwanke, B., Rehbein, M., Garner, C.C., Richter, D., and Kindler, S. (1999). Identification of a cis-acting dendritic targeting element in MAP2 mRNAs. J Neurosci *19*, 8818-8829.

Bliss, T.V., and Lomo, T. (1973). Long-lasting potentiation of synaptic transmission in the dentate area of the anaesthetized rabbit following stimulation of the perforant path. J Physiol *232*, 331-356.

Bloomer, W.A., VanDongen, H.M., and VanDongen, A.M. (2008). Arc/Arg3.1 translation is controlled by convergent N-methyl-D-aspartate and Gs-coupled receptor signaling pathways. J Biol Chem *283*, 582-592.

Bockers, T.M., Segger-Junius, M., Iglauer, P., Bockmann, J., Gundelfinger, E.D., Kreutz, M.R., Richter, D., Kindler, S., and Kreienkamp, H.J. (2004). Differential expression and dendritic transcript localization of Shank family members:

identification of a dendritic targeting element in the 3' untranslated region of Shank1 mRNA. Molecular and cellular neurosciences *26*, 182-190.

Bodian, D. (1965). A Suggestive Relationship of Nerve Cell Rna with Specific Synaptic Sites. Proc Natl Acad Sci U S A *53*, 418-425.

Bourne, J., and Harris, K.M. (2007). Do thin spines learn to be mushroom spines that remember? Curr Opin Neurobiol *17*, 381-386.

Bourne, J.N., and Harris, K.M. (2008). Balancing structure and function at hippocampal dendritic spines. Annu Rev Neurosci *31*, 47-67.

Bramham, C.R. (2007). Control of synaptic consolidation in the dentate gyrus: mechanisms, functions, and therapeutic implications. Prog Brain Res *163*, 453-471.

Burd, C.G., and Dreyfuss, G. (1994). Conserved structures and diversity of functions of RNA-binding proteins. Science *265*, 615-621.

Burgin, K.E., Waxham, M.N., Rickling, S., Westgate, S.A., Mobley, W.C., and Kelly, P.T. (1990). In situ hybridization histochemistry of Ca2+/calmodulin-dependent protein kinase in developing rat brain. J Neurosci *10*, 1788-1798.

Cao, Q., Kim, J.H., and Richter, J.D. (2006). CDK1 and calcineurin regulate Maskin association with eIF4E and translational control of cell cycle progression. Nat Struct Mol Biol *13*, 1128-1134.

Cao, Q., Padmanabhan, K., and Richter, J.D. (2010). Pumilio 2 controls translation by competing with eIF4E for 7-methyl guanosine cap recognition. RNA *16*, 221-227.

Cao, Q., and Richter, J.D. (2002). Dissolution of the maskin-eIF4E complex by cytoplasmic polyadenylation and poly(A)-binding protein controls cyclin B1 mRNA translation and oocyte maturation. EMBO J *21*, 3852-3862.

Carroll, M., Dyer, J., and Sossin, W.S. (2006). Serotonin increases phosphorylation of synaptic 4EBP through TOR, but eukaryotic initiation factor 4E levels do not limit somatic cap-dependent translation in aplysia neurons. Mol Cell Biol *26*, 8586-8598.

Centonze, D., Rossi, S., Napoli, I., Mercaldo, V., Lacoux, C., Ferrari, F., Ciotti, M.T., De Chiara, V., Prosperetti, C., Maccarrone, M., Fezza, F., Calabresi, P., Bernardi, G.,

and Bagni, C. (2007). The brain cytoplasmic RNA BC1 regulates dopamine D2 receptor-mediated transmission in the striatum. J Neurosci *27*, 8885-8892.

Chen, P.J., and Huang, Y.S. (2011). CPEB2-eEF2 interaction impedes HIF-1alpha RNA translation. EMBO J.

Chen, W.S., and Bear, M.F. (2007). Activity-dependent regulation of NR2B translation contributes to metaplasticity in mouse visual cortex. Neuropharmacology *52*, 200-214.

Chen, Y., Stevens, B., Chang, J., Milbrandt, J., Barres, B.A., and Hell, J.W. (2008). NS21: re-defined and modified supplement B27 for neuronal cultures. J Neurosci Methods *171*, 239-247.

Chiaruttini, C., Vicario, A., Li, Z., Baj, G., Braiuca, P., Wu, Y., Lee, F.S., Gardossi, L., Baraban, J.M., and Tongiorgi, E. (2009). Dendritic trafficking of BDNF mRNA is mediated by translin and blocked by the G196A (Val66Met) mutation. Proc Natl Acad Sci U S A *106*, 16481-16486.

Chowdhury, S., Shepherd, J.D., Okuno, H., Lyford, G., Petralia, R.S., Plath, N., Kuhl, D., Huganir, R.L., and Worley, P.F. (2006). Arc/Arg3.1 interacts with the endocytic machinery to regulate AMPA receptor trafficking. Neuron *52*, 445-459.

Connor, S.A., Hoeffer, C.A., Klann, E., and Nguyen, P.V. (2011). Fragile X mental retardation protein regulates heterosynaptic plasticity in the hippocampus. Learn Mem *18*, 207-220.

Costa-Mattioli, M., Gobert, D., Stern, E., Gamache, K., Colina, R., Cuello, C., Sossin, W., Kaufman, R., Pelletier, J., Rosenblum, K., Krnjevic, K., Lacaille, J.C., Nader, K., and Sonenberg, N. (2007). eIF2alpha phosphorylation bidirectionally regulates the switch from short- to long-term synaptic plasticity and memory. Cell *129*, 195-206.

Costa-Mattioli, M., Sossin, W.S., Klann, E., and Sonenberg, N. (2009). Translational control of long-lasting synaptic plasticity and memory. Neuron *61*, 10-26.

Costes, S.V., Daelemans, D., Cho, E.H., Dobbin, Z., Pavlakis, G., and Lockett, S. (2004). Automatic and quantitative measurement of protein-protein colocalization in live cells. Biophys J *86*, 3993-4003.

Davis, L., Banker, G.A., and Steward, O. (1987). Selective dendritic transport of RNA in hippocampal neurons in culture. Nature *330*, 477-479.

Delanoue, R., and Davis, I. (2005). Dynein anchors its mRNA cargo after apical transport in the Drosophila blastoderm embryo. Cell *122*, 97-106.

Dent, E.W., Merriam, E.B., and Hu, X. (2011). The dynamic cytoskeleton: backbone of dendritic spine plasticity. Curr Opin Neurobiol *21*, 175-181.

Dictenberg, J.B., Swanger, S.A., Antar, L.N., Singer, R.H., and Bassell, G.J. (2008). A direct role for FMRP in activity-dependent dendritic mRNA transport links filopodial-spine morphogenesis to fragile X syndrome. Dev Cell *14*, 926-939.

Dieterich, D.C., Hodas, J.J., Gouzer, G., Shadrin, I.Y., Ngo, J.T., Triller, A., Tirrell, D.A., and Schuman, E.M. (2010). In situ visualization and dynamics of newly synthesized proteins in rat hippocampal neurons. Nat Neurosci *13*, 897-905.

Dolen, G., Osterweil, E., Rao, B.S., Smith, G.B., Auerbach, B.D., Chattarji, S., and Bear, M.F. (2007). Correction of fragile X syndrome in mice. Neuron *56*, 955-962.

Doyle, M., and Kiebler, M.A. (2011). Mechanisms of dendritic mRNA transport and its role in synaptic tagging. EMBO J *30*, 3540-3552.

Du, L., and Richter, J.D. (2005). Activity-dependent polyadenylation in neurons. RNA *11*, 1340-1347.

Dunwiddie, T., and Lynch, G. (1978). Long-term potentiation and depression of synaptic responses in the rat hippocampus: localization and frequency dependency. J Physiol *276*, 353-367.

Eberwine, J., Belt, B., Kacharmina, J.E., and Miyashiro, K. (2002). Analysis of subcellularly localized mRNAs using in situ hybridization, mRNA amplification, and expression profiling. Neurochem Res *27*, 1065-1077.

Edbauer, D., Neilson, J.R., Foster, K.A., Wang, C.F., Seeburg, D.P., Batterton, M.N., Tada, T., Dolan, B.M., Sharp, P.A., and Sheng, M. (2010). Regulation of synaptic structure and function by FMRP-associated microRNAs miR-125b and miR-132. Neuron *65*, 373-384.

Ehlers, M.D. (2000). Reinsertion or degradation of AMPA receptors determined by activity-dependent endocytic sorting. Neuron *28*, 511-525.

Eom, T., Antar, L.N., Singer, R.H., and Bassell, G.J. (2003). Localization of a beta-actin messenger ribonucleoprotein complex with zipcode-binding protein modulates the density of dendritic filopodia and filopodial synapses. J Neurosci *23*, 10433-10444.

Ernoult-Lange, M., Wilczynska, A., Harper, M., Aigueperse, C., Dautry, F., Kress, M., and Weil, D. (2009). Nucleocytoplasmic traffic of CPEB1 and accumulation in Crm1 nucleolar bodies. Mol Biol Cell *20*, 176-187.

Esteban, J.A., Shi, S.H., Wilson, C., Nuriya, M., Huganir, R.L., and Malinow, R. (2003). PKA phosphorylation of AMPA receptor subunits controls synaptic trafficking underlying plasticity. Nat Neurosci *6*, 136-143.

Eulalio, A., Behm-Ansmant, I., and Izaurralde, E. (2007). P bodies: at the crossroads of post-transcriptional pathways. Nat Rev Mol Cell Biol *8*, 9-22.

Fahling, M., Mrowka, R., Steege, A., Kirschner, K.M., Benko, E., Forstera, B., Persson, P.B., Thiele, B.J., Meier, J.C., and Scholz, H. (2009). Translational regulation of the human achaete-scute homologue-1 by fragile X mental retardation protein. J Biol Chem *284*, 4255-4266.

Falley, K., Schutt, J., Iglauer, P., Menke, K., Maas, C., Kneussel, M., Kindler, S., Wouters, F.S., Richter, D., and Kreienkamp, H.J. (2009). Shank1 mRNA: dendritic transport by kinesin and translational control by the 5'untranslated region. Traffic *10*, 844-857.

Farina, K.L., and Singer, R.H. (2002). The nuclear connection in RNA transport and localization. Trends Cell Biol *12*, 466-472.

Feig, S., and Lipton, P. (1993). Pairing the cholinergic agonist carbachol with patterned Schaffer collateral stimulation initiates protein synthesis in hippocampal CA1 pyramidal cell dendrites via a muscarinic, NMDA-dependent mechanism. J Neurosci *13*, 1010-1021.

Ferretti, V., Roullet, P., Sargolini, F., Rinaldi, A., Perri, V., Del Fabbro, M., Costantini, V.J., Annese, V., Scesa, G., De Stefano, M.E., Oliverio, A., and Mele, A. (2010). Ventral striatal plasticity and spatial memory. Proc Natl Acad Sci U S A *107*, 7945-7950.

Fifkova, E., Anderson, C.L., Young, S.J., and Van Harreveld, A. (1982). Effect of anisomycin on stimulation-induced changes in dendritic spines of the dentate granule cells. J Neurocytol *11*, 183-210.

Finkenstadt, P.M., Kang, W.S., Jeon, M., Taira, E., Tang, W., and Baraban, J.M. (2000). Somatodendritic localization of Translin, a component of the Translin/Trax RNA binding complex. J Neurochem *75*, 1754-1762.

Fiore, R., Khudayberdiev, S., Christensen, M., Siegel, G., Flavell, S.W., Kim, T.K., Greenberg, M.E., and Schratt, G. (2009). Mef2-mediated transcription of the miR379-410 cluster regulates activity-dependent dendritogenesis by fine-tuning Pumilio2 protein levels. EMBO J *28*, 697-710.

Flexner, J.B., Flexner, L.B., and Stellar, E. (1963). Memory in mice as affected by intracerebral puromycin. Science *141*, 57-59.

Frey, S., Bergado-Rosado, J., Seidenbecher, T., Pape, H.C., and Frey, J.U. (2001). Reinforcement of early long-term potentiation (early-LTP) in dentate gyrus by stimulation of the basolateral amygdala: heterosynaptic induction mechanisms of late-LTP. J Neurosci *21*, 3697-3703.

Frey, S., Bergado, J.A., and Frey, J.U. (2003). Modulation of late phases of long-term potentiation in rat dentate gyrus by stimulation of the medial septum. Neuroscience *118*, 1055-1062.

Frey, U., and Morris, R.G. (1997). Synaptic tagging and long-term potentiation. Nature *385*, 533-536.

Gardiol, A., Racca, C., and Triller, A. (1999). Dendritic and postsynaptic protein synthetic machinery. J Neurosci *19*, 168-179.

Garner, C.C., Tucker, R.P., and Matus, A. (1988). Selective localization of messenger RNA for cytoskeletal protein MAP2 in dendrites. Nature *336*, 674-677.

Gazzaley, A.H., Benson, D.L., Huntley, G.W., and Morrison, J.H. (1997). Differential subcellular regulation of NMDAR1 protein and mRNA in dendrites of dentate gyrus granule cells after perforant path transection. J Neurosci *17*, 2006-2017.

Gelinas, J.N., Banko, J.L., Hou, L., Sonenberg, N., Weeber, E.J., Klann, E., and Nguyen, P.V. (2007). ERK and mTOR signaling couple beta-adrenergic receptors to

translation initiation machinery to gate induction of protein synthesis-dependent long-term potentiation. J Biol Chem *282*, 27527-27535.

Gelinas, J.N., and Nguyen, P.V. (2005). Beta-adrenergic receptor activation facilitates induction of a protein synthesis-dependent late phase of long-term potentiation. J Neurosci *25*, 3294-3303.

Gingras, A.C., Kennedy, S.G., O'Leary, M.A., Sonenberg, N., and Hay, N. (1998). 4E-BP1, a repressor of mRNA translation, is phosphorylated and inactivated by the Akt(PKB) signaling pathway. Genes Dev *12*, 502-513.

Gong, R., Park, C.S., Abbassi, N.R., and Tang, S.J. (2006). Roles of glutamate receptors and the mammalian target of rapamycin (mTOR) signaling pathway in activity-dependent dendritic protein synthesis in hippocampal neurons. J Biol Chem *281*, 18802-18815.

Goslin, K., and Banker, G. (1998). Culturing Nerve Cells, 2 edn (Cambridge, MA, MIT).

Groisman, I., Huang, Y.S., Mendez, R., Cao, Q., Theurkauf, W., and Richter, J.D. (2000). CPEB, maskin, and cyclin B1 mRNA at the mitotic apparatus: implications for local translational control of cell division. Cell *103*, 435-447.

Groisman, I., Ivshina, M., Marin, V., Kennedy, N.J., Davis, R.J., and Richter, J.D. (2006). Control of cellular senescence by CPEB. Genes Dev *20*, 2701-2712.

Grooms, S.Y., Noh, K.M., Regis, R., Bassell, G.J., Bryan, M.K., Carroll, R.C., and Zukin, R.S. (2006). Activity bidirectionally regulates AMPA receptor mRNA abundance in dendrites of hippocampal neurons. J Neurosci *26*, 8339-8351.

Gross, C., Berry-Kravis, E.M., and Bassell, G.J. (2011a). Therapeutic Strategies in Fragile X Syndrome: Dysregulated mGluR Signaling and Beyond. Neuropsychopharmacology : official publication of the American College of Neuropsychopharmacology.

Gross, C., Nakamoto, M., Yao, X., Chan, C.B., Yim, S.Y., Ye, K., Warren, S.T., and Bassell, G.J. (2010). Excess phosphoinositide 3-kinase subunit synthesis and activity as a novel therapeutic target in fragile X syndrome. J Neurosci *30*, 10624-10638.

Gross, C., Yao, X., Pong, D.L., Jeromin, A., and Bassell, G.J. (2011b). Fragile X mental retardation protein regulates protein expression and mRNA translation of the

potassium channel Kv4.2. The Journal of neuroscience : the official journal of the Society for Neuroscience *31*, 5693-5698.

Grosshans, D.R., Clayton, D.A., Coultrap, S.J., and Browning, M.D. (2002). LTP leads to rapid surface expression of NMDA but not AMPA receptors in adult rat CA1. Nat Neurosci *5*, 27-33.

Hake, L.E., Mendez, R., and Richter, J.D. (1998). Specificity of RNA binding by CPEB: requirement for RNA recognition motifs and a novel zinc finger. Mol Cell Biol *18*, 685-693.

Harris, K.M., Jensen, F.E., and Tsao, B. (1992). Three-dimensional structure of dendritic spines and synapses in rat hippocampus (CA1) at postnatal day 15 and adult ages: implications for the maturation of synaptic physiology and long-term potentiation. J Neurosci *12*, 2685-2705.

Harris, K.M., and Stevens, J.K. (1989). Dendritic spines of CA 1 pyramidal cells in the rat hippocampus: serial electron microscopy with reference to their biophysical characteristics. J Neurosci *9*, 2982-2997.

Havik, B., Rokke, H., Bardsen, K., Davanger, S., and Bramham, C.R. (2003). Bursts of high-frequency stimulation trigger rapid delivery of pre-existing alpha-CaMKII mRNA to synapses: a mechanism in dendritic protein synthesis during long-term potentiation in adult awake rats. Eur J Neurosci *17*, 2679-2689.

Hay, N., and Sonenberg, N. (2004). Upstream and downstream of mTOR. Genes Dev *18*, 1926-1945.

Hebb, D.O. (1949). The Organization of Behavior: A Neuropsychological Theory (New York, New York, Wiley).

Hellen, C.U., and Sarnow, P. (2001). Internal ribosome entry sites in eukaryotic mRNA molecules. Genes Dev *15*, 1593-1612.

Helmstetter, F.J., Parsons, R.G., and Gafford, G.M. (2008). Macromolecular synthesis, distributed synaptic plasticity, and fear conditioning. Neurobiol Learn Mem *89*, 324-337.

Hernandez, P.J., and Abel, T. (2008). The role of protein synthesis in memory consolidation: progress amid decades of debate. Neurobiol Learn Mem *89*, 293-311.

Hernandez, P.J., and Kelley, A.E. (2004). Long-term memory for instrumental responses does not undergo protein synthesis-dependent reconsolidation upon retrieval. Learn Mem *11*, 748-754.

Hodgman, R., Tay, J., Mendez, R., and Richter, J.D. (2001). CPEB phosphorylation and cytoplasmic polyadenylation are catalyzed by the kinase IAK1/Eg2 in maturing mouse oocytes. Development *128*, 2815-2822.

Hoeffer, C.A., Tang, W., Wong, H., Santillan, A., Patterson, R.J., Martinez, L.A., Tejada-Simon, M.V., Paylor, R., Hamilton, S.L., and Klann, E. (2008). Removal of FKBP12 enhances mTOR-Raptor interactions, LTP, memory, and perseverative/repetitive behavior. Neuron *60*, 832-845.

Hollingsworth, E.B., McNeal, E.T., Burton, J.L., Williams, R.J., Daly, J.W., and Creveling, C.R. (1985). Biochemical characterization of a filtered synaptoneurosome preparation from guinea pig cerebral cortex: cyclic adenosine 3':5'-monophosphate-generating systems, receptors, and enzymes. J Neurosci *5*, 2240-2253.

Horton, A.C., and Ehlers, M.D. (2003). Dual modes of endoplasmic reticulum-to-Golgi transport in dendrites revealed by live-cell imaging. J Neurosci *23*, 6188-6199.

Huang, Y.S., Carson, J.H., Barbarese, E., and Richter, J.D. (2003). Facilitation of dendritic mRNA transport by CPEB. Genes Dev *17*, 638-653.

Huang, Y.S., Jung, M.Y., Sarkissian, M., and Richter, J.D. (2002). N-methyl-D-aspartate receptor signaling results in Aurora kinase-catalyzed CPEB phosphorylation and alpha CaMKII mRNA polyadenylation at synapses. EMBO J *21*, 2139-2148.

Huang, Y.S., Kan, M.C., Lin, C.L., and Richter, J.D. (2006). CPEB3 and CPEB4 in neurons: analysis of RNA-binding specificity and translational control of AMPA receptor GluR2 mRNA. EMBO J *25*, 4865-4876.

Huang, Y.Y., and Kandel, E.R. (1995). D1/D5 receptor agonists induce a protein synthesis-dependent late potentiation in the CA1 region of the hippocampus. Proc Natl Acad Sci U S A *92*, 2446-2450.

Huang, Y.Y., Simpson, E., Kellendonk, C., and Kandel, E.R. (2004). Genetic evidence for the bidirectional modulation of synaptic plasticity in the prefrontal cortex by D1 receptors. Proc Natl Acad Sci U S A *101*, 3236-3241.

Huber, K.M., Gallagher, S.M., Warren, S.T., and Bear, M.F. (2002). Altered synaptic plasticity in a mouse model of fragile X mental retardation. Proc Natl Acad Sci U S A *99*, 7746-7750.

Huber, K.M., Kayser, M.S., and Bear, M.F. (2000). Role for rapid dendritic protein synthesis in hippocampal mGluR-dependent long-term depression. Science *288*, 1254-1257.

Hussey, G.S., Chaudhury, A., Dawson, A.E., Lindner, D.J., Knudsen, C.R., Wilce, M.C., Merrick, W.C., and Howe, P.H. (2011). Identification of an mRNP complex regulating tumorigenesis at the translational elongation step. Mol Cell *41*, 419-431.

Huttelmaier, S., Zenklusen, D., Lederer, M., Dictenberg, J., Lorenz, M., Meng, X., Bassell, G.J., Condeelis, J., and Singer, R.H. (2005). Spatial regulation of beta-actin translation by Src-dependent phosphorylation of ZBP1. Nature *438*, 512-515.

Irwin, S.A., Idupulapati, M., Gilbert, M.E., Harris, J.B., Chakravarti, A.B., Rogers, E.J., Crisostomo, R.A., Larsen, B.P., Mehta, A., Alcantara, C.J., Patel, B., Swain, R.A., Weiler, I.J., Oostra, B.A., and Greenough, W.T. (2002). Dendritic spine and dendritic field characteristics of layer V pyramidal neurons in the visual cortex of fragile-X knockout mice. American journal of medical genetics *111*, 140-146.

Jackson, R.J., Hellen, C.U., and Pestova, T.V. (2010). The mechanism of eukaryotic translation initiation and principles of its regulation. Nat Rev Mol Cell Biol *11*, 113-127.

Jeffery, W.R., Tomlinson, C.R., and Brodeur, R.D. (1983). Localization of actin messenger RNA during early ascidian development. Dev Biol *99*, 408-417.

Jin, P., Zarnescu, D.C., Ceman, S., Nakamoto, M., Mowrey, J., Jongens, T.A., Nelson, D.L., Moses, K., and Warren, S.T. (2004). Biochemical and genetic interaction between the fragile X mental retardation protein and the microRNA pathway. Nat Neurosci *7*, 113-117.

Jones, K.J., Korb, E., Kundel, M.A., Kochanek, A.R., Kabraji, S., McEvoy, M., Shin, C.Y., and Wells, D.G. (2008). CPEB1 regulates beta-catenin mRNA translation and cell migration in astrocytes. Glia *56*, 1401-1413.

Ju, W., Morishita, W., Tsui, J., Gaietta, G., Deerinck, T.J., Adams, S.R., Garner, C.C., Tsien, R.Y., Ellisman, M.H., and Malenka, R.C. (2004). Activity-dependent regulation of dendritic synthesis and trafficking of AMPA receptors. Nat Neurosci *7*, 244-253.

Jung, M.Y., Lorenz, L., and Richter, J.D. (2006). Translational control by neuroguidin, a eukaryotic initiation factor 4E and CPEB binding protein. Mol Cell Biol *26*, 4277-4287.

Kacharmina, J.E., Job, C., Crino, P., and Eberwine, J. (2000). Stimulation of glutamate receptor protein synthesis and membrane insertion within isolated neuronal dendrites. Proc Natl Acad Sci U S A *97*, 11545-11550.

Kanai, Y., Dohmae, N., and Hirokawa, N. (2004). Kinesin transports RNA: isolation and characterization of an RNA-transporting granule. Neuron *43*, 513-525.

Kandel, E.R. (2001). The molecular biology of memory storage: a dialogue between genes and synapses. Science *294*, 1030-1038.

Kang, H., and Schuman, E.M. (1996). A requirement for local protein synthesis in neurotrophin-induced hippocampal synaptic plasticity. Science *273*, 1402-1406.

Kanhema, T., Dagestad, G., Panja, D., Tiron, A., Messaoudi, E., Havik, B., Ying, S.W., Nairn, A.C., Sonenberg, N., and Bramham, C.R. (2006). Dual regulation of translation initiation and peptide chain elongation during BDNF-induced LTP in vivo: evidence for compartment-specific translation control. J Neurochem *99*, 1328-1337.

Kao, D.I., Aldridge, G.M., Weiler, I.J., and Greenough, W.T. (2010). Altered mRNA transport, docking, and protein translation in neurons lacking fragile X mental retardation protein. Proc Natl Acad Sci U S A *107*, 15601-15606.

Karachot, L., Shirai, Y., Vigot, R., Yamamori, T., and Ito, M. (2001). Induction of long-term depression in cerebellar Purkinje cells requires a rapidly turned over protein. J Neurophysiol *86*, 280-289.

Keleman, K., Kruttner, S., Alenius, M., and Dickson, B.J. (2007). Function of the Drosophila CPEB protein Orb2 in long-term courtship memory. Nat Neurosci *10*, 1587-1593.

Kessels, H.W., and Malinow, R. (2009). Synaptic AMPA receptor plasticity and behavior. Neuron *61*, 340-350.

Kiebler, M.A., and Bassell, G.J. (2006). Neuronal RNA granules: movers and makers. Neuron *51*, 685-690.

Kim, J.H., and Richter, J.D. (2006). Opposing polymerase-deadenylase activities regulate cytoplasmic polyadenylation. Mol Cell *24*, 173-183.

Kindler, S., Muller, R., Chung, W.J., and Garner, C.C. (1996). Molecular characterization of dendritically localized transcripts encoding MAP2. Brain Res Mol Brain Res *36*, 63-69.

Kirov, S.A., and Harris, K.M. (1999). Dendrites are more spiny on mature hippocampal neurons when synapses are inactivated. Nat Neurosci *2*, 878-883.

Kislauskis, E.H., and Singer, R.H. (1992). Determinants of mRNA localization. Curr Opin Cell Biol *4*, 975-978.

Kleiman, R., Banker, G., and Steward, O. (1990). Differential subcellular localization of particular mRNAs in hippocampal neurons in culture. Neuron *5*, 821-830.

Knowles, R.B., and Kosik, K.S. (1997). Neurotrophin-3 signals redistribute RNA in neurons. Proc Natl Acad Sci U S A *94*, 14804-14808.

Knowles, R.B., Sabry, J.H., Martone, M.E., Deerinck, T.J., Ellisman, M.H., Bassell, G.J., and Kosik, K.S. (1996). Translocation of RNA granules in living neurons. J Neurosci *16*, 7812-7820.

Kobayashi, H., Yamamoto, S., Maruo, T., and Murakami, F. (2005). Identification of a cis-acting element required for dendritic targeting of activity-regulated cytoskeleton-associated protein mRNA. Eur J Neurosci *22*, 2977-2984.

Kobayashi, S., Takashima, A., and Anzai, K. (1998). The dendritic translocation of translin protein in the form of BC1 RNA protein particles in developing rat hippocampal neurons in primary culture. Biochem Biophys Res Commun *253*, 448-453.

Koekkoek, S.K., Yamaguchi, K., Milojkovic, B.A., Dortland, B.R., Ruigrok, T.J., Maex, R., De Graaf, W., Smit, A.E., VanderWerf, F., Bakker, C.E., Willemsen, R., Ikeda, T., Kakizawa, S., Onodera, K., Nelson, D.L., Mientjes, E., Joosten, M., De Schutter, E., Oostra, B.A., Ito, M., and De Zeeuw, C.I. (2005). Deletion of FMR1

in Purkinje cells enhances parallel fiber LTD, enlarges spines, and attenuates cerebellar eyelid conditioning in Fragile X syndrome. Neuron *47*, 339-352.

Kopec, C.D., Real, E., Kessels, H.W., and Malinow, R. (2007). GluR1 links structural and functional plasticity at excitatory synapses. J Neurosci *27*, 13706-13718.

Kress, T.L., Yoon, Y.J., and Mowry, K.L. (2004). Nuclear RNP complex assembly initiates cytoplasmic RNA localization. J Cell Biol *165*, 203-211.

Krichevsky, A.M., and Kosik, K.S. (2001). Neuronal RNA granules: a link between RNA localization and stimulation-dependent translation. Neuron *32*, 683-696.

Krishnan, V., Han, M.H., Graham, D.L., Berton, O., Renthal, W., Russo, S.J., Laplant, Q., Graham, A., Lutter, M., Lagace, D.C., Ghose, S., Reister, R., Tannous, P., Green, T.A., Neve, R.L., Chakravarty, S., Kumar, A., Eisch, A.J., Self, D.W., Lee, F.S., Tamminga, C.A., Cooper, D.C., Gershenfeld, H.K., and Nestler, E.J. (2007). Molecular adaptations underlying susceptibility and resistance to social defeat in brain reward regions. Cell *131*, 391-404.

Kudoh, M., Sakai, M., and Shibuki, K. (2002). Differential dependence of LTD on glutamate receptors in the auditory cortical synapses of cortical and thalamic inputs. J Neurophysiol *88*, 3167-3174.

Kumar-Singh, S. (2011). Progranulin and TDP-43: mechanistic links and future directions. J Mol Neurosci *45*, 561-573.

Kuo, Y.M., Liang, K.C., Chen, H.H., Cherng, C.G., Lee, H.T., Lin, Y., Huang, A.M., Liao, R.M., and Yu, L. (2007). Cocaine-but not methamphetamine-associated memory requires de novo protein synthesis. Neurobiol Learn Mem *87*, 93-100.

Kurihara, Y., Tokuriki, M., Myojin, R., Hori, T., Kuroiwa, A., Matsuda, Y., Sakurai, T., Kimura, M., Hecht, N.B., and Uesugi, S. (2003). CPEB2, a novel putative translational regulator in mouse haploid germ cells. Biol Reprod *69*, 261-268.

Kwak, J.E., Drier, E., Barbee, S.A., Ramaswami, M., Yin, J.C., and Wickens, M. (2008). GLD2 poly(A) polymerase is required for long-term memory. Proc Natl Acad Sci U S A *105*, 14644-14649.

Kwon, H.B., and Castillo, P.E. (2008). Role of glutamate autoreceptors at hippocampal mossy fiber synapses. Neuron *60*, 1082-1094.

Lamphear, B.J., Kirchweger, R., Skern, T., and Rhoads, R.E. (1995). Mapping of functional domains in eukaryotic protein synthesis initiation factor 4G (eIF4G) with picornaviral proteases. Implications for cap-dependent and cap-independent translational initiation. J Biol Chem *270*, 21975-21983.

Lantz, V., Ambrosio, L., and Schedl, P. (1992). The Drosophila orb gene is predicted to encode sex-specific germline RNA-binding proteins and has localized transcripts in ovaries and early embryos. Development *115*, 75-88.

Lau, A.G., Irier, H.A., Gu, J., Tian, D., Ku, L., Liu, G., Xia, M., Fritsch, B., Zheng, J.Q., Dingledine, R., Xu, B., Lu, B., and Feng, Y. (2010). Distinct 3'UTRs differentially regulate activity-dependent translation of brain-derived neurotrophic factor (BDNF). Proc Natl Acad Sci U S A *107*, 15945-15950.

Lau, C.G., and Zukin, R.S. (2007). NMDA receptor trafficking in synaptic plasticity and neuropsychiatric disorders. Nat Rev Neurosci *8*, 413-426.

Lawrence, J.B., and Singer, R.H. (1986). Intracellular localization of messenger RNAs for cytoskeletal proteins. Cell *45*, 407-415.

Lee, M.C., Yasuda, R., and Ehlers, M.D. (2010). Metaplasticity at single glutamatergic synapses. Neuron *66*, 859-870.

Li, Z., Wu, Y., and Baraban, J.M. (2008). The Translin/Trax RNA binding complex: clues to function in the nervous system. Biochim Biophys Acta *1779*, 479-485.

Lin, C.L., Evans, V., Shen, S., Xing, Y., and Richter, J.D. (2010). The nuclear experience of CPEB: implications for RNA processing and translational control. RNA *16*, 338-348.

Linden, D.J. (1996). A protein synthesis-dependent late phase of cerebellar long-term depression. Neuron *17*, 483-490.

Link, W., Konietzko, U., Kauselmann, G., Krug, M., Schwanke, B., Frey, U., and Kuhl, D. (1995). Somatodendritic expression of an immediate early gene is regulated by synaptic activity. Proc Natl Acad Sci U S A *92*, 5734-5738.

Liu, J., Hu, J.Y., Wu, F., Schwartz, J.H., and Schacher, S. (2006). Two mRNA-binding proteins regulate the distribution of syntaxin mRNA in Aplysia sensory neurons. J Neurosci *26*, 5204-5214.

Liu, J., and Schwartz, J.H. (2003). The cytoplasmic polyadenylation element binding protein and polyadenylation of messenger RNA in Aplysia neurons. Brain Res *959*, 68-76.

Lu, W., Man, H., Ju, W., Trimble, W.S., MacDonald, J.F., and Wang, Y.T. (2001). Activation of synaptic NMDA receptors induces membrane insertion of new AMPA receptors and LTP in cultured hippocampal neurons. Neuron *29*, 243-254.

Lyford, G.L., Yamagata, K., Kaufmann, W.E., Barnes, C.A., Sanders, L.K., Copeland, N.G., Gilbert, D.J., Jenkins, N.A., Lanahan, A.A., and Worley, P.F. (1995). Arc, a growth factor and activity-regulated gene, encodes a novel cytoskeleton-associated protein that is enriched in neuronal dendrites. Neuron *14*, 433-445.

Maccarrone, M., Rossi, S., Bari, M., De Chiara, V., Rapino, C., Musella, A., Bernardi, G., Bagni, C., and Centonze, D. (2010). Abnormal mGlu 5 receptor/endocannabinoid coupling in mice lacking FMRP and BC1 RNA. Neuropsychopharmacology *35*, 1500-1509.

MacDonald, J.F., Jackson, M.F., and Beazely, M.A. (2006). Hippocampal long-term synaptic plasticity and signal amplification of NMDA receptors. Crit Rev Neurobiol *18*, 71-84.

Malinow, R., and Malenka, R.C. (2002). AMPA receptor trafficking and synaptic plasticity. Annu Rev Neurosci *25*, 103-126.

Mameli, M., Balland, B., Lujan, R., and Luscher, C. (2007). Rapid synthesis and synaptic insertion of GluR2 for mGluR-LTD in the ventral tegmental area. Science *317*, 530-533.

Manders, E.M.M., Verbeek, F.J., and Aten, J.A. (1993). Measurement of co-localization of object in dual-colour confocal images. Journal of Microscopy *169*, 375-382.

Mao, L.M., Zhang, G.C., Liu, X.Y., Fibuch, E.E., and Wang, J.Q. (2008). Group I metabotropic glutamate receptor-mediated gene expression in striatal neurons. Neurochem Res *33*, 1920-1924.

Massey, P.V., Bhabra, G., Cho, K., Brown, M.W., and Bashir, Z.I. (2001). Activation of muscarinic receptors induces protein synthesis-dependent long-lasting depression in the perirhinal cortex. Eur J Neurosci *14*, 145-152.

Mathews, M.B., Sonenberg, N., and Hershey, J.W.B. (2007). Origins and principles of translational control. In Translation Control in Biology and Medicine, M.B. Mathews, N. Sonenberg, and J.W.B. Hershey, eds. (Cold Spring Harbor, NY, Cold Spring Harbor Laboratory Press), pp. 1-40.

Matsuzaki, M., Honkura, N., Ellis-Davies, G.C., and Kasai, H. (2004). Structural basis of long-term potentiation in single dendritic spines. Nature *429*, 761-766.

McCoy, P.A., and McMahon, L.L. (2007). Muscarinic receptor dependent long-term depression in rat visual cortex is PKC independent but requires ERK1/2 activation and protein synthesis. J Neurophysiol *98*, 1862-1870.

McEvoy, M., Cao, G., Montero Llopis, P., Kundel, M., Jones, K., Hofler, C., Shin, C., and Wells, D.G. (2007). Cytoplasmic polyadenylation element binding protein 1-mediated mRNA translation in Purkinje neurons is required for cerebellar long-term depression and motor coordination. J Neurosci *27*, 6400-6411.

Mendez, R., Hake, L.E., Andresson, T., Littlepage, L.E., Ruderman, J.V., and Richter, J.D. (2000). Phosphorylation of CPE binding factor by Eg2 regulates translation of c-mos mRNA. Nature *404*, 302-307.

Menon, K.P., Sanyal, S., Habara, Y., Sanchez, R., Wharton, R.P., Ramaswami, M., and Zinn, K. (2004). The translational repressor Pumilio regulates presynaptic morphology and controls postsynaptic accumulation of translation factor eIF-4E. Neuron *44*, 663-676.

Merrick, W.C., and Nyborg, J. (2000). The Protein Biosynthesis Elongation Cycle. In Translational Control of Gene Expression, N. Sonenberg, M.B. Mathews, and J.W.B. Hershey, eds. (Cold Spring Harbor, NY, Cold Spring Harbor Laboratory Press), pp. 89-126.

Miki, T., Takano, K., and Yoneda, Y. (2005). The role of mammalian Staufen on mRNA traffic: a view from its nucleocytoplasmic shuttling function. Cell Struct Funct *30*, 51-56.

Mikl, M., Vendra, G., and Kiebler, M.A. (2011). Independent localization of MAP2, CaMKIIalpha and beta-actin RNAs in low copy numbers. EMBO Rep *12*, 1077-1084.

Miller, S., Yasuda, M., Coats, J.K., Jones, Y., Martone, M.E., and Mayford, M. (2002). Disruption of dendritic translation of CaMKIIalpha impairs stabilization of synaptic plasticity and memory consolidation. Neuron *36*, 507-519.

Millevoi, S., and Vagner, S. (2010). Molecular mechanisms of eukaryotic pre-mRNA 3' end processing regulation. Nucleic Acids Res *38*, 2757-2774.

Miniaci, M.C., Kim, J.H., Puthanveettil, S.V., Si, K., Zhu, H., Kandel, E.R., and Bailey, C.H. (2008). Sustained CPEB-dependent local protein synthesis is required to stabilize synaptic growth for persistence of long-term facilitation in Aplysia. Neuron *59*, 1024-1036.

Miyashiro, K., Dichter, M., and Eberwine, J. (1994). On the nature and differential distribution of mRNAs in hippocampal neurites: implications for neuronal functioning. Proc Natl Acad Sci U S A *91*, 10800-10804.

Moon, I.S., Cho, S.J., Seog, D.H., and Walikonis, R. (2009). Neuronal activation increases the density of eukaryotic translation initiation factor 4E mRNA clusters in dendrites of cultured hippocampal neurons. Exp Mol Med *41*, 601-610.

Mori, Y., Imaizumi, K., Katayama, T., Yoneda, T., and Tohyama, M. (2000). Two cis-acting elements in the 3' untranslated region of alpha-CaMKII regulate its dendritic targeting. Nat Neurosci *3*, 1079-1084.

Morris, D.R., and Geballe, A.P. (2000). Upstream open reading frames as regulators of mRNA translation. Mol Cell Biol *20*, 8635-8642.

Muddashetty, R.S., Kelic, S., Gross, C., Xu, M., and Bassell, G.J. (2007). Dysregulated metabotropic glutamate receptor-dependent translation of AMPA receptor and postsynaptic density-95 mRNAs at synapses in a mouse model of fragile X syndrome. J Neurosci *27*, 5338-5348.

Muddashetty, R.S., Nalavadi, V.C., Gross, C., Yao, X., Xing, L., Laur, O., Warren, S.T., and Bassell, G.J. (2011). Reversible inhibition of PSD-95 mRNA translation by miR-125a, FMRP phosphorylation, and mGluR signaling. Mol Cell *42*, 673-688.

Muramatsu, T., Ohmae, A., and Anzai, K. (1998). BC1 RNA protein particles in mouse brain contain two y-,h-element-binding proteins, translin and a 37 kDa protein. Biochem Biophys Res Commun *247*, 7-11.

Muslimov, I.A., Nimmrich, V., Hernandez, A.I., Tcherepanov, A., Sacktor, T.C., and Tiedge, H. (2004). Dendritic transport and localization of protein kinase Mzeta mRNA: implications for molecular memory consolidation. The Journal of biological chemistry *279*, 52613-52622.

Nagai, T., Takuma, K., Kamei, H., Ito, Y., Nakamichi, N., Ibi, D., Nakanishi, Y., Murai, M., Mizoguchi, H., Nabeshima, T., and Yamada, K. (2007). Dopamine D1 receptors regulate protein synthesis-dependent long-term recognition memory via extracellular signal-regulated kinase 1/2 in the prefrontal cortex. Learn Mem *14*, 117-125.

Naito, Y., Yamada, T., Ui-Tei, K., Morishita, S., and Saigo, K. (2004). siDirect: highly effective, target-specific siRNA design software for mammalian RNA interference. Nucleic Acids Res *32*, W124-129.

Nakamoto, M., Nalavadi, V., Epstein, M.P., Narayanan, U., Bassell, G.J., and Warren, S.T. (2007). Fragile X mental retardation protein deficiency leads to excessive mGluR5-dependent internalization of AMPA receptors. Proc Natl Acad Sci U S A *104*, 15537-15542.

Napoli, I., Mercaldo, V., Boyl, P.P., Eleuteri, B., Zalfa, F., De Rubeis, S., Di Marino, D., Mohr, E., Massimi, M., Falconi, M., Witke, W., Costa-Mattioli, M., Sonenberg, N., Achsel, T., and Bagni, C. (2008). The fragile X syndrome protein represses activity-dependent translation through CYFIP1, a new 4E-BP. Cell *134*, 1042-1054.

Navakkode, S., Sajikumar, S., and Frey, J.U. (2007). Synergistic requirements for the induction of dopaminergic D1/D5-receptor-mediated LTP in hippocampal slices of rat CA1 in vitro. Neuropharmacology *52*, 1547-1554.

Neasta, J., Ben Hamida, S., Yowell, Q., Carnicella, S., and Ron, D. (2010). Role for mammalian target of rapamycin complex 1 signaling in neuroadaptations underlying alcohol-related disorders. Proc Natl Acad Sci U S A *107*, 20093-20098.

Oe, S., and Yoneda, Y. (2010). Cytoplasmic polyadenylation element-like sequences are involved in dendritic targeting of BDNF mRNA in hippocampal neurons. FEBS Lett *584*, 3424-3430.

Okamoto, K., Nagai, T., Miyawaki, A., and Hayashi, Y. (2004). Rapid and persistent modulation of actin dynamics regulates postsynaptic reorganization underlying bidirectional plasticity. Nat Neurosci *7*, 1104-1112.

Oleynikov, Y., and Singer, R.H. (2003). Real-time visualization of ZBP1 association with beta-actin mRNA during transcription and localization. Curr Biol *13*, 199-207.

Ostareck-Lederer, A., Ostareck, D.H., Cans, C., Neubauer, G., Bomsztyk, K., Superti-Furga, G., and Hentze, M.W. (2002). c-Src-mediated phosphorylation of hnRNP K drives translational activation of specifically silenced mRNAs. Mol Cell Biol *22*, 4535-4543.

Ostareck, D.H., Ostareck-Lederer, A., Shatsky, I.N., and Hentze, M.W. (2001). Lipoxygenase mRNA silencing in erythroid differentiation: The 3'UTR regulatory complex controls 60S ribosomal subunit joining. Cell *104*, 281-290.

Ostroff, L.E., Fiala, J.C., Allwardt, B., and Harris, K.M. (2002). Polyribosomes redistribute from dendritic shafts into spines with enlarged synapses during LTP in developing rat hippocampal slices. Neuron *35*, 535-545.

Ouyang, Y., Kantor, D., Harris, K.M., Schuman, E.M., and Kennedy, M.B. (1997). Visualization of the distribution of autophosphorylated calcium/calmodulin-dependent protein kinase II after tetanic stimulation in the CA1 area of the hippocampus. J Neurosci *17*, 5416-5427.

Ouyang, Y., Rosenstein, A., Kreiman, G., Schuman, E.M., and Kennedy, M.B. (1999). Tetanic stimulation leads to increased accumulation of Ca(2+)/calmodulin-dependent protein kinase II via dendritic protein synthesis in hippocampal neurons. J Neurosci *19*, 7823-7833.

Paris, J., Swenson, K., Piwnica-Worms, H., and Richter, J.D. (1991). Maturation-specific polyadenylation: in vitro activation by p34cdc2 and phosphorylation of a 58-kD CPE-binding protein. Genes Dev *5*, 1697-1708.

Park, M., Salgado, J.M., Ostroff, L., Helton, T.D., Robinson, C.G., Harris, K.M., and Ehlers, M.D. (2006). Plasticity-induced growth of dendritic spines by exocytic trafficking from recycling endosomes. Neuron *52*, 817-830.

Parsons, R.G., Riedner, B.A., Gafford, G.M., and Helmstetter, F.J. (2006). The formation of auditory fear memory requires the synthesis of protein and mRNA in the auditory thalamus. Neuroscience *141*, 1163-1170.

Pause, A., Belsham, G.J., Gingras, A.C., Donze, O., Lin, T.A., Lawrence, J.C., Jr., and Sonenberg, N. (1994). Insulin-dependent stimulation of protein synthesis by phosphorylation of a regulator of 5'-cap function. Nature *371*, 762-767.

Pavlopoulos, E., Trifilieff, P., Chevaleyre, V., Fioriti, L., Zairis, S., Pagano, A., Malleret, G., and Kandel, E.R. (2011). Neuralized1 activates CPEB3: a function for nonproteolytic ubiquitin in synaptic plasticity and memory storage. Cell *147*, 1369-1383.

Pedroza-Llinas, R., Ramirez-Lugo, L., Guzman-Ramos, K., Zavala-Vega, S., and Bermudez-Rattoni, F. (2009). Safe taste memory consolidation is disrupted by a protein synthesis inhibitor in the nucleus accumbens shell. Neurobiol Learn Mem *92*, 45-52.

Peng, Y., Zhao, J., Gu, Q.H., Chen, R.Q., Xu, Z., Yan, J.Z., Wang, S.H., Liu, S.Y., Chen, Z., and Lu, W. (2010). Distinct trafficking and expression mechanisms underlie LTP and LTD of NMDA receptor-mediated synaptic responses. Hippocampus *20*, 646-658.

Perycz, M., Urbanska, A.S., Krawczyk, P.S., Parobczak, K., and Jaworski, J. (2011). Zipcode binding protein 1 regulates the development of dendritic arbors in hippocampal neurons. J Neurosci *31*, 5271-5285.

Petrini, E.M., Lu, J., Cognet, L., Lounis, B., Ehlers, M.D., and Choquet, D. (2009). Endocytic trafficking and recycling maintain a pool of mobile surface AMPA receptors required for synaptic potentiation. Neuron *63*, 92-105.

Pezawas, L., Verchinski, B.A., Mattay, V.S., Callicott, J.H., Kolachana, B.S., Straub, R.E., Egan, M.F., Meyer-Lindenberg, A., and Weinberger, D.R. (2004). The brain-derived neurotrophic factor val66met polymorphism and variation in human cortical morphology. J Neurosci *24*, 10099-10102.

Philpot, B.D., Cho, K.K., and Bear, M.F. (2007). Obligatory role of NR2A for metaplasticity in visual cortex. Neuron *53*, 495-502.

Pickering, B.M., and Willis, A.E. (2005). The implications of structured 5' untranslated regions on translation and disease. Semin Cell Dev Biol *16*, 39-47.

Poon, M.M., Choi, S.H., Jamieson, C.A., Geschwind, D.H., and Martin, K.C. (2006). Identification of process-localized mRNAs from cultured rodent hippocampal neurons. J Neurosci *26*, 13390-13399.

Quinlan, E.M., and Halpain, S. (1996). Postsynaptic mechanisms for bidirectional control of MAP2 phosphorylation by glutamate receptors. Neuron *16*, 357-368.

Quinlan, E.M., Philpot, B.D., Huganir, R.L., and Bear, M.F. (1999). Rapid, experience-dependent expression of synaptic NMDA receptors in visual cortex in vivo. Nat Neurosci *2*, 352-357.

Rebola, N., Lujan, R., Cunha, R.A., and Mulle, C. (2008). Adenosine A2A receptors are essential for long-term potentiation of NMDA-EPSCs at hippocampal mossy fiber synapses. Neuron *57*, 121-134.

Rial Verde, E.M., Lee-Osbourne, J., Worley, P.F., Malinow, R., and Cline, H.T. (2006). Increased expression of the immediate-early gene arc/arg3.1 reduces AMPA receptor-mediated synaptic transmission. Neuron *52*, 461-474.

Richter, J.D. (2007). CPEB: a life in translation. Trends Biochem Sci *32*, 279-285.

Richter, J.D., and Klann, E. (2009). Making synaptic plasticity and memory last: mechanisms of translational regulation. Genes Dev *23*, 1-11.

Richter, J.D., and Sonenberg, N. (2005). Regulation of cap-dependent translation by eIF4E inhibitory proteins. Nature *433*, 477-480.

Riedl, J., Crevenna, A.H., Kessenbrock, K., Yu, J.H., Neukirchen, D., Bista, M., Bradke, F., Jenne, D., Holak, T.A., Werb, Z., Sixt, M., and Wedlich-Soldner, R. (2008). Lifeact: a versatile marker to visualize F-actin. Nat Methods *5*, 605-607.

Riedl, J., Flynn, K.C., Raducanu, A., Gartner, F., Beck, G., Bosl, M., Bradke, F., Massberg, S., Aszodi, A., Sixt, M., and Wedlich-Soldner, R. (2010). Lifeact mice for studying F-actin dynamics. Nat Methods *7*, 168-169.

Roberts, L.A., Large, C.H., Higgins, M.J., Stone, T.W., O'Shaughnessy, C.T., and Morris, B.J. (1998). Increased expression of dendritic mRNA following the induction of long-term potentiation. Brain Res Mol Brain Res *56*, 38-44.

Ronesi, J.A., and Huber, K.M. (2008). Metabotropic glutamate receptors and fragile x mental retardation protein: partners in translational regulation at the synapse. Sci Signal *1*, pe6.

Rook, M.S., Lu, M., and Kosik, K.S. (2000). CaMKIIalpha 3' untranslated region-directed mRNA translocation in living neurons: visualization by GFP linkage. J Neurosci *20*, 6385-6393.

Ross, A.F., Oleynikov, Y., Kislauskis, E.H., Taneja, K.L., and Singer, R.H. (1997). Characterization of a beta-actin mRNA zipcode-binding protein. Mol Cell Biol *17*, 2158-2165.

Rouget, C., Papin, C., and Mandart, E. (2006). Cytoplasmic CstF-77 protein belongs to a masking complex with cytoplasmic polyadenylation element-binding protein in Xenopus oocytes. J Biol Chem *281*, 28687-28698.

Rouhana, L., Wang, L., Buter, N., Kwak, J.E., Schiltz, C.A., Gonzalez, T., Kelley, A.E., Landry, C.F., and Wickens, M. (2005). Vertebrate GLD2 poly(A) polymerases in the germline and the brain. RNA *11*, 1117-1130.

Rowlands, A.G., Panniers, R., and Henshaw, E.C. (1988). The catalytic mechanism of guanine nucleotide exchange factor action and competitive inhibition by phosphorylated eukaryotic initiation factor 2. J Biol Chem *263*, 5526-5533.

Salas-Marco, J., and Bedwell, D.M. (2004). GTP hydrolysis by eRF3 facilitates stop codon decoding during eukaryotic translation termination. Mol Cell Biol *24*, 7769-7778.

Sarkissian, M., Mendez, R., and Richter, J.D. (2004). Progesterone and insulin stimulation of CPEB-dependent polyadenylation is regulated by Aurora A and glycogen synthase kinase-3. Genes Dev *18*, 48-61.

Sasaki, Y., Welshhans, K., Wen, Z., Yao, J., Xu, M., Goshima, Y., Zheng, J.Q., and Bassell, G.J. (2010). Phosphorylation of zipcode binding protein 1 is required for brain-derived neurotrophic factor signaling of local beta-actin synthesis and growth cone turning. J Neurosci *30*, 9349-9358.

Scheetz, A.J., Nairn, A.C., and Constantine-Paton, M. (2000). NMDA receptor-mediated control of protein synthesis at developing synapses. Nat Neurosci *3*, 211-216.

Schenck, A., Bardoni, B., Langmann, C., Harden, N., Mandel, J.L., and Giangrande, A. (2003). CYFIP/Sra-1 controls neuronal connectivity in Drosophila and links the Rac1 GTPase pathway to the fragile X protein. Neuron *38*, 887-898.

Schenck, A., Qurashi, A., Carrera, P., Bardoni, B., Diebold, C., Schejter, E., Mandel, J.L., and Giangrande, A. (2004). WAVE/SCAR, a multifunctional complex coordinating different aspects of neuronal connectivity. Dev Biol *274*, 260-270.

Schicknick, H., Schott, B.H., Budinger, E., Smalla, K.H., Riedel, A., Seidenbecher, C.I., Scheich, H., Gundelfinger, E.D., and Tischmeyer, W. (2008). Dopaminergic modulation of auditory cortex-dependent memory consolidation through mTOR. Cereb Cortex *18*, 2646-2658.

Schilstrom, B., Yaka, R., Argilli, E., Suvarna, N., Schumann, J., Chen, B.T., Carman, M., Singh, V., Mailliard, W.S., Ron, D., and Bonci, A. (2006). Cocaine enhances NMDA receptor-mediated currents in ventral tegmental area cells via dopamine D5 receptor-dependent redistribution of NMDA receptors. J Neurosci *26*, 8549-8558.

Schratt, G. (2009). microRNAs at the synapse. Nat Rev Neurosci *10*, 842-849.

Shang, Y., Wang, H., Mercaldo, V., Li, X., Chen, T., and Zhuo, M. (2009). Fragile X mental retardation protein is required for chemically-induced long-term potentiation of the hippocampus in adult mice. J Neurochem *111*, 635-646.

Shepherd, J.D., Rumbaugh, G., Wu, J., Chowdhury, S., Plath, N., Kuhl, D., Huganir, R.L., and Worley, P.F. (2006). Arc/Arg3.1 mediates homeostatic synaptic scaling of AMPA receptors. Neuron *52*, 475-484.

Shiina, N., Shinkura, K., and Tokunaga, M. (2005). A novel RNA-binding protein in neuronal RNA granules: regulatory machinery for local translation. J Neurosci *25*, 4420-4434.

Shin, C.Y., Kundel, M., and Wells, D.G. (2004). Rapid, activity-induced increase in tissue plasminogen activator is mediated by metabotropic glutamate receptor-dependent mRNA translation. J Neurosci *24*, 9425-9433.

Si, K., Giustetto, M., Etkin, A., Hsu, R., Janisiewicz, A.M., Miniaci, M.C., Kim, J.H., Zhu, H., and Kandel, E.R. (2003a). A neuronal isoform of CPEB regulates local

protein synthesis and stabilizes synapse-specific long-term facilitation in aplysia. Cell *115*, 893-904.

Si, K., Lindquist, S., and Kandel, E.R. (2003b). A neuronal isoform of the aplysia CPEB has prion-like properties. Cell *115*, 879-891.

Silva, A.J., and Giese, K.P. (1994). Plastic genes are in! Curr Opin Neurobiol *4*, 413-420.

Simon, R., Wu, L., and Richter, J.D. (1996). Cytoplasmic polyadenylation of activin receptor mRNA and the control of pattern formation in Xenopus development. Dev Biol *179*, 239-250.

Simonato, M., Bregola, G., Armellin, M., Del Piccolo, P., Rodi, D., Zucchini, S., and Tongiorgi, E. (2002). Dendritic targeting of mRNAs for plasticity genes in experimental models of temporal lobe epilepsy. Epilepsia *43 Suppl 5*, 153-158.

Slipczuk, L., Bekinschtein, P., Katche, C., Cammarota, M., Izquierdo, I., and Medina, J.H. (2009). BDNF activates mTOR to regulate GluR1 expression required for memory formation. PLoS One *4*, e6007.

Smart, F.M., Edelman, G.M., and Vanderklish, P.W. (2003). BDNF induces translocation of initiation factor 4E to mRNA granules: evidence for a role of synaptic microfilaments and integrins. Proc Natl Acad Sci U S A *100*, 14403-14408.

Smith, G.B., Heynen, A.J., and Bear, M.F. (2009). Bidirectional synaptic mechanisms of ocular dominance plasticity in visual cortex. Philos Trans R Soc Lond B Biol Sci *364*, 357-367.

Smith, W.B., Starck, S.R., Roberts, R.W., and Schuman, E.M. (2005). Dopaminergic stimulation of local protein synthesis enhances surface expression of GluR1 and synaptic transmission in hippocampal neurons. Neuron *45*, 765-779.

Snyder, E.M., Philpot, B.D., Huber, K.M., Dong, X., Fallon, J.R., and Bear, M.F. (2001). Internalization of ionotropic glutamate receptors in response to mGluR activation. Nat Neurosci *4*, 1079-1085.

Sobczyk, A., and Svoboda, K. (2007). Activity-dependent plasticity of the NMDA-receptor fractional Ca2+ current. Neuron *53*, 17-24.

Sokol, D.K., Maloney, B., Long, J.M., Ray, B., and Lahiri, D.K. (2011). Autism, Alzheimer disease, and fragile X: APP, FMRP, and mGluR5 are molecular links. Neurology *76*, 1344-1352.

Soliman, F., Glatt, C.E., Bath, K.G., Levita, L., Jones, R.M., Pattwell, S.S., Jing, D., Tottenham, N., Amso, D., Somerville, L.H., Voss, H.U., Glover, G., Ballon, D.J., Liston, C., Teslovich, T., Van Kempen, T., Lee, F.S., and Casey, B.J. (2010). A genetic variant BDNF polymorphism alters extinction learning in both mouse and human. Science *327*, 863-866.

Song, B., Lai, B., Zheng, Z., Zhang, Y., Luo, J., Wang, C., Chen, Y., Woodgett, J.R., and Li, M. (2010). Inhibitory phosphorylation of GSK-3 by CaMKII couples depolarization to neuronal survival. J Biol Chem *285*, 41122-41134.

Sorg, B.A., and Ulibarri, C. (1995). Application of a protein synthesis inhibitor into the ventral tegmental area, but not the nucleus accumbens, prevents behavioral sensitization to cocaine. Synapse *20*, 217-224.

Sossin, W.S., and DesGroseillers, L. (2006). Intracellular trafficking of RNA in neurons. Traffic *7*, 1581-1589.

Stebbins-Boaz, B., Cao, Q., de Moor, C.H., Mendez, R., and Richter, J.D. (1999). Maskin is a CPEB-associated factor that transiently interacts with eIF-4E. Mol Cell *4*, 1017-1027.

Stein, J.M., Bergman, W., Fang, Y., Davison, L., Brensinger, C., Robinson, M.B., Hecht, N.B., and Abel, T. (2006). Behavioral and neurochemical alterations in mice lacking the RNA-binding protein translin. J Neurosci *26*, 2184-2196.

Steward, O., and Halpain, S. (1999). Lamina-specific synaptic activation causes domain-specific alterations in dendritic immunostaining for MAP2 and CAM kinase II. J Neurosci *19*, 7834-7845.

Steward, O., and Levy, W.B. (1982). Preferential localization of polyribosomes under the base of dendritic spines in granule cells of the dentate gyrus. J Neurosci *2*, 284-291.

Steward, O., and Reeves, T.M. (1988). Protein-synthetic machinery beneath postsynaptic sites on CNS neurons: association between polyribosomes and other organelles at the synaptic site. J Neurosci *8*, 176-184.

Steward, O., and Schuman, E.M. (2001). Protein synthesis at synaptic sites on dendrites. Annu Rev Neurosci *24*, 299-325.

Steward, O., Wallace, C.S., Lyford, G.L., and Worley, P.F. (1998). Synaptic activation causes the mRNA for the IEG Arc to localize selectively near activated postsynaptic sites on dendrites. Neuron *21*, 741-751.

Steward, O., and Worley, P.F. (2001). Selective targeting of newly synthesized Arc mRNA to active synapses requires NMDA receptor activation. Neuron *30*, 227-240.

Straube, T., Korz, V., Balschun, D., and Frey, J.U. (2003). Requirement of beta-adrenergic receptor activation and protein synthesis for LTP-reinforcement by novelty in rat dentate gyrus. J Physiol *552*, 953-960.

Sun, X., and Wolf, M.E. (2009). Nucleus accumbens neurons exhibit synaptic scaling that is occluded by repeated dopamine pre-exposure. Eur J Neurosci *30*, 539-550.

Sutton, M.A., Ito, H.T., Cressy, P., Kempf, C., Woo, J.C., and Schuman, E.M. (2006). Miniature neurotransmission stabilizes synaptic function via tonic suppression of local dendritic protein synthesis. Cell *125*, 785-799.

Sutton, M.A., and Schuman, E.M. (2006). Dendritic protein synthesis, synaptic plasticity, and memory. Cell *127*, 49-58.

Swanger, S.A., and Bassell, G.J. (2011). Making and breaking synapses through local mRNA regulation. Curr Opin Genet Dev *21*, 414-421.

Swanger, S.A., Bassell, G.J., and Gross, C. (2011a). High-resolution fluorescence in situ hybridization to detect mRNAs in neuronal compartments in vitro and in vivo. Methods Mol Biol *714*, 103-123.

Swanger, S.A., Yao, X., Gross, C., and Bassell, G.J. (2011b). Automated 4D analysis of dendritic spine morphology: applications to stimulus-induced spine remodeling and pharmacological rescue in a disease model. Mol Brain *4*, 38.

Takei, N., Inamura, N., Kawamura, M., Namba, H., Hara, K., Yonezawa, K., and Nawa, H. (2004). Brain-derived neurotrophic factor induces mammalian target of rapamycin-dependent local activation of translation machinery and protein synthesis in neuronal dendrites. J Neurosci *24*, 9760-9769.

Takei, N., Kawamura, M., Ishizuka, Y., Kakiya, N., Inamura, N., Namba, H., and Nawa, H. (2009). Brain-derived neurotrophic factor enhances the basal rate of protein

synthesis by increasing active eukaryotic elongation factor 2 levels and promoting translation elongation in cortical neurons. J Biol Chem *284*, 26340-26348.

Tanaka, J., Horiike, Y., Matsuzaki, M., Miyazaki, T., Ellis-Davies, G.C., and Kasai, H. (2008). Protein synthesis and neurotrophin-dependent structural plasticity of single dendritic spines. Science *319*, 1683-1687.

Tang, S.J., Reis, G., Kang, H., Gingras, A.C., Sonenberg, N., and Schuman, E.M. (2002). A rapamycin-sensitive signaling pathway contributes to long-term synaptic plasticity in the hippocampus. Proc Natl Acad Sci U S A *99*, 467-472.

Tay, J., Hodgman, R., Sarkissian, M., and Richter, J.D. (2003). Regulated CPEB phosphorylation during meiotic progression suggests a mechanism for temporal control of maternal mRNA translation. Genes Dev *17*, 1457-1462.

Theis, M., Si, K., and Kandel, E.R. (2003). Two previously undescribed members of the mouse CPEB family of genes and their inducible expression in the principal cell layers of the hippocampus. Proc Natl Acad Sci U S A *100*, 9602-9607.

Tiedge, H., and Brosius, J. (1996). Translational machinery in dendrites of hippocampal neurons in culture. J Neurosci *16*, 7171-7181.

Tiruchinapalli, D.M., Caron, M.G., and Keene, J.D. (2008). Activity-dependent expression of ELAV/Hu RBPs and neuronal mRNAs in seizure and cocaine brain. J Neurochem *107*, 1529-1543.

Tiruchinapalli, D.M., Oleynikov, Y., Kelic, S., Shenoy, S.M., Hartley, A., Stanton, P.K., Singer, R.H., and Bassell, G.J. (2003). Activity-dependent trafficking and dynamic localization of zipcode binding protein 1 and beta-actin mRNA in dendrites and spines of hippocampal neurons. J Neurosci *23*, 3251-3261.

Tischmeyer, W., Schicknick, H., Kraus, M., Seidenbecher, C.I., Staak, S., Scheich, H., and Gundelfinger, E.D. (2003). Rapamycin-sensitive signalling in long-term consolidation of auditory cortex-dependent memory. Eur J Neurosci *18*, 942-950.

Tongiorgi, E., Armellin, M., Giulianini, P.G., Bregola, G., Zucchini, S., Paradiso, B., Steward, O., Cattaneo, A., and Simonato, M. (2004). Brain-derived neurotrophic factor mRNA and protein are targeted to discrete dendritic laminas by events that trigger epileptogenesis. J Neurosci *24*, 6842-6852.

Tongiorgi, E., Righi, M., and Cattaneo, A. (1997). Activity-dependent dendritic targeting of BDNF and TrkB mRNAs in hippocampal neurons. J Neurosci *17*, 9492-9505.

Torre, E.R., and Steward, O. (1992). Demonstration of local protein synthesis within dendrites using a new cell culture system that permits the isolation of living axons and dendrites from their cell bodies. J Neurosci *12*, 762-772.

Torre, E.R., and Steward, O. (1996). Protein synthesis within dendrites: glycosylation of newly synthesized proteins in dendrites of hippocampal neurons in culture. J Neurosci *16*, 5967-5978.

Traynelis, S.F., Wollmuth, L.P., McBain, C.J., Menniti, F.S., Vance, K.M., Ogden, K.K., Hansen, K.B., Yuan, H., Myers, S.J., and Dingledine, R. (2010). Glutamate receptor ion channels: structure, regulation, and function. Pharmacol Rev *62*, 405-496.

Troca-Marin, J.A., Alves-Sampaio, A., and Montesinos, M.L. (2011). An increase in basal BDNF provokes hyperactivation of the Akt-mammalian target of rapamycin pathway and deregulation of local dendritic translation in a mouse model of Down's syndrome. J Neurosci *31*, 9445-9455.

Udagawa, T., Swanger, S.A., Takeuchi, K., Kim, J.H., Nalavadi, V., Shin, J., Lorenz, L.J., Zukin, R.S., Bassell, G.J., and Richter, J.D. (in press). Bidirectional control of mRNA translation and synaptic plasticity by the cytoplasmic polyadenylation complex. Mol Cell.

Vessey, J.P., Schoderboeck, L., Gingl, E., Luzi, E., Riefler, J., Di Leva, F., Karra, D., Thomas, S., Kiebler, M.A., and Macchi, P. (2010). Mammalian Pumilio 2 regulates dendrite morphogenesis and synaptic function. Proc Natl Acad Sci U S A *107*, 3222-3227.

Vessey, J.P., Vaccani, A., Xie, Y., Dahm, R., Karra, D., Kiebler, M.A., and Macchi, P. (2006). Dendritic localization of the translational repressor Pumilio 2 and its contribution to dendritic stress granules. J Neurosci *26*, 6496-6508.

Vogler, C., Spalek, K., Aerni, A., Demougin, P., Muller, A., Huynh, K.D., Papassotiropoulos, A., and de Quervain, D.J. (2009). CPEB3 is associated with human episodic memory. Front Behav Neurosci *3*, 4.

Volk, L.J., Pfeiffer, B.E., Gibson, J.R., and Huber, K.M. (2007). Multiple Gq-coupled receptors converge on a common protein synthesis-dependent long-term depression that is affected in fragile X syndrome mental retardation. J Neurosci *27*, 11624-11634.

Walling, S.G., and Harley, C.W. (2004). Locus ceruleus activation initiates delayed synaptic potentiation of perforant path input to the dentate gyrus in awake rats: a novel beta-adrenergic- and protein synthesis-dependent mammalian plasticity mechanism. J Neurosci *24*, 598-604.

Wang, D.O., Kim, S.M., Zhao, Y., Hwang, H., Miura, S.K., Sossin, W.S., and Martin, K.C. (2009). Synapse- and stimulus-specific local translation during long-term neuronal plasticity. Science *324*, 1536-1540.

Wang, H., Kim, S.S., and Zhuo, M. (2010a). Roles of fragile X mental retardation protein in dopaminergic stimulation-induced synapse-associated protein synthesis and subsequent alpha-amino-3-hydroxyl-5-methyl-4-isoxazole-4-propionate (AMPA) receptor internalization. J Biol Chem *285*, 21888-21901.

Wang, X., Luo, Y.X., He, Y.Y., Li, F.Q., Shi, H.S., Xue, L.F., Xue, Y.X., and Lu, L. (2010b). Nucleus accumbens core mammalian target of rapamycin signaling pathway is critical for cue-induced reinstatement of cocaine seeking in rats. J Neurosci *30*, 12632-12641.

Wang, X.B., Yang, Y., and Zhou, Q. (2007). Independent expression of synaptic and morphological plasticity associated with long-term depression. J Neurosci *27*, 12419-12429.

Wang, X.P., and Cooper, N.G. (2010). Comparative in silico analyses of cpeb1-4 with functional predictions. Bioinform Biol Insights *4*, 61-83.

Waung, M.W., Pfeiffer, B.E., Nosyreva, E.D., Ronesi, J.A., and Huber, K.M. (2008). Rapid translation of Arc/Arg3.1 selectively mediates mGluR-dependent LTD through persistent increases in AMPAR endocytosis rate. Neuron *59*, 84-97.

Weiler, I.J., Irwin, S.A., Klintsova, A.Y., Spencer, C.M., Brazelton, A.D., Miyashiro, K., Comery, T.A., Patel, B., Eberwine, J., and Greenough, W.T. (1997). Fragile X mental retardation protein is translated near synapses in response to neurotransmitter activation. Proc Natl Acad Sci U S A *94*, 5395-5400.

Wells, D.G., Dong, X., Quinlan, E.M., Huang, Y.S., Bear, M.F., Richter, J.D., and
Fallon, J.R. (2001). A role for the cytoplasmic polyadenylation element in NMDA
receptor-regulated mRNA translation in neurons. J Neurosci *21*, 9541-9548.

Wells, S.E., Hillner, P.E., Vale, R.D., and Sachs, A.B. (1998). Circularization of mRNA
by eukaryotic translation initiation factors. Mol Cell *2*, 135-140.

Welshhans, K., and Bassell, G.J. (2011). Netrin-1-induced local beta-actin synthesis and
growth cone guidance requires zipcode binding protein 1. J Neurosci *31*, 9800-
9813.

Wharton, R.P., Sonoda, J., Lee, T., Patterson, M., and Murata, Y. (1998). The Pumilio
RNA-binding domain is also a translational regulator. Mol Cell *1*, 863-872.

Williams, J.M., Guevremont, D., Kennard, J.T., Mason-Parker, S.E., Tate, W.P., and
Abraham, W.C. (2003). Long-term regulation of N-methyl-D-aspartate receptor
subunits and associated synaptic proteins following hippocampal synaptic
plasticity. Neuroscience *118*, 1003-1013.

Williams, J.M., Mason-Parker, S.E., Abraham, W.C., and Tate, W.P. (1998). Biphasic
changes in the levels of N-methyl-D-aspartate receptor-2 subunits correlate with
the induction and persistence of long-term potentiation. Brain Res Mol Brain Res
60, 21-27.

Wu, L., Wells, D., Tay, J., Mendis, D., Abbott, M.A., Barnitt, A., Quinlan, E., Heynen,
A., Fallon, J.R., and Richter, J.D. (1998). CPEB-mediated cytoplasmic
polyadenylation and the regulation of experience-dependent translation of alpha-
CaMKII mRNA at synapses. Neuron *21*, 1129-1139.

Wu, Y.C., Williamson, R., Li, Z., Vicario, A., Xu, J., Kasai, M., Chern, Y., Tongiorgi, E.,
and Baraban, J.M. (2011). Dendritic trafficking of brain-derived neurotrophic
factor mRNA: regulation by translin-dependent and -independent mechanisms. J
Neurochem *116*, 1112-1121.

Yang, Y., Wang, X.B., Frerking, M., and Zhou, Q. (2008). Spine expansion and
stabilization associated with long-term potentiation. J Neurosci *28*, 5740-5751.

Yashiro, K., and Philpot, B.D. (2008). Regulation of NMDA receptor subunit expression
and its implications for LTD, LTP, and metaplasticity. Neuropharmacology *55*,
1081-1094.

Ye, B., Petritsch, C., Clark, I.E., Gavis, E.R., Jan, L.Y., and Jan, Y.N. (2004). Nanos and Pumilio are essential for dendrite morphogenesis in Drosophila peripheral neurons. Curr Biol *14*, 314-321.

Yoshimura, A., Fujii, R., Watanabe, Y., Okabe, S., Fukui, K., and Takumi, T. (2006). Myosin-Va facilitates the accumulation of mRNA/protein complex in dendritic spines. Curr Biol *16*, 2345-2351.

Zalfa, F., Giorgi, M., Primerano, B., Moro, A., Di Penta, A., Reis, S., Oostra, B., and Bagni, C. (2003). The fragile X syndrome protein FMRP associates with BC1 RNA and regulates the translation of specific mRNAs at synapses. Cell *112*, 317-327.

Zearfoss, N.R., Alarcon, J.M., Trifilieff, P., Kandel, E., and Richter, J.D. (2008). A molecular circuit composed of CPEB-1 and c-Jun controls growth hormone-mediated synaptic plasticity in the mouse hippocampus. J Neurosci *28*, 8502-8509.

Zhang, G., Neubert, T.A., and Jordan, B.A. (2012). RNA binding proteins accumulate at the postsynaptic density with synaptic activity. J Neurosci *32*, 599-609.

Zhang, H., Xing, L., Rossoll, W., Wichterle, H., Singer, R.H., and Bassell, G.J. (2006). Multiprotein complexes of the survival of motor neuron protein SMN with Gemins traffic to neuronal processes and growth cones of motor neurons. J Neurosci *26*, 8622-8632.

Zhang, H.L., Eom, T., Oleynikov, Y., Shenoy, S.M., Liebelt, D.A., Dictenberg, J.B., Singer, R.H., and Bassell, G.J. (2001). Neurotrophin-induced transport of a beta-actin mRNP complex increases beta-actin levels and stimulates growth cone motility. Neuron *31*, 261-275.

Zhong, J., Zhang, T., and Bloch, L.M. (2006a). Dendritic mRNAs encode diversified functionalities in hippocampal pyramidal neurons. BMC Neurosci *7*, 17.

Zhong, W.X., Dong, Z.F., Tian, M., Cao, J., Xu, L., and Luo, J.H. (2006b). N-methyl-D-aspartate receptor-dependent long-term potentiation in CA1 region affects synaptic expression of glutamate receptor subunits and associated proteins in the whole hippocampus. Neuroscience *141*, 1399-1413.

Zimyanin, V.L., Belaya, K., Pecreaux, J., Gilchrist, M.J., Clark, A., Davis, I., and St Johnston, D. (2008). In vivo imaging of oskar mRNA transport reveals the mechanism of posterior localization. Cell *134*, 843-853.

Zukin, R.S., Richter, J.D., and Bagni, C. (2009). Signals, synapses, and synthesis: how new proteins control plasticity. Front Neural Circuits *3*, 14.

APPENDIX 1

Automated 4D analysis of dendritic spine morphology: applications to stimulus-induced spine remodeling and pharmacological rescue in a disease model

Parts of this chapter are adapted from:

Swanger, S.A., Gross, C., Yao, X., and Bassell, G.J. Automated 4D analysis of dendritic spine morphology: applications to stimulus-induced spine remodeling and pharmacological rescue in a disease model. *Mol Brain*. 2011 Oct 7;4:38.

A1.1   Introduction

Dendritic spines are dynamic, actin-rich protrusions that form the postsynaptic compartment at most glutamatergic synapses (Edwards, 1995). Synapse strength is closely correlated with dendritic spine morphology, and synaptic activity regulates spine number and shape during brain development, behavioral learning, and aging (Alvarez and Sabatini, 2007; Holtmaat and Svoboda, 2009; Kasai et al., 2010). In addition, abnormal spine morphology is prevalent in neurological diseases such as intellectual disabilities, autism spectrum disorders, schizophrenia, mood disorders, and Alzheimer's disease (Glantz and Lewis, 2001; Lee et al., 2005; Penzes et al., 2011). Although many details regarding the spine structure-synapse function relationship remain unclear, it is evident that spine morphology can impact excitatory neurotransmission and is an important aspect of neuronal development, plasticity, and disease (Bourne and Harris, 2008, 2010; Hayashi and Majewska, 2005; Lee et al., 2005).

The lack of automated methods for quantifying spine number and geometry has hindered analysis of the mechanisms linking spine structure to synapse function (Svoboda, 2011). Cultured neurons are the primary model system for studying the basic mechanisms regulating neuronal structure and function as these mechanistic studies require complex designs and large sample sizes in order to produce meaningful results. While several recent reports have described automated algorithms for analyzing neuron morphology in vivo (Janoos et al., 2009; Mukai et al., 2011; Rodriguez et al., 2008; Rodriguez et al., 2006; Wearne et al., 2005; Zhang et al., 2010; Zhang et al., 2007), few independent studies have validated these methods (Bloss et al., 2011; Scotto-Lomassese et al., 2011) and there are no established methods for automated 3D spine analysis in

cultured neurons. Son et al. developed an automated spine analysis algorithm using 2D

images of cultured neurons, but 2D analyses do not consider a significant amount of

information including all protrusions extending into the z-plane (Son et al., 2011; Stevens

and Trogadis, 1986). The majority of spine morphology studies have relied on manual

measurements, which are time consuming, often biased by experimenter error and

fatigue, and have limited reproducibility (Wearne et al., 2005).

Here, we present, validate, and apply an automated 3D approach using the

commercially available software program Filament Tracer (Imaris, Bitplane, Inc.).

Filament Tracer has been used for automated spine detection *in vivo,* but geometric

measurements were limited to spine head width (Shen et al., 2008; Staffend et al., 2011).

Also, we have used Filament Tracer to facilitate spine density calculations in cultured

neurons, but this analysis required manual validation and extensive editing of false-

positive spines (Gross et al., 2010; Gross et al., 2011b). Now, our improved approach

generates an accurate 3D reconstruction without any manual validation. Moreover, our

approach can be applied to either fixed or live neurons as well as images acquired using

either widefield fluorescence or confocal microscopy.

To demonstrate the applicability of our approach, we analyzed changes in spine

morphology following acute brain-derived neurotrophic factor (BDNF) application in

live hippocampal neurons. We verified our method by showing that acute BDNF

treatment increased spine head volume, as was previously published (Tanaka et al.,

2008). Furthermore, we demonstrated that BDNF application induced rapid alterations in

spine neck and length geometry and resulted in an overall maturation of the dendritic

spine population within 60 minutes. We also applied our method to the study of aberrant

spine morphology in a mouse model of fragile X syndrome (FXS), an inherited

intellectual disability (Bassell and Warren, 2008). We not only accurately detected the

established spine abnormalities in cultured neurons from this mouse model, but we also

demonstrated that these abnormalities were rescued by inhibiting phosphoinositide-3

kinase activity, a potential therapeutic strategy for FXS (Gross et al., 2010). These

findings demonstrate that our approach is an efficient and accurate method for

investigating dendritic spine development and plasticity as well as neurological disease

mechanisms and therapies.

A1.2 Results and Discussion

A1.2.1 Automated detection and 3D measurement of dendritic spines

The accurate study of dendritic spine morphology requires a method that

incorporates effective neuron labeling with unbiased spine detection and measurement.

To establish the most effective method for labeling and detecting spines in cultured

hippocampal neurons, we tested several fluorescent markers including the lipophilic dye

DiI and plasmids encoding soluble eGFP, membrane-tagged eGFP, and mRFPruby-

tagged Lifeact, a small actin binding peptide (Riedl et al., 2008). The labeled neurons

were fixed, and z-series images were acquired using a widefield fluorescence

microscope. Following deconvolution, the images were analyzed with two different

software programs: NeuronStudio, a program used for automated 3D neuron tracing *in*

vivo (Rodriguez et al., 2008) , and Filament Tracer (Imaris, Bitplane, Inc.), a

commercially available 3D tracing software. Universal parameters for accurate automated

tracing of a large dataset could not be identified using NeuronStudio with any fluorescent

label or using Filament Tracer with DiI-labeled or GFP-expressing neurons (data not shown). However, accurate 3D traces were automatically generated from images of Lifeact-ruby-expressing neurons (Fig. 1a). While GFP is commonly used for morphological analyses, we found that generating accurate traces of GFP-expressing neurons required extensive manual editing of false-positive spines. Images of Lifeact-expressing neurons could be used to generate automated traces with universal parameters and no manual editing. Of note, Lifeact-expressing neurons have been previously shown to exhibit normal actin dynamics and dendritic spine morphology (Riedl et al., 2008; Riedl et al., 2010). Consequently, we describe here the validation and application of an automated spine analysis method using Filament Tracer and images of Lifeact-expressing neurons.

To generate the 3D reconstructions for spine analysis, we selected a dendritic region that was 40 – 60 µm in length and void of dendritic branch points and crossing neurites. A point within the dendrite and at the edge of the selected region was assigned as the dendrite starting point, and the following parameters were set: *minimum dendrite end diameter* (0.75 µm; empirically determined to be the minimum dendritic width enabling accurate tracing), *minimum spine end diame*ter (0.215 µm; 2 times the pixel width), and *maximum spine len*gth (5 µm) (Papa et al., 1995). The dendritic segment was then traced and volume rendered using automatic thresholds without any additional manual input or editing. On occasion the algorithm inappropriately assigned dendritic protrusions as dendrites instead of spines, so we applied a mathematical filter that selected all dendritic protrusions ≤ 5 µm in length and assigned them as spines. To validate the automated spine detection, spine density was calculated within the same

dendritic regions using manual and automated analyses (Fig. 1b). The automated

measures accurately predicted the manual spine counts as determined by linear regression

analysis (Fig. 1c) (Ludbrook, 2010). The mean spine density (spines per 10 μm) did not

significantly differ between the manual (4.36 ± 0.46) and automated (4.47 ± 0.41)

analyses (Student's t-test, $P = 0.836$), but there was a consistent trend toward higher

spine density using the automated method. The coefficient of variation was lower for the

automated results (0.9) as compared to the manual measurements (0.11), suggesting that

automated spine detection was slightly more reproducible than manual detection.

While spine number reflects the quantity of excitatory synapses, spine geometry is

linked with excitatory synapse function and is also an important outcome measure in

dendritic spine studies (Bourne and Harris, 2008). Spine head size is positively correlated

with postsynaptic density (PSD) size, cell surface GluA receptor number, and synaptic

vesicle content in the associated presynaptic terminal (Harris and Stevens, 1989; Kasai et

al., 2003). Spine length and neck width likely affect calcium signaling within spines as

well as signaling from the spine to the dendrite shaft (Biess et al., 2007; Korkotian et al.,

2004; Noguchi et al., 2005). To evaluate how effectively our approach measured spine

geometry, automated measurements of spine head width, neck width, and length were

compared to manual measurements (Table 1). Unexpectedly, the distributions for each

parameter significantly differed between the manual and automated methods ($N_{manual} =$

411; $N_{auto} = 423$ spines; Kolmogorov-Smirnov Test; head width: $D = 0.394$; neck width:

$D = 0.510$; length: $D = 0.178$; all $P < 0.001$). Given these conflicting results, we

evaluated the precision and accuracy of the automated and manual methods. To analyze

precision, we evaluated specific characteristics of each dataset and found that the

standard deviation and coefficient of variation were consistently smaller for the

automated method (Table 1). Furthermore, the manual measurement distributions were

more skewed than the automated distributions, indicating that the manual method yields

distributions shifted further from the normal distribution as compared to automated

analyses. Together, these data indicate that our automated approach is a more precise

spine analysis method than manual measurements. To evaluate the accuracy of our

approach, we used published ultrastructural data to estimate population statistics for spine

head width, neck width, and length (Bourne and Harris, 2008; Harris and Stevens, 1989;

Noguchi et al., 2005; Papa et al., 1995). For each geometric parameter, the mean, median,

and range values of the automated distributions (shown in Table 1) were more similar to

the estimated population statistics (Table 2) than the manual values. For example, the

estimated median head and neck widths garnered from several published ultrastructural

studies were 0.40 µm and 0.15 µm, respectively. Our automatically determined median

head and neck widths were 0.46 µm and 0.11 µm, respectively; whereas, our manually

determined median head and neck widths were 0.60 µm and 0.23 µm, respectively. These

data suggest that the automated approach generated data that was more accurate than

manual measurements.

In addition, dendritic spines were classified as stubby, mushroom, or thin using

the aforementioned geometric measures; this is a widely used scheme to assess the

proportions of mature and immature spines within a population (Bourne and Harris,

2008; Harris et al., 1992; Peters and Kaiserman-Abramof, 1970). While similar

proportions of mushroom and thin spines were reported by both methods, the manual

method reported a significantly lower proportion of stubby spines than the automated

method (Table 3). On close examination, we observed that spines classified as stubby by the automated method were often manually classified as thin, due to an increased length measurement, or were manually determined to be a region of the dendrite shaft rather than a protrusion. In agreement with these observations, it is evident from the literature that manual spine analyses consistently underestimate the proportion of stubby spines and overestimate spine length at the low end of the distribution when compared to automated and semi-automated methods (Fan et al., 2009; Koh et al., 2002; Rodriguez et al., 2008; Zhang et al., 2007). It is important to note that, given the resolution limit of light microscopy, some spine heads may not be distinguishable from short and wide spine necks. While electron microscopy affords the resolution to make such distinctions, light microscopy is a more versatile and practical approach for mechanistic studies of dendritic spine structure. Altogether, these results indicate that our method accurately and precisely reports spine number and geometry in cultured neurons. Moreover, our method is a significant advance over current spine analysis methods as dendritic spine detection and 3D measurements are entirely automated, thus greatly reducing the time burden and removing experimenter biases.

A1.2.2 Automated tracking of dendritic spines in live neurons

Dendritic spine density and morphology are dynamically regulated by many extracellular cues and neurotransmitters. For example, many more dendritic protrusions are formed during development than remain into adulthood, indicating that spine formation and morphogenesis are highly regulated processes; yet, the mechanisms determining which spines become stabilized remain unclear. In the adult brain, stimulus

induced potentiation of the postsynaptic response can convert spines with small heads to large spines, whereas large spines can shrink in response to long-term depression of the postsynaptic response (Matsuzaki et al., 2004; Zhou et al., 2004). However, the detailed mechanisms governing these differential responses remain poorly understood. Therefore, time-lapse imaging in living neurons is an essential tool for studying stimulus-induced synapse development and plasticity.

To test how effectively our automated approach tracked dendritic protrusions in live hippocampal neurons, 12 *DIV* neurons expressing Lifeact-ruby were imaged at 5 min intervals for 1 hr. The 3D reconstructions were generated as described above with a few modifications. A dendrite starting point was defined for each time point using the AutoDepth mode in Imaris Filament Tracer. The automated trace was built using these existing dendrite start points and the following geometric parameters: *minimum dendrite end diameter* (0.75 µm), *minimum spine end diameter* (0.3 µm; empirically determined to be the minimum end diameter allowing accurate spine detection), and *maximum spine length* (15.0 µm). The *maximum spine length* was set at 15 µm to include dendritic filopodia, which are long and dynamic protrusions involved in spine and dendrite development (Heiman and Shaham, 2010; Yoshihara et al., 2009). Filopodia are included in this analysis because they are abundant on the 12 *DIV* neurons used for these experiments, whereas they are nearly absent on the mature neurons (17 *DIV*) used for the fixed neuron experiments described in Figure 1 and Table 1. The proportions of stable, new, and pruned dendritic protrusions (spines and filopodia) measured with the automated method were similar to those determined manually, suggesting that our automated approach allows detection and tracking of individual spines across time (Fig.

2a). Moreover, we demonstrated that the morphology of individual spines can be tracked (Fig. 2b) and quantified (Fig. 2c and 2d) over time using our automated approach. Taken together, these data indicate that Lifeact-expressing neurons combined with this automated spine analysis approach is a valid method for the 4D tracking of dendritic protrusions in live neurons.

A1.2.3 Acute BDNF treatment induces synapse maturation through spine remodeling

To test the usefulness of our approach, we analyzed the acute effects of BDNF on spine morphology in live neurons (Fig. 3a). BDNF is a neurotrophin that not only supports neuron differentiation and survival, but it is also an important regulator of synaptic signaling and plasticity (Gottmann et al., 2009). The canonical mechanism for BDNF-induced synapse maturation is through chronic exposure and a transcription-dependent pathway (Chapleau et al., 2009). However, BDNF also enhances glutamatergic neurotransmission through rapid, local signaling events (Gottmann et al., 2009), and recently Tanaka et al. showed that acute BDNF treatment increased dendritic spine head volume by ~150% within 25 minutes (Tanaka et al., 2008). Here, we used cultured hippocampal neurons and our automated 4D approach to investigate the effects of acute BDNF application on dendritic spine morphology. Similar to the previous study, BDNF increased mean head volume by ~160% within 20 min, and this effect was maintained for 60 min (Fig. 3a). In addition, we found that BDNF increased mean neck width by 125% (Fig. 3b) and decreased mean protrusion length by 45% (Fig. 3c). Spine classification analysis revealed significant increases in stubby and mushroom spine proportions and a decrease in the proportion of thin protrusions following BDNF treatment (Fig. 3d).

Finally, BDNF increased protrusion number by ~25% (Fig. 3e). Together, these findings indicate that acute BDNF treatment leads to an overall maturation of the dendritic spine population in a manner consistent with enhanced synaptic efficacy.

In support of the above assertion, the observed increases in head and neck width and the decrease in protrusion length are associated with increased signaling between the dendritic spine and shaft, which promotes greater signal integration within the neuron (Biess et al., 2007; Korkotian et al., 2004; Noguchi et al., 2005). Furthermore, we observed an increased proportion of mushroom-shaped spines, which have many GluA receptors and large PSDs; whereas, BDNF decreased the proportion of thin protrusions, which often lack surface GluA receptors and have less defined PSDs (Bourne and Harris, 2007). Importantly, our results agree with previous studies showing that acute BDNF enhances postsynaptic glutamate receptor function, increases excitatory postsynaptic currents, and increases intracellular calcium concentration in hippocampal neurons (Gottmann et al., 2009). Thus, our observations provide extensive morphological evidence supporting a role for BDNF in the acute regulation of synapse structure.

To determine how dendritic protrusions were remodeled to achieve the population effects described above, we tracked individual protrusions across time and quantified their morphogenesis. In this analysis, we asked three basic questions regarding remodeling: 1) does initial protrusion morphology affect remodeling, 2) what are the incidences of specific types of remodeling, and 3) what, if any, geometric parameters are associated with specific changes in morphology? We also evaluated whether BDNF treatment impacted these aspects of protrusion dynamics. Qualitatively, we observed several types of spine and filopodia remodeling such as: transient and highly dynamic

thin protrusions, the morphogenesis of long, thin protrusions into mushroom-shaped spines, the growth of stubby-spines into mushroom-shaped spines, and de novo mushroom spine formation (Fig. 4a-d and sample movie in Additional File 1).

To quantitatively analyze remodeling, we calculated the percentages of each protrusion type (stubby, mushroom, or thin) that maintained classification, remodeled into another protrusion type, or were pruned over 60 min. All newly formed spines were excluded from this analysis. Under control conditions, similar proportions of thin protrusions and stubby spines were either remodeled into mushroom spines (28.9% and 27.3%, respectively) or pruned (26.3% and 18.2%, respectively), whereas 78.6% of mushroom spines maintained their shape and only 7.1% were pruned (Fig. 4a). Acute BDNF treatment increased the remodeling of both thin and stubby protrusions into mushroom spines (40.5% and 42.9%, respectively) as well as the percentage of mushroom spines (26.7%) and thin protrusions (40.5%) that were pruned. However, BDNF slightly decreased the percentage of stubby spines that were pruned (14.3%). Interestingly, thin- and mushroom-shaped protrusions rarely morphed into stubby spines, and stubby spines were never observed to remodel into thin protrusions. These observations suggest that stubby and thin protrusions have similar propensities for remodeling into mushroom spines, but they likely do so through distinct mechanisms.

Among the total spine population, thin protrusions had the highest incidence of remodeling, and mushroom spines showed the lowest incidence of remodeling (Fig 4b). Following BDNF treatment, stubby spines had the lowest incidence of remodeling (see sample movie in Additional File 2), suggesting that stubby spines may not be simply a transitional structure, but that they might have an important end function as a stable

structure under certain conditions. The BDNF-induced increases in the proportion and stability of stubby spines, reported in Fig. 3, are difficult to interpret, because the role of stubby spines in neuronal function remains controversial. Stubby spines do not maintain or recruit GluA receptors as efficiently as mushroom spines, nor do they form synapses as often (Ashby et al., 2006; Fiala et al., 1998; Harris, 1999; Matsuo et al., 2008). On the other hand, stubby spines might have enhanced coupling to the dendritic shaft as compared to the other spine types (Richardson et al., 2009). Also, stubby spine incidence is increased during learning *in vivo*, and it has been theorized that they are transitional structures that will be enlarged/stabilized or have undergone shrinkage due to synaptic weakening (Bourne and Harris, 2007; Holtmaat and Svoboda, 2009; Holtmaat et al., 2005; Lee et al., 2005; Zhou et al., 2004; Zuo et al., 2005). Our data suggest that it is unlikely for an increase in stubby spines to result from the weakening of mushroom spines or the retraction of thin protrusions, but it is possible that the increase in stubby spines is linked to the increase in total protrusion number following BDNF stimulation. Future studies in systems having a higher overall incidence of stubby spines, perhaps neurons in an earlier developmental stage, will be important for advancing our understanding stubby spine formation, remodeling, and function.

These results also have implications regarding spine formation. Several mechanisms have been proposed for how stable, mushroom-shaped spines are formed, including growth of mushroom spines from the dendritic shaft, morphogenesis of a filopodia into a mushroom spine, and retraction of filopodia into the dendritic shaft resulting in a shaft or stubby spine synapse followed by growth of a mushroom spine at the same location (Fiala et al., 2002; Papa and Segal, 1996; Yuste and Bonhoeffer, 2004;

Ziv and Smith, 1996). Our data clearly support the formation of mushroom spines de novo and through morphogenesis of an existing filopodia (Fig. 4) as has been previously observed *in vitro* and *in vivo* (Knott et al., 2006; Konur and Yuste, 2004; Kwon and Sabatini, 2011; Lohmann et al., 2005; Marrs et al., 2001; Nagerl et al., 2007; Okabe et al., 2001; Papa and Segal, 1996; Ziv and Smith, 1996; Zuo et al., 2005). However, our data suggest that mushroom spine formation via filopodia retraction into a stubby spine followed by re-growth is not a common occurrence, at least in this model system, as we rarely observed morphogenesis of a filopodia into a stubby spine. Whether filopodia were retracted fully into the shaft and re-emerged as mushroom spines at the same locus was not evaluated in the current study, but this analysis is possible using our automated method and can be investigated in future studies.

To investigate whether any geometric parameters were associated with BDNF-induced remodeling, the initial (t = 0) mean head width, neck width, and protrusion length were compared among stable, remodeled, and pruned mushroom spines or stable, remodeled, and pruned thin protrusions (Fig. 4g,h). Large neck width was the best predictor of mushroom spine stability, whereas head width was not significantly different between stable and remodeled mushroom spines (Fig. 4g). Mushroom spine pruning was associated with reduced head and neck width and increased length compared to the other two groups (Fig. 4g). For thin protrusions, a high ratio of head width to neck width was the best indicator of stability (see Fig. 4d and the sample movie in Additional File 3). Interestingly, these data are consistent with functional studies reporting that large neck width is associated with greater synaptic strength (Noguchi et al., 2005) and synaptic potentiation of thin protrusions is promoted by maintaining high concentrations of

signaling molecules within the head, which might be due to a high ratio of head width to neck width (Bourne and Harris, 2007; Grunditz et al., 2008).

An interesting observation was that BDNF decreased the percentage of mushroom spines that remained as mushroom spines from 79% to 53% (Fig. 4e). Moreover, 26% of mushroom spines were pruned following BDNF. Both observations imply BDNF-induced turnover of mushroom spines, suggesting that the overall net gain in spine maturation (increased density and spine width, reduced length) (Fig. 3) involves extensive remodeling. This process may involve pruning of mushroom spines that passed certain thresholds approaching immature phenotypes (e.g. low head or neck width, or increased length), which are apparently replaced by more mature mushroom spines developed from other less mature populations (thin, stubby).

In the future, it will be important to study the different mechanisms underlying specific types of spine formation and remodeling, such as the distinctions between stubby and thin protrusion remodeling into mushroom spines. Furthermore, there is still much debate regarding the functional significance of different spine morphologies in brain development, plasticity, and disease. One necessary step towards understanding the structure-function relationship of dendritic spines is generating reproducible and interpretable spine morphology data. The accuracy and speed of our method makes it well-suited for studies of this type, and we anticipate that our approach will facilitate studies on spine structure and its relation to synapse function.

In addition to advancing morphological studies, the described technique has the potential to facilitate studies evaluating the synaptic localization of specific molecules. The fluorescence intensity of multiple channels can be automatically quantified within

each dendritic spine; thus, one could evaluate whether a particular fluorescently tagged or stained molecule is differentially localized between spine types or shows altered localization following a pharmacological, molecular, or genetic manipulation. Therefore, the combination our optimized spine analysis method with automated quantification of spine fluorescence creates a powerful and efficient technique for simultaneously studying spine morphology and the molecules regulating synapse structure and function.

A1.2.4 Inhibiting PI3 kinase activity rescues dendritic spine defects in neurons from Fmr1 KO mice

The importance of dendritic spine morphology is emphasized by the fact that spine abnormalities are associated with varied neurological diseases such as intellectual disabilities, neurodegenerative diseases, and psychiatric disorders (Penzes et al., 2011). Cultured neurons are a valuable model system for studying the mechanisms underlying brain diseases; as such, it is critical that spine analysis methods effectively detect aberrant spine phenotypes in disease models and identify treatments that ameliorate disease phenotypes. Here, we used our approach to study spine morphology in neurons from *Fmr1* knockout mice, a mouse model of fragile X syndrome (FXS).

FXS is an inherited intellectual disability caused by the loss of fragile X mental retardation protein (FMRP), an RNA binding protein that regulates mRNA transport and local protein synthesis at synapses (Bassell and Warren, 2008). Patients with FXS display increased dendritic spine density, an increased incidence of thin spines, and increased mean spine length, and these abnormalities are recapitulated in neurons from *Fmr1* knockout mice (Antar et al., 2006; Cruz-Martin et al., 2010; Irwin et al., 2002; Irwin et

al., 2001). In a previous study, we detected increased spine density in cultured hippocampal neurons from *Fmr1* knockout mice using a semi-automated spine analysis method in which the experimenter manually edited an automated trace; however, we were unable to detect any other defects in spine morphology with this method [(Gross et al., 2010) and unpublished observations]. Using our fully automated method, we accurately detected the established spine phenotypes in 18 *DIV* hippocampal neurons from *Fmr1* knockout mice: increased spine density, decreased spine head width, increased spine length, and decreased spine volume (Fig. 5). Furthermore, there were less mushroom-shaped spines and more thin spines in FMRP-deficient neurons, which is in line with previous reports (Bilousova et al., 2009; de Vrij et al., 2008; Galvez and Greenough, 2005; Irwin et al., 2002). These data further demonstrate the validity of our approach as well as its usefulness for studying neurological diseases.

Next, we investigated whether treating hippocampal neurons with a phosphoinositide-3-kinase (PI3K) inhibitor affected spine morphology. Previously, we discovered that inhibiting PI3K activity is a potential therapeutic strategy for FXS. We showed that the loss of FMRP leads to excess PI3K activity and treatment with a PI3K inhibitor, LY294002, rescues several neuronal phenotypes in *Fmr1* knockout mice, including aberrant synaptic protein synthesis, GluA receptor internalization, and dendritic spine density (Gross et al., 2010). Here, using our automated approach, we reproduced our previous findings by demonstrating that LY294002 treatment (10 µM for 72 hrs) reduced spine density in hippocampal neurons from *Fmr1* knockout mice to wild type levels (Fig. 5b). Furthermore, our analysis revealed that LY294002 treatment significantly increased spine head width, decreased spine length, and increased spine

volume in neurons from *Fmr1* KO mice (Fig. 5c-e). Additionally, LY294002 significantly increased mushroom-shaped spines and decreased thin spines in FMRP-deficient neurons such that all spine proportions were similar to those of wild type neurons (Fig. 5f). These data indicate that inhibiting PI3K activity not only rescues increased spine density in a mouse model of FXS, but also restores aberrant spine shape to the wild type morphology. These findings are an important advance of our previous findings and further support the pharmacological inhibition of PI3K as a potential FXS treatment strategy (Gross et al., 2011a). More broadly, these data demonstrate that our automated approach can be used to study dendritic spine abnormalities and potential pharmacotherapeutics in neurological disorders.

Although spine defects are apparent in many brain diseases, a vital unanswered question is whether altered spine morphology contributes to disease onset and progression or is secondary to disordered neuronal activity (Penzes et al., 2011; Portera-Cailliau, 2011). Of note, cortical neurons in a mouse model of Alzheimer's disease exhibit reduced spine density, a phenotype evident in patients with Alzheimer's disease, but these neurons do not show overt electrophysiological impairments; whereas, other mouse models of Alzheimer's disease show both structural and functional phenotypes in cortical neurons (Rocher et al., 2008). In addition, it is possible to alter synaptic efficacy without inducing long-term changes in spine morphology, and altering spine morphology through manipulating the neuronal cytoskeleton is not always sufficient to alter synapse function (Alvarez and Sabatini, 2007). These data highlight the complexity inherent in the spine structure-synapse function relationship and emphasize the importance of

developing powerful techniques for studying the mechanisms regulating spine

morphology in brain development, plasticity, and disease.

A1.3 Conclusions

We have developed an automated 3D approach for dendritic spine analysis using

neurons expressing fluorescently labeled Lifeact. This versatile method can be applied to

images of either fixed or live cultured neurons that were collected using widefield

fluorescence or confocal microscopy. The increased speed and accuracy of our automated

spine analysis, as compared to manual spine assessments, is critical for uncovering the

complicated mechanisms underlying normal and aberrant dendritic spine formation and

remodeling. Using our automated approach, we showed that acute BDNF treatment leads

to rapid spine remodeling consistent with enhanced synaptic efficacy. We also found that

inhibiting PI3 kinase activity rescues aberrant spine shape in neurons from a mouse

model of FXS. We predict that this method will significantly advance studies of

glutamatergic synapse structure and function in neuronal health and disease.

Table A1.1 Statistical comparison of geometric spine measurements.

	Head width		Neck width		Length	
	Manual	Auto	Manual	Auto	Manual	Auto
Neurons						
Mean (µm)	0.67	0.40	0.27	0.17	1.91	1.73
SD	±0.22	±0.08	±0.07	±0.03	±0.73	±0.26
CV	0.32	0.20	0.27	0.20	0.38	0.15
Spines						
Median (µm)	0.60	0.44	0.23	0.11	1.50	1.33
Range (µm)	2.36	0.79	1.50	0.57	4.60	4.85
Skewness	1.25	0.10	2.66	2.09	1.03	0.84

Table A1.1 The mean, standard deviation (SD), and coefficient of variation (CV) were calculated for the manual and automated measurements of average spine head width, neck width, and length per neuron (µm; $N = 28$ neurons). The median, range, and skewness were calculated for the distributions of spine head width, neck width, and length determined using the manual ($N = 411$ spines) and automated methods ($N = 423$ spines) on the same 28 neurons.

Table A1.2 Estimated population statistics based on published electron microscopy studies.

	Head width	Neck width	Length
Median	0.40	0.15	1.36
Mean	0.46	0.15	1.50
Range	0.84	0.42	4.80

Table A1.2 Geometric spine measurements (µm) from previously published electron microscopy studies were pooled to generate estimated median, mean, and range values for the population of dendritic spines on hippocampal neurons (Bourne and Harris, 2008; Harris et al., 1992; Harris and Stevens, 1989; Papa et al., 1995; Sorra and Harris, 2000).

Table A1.3 Statistical comparison of spine shape classification.

	Stubby		Mushroom		Thin	
	Manual	Auto	Manual	Auto	Manual	Auto
Median	7.0%	13.5%	65.5%	59.4%	11.7%	9.3%
SD	±11.4	±7.1	±20.0	±10.9	±15.5	±10.1
CV	1.10	0.49	0.33	0.18	0.99	0.80
P	0.033*		0.895		0.346	

Table A1.3 Dendritic spines were classified as stubby, mushroom, or thin using the manually or automatically generated geometric measurements. *P*: The Kolmogorov Smirnov test was used to compare the manual and automated distributions (*significant difference between the manual and automated measures).

Figure A1.1
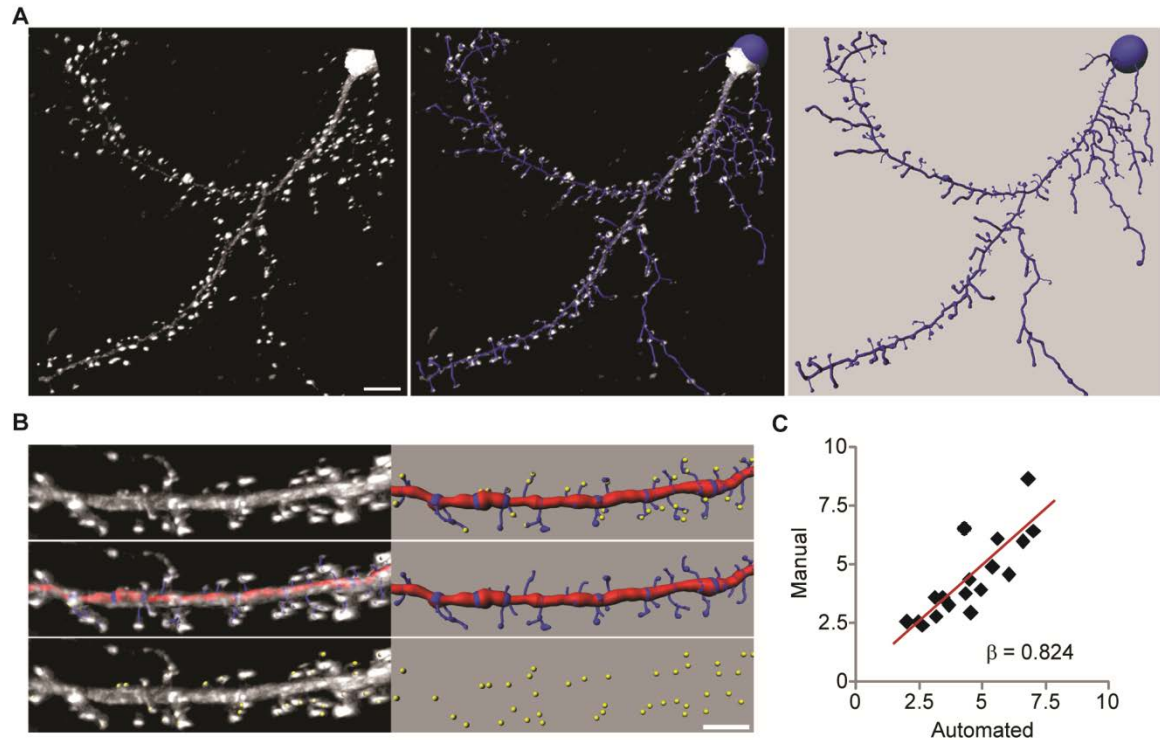
Figure A1.1 Automated detection of dendritic spines using images of Lifeact-expressing neurons. *(a)* Images depict a representative 3D reconstruction of a 17 *DIV* rat hippocampal neuron expressing Lifeact-ruby (white) and the automated trace generated by Filament Tracer (blue). Scale bar is 10 µm. *(b)* Automated and manual spine counts were performed within the same dendritic regions. Top: A dendritic segment of a Lifeact-ruby-expressing neuron (white) and the corresponding automated trace (dendrite: red, spines: blue) as well as manually marked spines (yellow spheres) are shown. Middle: Lifeact-ruby signal (white) is overlayed by the automated trace (shown alone at right). Bottom: Lifeact-ruby signal (white) is overlayed by manual spine marks (yellow; shown alone at right). *(c)* For each dendritic segment, the manual spine count was plotted against the automated count. Linear regression analysis showed that manual and automated spine detection were significantly correlated (n = 28; β = 0.824; p<0.001).

Figure A1.2 Automated tracking of dendritic protrusions in live neurons. 11 *DIV* hippocampal neurons were transfected with a vector expressing Lifeact-ruby, and 24 hrs later were imaged at 5 min intervals for 1 hr. *(a)* Individual protrusions were tracked across the time series manually and with our automated method. This histogram shows the percentages of stable, new, and pruned protrusions for both methods. *(b)* Images depict 12 *DIV* neurons expressing Lifeact-ruby (white; top) overlayed with automated 3D reconstructions (bottom). The dendrite shaft is red and each tracked protrusion is labeled 1 through 4 (shades of blue and green). Images from t = 0 and 60 min are shown, and the scale bar is 5 µm. *(c)* Head width and *(d)* protrusion length were plotted versus time for each protrusion; the labels 1 through 4 in the legend correspond to the labels 1 through 4 in panel (b).

Figure A1.2
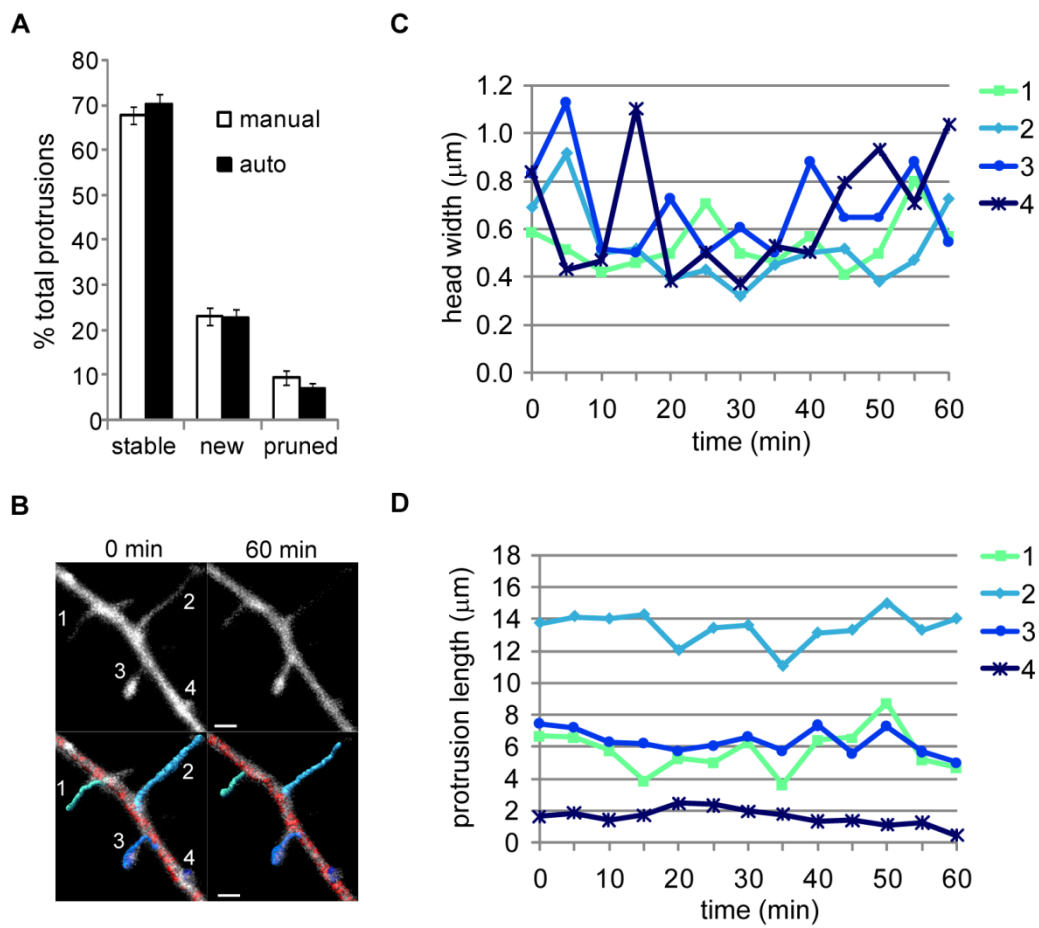
Figure A1.3 Acute BDNF treatment induces maturation of the dendritic spine population. 11 *DIV* hippocampal neurons were transfected with a vector expressing Lifeact-ruby, and 24 hrs later, the neurons were treated with vehicle or 100 ng/ml BDNF followed by time-lapse imaging every 5 minutes for 1 hr. Each protrusion was tracked across time and measured using the automated method. *(a)* Head volume was plotted as the percent change from the initial time point (T_0). Statistical analyses were performed to compare protrusion head volume at T_0 and T_{60} ($N = 105 – 135$ spines; Kruskal Wallis test with repeated measures; Control: $P = 0.548$; BDNF: $P = 0.001$). *(b)* Neck width was plotted and analyzed as above (Control: $P = 0.91$; BDNF: $P = 0.0002$). *(c)* Dendritic protrusion length was plotted and analyzed as above (Control: $P = 0.648$; BDNF: $P = 0.017$). *(d)* Dendritic protrusions were classified as stubby, mushroom, or thin at each time point. The percentages of total protrusions within each class are presented for T_0 and T_{60} (*$P = 0.038$, ‡$P = 0.044$, #$P = 0.015$). *(e)* The number of protrusions within a dendritic region was determined using Imaris Filament Tracer and compared between T_0 and T_{60} ($N = 25 - 30$ neurons; repeated measures ANOVA, post-hoc Tukey's test [Control: $P = 0.219$; BDNF: $P = 0.014$]).

Figure A1.3
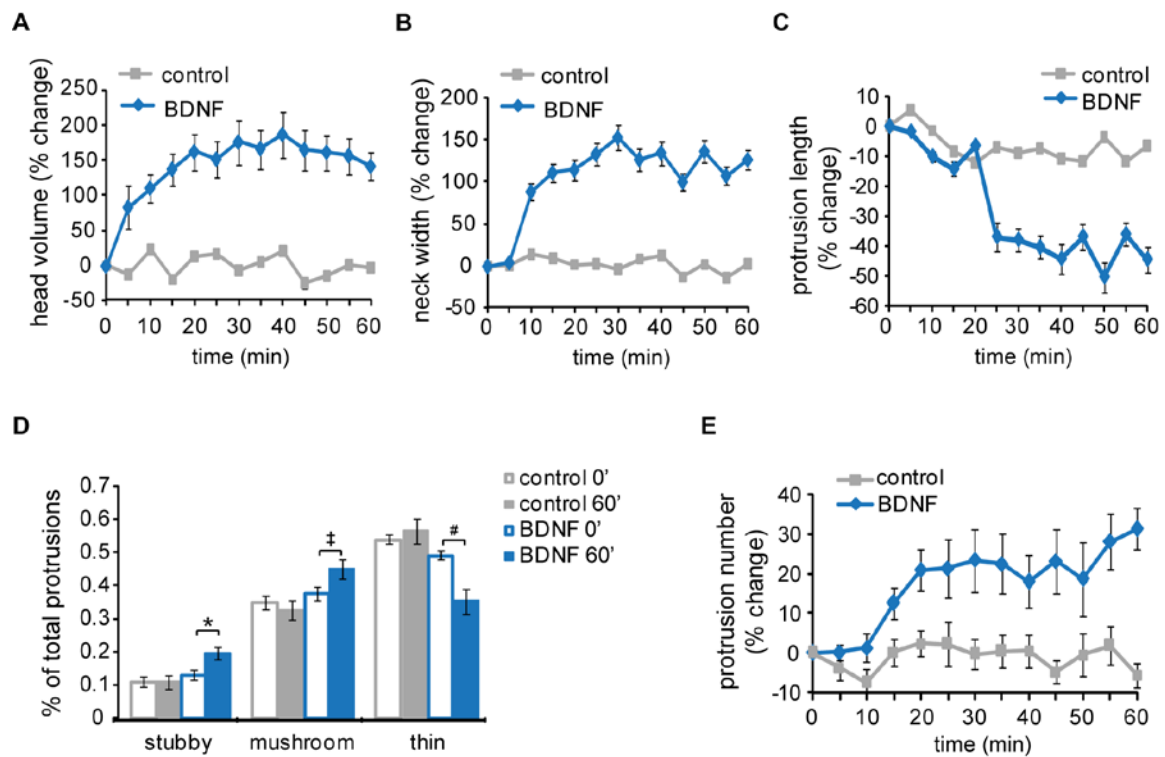
Figure A1.4 Acute BDNF induces specific types of spine remodeling. 12 *DIV*

hippocampal neurons expressing Lifeact-ruby were treated with vehicle or 100 ng/ml

BDNF and imaged at 5 min intervals for 1 hr. Each protrusion was classified as stubby,

mushroom, or thin at t = 0 and 60 min. *(a-d)* At left, each each time series (0 – 60 min)

depicts a representative type of dendritic protrusion remodeling observed during our

analysis. At right, the automated 3D reconstructions illustrate the classification of each

protrusion at t = 0 and 60 min (stubby: yellow, mushroom: green, thin: blue). *(e)* The

diagram shows the percentages of pre-existing stubby, mushroom, and thin protrusions

that were remodeled (to stubby, to mushroom, to thin) or pruned under control and

BDNF-treated conditions. *(f)* Using the same dataset as in (e), we calculated the total

incidence for each type of remodeling under control and BDNF-treated conditions. The

histogram depicts the percentages of total protrusions that were initially stubby,

mushroom, or thin and were either remodeled (to stubby, to mushroom, or to thin) or

pruned. *(g)* The initial (t=0) mean protrusion head width, neck width and length as well

as the head width/neck width ratio were determined for mushrooms spines that were

either stable (maintained mushroom morphology), remodeled into thin protrusions, or

pruned within the 60 min imaging period following BDNF treatment ($N = 24 – 32$ spines;

ANOVA, post-hoc Tukey's test; head width: [‡]$P = 0.032$, *$P = 0.017$; neck width: *$P =$

0.020, [‡]$P = 0.037$; length: [‡]$P = 0.032$, *$P = 0.017$; head/neck ratio: *$P = 0.002$, [‡]$P =$

0.001). *(h)* The group means listed above were determined for thin protrusions (t=0) that

were stable (maintained thin morphology), remodeled into mushroom spines, or pruned

during 30 min. BDNF treatment ($N = 36 – 47$ spines; ANOVA, post-hoc Tukey's test;

length: *$P = 0.002$; head/neck ratio: *$P = 0.037$).

Figure A1.4
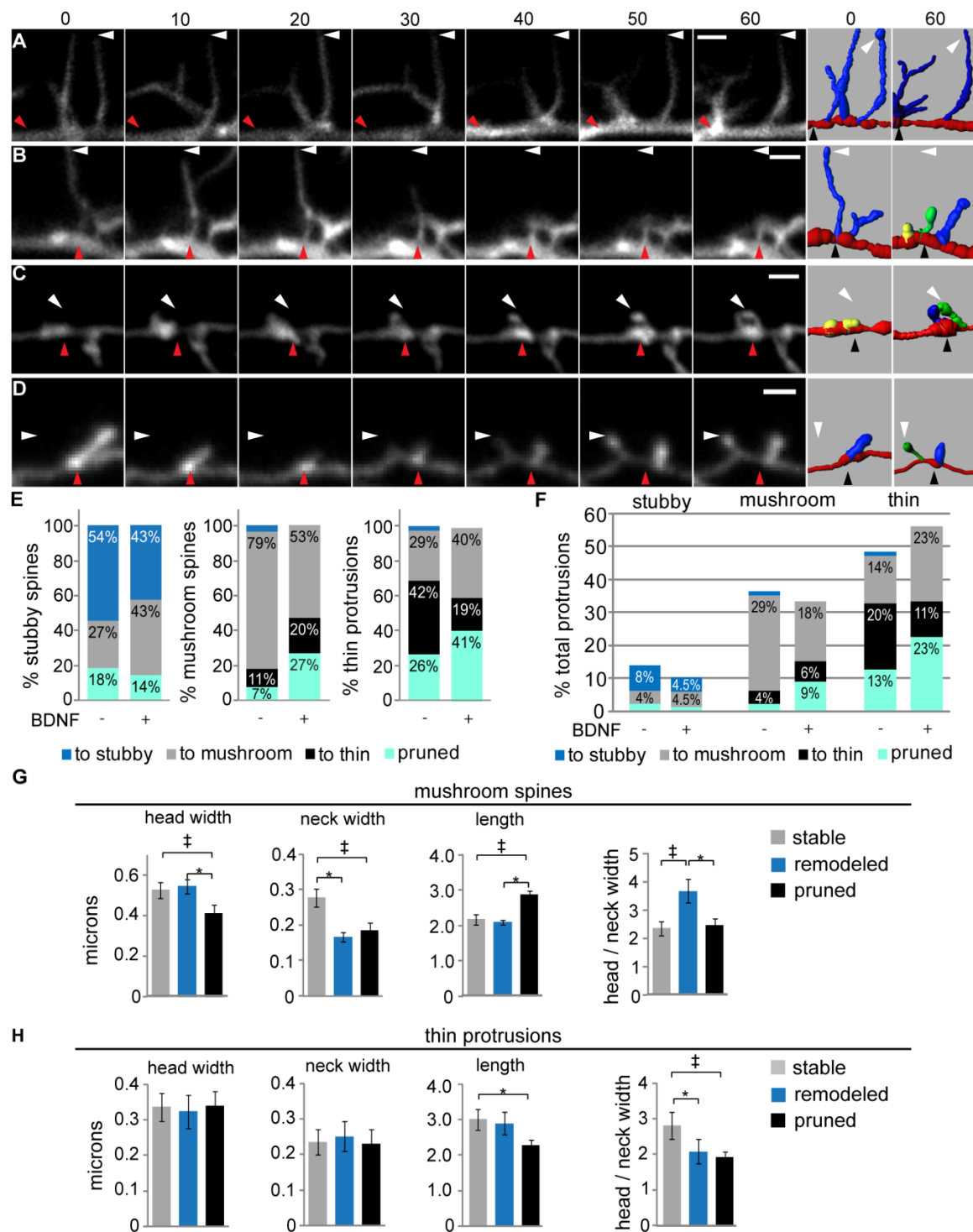
Figure A1.5 A PI3 kinase inhibitor rescues spine morphology in neurons from *Fmr1* knockout mice. *(a)* Hippocampal neurons cultured from wild type (WT) or *Fmr1* knockout (KO) mice were treated with vehicle or a PI3 kinase inhibitor (LY294, 10 µM) for 72 hours starting at 15 *DIV*. Neurons were transfected with a plasmid encoding Lifeact-ruby at 17 *DIV* and fixed 24 hours later. The images depict representative dendritic regions from deconvolved z-series images (scale bar is 5µm). *(b)* Spine density was measured using our automated approach for WT and KO neurons treated with either vehicle or LY294 (n = 55-60 neurons; ANOVA [$F = 3.996$, $P = 0.009$]; post-hoc Fisher's LSD: *$P = 0.017$, #$P = 0.028$). Cumulative distributions of *(c)* spine head width, *(d)* length, and *(e)* volume were plotted for each group (Kolmogorov-Smirnov test: head width [WT vs. KO: $P = 0.002$, WT vs. WT LY294: $P = 0.235$, KO vs. KO LY294: $P = 0.009$], spine length [WT vs. KO: $P = 0.009$, WT vs. WT LY294: $P = 0.537$, KO vs. KO LY294: $P = 0.014$], spine volume [WT vs. KO: $P < 0.001$, WT vs. WT LY294: $P = 0.158$, KO vs. KO LY294: $P < 0.001$]). *(f)* Spines were classified as stubby, mushroom, and thin based on the automated geometric measurement, and the values were plotted as percentage of total spines per treatment group (n = 55 - 60 neurons; ANOVA with post-hoc Fisher's LSD: *$P = 0.043$, #$P = 0.006$, ‡$P = 0.043$).

Figure A1.5
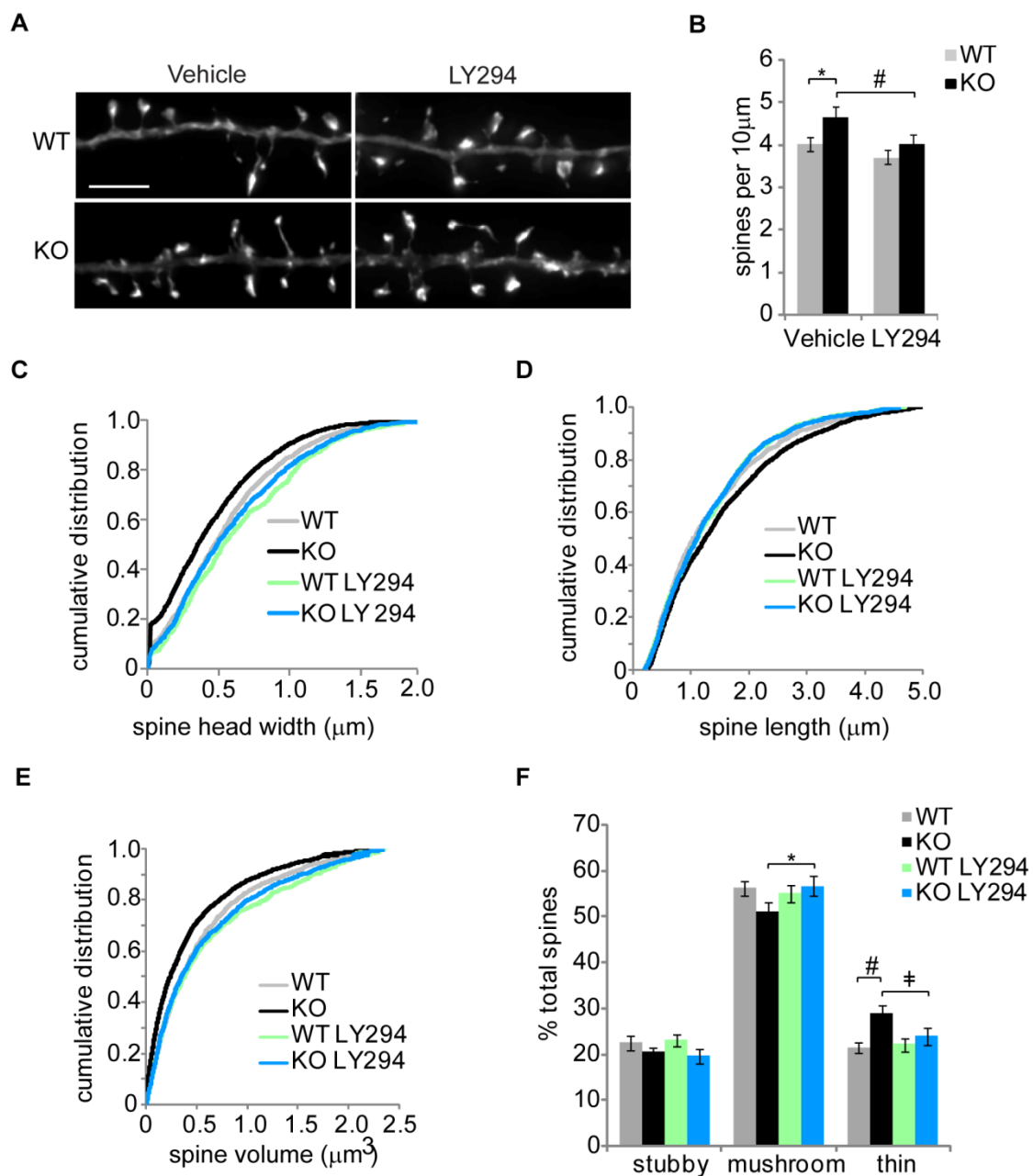
A1.4 Experimental Procedures

Neuron culture, transfection, and drug treatments

Hippocampal neurons were isolated from embryos at E18 (rat) or E17 (mouse) and cultured at high-density as previously described with minor modifications (Tiruchinapalli et al., 2003). Rat hippocampal neurons were cultured in Neurobasal medium (Invitrogen) supplemented with NS21 (Chen et al., 2008). Neurons were either plated on 15 mm glass coverslips and co-cultured with glia, or plated on 35 mm MatTek glass bottom dishes in glia-conditioned media that was exchanged every 2 days with new glia-conditioned media.

Fixed neuron experiments: 16-17 *DIV* neurons were transfected with plasmids encoding Lifeact-ruby (a generous gift from Dr. Roland Wedlich-Soldner, Max Planck Institute, Martinsried, Germany), Lifeact-GFP, GFP, or membrane-tagged GFP using NeuroMag (OZBiosciences). DiI labeling was performed on 16 *DIV* neurons by incubating the coverslips covered with a small volume of neuronal culture media containing Vybrant DiI solution (Invitrogen) for 25 min at 37°C. For LY294002 experiments, 15 *DIV* neurons were treated with 10 µM LY294002 or an equivalent volume of DMSO for 72 hrs total; the culture media was exchanged with conditioned media containing freshly prepared drug (or vehicle) after 24 and 48 hrs.

Live neuron experiments: 11 *DIV* rat hippocampal neurons were transfected with a plasmid encoding Lifeact-ruby using Lipofectamine 2000 and used for imaging 24 hrs later. Thirty minutes prior to imaging, neurons were equilibrated to glia-conditioned imaging media (phenol red-free Neurobasal media supplemented with HEPES, sodium pyruvate, NS21, and Glutamax). For BDNF experiments: One hour prior to imaging,

neurons were starved in glia-conditioned imaging media without NS21, and immediately prior to time lapse imaging neurons were treated with BDNF (100ng/ml; Peprotech) or vehicle (H_2O).

Microscopy

Widefield fluorescence: Twenty-four hours after transfection, hippocampal neurons were fixed with 4% paraformaldehyde in 1x phosphate-buffered saline (PBS), washed 3 times with 1x PBS, and the coverslips were mounted on microscope slides with propyl gallate-containing polyvinyl alcohol. Neurons were imaged on a Nikon Eclipse Ti microscope with a Nikon Intensilight and Photometrics Coolsnap HQ2 camera. GFP was imaged using a 480/40 excitation filter, a 535/50 emission filter, and a 505 dichroic (Nikon), and ruby and DiI were imaged using a 545/30 excitation filter, a 620/60 emission filter, and a 570 dichroic. Images were acquired using a 60X oil-immersion objective (Nikon Plan Apo, N.A. 1.40). Z-series images were acquired at 0.15 μm increments through the entire visible dendrite.

Confocal laser scanning: Time lapse imaging was performed on a Nikon A1R confocal encased in a plexiglass humidified chamber maintained at 37°C and 5% CO_2 using a 60X oil immersion objective (Nikon Plan Apo, N.A. 1.40). Images of Lifeact-ruby were collected using a 561 nm laser for excitation and a 650 emission filter. Z-series were acquired at 0.15 μm increments, and a Nikon Perfect Focus system was enabled for the duration of the experiment.

Image processing

Images were deconvolved in AutoQuant X (MediaCybernetics) using the blind algorithm, which employs an iteratively refined theoretical PSF. No further processing was performed prior to image analysis. For preparation of figures, maximum intensity Z-projections were created in Imaris (Figs 1 and 5) or average intensity Z-projections were created using ImageJ (Figs 2 and 4). For visualization, brightness and contrast levels were adjusted using ImageJ.

Automated image analysis

In Imaris Surpass mode, a new filament was created using the Autopath mode and a region of interest (ROI) was selected. To select an ROI, we identified a dendritic region 40 – 60 µm length that was distal to a dendritic branch point and void of crossing neurites or any additional dendritic branch points. A *minimum dendrite end diameter* of 0.75 µm was entered and a single dendrite starting point was assigned at the edge of the ROI. For time-lapse image series, a single dendrite starting point was assigned at each timepoint by using the AutoDepth mode. Automatic thresholds were used for assigning dendrite end points and dendrite surface rendering. To trace spines, the *maximum spine length* and *minimum spine end diameter* were set at 5 µm and 0.215 µm, respectively, for fixed neuron experiments and 15 µm and 0.3 µm, respectively, for live imaging experiments. Automatic thresholds were used for generating spine seed points and surface rendering. After generating the trace, a filter was applied to ensure all dendritic protrusions ≤ 5 µm (or 15 µm) were assigned as spines; to do so, we created a filter that selected all dendritic segments with "Branch level" = 2 and "length" ≤ 5 (or 15) and the selected segments

were assigned as spines by choosing "Assign as spine" under the *Edit* tab. All of the

geometric parameters and filters were set, or loaded from a previously analyzed image, at

the start of the analysis session after which the software maintained these values. For

each subsequent image processed, an ROI was selected, a dendrite starting point was

assigned, and then the trace was built by clicking "Finish". To apply the filter, the *Filter*

tab was opened (which automatically selected the appropriate segments), then by clicking

on the *Edit* tab followed by "Assign as spine" the final 3D trace was generated. Filament

statistics were exported into Excel (Microsoft), where they were compiled and graphed.

Manual image analysis

Manual analyses were performed in Imaris Surpass mode using the same dendritic

ROIs as above. The dendrite length was measured using Measurement Points and each

spine was marked using Spots (Imaris). Using Measurement Points, head width was

measured at the maximum width of the spine tip, neck width was measured at the

minimum point along the spine length, and spine length was measured from the dendrite

shaft to the spine tip. Each ROI was processed in duplicate and the values were averaged.

Spine classifications

Spines were classified into groups termed stubby, mushroom, and thin. These groups

were established as follows: stubby (length ≤1 µm and neck width/head width < 1.5),

mushroom (neck width/head width ≥ 1.5 and length ≤5 µm), and thin (1 < length ≤ 5 µm

and neck width/head width < 1.5) (Harris et al., 1992). Classification for both manual and

Filament Tracer, were computed in Excel using the following formulas:

Stubby:	=IF(AND(length ≤ 5, head/neck ≤ 1.5),1,0)
Mushroom:	=IF(AND(length ≤ 5, head/neck ≥ 1.5),1,0)
Thin:	=IF(AND(length ≤ 5, length >1, head/neck ≤ 1.5),1,0)

These logic statements return a value of 1 if true and 0 if false. The total number of spines in each class was tallied by summing the results of the logic statements. For live imaging experiments, a maximum length of 15 µm was used instead of 5 µm.

Statistics

Unless otherwise noted, statistics were completed using PASW Statistics 18 (SPSS, Inc). All datasets were analyzed for equal variance using Levene's test and normality using the Kolmogorov Smirnov test. Normally distributed datasets were compared using either Student's t-test or an ANOVA followed by post-hoc tests as noted in figure legends. Non-normal datasets were compared using the Mann-Whitney U test or Kruskal Wallis test. Cumulative distributions were compared using the Kolmogorov-Smirnov test. Alpha was set at 0.05 for all comparisons. Power analysis was performed using G*Power 3.1.2 (University of Kiel, Germany) with $\beta=0.8$ and $\alpha=0.05$, and effect size and standard deviation were determined using pilot experiment results. The experimenter was blind to treatment and genotype during all image analysis.

A1.5 REFERENCES

Alvarez, V.A., and Sabatini, B.L. (2007). Anatomical and physiological plasticity of dendritic spines. Annu Rev Neurosci *30*, 79-97.

Antar, L.N., Li, C., Zhang, H., Carroll, R.C., and Bassell, G.J. (2006). Local functions for FMRP in axon growth cone motility and activity-dependent regulation of filopodia and spine synapses. Molecular and cellular neurosciences *32*, 37-48.

Ashby, M.C., Maier, S.R., Nishimune, A., and Henley, J.M. (2006). Lateral diffusion drives constitutive exchange of AMPA receptors at dendritic spines and is regulated by spine morphology. J Neurosci *26*, 7046-7055.

Bassell, G.J., and Warren, S.T. (2008). Fragile X syndrome: loss of local mRNA regulation alters synaptic development and function. Neuron *60*, 201-214.

Biess, A., Korkotian, E., and Holcman, D. (2007). Diffusion in a dendritic spine: the role of geometry. Phys Rev E Stat Nonlin Soft Matter Phys *76*, 021922.

Bilousova, T.V., Dansie, L., Ngo, M., Aye, J., Charles, J.R., Ethell, D.W., and Ethell, I.M. (2009). Minocycline promotes dendritic spine maturation and improves behavioural performance in the fragile X mouse model. J Med Genet *46*, 94-102.

Bloss, E.B., Janssen, W.G., Ohm, D.T., Yuk, F.J., Wadsworth, S., Saardi, K.M., McEwen, B.S., and Morrison, J.H. (2011). Evidence for reduced experience-dependent dendritic spine plasticity in the aging prefrontal cortex. The Journal of neuroscience : the official journal of the Society for Neuroscience *31*, 7831-7839.

Bourne, J., and Harris, K.M. (2007). Do thin spines learn to be mushroom spines that remember? Curr Opin Neurobiol *17*, 381-386.

Bourne, J.N., and Harris, K.M. (2008). Balancing structure and function at hippocampal dendritic spines. Annu Rev Neurosci *31*, 47-67.

Bourne, J.N., and Harris, K.M. (2010). Coordination of size and number of excitatory and inhibitory synapses results in a balanced structural plasticity along mature hippocampal CA1 dendrites during LTP. Hippocampus.

Chapleau, C.A., Larimore, J.L., Theibert, A., and Pozzo-Miller, L. (2009). Modulation of dendritic spine development and plasticity by BDNF and vesicular trafficking: fundamental roles in neurodevelopmental disorders associated with mental retardation and autism. J Neurodev Disord *1*, 185-196.

Chen, Y., Stevens, B., Chang, J., Milbrandt, J., Barres, B.A., and Hell, J.W. (2008).
NS21: re-defined and modified supplement B27 for neuronal cultures. J Neurosci
Methods *171*, 239-247.

Cruz-Martin, A., Crespo, M., and Portera-Cailliau, C. (2010). Delayed stabilization of
dendritic spines in fragile X mice. J Neurosci *30*, 7793-7803.

de Vrij, F.M., Levenga, J., van der Linde, H.C., Koekkoek, S.K., De Zeeuw, C.I., Nelson,
D.L., Oostra, B.A., and Willemsen, R. (2008). Rescue of behavioral phenotype
and neuronal protrusion morphology in Fmr1 KO mice. Neurobiology of disease
31, 127-132.

Edwards, F.A. (1995). Anatomy and electrophysiology of fast central synapses lead to a
structural model for long-term potentiation. Physiol Rev *75*, 759-787.

Fan, J., Zhou, X., Dy, J.G., Zhang, Y., and Wong, S.T. (2009). An automated pipeline for
dendrite spine detection and tracking of 3D optical microscopy neuron images of
in vivo mouse models. Neuroinformatics *7*, 113-130.

Fiala, J.C., Feinberg, M., Popov, V., and Harris, K.M. (1998). Synaptogenesis via
dendritic filopodia in developing hippocampal area CA1. J Neurosci *18*, 8900-
8911.

Fiala, J.C., Spacek, J., and Harris, K.M. (2002). Dendritic spine pathology: cause or
consequence of neurological disorders? Brain Res Brain Res Rev *39*, 29-54.

Galvez, R., and Greenough, W.T. (2005). Sequence of abnormal dendritic spine
development in primary somatosensory cortex of a mouse model of the fragile X
mental retardation syndrome. Am J Med Genet A *135*, 155-160.

Glantz, L.A., and Lewis, D.A. (2001). Dendritic spine density in schizophrenia and
depression. Arch Gen Psychiatry *58*, 203.

Gottmann, K., Mittmann, T., and Lessmann, V. (2009). BDNF signaling in the formation,
maturation and plasticity of glutamatergic and GABAergic synapses.
Experimental brain research Experimentelle Hirnforschung Experimentation
cerebrale *199*, 203-234.

Gross, C., Berry-Kravis, E.M., and Bassell, G.J. (2011a). Therapeutic Strategies in
Fragile X Syndrome: Dysregulated mGluR Signaling and Beyond.

Neuropsychopharmacology : official publication of the American College of Neuropsychopharmacology.

Gross, C., Nakamoto, M., Yao, X., Chan, C.B., Yim, S.Y., Ye, K., Warren, S.T., and Bassell, G.J. (2010). Excess phosphoinositide 3-kinase subunit synthesis and activity as a novel therapeutic target in fragile X syndrome. J Neurosci *30*, 10624-10638.

Gross, C., Yao, X., Pong, D.L., Jeromin, A., and Bassell, G.J. (2011b). Fragile X mental retardation protein regulates protein expression and mRNA translation of the potassium channel Kv4.2. The Journal of neuroscience : the official journal of the Society for Neuroscience *31*, 5693-5698.

Grunditz, A., Holbro, N., Tian, L., Zuo, Y., and Oertner, T.G. (2008). Spine neck plasticity controls postsynaptic calcium signals through electrical compartmentalization. J Neurosci *28*, 13457-13466.

Harris, K.M. (1999). Structure, development, and plasticity of dendritic spines. Curr Opin Neurobiol *9*, 343-348.

Harris, K.M., Jensen, F.E., and Tsao, B. (1992). Three-dimensional structure of dendritic spines and synapses in rat hippocampus (CA1) at postnatal day 15 and adult ages: implications for the maturation of synaptic physiology and long-term potentiation. J Neurosci *12*, 2685-2705.

Harris, K.M., and Stevens, J.K. (1989). Dendritic spines of CA 1 pyramidal cells in the rat hippocampus: serial electron microscopy with reference to their biophysical characteristics. J Neurosci *9*, 2982-2997.

Hayashi, Y., and Majewska, A.K. (2005). Dendritic spine geometry: functional implication and regulation. Neuron *46*, 529-532.

Heiman, M.G., and Shaham, S. (2010). Twigs into branches: how a filopodium becomes a dendrite. Current opinion in neurobiology *20*, 86-91.

Holtmaat, A., and Svoboda, K. (2009). Experience-dependent structural synaptic plasticity in the mammalian brain. Nat Rev Neurosci *10*, 647-658.

Holtmaat, A.J., Trachtenberg, J.T., Wilbrecht, L., Shepherd, G.M., Zhang, X., Knott, G.W., and Svoboda, K. (2005). Transient and persistent dendritic spines in the neocortex in vivo. Neuron *45*, 279-291.

Irwin, S.A., Idupulapati, M., Gilbert, M.E., Harris, J.B., Chakravarti, A.B., Rogers, E.J., Crisostomo, R.A., Larsen, B.P., Mehta, A., Alcantara, C.J., Patel, B., Swain, R.A., Weiler, I.J., Oostra, B.A., and Greenough, W.T. (2002). Dendritic spine and dendritic field characteristics of layer V pyramidal neurons in the visual cortex of fragile-X knockout mice. American journal of medical genetics *111*, 140-146.

Irwin, S.A., Patel, B., Idupulapati, M., Harris, J.B., Crisostomo, R.A., Larsen, B.P., Kooy, F., Willems, P.J., Cras, P., Kozlowski, P.B., Swain, R.A., Weiler, I.J., and Greenough, W.T. (2001). Abnormal dendritic spine characteristics in the temporal and visual cortices of patients with fragile-X syndrome: a quantitative examination. American journal of medical genetics *98*, 161-167.

Janoos, F., Mosaliganti, K., Xu, X., Machiraju, R., Huang, K., and Wong, S.T. (2009). Robust 3D reconstruction and identification of dendritic spines from optical microscopy imaging. Med Image Anal *13*, 167-179.

Kasai, H., Fukuda, M., Watanabe, S., Hayashi-Takagi, A., and Noguchi, J. (2010). Structural dynamics of dendritic spines in memory and cognition. Trends Neurosci *33*, 121-129.

Kasai, H., Matsuzaki, M., Noguchi, J., Yasumatsu, N., and Nakahara, H. (2003). Structure-stability-function relationships of dendritic spines. Trends Neurosci *26*, 360-368.

Knott, G.W., Holtmaat, A., Wilbrecht, L., Welker, E., and Svoboda, K. (2006). Spine growth precedes synapse formation in the adult neocortex in vivo. Nat Neurosci *9*, 1117-1124.

Koh, I.Y., Lindquist, W.B., Zito, K., Nimchinsky, E.A., and Svoboda, K. (2002). An image analysis algorithm for dendritic spines. Neural Comput *14*, 1283-1310.

Konur, S., and Yuste, R. (2004). Imaging the motility of dendritic protrusions and axon terminals: roles in axon sampling and synaptic competition. Molecular and cellular neurosciences *27*, 427-440.

Korkotian, E., Holcman, D., and Segal, M. (2004). Dynamic regulation of spine-dendrite coupling in cultured hippocampal neurons. Eur J Neurosci *20*, 2649-2663.

Kwon, H.B., and Sabatini, B.L. (2011). Glutamate induces de novo growth of functional spines in developing cortex. Nature *474*, 100-104.

Lee, K.J., Kim, H., and Rhyu, I.J. (2005). The roles of dendritic spine shapes in Purkinje cells. Cerebellum *4*, 97-104.

Lohmann, C., Finski, A., and Bonhoeffer, T. (2005). Local calcium transients regulate the spontaneous motility of dendritic filopodia. Nature neuroscience *8*, 305-312.

Ludbrook, J. (2010). Linear regression analysis for comparing two measurers or methods of measurement: but which regression? Clin Exp Pharmacol Physiol *37*, 692-699.

Marrs, G.S., Green, S.H., and Dailey, M.E. (2001). Rapid formation and remodeling of postsynaptic densities in developing dendrites. Nature neuroscience *4*, 1006-1013.

Matsuo, N., Reijmers, L., and Mayford, M. (2008). Spine-type-specific recruitment of newly synthesized AMPA receptors with learning. Science *319*, 1104-1107.

Matsuzaki, M., Honkura, N., Ellis-Davies, G.C., and Kasai, H. (2004). Structural basis of long-term potentiation in single dendritic spines. Nature *429*, 761-766.

Mukai, H., Hatanaka, Y., Mitsuhashi, K., Hojo, Y., Komatsuzaki, Y., Sato, R., Murakami, G., Kimoto, T., and Kawato, S. (2011). Automated Analysis of Spines from Confocal Laser Microscopy Images: Application to the Discrimination of Androgen and Estrogen Effects on Spinogenesis. Cerebral cortex.

Nagerl, U.V., Kostinger, G., Anderson, J.C., Martin, K.A., and Bonhoeffer, T. (2007). Protracted synaptogenesis after activity-dependent spinogenesis in hippocampal neurons. The Journal of neuroscience : the official journal of the Society for Neuroscience *27*, 8149-8156.

Noguchi, J., Matsuzaki, M., Ellis-Davies, G.C., and Kasai, H. (2005). Spine-neck geometry determines NMDA receptor-dependent Ca2+ signaling in dendrites. Neuron *46*, 609-622.

Okabe, S., Miwa, A., and Okado, H. (2001). Spine formation and correlated assembly of presynaptic and postsynaptic molecules. The Journal of neuroscience : the official journal of the Society for Neuroscience *21*, 6105-6114.

Papa, M., Bundman, M.C., Greenberger, V., and Segal, M. (1995). Morphological analysis of dendritic spine development in primary cultures of hippocampal neurons. J Neurosci *15*, 1-11.

Papa, M., and Segal, M. (1996). Morphological plasticity in dendritic spines of cultured hippocampal neurons. Neuroscience *71*, 1005-1011.

Penzes, P., Cahill, M.E., Jones, K.A., Vanleeuwen, J.E., and Woolfrey, K.M. (2011). Dendritic spine pathology in neuropsychiatric disorders. Nat Neurosci *14*, 285-293.

Peters, A., and Kaiserman-Abramof, I.R. (1970). The small pyramidal neuron of the rat cerebral cortex. The perikaryon, dendrites and spines. Am J Anat *127*, 321-355.

Portera-Cailliau, C. (2011). Which Comes First in Fragile X Syndrome, Dendritic Spine Dysgenesis or Defects in Circuit Plasticity? The Neuroscientist : a review journal bringing neurobiology, neurology and psychiatry.

Richardson, R.J., Blundon, J.A., Bayazitov, I.T., and Zakharenko, S.S. (2009). Connectivity patterns revealed by mapping of active inputs on dendrites of thalamorecipient neurons in the auditory cortex. J Neurosci *29*, 6406-6417.

Riedl, J., Crevenna, A.H., Kessenbrock, K., Yu, J.H., Neukirchen, D., Bista, M., Bradke, F., Jenne, D., Holak, T.A., Werb, Z., Sixt, M., and Wedlich-Soldner, R. (2008). Lifeact: a versatile marker to visualize F-actin. Nat Methods *5*, 605-607.

Riedl, J., Flynn, K.C., Raducanu, A., Gartner, F., Beck, G., Bosl, M., Bradke, F., Massberg, S., Aszodi, A., Sixt, M., and Wedlich-Soldner, R. (2010). Lifeact mice for studying F-actin dynamics. Nat Methods *7*, 168-169.

Rocher, A.B., Kinson, M.S., and Luebke, J.I. (2008). Significant structural but not physiological changes in cortical neurons of 12-month-old Tg2576 mice. Neurobiology of disease *32*, 309-318.

Rodriguez, A., Ehlenberger, D.B., Dickstein, D.L., Hof, P.R., and Wearne, S.L. (2008). Automated three-dimensional detection and shape classification of dendritic spines from fluorescence microscopy images. PLoS One *3*, e1997.

Rodriguez, A., Ehlenberger, D.B., Hof, P.R., and Wearne, S.L. (2006). Rayburst sampling, an algorithm for automated three-dimensional shape analysis from laser scanning microscopy images. Nature protocols *1*, 2152-2161.

Scotto-Lomassese, S., Nissant, A., Mota, T., Neant-Fery, M., Oostra, B.A., Greer, C.A., Lledo, P.M., Trembleau, A., and Caille, I. (2011). Fragile X mental retardation protein regulates new neuron differentiation in the adult olfactory bulb. The Journal of neuroscience : the official journal of the Society for Neuroscience *31*, 2205-2215.

Shen, H., Sesack, S.R., Toda, S., and Kalivas, P.W. (2008). Automated quantification of dendritic spine density and spine head diameter in medium spiny neurons of the nucleus accumbens. Brain Struct Funct *213*, 149-157.

Son, J., Song, S., Lee, S., Chang, S., and Kim, M. (2011). Morphological change tracking of dendritic spines based on structural features. J Microsc *241*, 261-272.

Sorra, K.E., and Harris, K.M. (2000). Overview on the structure, composition, function, development, and plasticity of hippocampal dendritic spines. Hippocampus *10*, 501-511.

Staffend, N.A., Loftus, C.M., and Meisel, R.L. (2011). Estradiol reduces dendritic spine density in the ventral striatum of female Syrian hamsters. Brain Struct Funct *215*, 187-194.

Stevens, J.K., and Trogadis, J. (1986). Reconstructive three-dimensional electron microscopy. A routine biologic tool. Anal Quant Cytol Histol *8*, 102-107.

Svoboda, K. (2011). The past, present, and future of single neuron reconstruction. Neuroinformatics *9*, 97-98.

Tanaka, J., Horiike, Y., Matsuzaki, M., Miyazaki, T., Ellis-Davies, G.C., and Kasai, H. (2008). Protein synthesis and neurotrophin-dependent structural plasticity of single dendritic spines. Science *319*, 1683-1687.

Tiruchinapalli, D.M., Oleynikov, Y., Kelic, S., Shenoy, S.M., Hartley, A., Stanton, P.K., Singer, R.H., and Bassell, G.J. (2003). Activity-dependent trafficking and dynamic localization of zipcode binding protein 1 and beta-actin mRNA in dendrites and spines of hippocampal neurons. J Neurosci *23*, 3251-3261.

Wearne, S.L., Rodriguez, A., Ehlenberger, D.B., Rocher, A.B., Henderson, S.C., and Hof, P.R. (2005). New techniques for imaging, digitization and analysis of three-dimensional neural morphology on multiple scales. Neuroscience *136*, 661-680.

Yoshihara, Y., De Roo, M., and Muller, D. (2009). Dendritic spine formation and stabilization. Current opinion in neurobiology *19*, 146-153.

Yuste, R., and Bonhoeffer, T. (2004). Genesis of dendritic spines: insights from ultrastructural and imaging studies. Nature reviews Neuroscience *5*, 24-34.

Zhang, Y., Chen, K., Baron, M., Teylan, M.A., Kim, Y., Song, Z., Greengard, P., and Wong, S.T. (2010). A neurocomputational method for fully automated 3D

dendritic spine detection and segmentation of medium-sized spiny neurons. NeuroImage *50*, 1472-1484.

Zhang, Y., Zhou, X., Witt, R.M., Sabatini, B.L., Adjeroh, D., and Wong, S.T. (2007). Dendritic spine detection using curvilinear structure detector and LDA classifier. NeuroImage *36*, 346-360.

Zhou, Q., Homma, K.J., and Poo, M.M. (2004). Shrinkage of dendritic spines associated with long-term depression of hippocampal synapses. Neuron *44*, 749-757.

Ziv, N.E., and Smith, S.J. (1996). Evidence for a role of dendritic filopodia in synaptogenesis and spine formation. Neuron *17*, 91-102.

Zuo, Y., Lin, A., Chang, P., and Gan, W.B. (2005). Development of long-term dendritic spine stability in diverse regions of cerebral cortex. Neuron *46*, 181-189.